Alma Mater Studiorum – Università di Bologna

DOTTORATO DI RICERCA IN

Ingegneria Chimica dell'Ambiente e della Sicurezza

Ciclo XXVIII

Settore Concorsuale di afferenza: AREA 09/D2

Settore Scientifico disciplinare: ING/IND-24

POLYMERIC MEMBRANES FOR CO_2 CAPTURE

Presentata da: Luca Olivieri

Coordinatore Dottorato:

Prof.ssa Serena Bandini

Relatori:

Prof.ssa Maria Grazia De Angelis

Prof. Giulio Cesare Sarti

Esame finale anno 2016

List of Figures

List of Tables

Table of content

Thesis abstract

The object of this PhD work is the study of innovative, composite and nanostructured polymeric materials for membrane-based separation and removal of CO_2 from gaseous streams.

The research on gas separation membranes, in the last two decades was largely devoted to the synthesis and fabrication of new, multiphasic materials, such as copolymers, composite materials bearing fillers dispersed in the polymeric matrix, or functionalized materials having selective functional groups attached to the polymer backbone. The materials investigated in this thesis can be divided in three classes:

i) Copolyetherimides: copolymers formed by a glassy polyimide phase, which confers mechanical and thermal resistance to the polymer matrix, and a rubber polyether phase, which has stronge affinity with carbon dioxide. This work originated from a collaboration with the University of Valladolid;

ii) Composite membranes, commonly defined as Mixed Matrix Membranes, obtained by physically dispersing of an inorganic, graphenic filler, phase into an organic polymeric phase (in collaboration with the start-up company GNext).

iii) Functionalized materials obtained by chemically attaching amine moieties to a polymeric backbone for the instauration, in appropriate operative conditions, of the facilitated transport mechanism of CO_2. Such work was carried out in collaboration with the Department of Industrial Engineering of University of Padua.

All the above materials have the advantage that their transport properties, in terms of solubility, diffusivity and thus of gas permeability and selectivity, can be tuned and adjusted for the practical purpose. To this end, in this work, an experimental campaign devoted to the measurement of transport properties will be supported by a modeling approach on the continuous scale, for better understanding mass transport properties and the influence of material formulation on them, and develop easily accessible models for the prediction of materials behavior.

In the first part of the thesis a description of gas separation with membranes will be shown, together with a brief description of materials studied in this work and the motivations driving this study.

After this introductive chapter, experimental methods and apparatuses will be described and a brief mathematical approach for the measurements of transport properties will be presented, followed by the description of the materials object of the study, of their formulation and preparation protocol.

Experimental results will be report separately for the different materials, observing as first in copolyetherimides the effect of temperature and copolymer composition on solubility and diffusivity of carbon dioxide, to give a deep explanation of previous results obtained by CSIC research group and on the dependence of gas separation performance on copolymer formulation. In addition the effect of water vapor will be investigate to evaluate performance more near to the reality of gases separation, which involves the presence of water vapor. It will be observed a similar dependence of two different gases permeability on relative humidity, which does not compromise separation performances and does not deplete gas fluxes across the membrane hanks to the presence of hydrophilic moieties in the polymeric composite membrane.

For Mixed Matrix Membranes, based on PTMSP and graphene based fillers it will be observed the effect of the different fillers on gases permeabilities, relating it on aspect ratio of nanoplatelets and on their ability to modify polymer chain packing. Moreover the effect of the filler will be investigate also during polymer physical ageing, observing that the filler can act as a mechanical constraint for volume relaxation if it is characterized by a sufficient size able to reduce and slow the ageing process.

Experimental results on functionalized material based on PAN, will be shown observing the effect of amine groups on carbon dioxide solubility and permeability in dry and humid condition and verifying the instauration of a facilitated transport mechanism in presence of water vapor.

Finally, models for the prediction of transport properties will be described with particular attention on solubility modeling in copolyetherimides, describing procedures for obtaining models parameters and their ability to predict solubility of composite membranes.

Introduction

The last century saw a rapid increase of population, growth of country industrialization and energy consumption, raw material utilization and consequent increase of environmental impact. Environmental issues due to emissions of pollutant and non-pollutant compounds from combustion of fossil fuel, process industry or, in general, from anthropologic activity have assumed a global character. [1] One of those is represented by emission of greenhouse gases, such as methane and carbon dioxide, which, becoming increasingly interesting topics for scientific research studies, have been identified as the cause of climate change. Recent studies affirm that the world population was more than 6.8 billion in 2010 and it is expected to increase to about 9.2 billion in 2050; this expansion is expected to be accompanied by equivalent increase in overall energy consumption from 15 TW to more than 40 TW [2]. The International Energy Agency (IEA) states that in 2013 global CO_2 emissions reached 32.2 Gt of CO_2, which is an increase of 2.2% with respect to 2012 levels [3]. This was a growth higher than in 2012 (0.6%), but lower than the average annual growth rate since 2000 (2.5%). Moreover the increase is strictly connected to increase of emission due to electricity and heat generation [3].

In this scenario it seems necessary to adopt a strategic program whose targets are: (i) the energy intensity reduction by more efficient energy conversion processes, (ii) the reduction of carbon intensity by switching to non-fossil fuels such as hydrogen and renewable energies, (iii) the development of economically feasible technologies to capture and sequester carbon dioxide [1–5].

Carbon capture and storage (CCS) has attracted the attention of many academic and industrial researchers, to improve existing and traditional capturing technologies such as pre-combustion, post-combustion and oxy-fuel combustion capture. The main disadvantages of traditional technologies which are commercially available, such as chemical absorption with amines, are low CO_2 loading capacity, high equipment corrosion rate, amine degradation by SO_2, NO_2 and HCl and high energy consumption during high temperature solvent regeneration [1,2,5]. It is possible to say that the regeneration step obtained in a stripping column consumes between 4 and 6 GJ/ton of CO_2 recovered, which is a too high energy consumption that should be largely reduced to make this process economically feasible [6].

These are some of the motivations that in the last three decades drive interest of researchers to study the thermodynamics and transport phenomena of CO_2 in polymeric materials. In opposition to high costs of absorption process, with a membrane module it could be possible to reduce energy consumption to 0.5–1 GJ/ton of CO_2 recovered [6]. In spite of this, membrane separation processes are energy efficient. They are versatile in application and characterized by operational simplicity. Moreover it has been proved in a previous study that the use of hybrid membrane/amine processes could be more economical than conventional absorption processes [7,8].

So the CO_2 related membrane research activity has been oriented on the fabrication and operative characterization of innovative performing polymer based materials to be used in gas separation systems. High attention has been dedicated to the study and characterization of polyimides, which, having superior thermal and chemical resistance, have been intensively studied as gas separation membranes due to their high selectivity [9]. In particular in a membrane separation process, it is important to have a membrane that guarantees high flux of the more permeable component and high separation factor that correspond to high values of permeability and selectivity, respectively. It is well known, however, that it is difficult to

obtain materials that combine high permeability and selectivity. Indeed, given a certain value of permeability, there is a maximum selectivity that can be achieved with polymeric membranes, and vice versa, according to an upper bound drawn by Robeson using the data of all the polymeric materials known in the literature [10,11]. Usually, due to their rigid structure, glassy polymers and in particular polyimides show good mechanical properties, thermal and chemical resistance but modest permeability [9]. On the contrary, high permeability values can be observed in many rubbery polymers due to the flexibility of polymeric chains, which however have lower thermo-chemical resistance.

According to the previous considerations, therefore, a possible solution is the design of copolymers formed by rubbery and glassy domains, in which the properties can be optimized by a careful choice of the type and amount of different monomers.

In this thesis study attention will be focused on the characterization of two series of co(polyether-imide)s. These materials are block copolymers formed by two segregated phases, a glassy phase and a rubbery phase: the first one is a polyimide with rigid structure and mechanical resistance, and the second one is made of polyether flexible chains which can guarantee high CO_2 permeability [12,13], due to their mobile structure but also to a high affinity with CO_2. In particular, the materials studied in this work are two series of copolymers characterized by a different couple of polyimide and polyether segments, which have been synthetized by research group of the *Instituto de Ciencia y Tecnología de Polímeros,* CSIC in Madrid, in collaboration with the University of Valladolid. The first set of materials is made by 3,3',4,4′-bypheniltetracarboxyilic dianhydride (BPDA), 4,4'-oxydianiline (ODA) and bis(2-aminopropyl) poly (propylene oxide) (PPO) with nominal molecular weight of 4000 g/mol. (BPDA-PPO4000-ODA) [12] The second set of copolymers is made by 3',4,4'- Benzophenone tetracarboxylic dianhydride (BKDA), 4-4'

oxydianiline (ODA) and α,ω-Diamine poly(ethylene oxide) (PEO) with nominal molecular weight of 6000 g/mol (BKDA-PEO6000-ODA) [13].

Another class of materials which has attracted research attention after their synthesis is represented by high free volume glassy polymers such as poly(1-trimethylsilyl-1-propyne) (PTMSP), synthetized by Masuda in 1983 [14], amorphous Teflon AF1600 and AF2400, synthetized by DuPont [15]. The performance of high free volume glassy polymers lies very close to the upper bound for several gas couples, in the region characterized by high permeability and medium-low selectivity. However, the majority of such glassy membranes shows physical ageing, that is a reduction of free volume and gas permeability with time. Such phenomenon is due to the rearrangement of polymeric chains aimed at the reduction of the non-equilibrium excess free volume. The ageing process thus arises from the non-equilibrium state of glassy systems, and can hardly be reduced or hindered without sacrificing gas permeability: for such reason, high free volume glassy polymers are not yet applied in real separation processes [16–19]. In this work, in collaboration with the company *GNext* in Bologna, the effect of the addition of graphene (G) and graphene oxide (GO) nanoplatelets on the gas permeability, selectivity and ageing of PTMSP will be investigated. The amount of platelets added was deliberately small (<1wt%), in order to have a small impact on the cost of such membranes, and to avoid filler precipitation or agglomeration. It is indeed known that, for real gas separation applications, the membranes must be obtained in the form of very thin films (1 μm and lower) and that the presence of clusters of fillers of similar size can cause defects. Moreover we will study the effect of different preparation protocols on the final gas transport properties, as it is well known that graphene-based composites have a strong dependence on the preparation route, and extend the analysis also to thin samples of the order of a few microns, in order to monitor the ageing in conditions closer to real applications.

Furthermore, the last class of materials taken in consideration is represented by facilitated transport membranes, produced and characterized in collaboration with the *Department of Industrial Engineering*, at the University of Padova. In this kind of materials the addition of chemical functionalization groups, which can selectively react with CO_2, leads to enhancement of transport properties, both in terms of permeability and selectivity, with the capability to overcome the Robeson upperbound. Many polymers have been functionalized and also Polyacrylonitrile [20]. Polyacrylonitrile (PAN) is an important polymer which has many desirable properties and active nitrile groups present in it allow for the introduction of new functional groups by specific reactions [20]. In this work we will focus the attention on the experimental fabrication and preliminary characterization of Polyacryolonitrile functionalized membranes. The target is to obtain nanofibers by electrospinning of functionalized PAN, which can be used directly as sorbent materials or can be pressed to compact the structure, and be used in gas permeation systems. Moreover different functionalization routes with hexamethylene diamine, ethylene diamine and PAN basic hydrolysis will be analyzed and materials will be characterized for CO_2 separation purpose.

1. State of the art: Membrane separation for CO_2 capture

CO_2 capture is emerging as an essential and crucial point in many industrial application. As first it is necessary to remove carbon dioxide from natural gas (NG) streams for two main reasons: increasing calorific value and prevent pipe corrosion in presence of water during NG transportation, reaching American standard of maximum CO_2 content of 2 mol% [1–7]. CO_2 is contained in relevant amount also in syn gas produced with biomass gasification and sequent water gas shift reaction to convert CO to CO_2 [21]. Biogas upgrading represent an important field to develop and apply CO_2 capture technology. It is reported that CO_2 concentration after microbial anaerobic digester is around 25-50% [22,23]. Last but not least it has to be remind CO_2 removal from flue gas where concentration of CO2 is around 15 vol% in coal fired power plants and 4 vol% in natural gas based power plants [1–3]. For each of these applications it has been widely documented that gas separation processes with polymeric membranes can compete with traditional and commercially available technologies [7,8,24,25].

The removal of CO_2 from gaseous stream, i.e. flue gases, natural gas, can be performed by absorption, adsorption, cryogenic separation or membrane based separation. In the following a brief description of each technology will be presented with particular emphasis to the reasons which move the attention to polymeric membranes.

CO_2 capture is usually performed by absorption with amine solutions. In particular two columns are implemented and, in the first one, the gas stream, at a pressure generally higher than atmospheric, and the solvent stream flow countercurrent to each other. In such a way the

liquid absorbs acid component like CO_2 and H_2S, heavier hydrocarbons and water and is removed from the bottom of the column. From the bottom, the liquid is heated and is sent to the stripping column, operated at lower pressure, so that heat and low pressure condition favors the removal of absorbed compounds, which leave the column from the top, while the regenerated solvent is recirculated to the first absorption column. Absorption is a well accepted technology; however the height of the column is proportional to the mass of component which has to be absorbed. For instance natural gas sweetening requires the removal of 10%-20% of the total gas stream, which requires large amounts of absorbent solvent in large towers [8]. Moreover the need to heat and cool down fluids requires well monitored operative procedures and, in addition, corrosion is a critical issue. Amines are the most common fluids for acid gas scrubbing, but their degradation leads to the formation of corrosive mixture which can destroy the system in short time [4–7]. Thus it is evident the importance and the necessity of constant monitoring of the plant, which limits the use of absorption technology in remote locations. The cost of absorption process is composed as usual by capital cost, connected to the cost of the two columns, heat exchangers, pumps and operative costs, mainly due to pumping work, vapor utility and solvent make up.

An alternative to absorption is represented by adsorption in solid porous media. With adsorption, gas separation is achieved thanks to the different sorption capacity of gaseous components in the solid material. Together with good mechanical properties, a promising adsorbent should possess high selectivity, good adsorption kinetics, regenerability, thermal resistance, high surface area and pore size to allow adsorbed molecules to entry the internal disposable surface [26]. On industrial point Active Carbons (AC) and Zeolites have been used in fixed bed columns, in which the gas stream is fed to the filter, CO_2 is adsorbed on the adsorbent bed and, from the top of the column, the purified gas is obtained. Once the break-through limit is reached the bed has to be regenerated, i.e. the adsorbed component has to be

desorbed by Pressure Swing Adsorption (PSA) or Thermal Swing Adsorption (TSA) [26,27]. In PSA, adsorption is performed at higher pressure than atmospheric one, while desorption is performed at atmospheric pressure. In TSA, the regeneration is achieved by hot air or steam and components are practically stripped from the solid sorbent. In both cases, to achieve continuous removal of CO_2 from the stream, a number of dual columns are necessary, which depends on the time needed for CO_2 to be adsorbed, for regeneration of the exhausted bed, and cooling of the regenerated column. In general, the technical feasibility of the process depends on the adsorption step, while the desorption step should control the economic viability. Strong affinity of the adsorbent for removing undesired components from the gas mixture is essential for an effective adsorption step, but the stronger the affinity, the more difficult is to desorb the gas and the higher energy is consumed in regenerating the bed for reuse in next cycle [28].

A relatively novel capture technology is based on cryogenic removal of carbon dioxide. Two advantages of the cryogenic operation with respect to absorption is that no chemical absorbents are required and that the process can be operated at atmospheric pressure. The main disadvantage is represented by very low temperature to be reached to liquefy CO_2 [1,2,5]. Moreover the water content should be minimal to prevent plugging by ice and unacceptably high pressure drop in the system. In addition, during liquefaction of carbon dioxide, heat transfer coefficient in heat exchangers can dramatically decrease due to the formation of a layer of solid CO_2, which reduce the process efficiency and constrict heat transfer apparatuses to be regenerated at higher temperature, avoiding excessive mechanical stresses of the structures [28].

Membrane based gas separation involves the presence of dense layer of membrane, which can be considered as a selective thin barrier that discriminates the permeation of targeted gases depending on favorable interaction or molecular sieving ability. In general membrane gas

separations are pressure driven processes, thus the driving force for the separation is given by a difference in partial pressure of components in the feed and permeate stream. Usually the feed stream is compressed at a pressure higher than atmospheric pressure and is sent to the permeation module, from which two streams are obtained, the permeate, enriched in the more permeable components, and the retentate, enriched in the less permeable components. In natural gas sweetening it is possible to use the high pressure of the gas well as the driving force of the process, reducing operative costs connected with large volume gas compression. As an alternative if the process stream is near atmospheric pressure, i.e. in flue gas CO_2 separation, the driving force for the process can be created maintaining the feed at atmospheric pressure while the permeate can be processed under vacuum. in membrane processes, different configurations can be considered depending on the desired product and on the purification grade desired. In Figure 1.1 schematic sketches of CO_2 separation from natural gas are reported. With one single stage the loss of methane can be considerable due to not negligible flux of methane through polymeric membranes. With a two stage configuration, methane losses are reduced and achieved by feeding the permeate of the first module to a second module, resulting in a more economically viable solution.

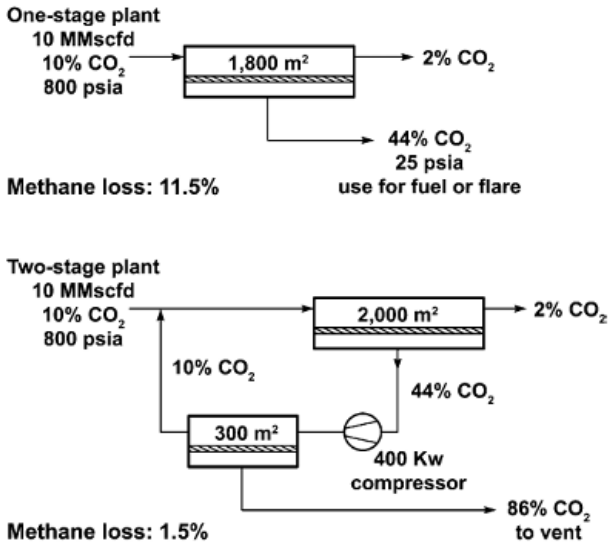

Figure 1.1: Sketch of gas permeation membrane plant configurations.

Currently membranes used for gas separation applications are produced as hollow fibers or flat sheets packaged as spiral-wound modules, as reported in Figure 1.2. Hollow fiber modules, in particular, allow large areas of membrane to be packaged into compact membrane modules. Up to now two thirds of the total market of gas separation involves nitrogen or water separation from air and hydrogen from ammonia purge stream or syngas. These are gas streams relatively clean and free of fouling or plasticizer components, so hollow fiber modules can work well. However growing application areas for membrane separation technology are in natural gas sweetening or refinery and petrochemical plants, where gas streams contain multiple components, such as heavy hydrocarbons, aromatics, CO_2 and H_2S which can degrade and plasticize the membrane. Moreover the gas is typically at high pressure, 30-60 bar, so under these operative conditions flat sheet membranes assembled as spiral wound modules should be preferred. Currently both kinds of modules are produced by different companies as reported in Table 1.1.

Table 1.1: Principal suppliers of Membrane Natural Gas separation systems [8].

Company	Module type	Polymeric material
Medal (Air Liquide)	Hollow Fiber	Polyimide
W. R. Grace	Spiral Wound	Cellulose Acetate
Separex (UOP)	Spiral Wound	Cellulose Acetate
Cynara (Natco)	Hollow Fiber	Cellulose Acetate
ABB/MTR	Spiral Wound	Perfluoro polymers dilicone rubber
Permea (Air Products)	Hollow Fiber	Polysulfone

(a)

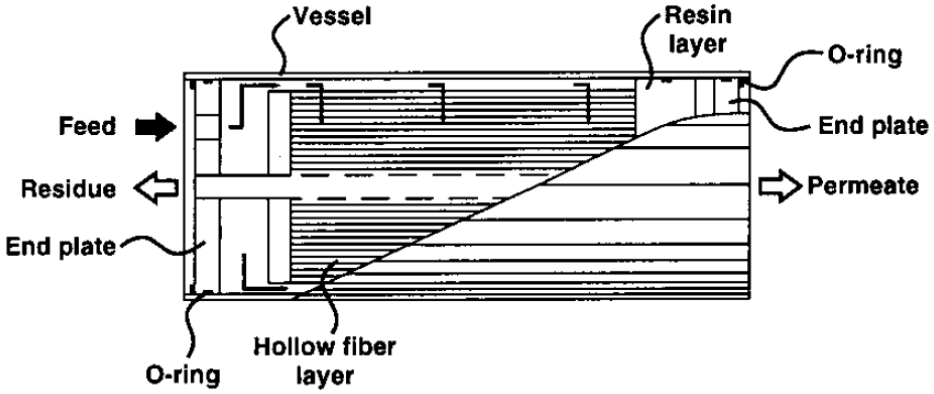

(b)

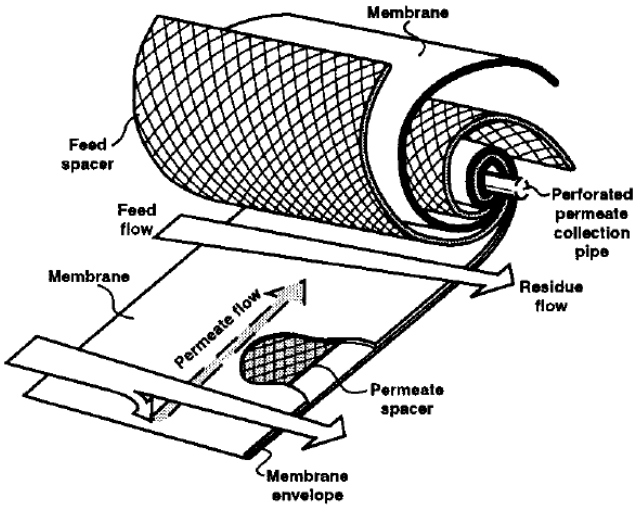

Figure 1.2: Schematic representation of Hollow fibers and Spiral Wound membrane modules [30].

The first membrane system for CO_2 separation from natural gas stream was produced by Grace Membrane System (a division of W. R. Grace), Separex (at now a part of UOP) and Cynara (now part of Natco). These companies used asymmetric cellulose acetate membranes produced according to Loeb-Sourirajan technique. Cellulose acetate is still widely used but

has begun to be challenged by new kind of membranes made in polyimide and perfluoropolymers [7,8].

One of the main trend in commercial membranes is to produce composite membranes instead of asymmetric ones. Asymmetric membranes have typically a dense, thin (0.1÷1 μm), selective layer that performs the separation on a microporous substrate mad in the same material, which provides mechanical support and resistance. However the method used to prepare anisotropic phase inversion membranes limits the number of materials that can be considered to give high performance membranes [7]. For these reasons membranes are increasingly forms as composite structures. Moreover composite membranes contain less than 1 g of selective polymer per square meter of the membrane, on the contrary Loeb-Sourirajan membranes can use 40÷60 g of the selective material per square meter of membrane. In addition new membrane applications require expensive polymers for the selective layer realization, which can cost up to 10÷20 $/g or more and could not be economically fabricated as asymmetric membranes [30]. In Figure 1.3 a schematic representation of asymmetric and composite membrane is reported, taken from [30].

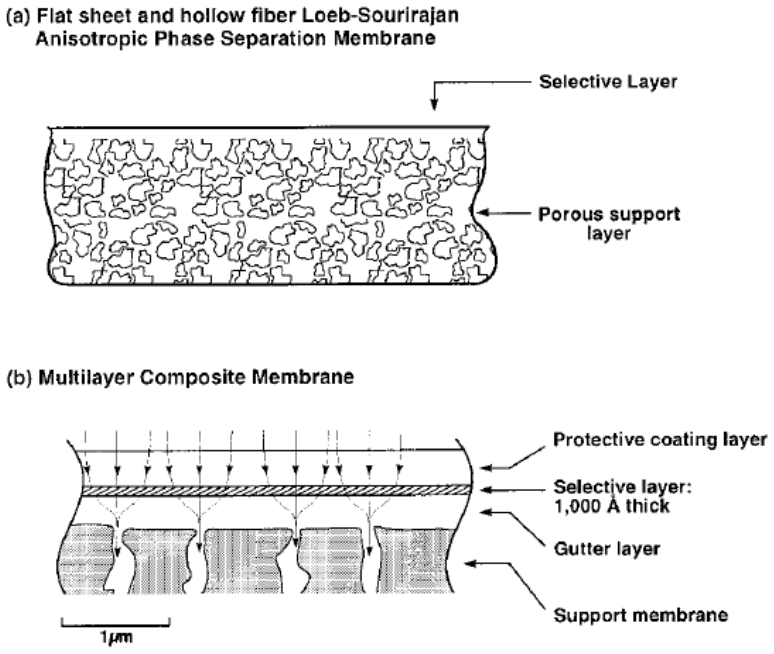

Figure 1.3: Schematic representation of asymmetric membranes (a) and composite membranes (b).

Composite membranes consist of two or more layers of different materials. The support layer is microporous, does not perform any separation and does not any resistance to mass transport, but is mechanically strong, chemically stable and can be made from a number of low cost polymers, such as polypropylene, nylon. The selective layer can be coated directly over the support, but better performing membranes are obtained when a gutter layer made from a highly permeable polymer is used. It also serves to conduct the permeating gases to the pores of the microporous support. Finally a protective layer of 1÷2 μm, of highly permeable polymer, should be deposited over the skin to protect the membrane from chemicals or mechanical abrasion [8,30].

So about the capital cost of the separation process it can be said that the cost of the membrane used is only a small fraction, around 4%, of the final membrane skid cost, which is attested to be around 500 $/m^2 of membrane. High skid costs arise because of many pressure vessels, pipes, flanges and valves required [8].

On a practical point of view it has been reported that membrane systems are conveniently installed for small size natural gas sweetening application, for feed less than 6000 Nm^3/h and remote locations, since amine absorption is too complicated for small productions. In addition membranes results competitive for systems up to 50000 Nm^3/h and also higher, up to 80000 Nm3/h in the case of off-shore platforms [7]. Considering also the fact that there are not moving equipments, except for compressors, and complex control schemes, membrane processes offer a simple and low maintenance process option. In definitive membrane gas separations represent advantages for off-shore industry and membrane technology is an environmentally friendly alternative to traditional amine absorption, because of no requirements for phase change or chemical additives.

In addition Favre et al. [6] provided a comparison between polymeric dense membranes and amine absorption in post-combustion CO_2 capture. They observed that the energy requirement

for membrane processes is connected to CO_2 concentration in the flue gas. In particular for separating a mixture containing 10% of carbon dioxide, the energy consumption is higher than that of absorption. However for concentration of CO_2 higher than 20% the energy requirement is comparable or even lower than that of absorption.

Moreover it has to be considered that membrane processes can be very easily expanded, since it only requires the addition of identical modules and it is not necessary to predict the possible expansion during the design step. On the contrary, cryogenic units can not be expanded if it is not foreseen during the design, while absorption can be expanded, but it requires additional design considerations and calculations [29].

Furthermore, it has been demonstrated that integrated processes such as amine scrubbing followed by membrane gas separation modules can achieve higher CO_2 removal efficiency and can represent higher economically solutions [7,8]. In addition membrane separation technology should be preferred in those applications, in which for logistic issues, it is necessary to operate with simplified and compacted plants.

1.1 Theoretical background

Dense polymeric membranes are commonly considered for membrane based gas separation application, because of their structural, conformational and sorption properties, they are able to separate mixtures of gaseous compound. Two main quantities have to be considered regarding dense membrane for gas separation: the permeability, which is related to process productivity and the selectivity which is related to membrane separation ability.

Membrane gas separation is a pressure-driven process and the permeability of a gaseous species *i* is defined as follow:

$$P_i = \frac{J_i \cdot l}{p_i^{up} - p_i^{down}} \tag{1.1}$$

In equation 1.1 J_i is the diffusive flux through the membrane, l is the membrane thickness and $\left(p_i^{up} - p_i^{down}\right)$ is the partial pressure difference of the component i across upstream and downstream side of the membrane. So the permeability of a gas is defined as its flux divided by its partial pressure gradient across the membrane.

Many units can be considered to report permeability data but the most used is the Barrer

$$1Barrer = 10^{-10} \frac{cm^3(STP) \cdot cm}{cm^2 \cdot cmHg \cdot s} \tag{1.2}$$

The transport of light gaseous species in dense polymeric membranes can be described by the solution-diffusion mechanism, illustrated in Figure 1.4, which assumes that permeating species dissolve in membrane and diffuse through it. On a practical point of view the permeation can be summarized as the sequence of three steps: (i) the sorption of the interest gas on the upstream side of the membrane, (ii) the diffusion of the gas inside the membrane, (iii) the desorption of the gas in the downstream side of the membrane.

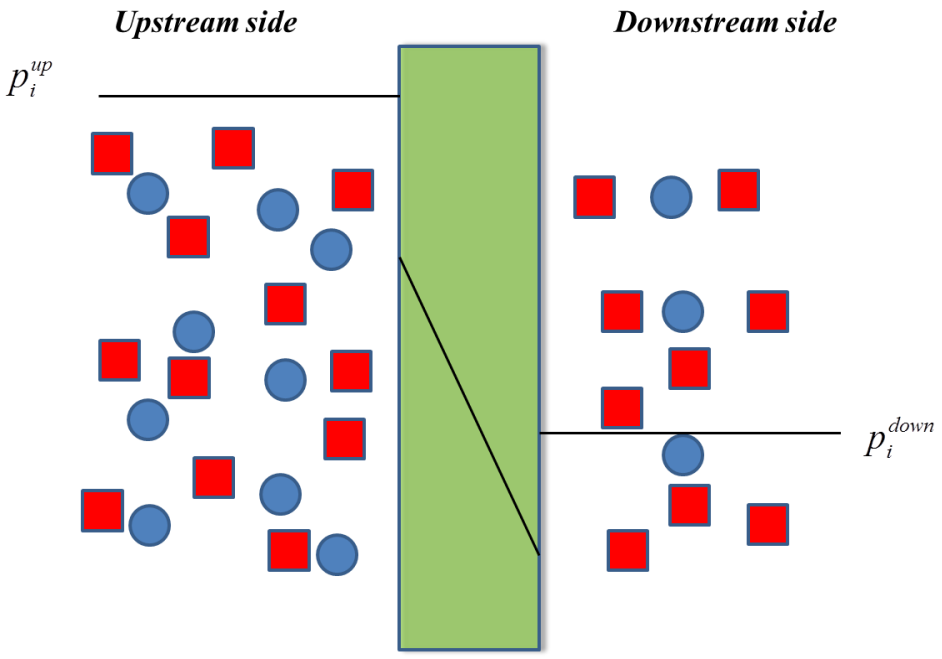

Figure 1.4: Illustration of solution-diffusion tansport mechanism.

The dissolution of the gas is usually described by Henry low as reported in equation 1.3 which substituted in Fick law, generalized for unidirectional transport, reported in equation 1.4, results in solution-diffusion model, as reported in equation 1.5. In these equations S_i is the solubility coefficient and D_i is the diffusion coefficient.

$$c_i = S_i \cdot p_i \tag{1.3}$$

$$J_i = D_i \frac{c_i^{up} - c_i^{down}}{l} \tag{1.4}$$

$$J_i = D_i \cdot S_i \frac{p_i^{up} - p_i^{down}}{l} \tag{1.5}$$

Comparing equation 1.1 and 1.4, it is possible to observe that the permeability can be calculated as the product of a kinetic factor D_i, and a thermodynamic one, S_i, as reported in equation 1.6.

$$P_i = D_i \cdot S_i \tag{1.6}$$

Diffusivity is a kinetic parameter which indicates the mobility of molecules thorough polymeric chains and thus it depends mainly on temperature, polymer free volume and gas molecules size. Solubility is a thermodynamic parameter which gives information about the sorption uptake of the gas in the polymer and is mainly affected by temperature and penetrant condensability, the latter connected to penetrant critical temperature.

Diffusivity dependence on temperature can be well described by Arrenhius type equation, while solubility by Van't Hoff equation reported as follow in equations 1.7 and 1.8, in which E_D is the diffusion activation energy and $\Delta\tilde{H}_S$ is the sorption enthalpy, *R* is the universal gas constant and *T* is the temperature:

$$\left(\frac{\partial \ln D}{\partial (1/T)}\right)_{c_i} = -\frac{E_D}{R} \tag{1.7}$$

$$\left(\frac{\partial \ln S}{\partial (1/T)}\right)_{c_i} = -\frac{\Delta \tilde{H}_S}{R} \tag{1.8}$$

Generally E_D is positive because diffusion is an activated process, while ΔH_S is a negative number because of exothermicity of sorption. As a consequence of solution-diffusion model, permeability dependence on temperature can be expressed with equation 1.9, in which E_P is the activation energy for permeation and, usually, it is positive in number, leading to permeability increase with temperature:

$$\left(\frac{\partial \ln P}{\partial (1/T)}\right)_{p_i} = -\frac{E_P}{R} = -\frac{E_D + \Delta H_S}{R} \tag{1.9}$$

The separation factor for membranes application is usually named selectivity and represents the efficiency of the separation offered by the material. In general it depends on components permeabilities and partial pressures in the feed and permeate side, but in the limit of negligible pressure in the permeate side it can be calculated as the ratio of component permeability as follow:

$$\alpha_{i/j} = \frac{y_i^{up} / y_i^{down}}{y_j^{up} / y_j^{down}} \underset{p^{down} \to 0}{\approx} \frac{P_i}{P_j} = \frac{D_i \cdot S_i}{D_j \cdot S_j} = \alpha_D \alpha_S \tag{1.10}$$

Moreover from the application of solution-diffusion model the selectivity can be decoupled in two terms: diffusivity selectivity, α_D, and solubility selectivity, α_S, and depending on the material the first or the latter can be predominant. Diffusivity selectivity is strongly influenced by the size difference between the penetrant molecules and the size-sieving ability of the polymer matrix, whereas solubility selectivity is controlled by the relative condensability of the penetrants and the relative affinity between the penetrants and the polymer matrix.

It has to be remind that rigorously in equation 1.10 the permeability should come from mixed gas state, but to have an indication of the separation performance one can consider the ideal selectivity which refers to pure gases measurements as follow:

$$\alpha_{i/j}^{IDEAL} = \frac{P_{i,pure}}{P_{j,pure}} \tag{1.11}$$

It is well known that a trade-off exists between selectivity and permeability and in particular that an increase of permeability is usually accompanied by a decrease of selectivity, and vice versa. This permeability-selectivity trade-off was demonstrated and revised by Robeson, respectively in 1991 [10] and 2008 [11], who analysed a wide number of polymers and observed that the permeability of the more permeable gas is related to the gas pair selectivity by the following empirical law:

$$P_i = k\alpha_{i/j}^{n} \tag{1.12}$$

In Figure 1.5 trade-off curve is reported for gas pair CO_2/CH_4, in which it can be observed only a modest shift of the upperbound from 1991 to 2008 one.

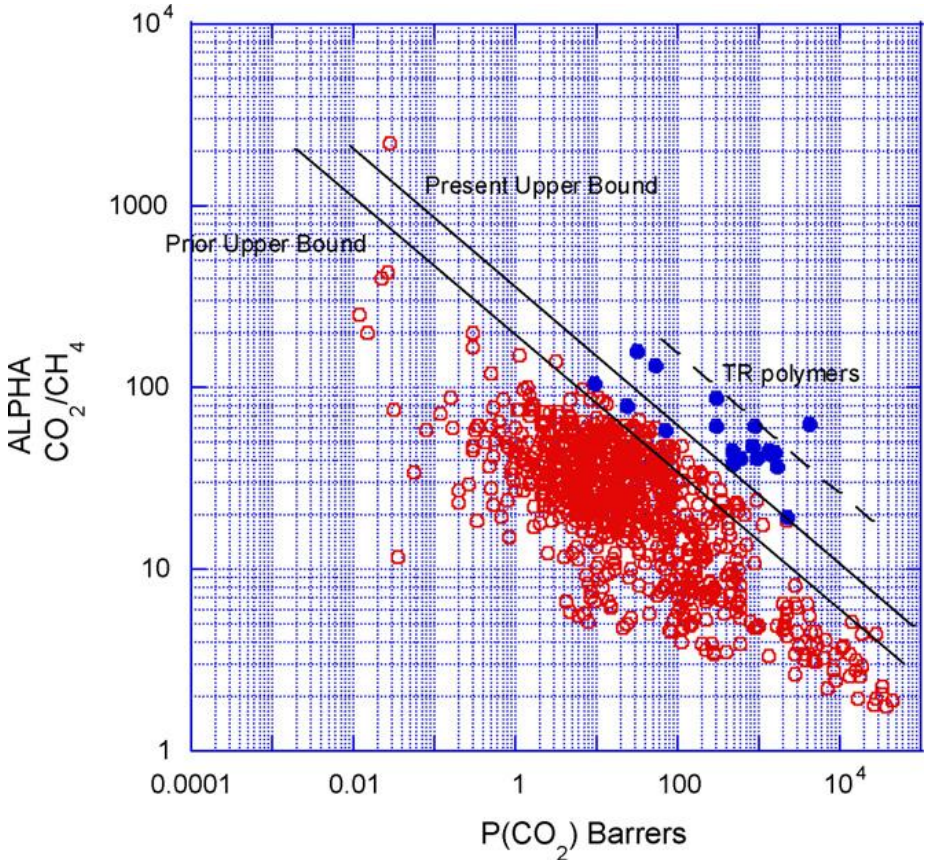

Figure 1.5: Robeson plot for the gas couple CO_2/CH_4, taken from ref [10].

It was observed that a linear relationship exists between $-1/n$ and the difference of the gas molecular diameters ($d_j - d_i$). This observation revealed that the diffusion coefficient governed the upper bound limits [11].

At now while many materials have surpassed the upperbound of 1991, only few materials have been surpassed the revised bound of 2008 and some of them are thermally rearranged polymers, polymers of intrinsic microporosity, facilitated transport membranes. One of the challenge nowadays in membrane gas separation research is to overcome Robeson upperbound to demonstrate the superiority of the transport properties of the synthetized materials.

1.2 Trends on CO_2 separation membranes

A large number of polymeric materials has been investigated and developed for gas separations, but the number of polymers used in commericial systems is still limited and the main rubbery and glassy polymers used are reported in Table 1.2.

Table 1.2: Most important glassy and rubbery polymers used in industrial membrane separation [7].

Rubbery polymers	Glassy polymers
- Poly(dimethylsiloxane) - Ethylene oxide/propylene oxide – amide copolymes	- Cellulose acetate - Polycarbonates - Polyimides - Poly(phenyleneoxide) - Polysulfone

Almost all industrial gas separation systems utilize glassy polymers because of high selectivity and mechanical properties. In the last years high interest has been concentrated on glassy polyimides [31–36], which have high separation performances together with high

chemical, thermal and mechanical resistance. The most interesting polyimides are heterocyclic aromatic polyimides, which have very high mechanical and physical properties. Their selectivity is conferred by high rigidity due to high intermolecular bond between carbonyl groups, nitrogen atom, and aromatic elements in the chain which give strong constraints to chain mobility. Even if they are very stable, due to very high glass transition temperatures, some of them tend to relax in presence of carbon dioxide or other plasticizing components.

Recently Thermally Rearranged polymers, TR polymers, have been studied as membrane materials [37–41]. They are aromatic polymers with heterocyclic rings prepared by thermal conversion of polyimides with ortho-functional groups [39]. TR polymers have aromatic structure with rigid polymeric backbone and have not processability. However, the precursor polymer is an aromatic polyimide, which is used in many industrial applications, can be processed, and so it is easy to form TR polymers into any shape such as flat sheet films or hollow fibers [32]. CO_2 permeability in TR materials is enhanced by more than two orders of magnitude over that of the precursor polymer and typical glassy polymers. In addition separation properties can be controlled by the degree of thermal rearrangement, which is determined by thermal treatment conditions.

Polyacetilene-based polymers have been studied extensively for gas and vapor separation applications [42–50]. These amorphous glassy materials are characterized by very high glass transition temperature, usually higher than 200°C, low density and very high gas permeability. In particular poly(1-trimethylsylil-1-propyne), PTMSP, has the highest gas permeability of all known polymers, which results from its high excess free volume and interconnectivity of free volume elements. Its very open structure leads the separation to be governed by solubility selectivity.

Another interesting high free volume glassy polymer is amorphous Teflon AF2400, which possesses many advantages as membrane material, including chemical stability and low susceptibility to swelling [15]. Together with Teflon AF1600, Teflon AF2400 is the most permeable perfluoropolymer with CO_2 permeability of 3900 Barrer and CO_2/CH_4 ideal selectivity around 7. Moreover unusually low hydrocarbon vapor sorption has been shown, due to unfavorable interaction between hydrocarbon and fluorocarbon polymers [7].

Polymers of intrinsic microporosity [51], PIMs, have been recently synthetized by Mc Keown et al. These materials are obtained by forming a backbone that has no conformational freedom but is sufficiently contorted to prevent an effective packing. In suh a way they show high surface area per unit volume similar to inorganic porous materials and high thermal resistance. Differently from conventional non soluble microporous materials, they have good solubility in common solvents and easy processability. PIM polymers have shown to be selective towards CO_2 with very high permeability, around 1000 Barrer, that locate their performances separation very close to the Robeson upperbound.

Many interesting physical and separation properties have been observed for different glassy materials, as aforementioned, but typical critical issues encountered with glassy membranes are CO_2 induced plasticization and physical ageing.

1.3 CO_2 induced plasticization

In CO_2 membrane separation, it is well known that CO_2 acts as a plasticizer [52–55]. On a practical point of view, plasticization of the polymer occurs when the CO_2 concentration is high enough to swell the material and increase the segmental chain mobility. In general plasticization of glassy polymers is defined as the increase of CO_2 permeability as a function of feed stream pressure and the minimum pressure necessary to induce the permeability increase is called plasticization pressure.

Due to the swelling of the matrix also CH_4, or in general less permeable components, permeations are accelerated and as a consequence the membrane loose its selectivity. So the difference between pure gas membrane selectivity and the selectivity measured with high pressure natural gas is due to membrane plasticization. In addition to CO_2, natural gas contains few percents of heavy hydrocarbons and variable quantities of hydrogen sulfide, which are absorbed by membranes and often have effect on membrane plasticization as carbon dioxide .

Several strategies have been used to overcome membrane plasticization:

- Feed pretreatments, to remove aromatics and heavy hydrocarbons
- Crosslinking, to make the membrane more resistant to plasticization [60–63]
- Use of polymers such as Teflon-like perfluoropolymers which are resistant to plasticization of CO_2, H_2S and hydrocarbons [64].

1.4 Physical ageing

Rubbery polymers are equilibrium structure and they can be theoretically approximate to very viscous liquid.

Imaging to cool down a rubber, measuring its specific volume during the temperature variation, one should obtain the qualitative output reported in Figure 1.6.

Behind the glass transition temperature the slope of the curve specific volume versus temperature decreases indicating that the glassy state is reached. Glassy materials are not equilibrium structures and their properties are strongly dependent on their preparation protocol and time-temperature history. Because of their non-equilibrium state glassy polymers are characterized by excess properties such as enthalpy, entropy and volume. Due to excess free volume with respect to equilibrium they tend to evolve toward the equilibrium with a process known as physical ageing, which leads to properties variation during time [16–18].

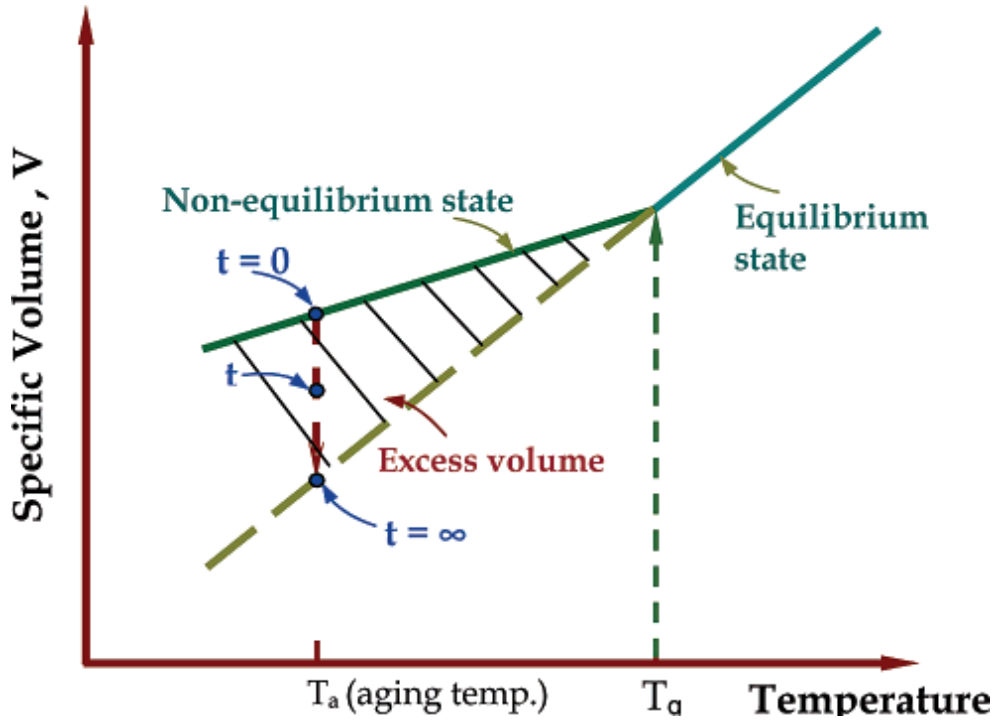

Figure 1.6: Polymers specific volume dependence with temperature and schematic representation of physical ageing, taken from ref [65].

Physical ageing consists in a volume relaxation and densification, which affect those properties that are dependent on free volume such as permeability, enthalpy, brittleness and many other properties. On a practical point of view materials subject to physical ageing could not be used as membranes due to their instability during time, which causes a permeability drop and consequent decrease of expected performances. Nevertheless physical ageing is a thermoreversible process. It means that the thermal treatment of a polymer above its glass transition temperature, lead it to rapidly reach the equilibrium condition and forget any previous history that it could have undergone below T_g [18].

A wide number of studies has been carried out on glassy polymers suitable for gas separation, such as Matrimid®, PSf, PPO, monitoring their ageing on gas permeability measurements and free volume measurements by ellipsometry an observing the effect of thickness on the phenomena. [16,65–68]. What has been observed is that ageing rate is a function of film thickness. In particular for thicknesses in the range of several micrometers up to millimeter scale ageing rate is not a function of film size; this is the case of so called bulk films for

which it is expected that properties are independent on film thickness. For films with thickness in the range from 100 nm up to several micrometers, which is the range of interest for membrane applications, it is possible to observe a dependence of ageing rate with film thickness, and in particular the relaxation rate increases by decreasing the film thickness [16,65]. Also for PTMSP Dorenkoo and Pfromm observed a dependence of ageing with film thickness [19]. At 35°C bulk film with 85 μm thickness did not show a significant decline of He and N_2 permeabilities over 7 days testing, while thin films encountered accelerated ageing, showing for He a decrease of the permeability of 50% and 92% and for N_2 a decrease of 63% 96%, respectively for 1 and 3 μm thick samples [19]. On a general point of view it can be assumed that during physical ageing holes and vacancies diffuses through the surface of the sample and escape from them. So it can be regarded as a diffusive process in which the driving force is the gradient of time and special dependent free volume. This assumption is validated by the ageing rate linear correlation with t / l^2 [16].

As polymer free volume decreases during physical aging, the permeability of larger gas molecules declines more rapidly than that of smaller ones. Thus, the relative permeability decline of CH_4 will be greater than that of CO_2 (since CH_4 is the larger molecule), and an increase of CO_2/CH_4 selectivity will be observed as the polymer ages. Furthermore, usually, physical ageing leads polymer performances moving parallel to Robeson upperbound and, consisting to this, a decrease in permeability is followed by increase of selectivity.

1.5 Materials studied in this work

1.5.1 Copoly(ether imides)

As said in introductive section, glassy polyimides represent an important class of material tested for gas separation. Unlikely due to their glassy state at room temperature, as reported by many authors [16,65–68], they are affected by physical ageing, which makes them less

attractive for membrane separation systems. In addition polyimides are sensitive to plasticization, which leads to increase of permeability but a rapid decrease of process selectivity [69]. Moreover polyimides are hydrophobic or weakly hydrophilic [9]. On a practical point, it is well known that condensable components, in particular water, present in the gaseous mixture, undergo competitive sorption with CO_2 in hydrophobic membrane. The higher condensability promotes H_2O in the competition with other penetrants for sorption in the microvoids of the material. The CO_2 and CH_4 permeabilities are reported to decrease up to 60% in 6FDA-TMPDA and Matrimid polyimides increasing the water activity of the feed stream [70]. Ansaloni et al. [71] extensively studied the effect of water on the permeation of He, N_2, CH_4 and CO_2 in Matrimid®, observing that permeabilities decrease in the same way for all gases up to 50% at 75% R.H. with respect to dry condition. It can be hypothesized that the decrease in permeability with R.H. can be due to the partial occupation of polymer free volume with consequent reduction of diffusive pathways for gas molecules, as confirmed by modeling analysis [71].

Finally it has to be reminded that polyimides, because of tunable free cavities, possesses extraordinary ability to separate complex mixture of gases in many application. Usually these materials have high selectivity to CO_2 but do not exhibit sufficiently high permeability [9]. In order to increase permeability without compromising permselectivity, an approach may be the introduction of CO_2-phylic moieties able to interact with the targeted gas [12,13,72].

Okamoto et al. [73], synthetized PEO containing poly(ether imide) copolymers with microphase-separated structures, consisting of microdomains of rubbery polyether segments and of glassy polyimide segments. It was observed that the permeation occurred through PEO domains while the glassy phase contributed to film formation and mechanical properties [73]. In these materials high CO_2 solubility in the polyether phase guaranteed high separation performance both in terms of productivity and separation efficiency. In particular for different

polyimides considered, both CO_2 permeability and CO_2/N_2 selectivity increased by increasing PEO content in the copolymers, which guaranteed solubility selectivity to materials predominant to diffusivity selectivity. Moreover increasing the polyether chain length it was observed an increasing CO_2 permeability, because of higher phase segregation in the membranes.

After the work of Okamoto, many researchers have intensively investigated PEO-containing poly(ether imide) copolymers membranes for CO_2 separation applications. In recent years Tena et al. [13] have found direct relationship between permeability and phase segregation, which increases with thermal treatment of copolymers. It has been observed that permeability increases when polyether content increases in the material, without substantial effect on ideal permselectivity, and similar results have been obtained also for copoly(ether imides) obtained from BPDA-ODA and polypropyleneoxide [12]. Another positive aspect is the relative low temperature necessary for the complete imidization of copolymers, compared with high temperatures, above 300°C, to achieve complete imidization of polyimides. Finally these copoly(ether imides) result CO_2 selective due to high affinity of polyether with carbon dioxide, which guarantee high solubility selectivity.

Moreover the incorporation of rubbery phase into glassy phase may be a way to reduce or avoid physical ageing. Furthermore the presence of highly hydrophilic domains, such as PEO or PPO, inside the glassy matrix may be able to give better behavior during humid gas permeation, which is a real aspect to face in membrane based gas separation.

1.5.2 Mixed Matrix Membranes

The performance of polymeric membranes can be improved by incorporating inorganic fillers to form Mixed Matrix Membranes, MMMs [74–88]. In MMMs it is important to use as small as possible particle to yield more polymer/particle interfacial area and potentially improve membrane separation performance through affecting polymers chain packing and molecular

transport. Moreover the use of nano-sized particle is necessary during thin film fabrication. Another important aspect is to avoid filler agglomeration caused by sedimentation, which could cause inhomogeneity during filled membrane formation.

Both porous permeable and dense impermeable fillers have been used to improve membranes gas separation performances. Porous micrometric inorganic fillers endowed with high permselectivity can be employed for this purpose, as it was verified for instance by adding carbon molecular sieves to commercial polyimides [76]. In most cases inorganic fillers have superior selective properties than polymeric matrices and so incorporation of small amount of them inside the organic phase can result in a significant enhancement of the separation factor. Recently Metal Organic Frameworks have been employed in MMMs fabrication. Up to 20% of IRMOF-1 was dispersed in Matrimid® and Ultem® observing up to 3 fold improvements in CO_2 permeability without significant loss of selectivity [89]. After this first successful result many other MOFs, such as HKUST-1, due to its zeolite-like structure, have been considered for CO_2/CH_4, CO_2/N_2 due to their high sorption capacity and selective behavior toward CO_2 [89].

Contrary to the aforementioned MMMs consisting of porous filler and polymeric matrices, impermeable nanometric fillers can be used to tune separation performances of polymeric membranes. Impermeable, non- porous, nano-size particles, like fumed silica, added to glassy polymers in solution allow to enhance gas permeability and, in some cases, the selectivity [77-88]. Indeed, such nanoparticles seem to reduce the packing and aggregation of polymer chains during film formation, thus enhancing the free volume, as it was confirmed by both experiments and models [84-88]. On the other hand, when silica particles are generated *in situ* in polymeric solutions, the free volume and mass transport coefficients of the composite film are lower than those of the pure polymer, which is exactly opposite to the result obtained when preformed silica nanoparticles are added to the solution [81]. Such behavior was

explained by assuming that, if silica particles are formed after contact with the polymeric solution, rather than before it, the final film is a hybrid organic/inorganic structure, in which polymeric chains and inorganic domains are deeply connected. Such network shows a lower free volume and smaller fluid transport rates than the neat polymer [86]. It is thus evident that some inorganic fillers, although nearly impermeable like fumed silica, when added in solution to glassy polymeric materials can modify the solid microstructure and the separation performance of the resulting membranes.

The discovery of graphene with its combination of extraordinary physical properties, such as thermal and electrical conductivity, and ability to be dispersed in various polymer matrices, has created a new class of polymer nanocomposites [90–92]. Defect free graphene sheets are impermeable to all gas molecules, and so the combination of polymeric membranes with graphene makes possible large scale barrier membranes with mechanical integrity. Recently graphene and graphene oxide sheets have been considered as molecular filters to separate gas molecules [93]. As said before graphene is impermeable, however during graphene deposition over polymeric substrates, irregularly alignment leads to the formation of gas permeable interlayer spacing, which can results in the realization of an ideal membrane in terms of selectivity and permeability. Kim and coworkers prepared ultrathin GO membranes on a polyethersulfone (PES) support membrane, obtaining selective transport of CO_2 over hydrogen, methane and nitrogen [94]. In particular it was observed that selective gas diffusion can be achieved by controlling gas flow pathways and pores. Li et al. showed that structural defects on molecular sieving GO membranes provided highly H_2 permeation over CO_2 and N_2 [95]. So it seems that different fabrication approaches lead to GO membranes with different microstructures and separation properties. Shen et al reported a methodology for fabricating membranes that involves GO assembly in polymeric environment, utilizing favorable interaction between GO and the polymer to provide the stacking of nanosheets into weel

defined GO laminates in which the interlayer spaces could provide molecular sieving channels [96]. The polymer considered was commercial PEBAX and they observed that membranes allowed fastest transport of CO_2 and very low permeation of other gases like methane and nitrogen. In particular GO was considered to create a large number of cavities and in addition the interlayer spacing of the GO laminates was approximately 0.35 nm which allows a cut-off in permeation of molecules with kinetic diameter greater than this value, i.e. N_2 and CH_4. The CO_2 permeability reached 100 Barrer and CO_2/N_2 selectivity was 91, breaking the permeability/selectivity trade-off relation in polymeric membranes. Recently Li et al, considered the combination of carbon nanotubes, CNTs, and GO nanosheets in commercial polyimide Matrimid [97]. It was observed that mixed matrix membranes showed higher T_g with respect to pure polymer, due to filler polymer interfacial interactions and polymer chain rigidification. In particular an optimal formulation was for 5% of GO and 5% of CNTs content which lead to an increase of free volume cavity size due to disruption of polymer chain packing and thus to enhancement in CO_2 permselectivity. Similarly the addition of GO in a commericial polyimide BPDA-ODA, influenced transport properties, depending on the total amount of nanofiller in the polymer matrix [98]. The optimal formulation resulted to be 1% wt. with simultaneous maximization of CO_2 permeability and CO_2/N_2 selectivity.

It is reasonable to expect that the addition of filler also affects the ageing kinetics of glassy membranes, that is ultimately related to their relaxation time. Some studies indeed evaluated the reduction of ageing obtained by adding functionalized carbon nanotubes to a high free volume structure such as the polymer of intrinsic microporosity (PIM-1) [99], or by adding microparticles of porous aromatic frameworks (PAF) to different glassy polymers [100]. Kelman et al. found that the addition of 10wt% polysiloxysilsesquioxanes (POSS) nanoparticles reduces the ageing of poly(trimethyl silyl propyne) (PTMSP), evaluated in

terms of loss of O_2, N_2 and CH_4 permeability over 6 months on thick (100 μm) samples. However, the POSS-filled polymer has much lower gas permeability than pure PTMSP, even after 6 months [101] Matteucci et al. studied the effect of MgO and TiO_2 nanoparticles on the ageing behavior of PTMSP samples through changes of CO_2 permeability over 40 d. They found, in particular, that addition of TiO_2 nanoparticles up to a volume fraction of 20% (corresponding to about 55wt%) reduces the physical ageing of PTMSP, while the same amount of MgO particles does not affect ageing of PTMSP. A fairly large volume fraction (75%) of MgO is required to reduce ageing of PTMSP [102-103].

1.5.3 Facilitated Transport Membranes

Facilitated transport membranes is taking on great importance in membrane based gas separation processes, since Scholander [104] demonstrated oxygen facilitated transport with hemoglobin carriers. Several researchers reported that fixed site carrier membranes are attractive candidate for facilitated transport and show enhanced stability with respect to mobile carriers membranes. Facilitated transport membranes were fabricated and tested by many authors for different applications. Funke et al. [105] immobilized Ag^+ ions in Nafion membrane to separate butane isomers via facilitated diffusion. Fixed amine carriers were incorporated by Huang et al. [106] in poly vinyl alcohol (PVA) and used to increase CO_2/N_2 selectivity up to 170°C. Deng et al. [107] fabricated poly vinyl alcohol (PVA) and polyvinyl amine (PVAm) blends, obtaining CO_2/N_2 separation factor around 174 and CO_2 permeance up to 0.58 $m^3(STP)/m^{-2}\ h^{-1}\ bar^{-1}$, in particular it was observed that PVAm with fixed amino carriers facilitates CO_2 transport while PVA added mechanical strength to the membrane. In these membranes high selectivity and gas permeability can be achieved thanks to the fact that a targeted gas, like CO_2, can permeate selectively by a reversible reaction with carriers, bound covalently to solid polymer, while other gases, like N_2, can permeate only by solution-diffusion mechanism. Moreover the presence of water, due to CO_2 hydration reaction taking

place in water-swollen membrane, should enhance the facilitation effect with respect to dry condition [105–107].

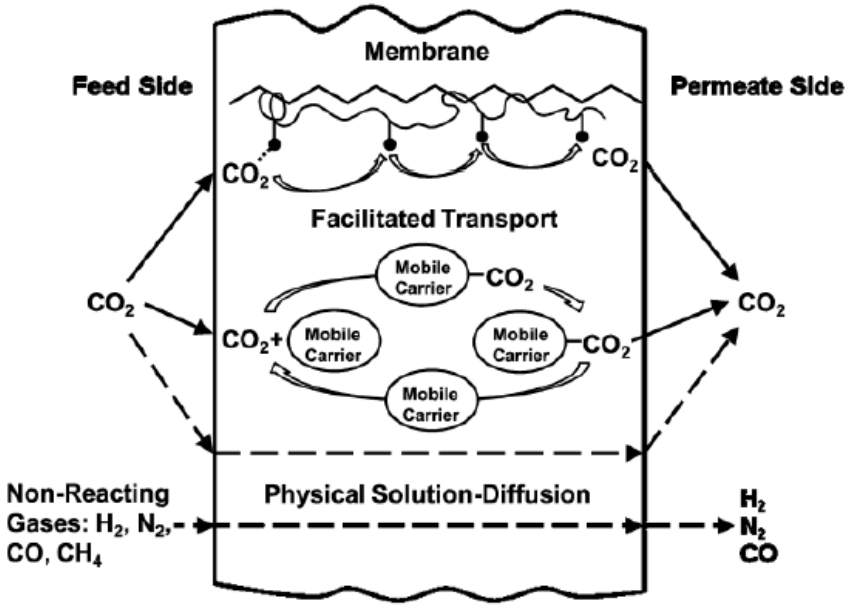

Figure 1.7: Schematic description of CO2 facilitated transport, taken from ref. [60].

The reaction of CO_2 mechanism can be described by the zwitterion mechanism, according to which as firs CO_2 reacts with primary to form zwitterion as an intermediate (eq. 1.13), which is then deprotonated by amines and water to form carbamater ion (eq. 1.14 and eq. 1.15), which can react with water to form bicarbonate (eq. 1.16).

$$CO_2 + RRH'NH \leftrightarrow RR'NH^+COO^- \quad (1.13)$$

$$RR'NH^+COO^- + RR'NH \leftrightarrow RR'NCOO^- + RR'NH_2^+ \quad (1.14)$$

$$RR'NH^+COO^- + H_2O \leftrightarrow RR'NCOO^- + H_3O^+ \quad (1.15)$$

$$RR'NHCOO^- + H_2O \leftrightarrow RR'NH + HCO_3^- \quad (1.16)$$

There are a number of studies investigating the facilitated transport of CO_2 and these studies are oriented on the comprehension of the mechanism of transport and on the evaluation of the technical feasibility of separation processes based on facilitated transport [105–120].

The main target of materials characterization is the evaluation of the facilitation factor, which is defined as the ratio between the total solute flux with facilitation to the solute flux without facilitation. This factor depends on operative conditions like temperature and pressure and has been demonstrated its dependence with membrane thickness [108,109].

Feasibility studies have been conducted about the application of facilitated transport mechanism in natural gas sweetening and CO_2 capture from flue gases. The results have shown that a membrane process using the facilitated transport membrane is feasible, even for low CO_2 concentration (10%) in flue gas, compared to amine absorption in terms of energy requirement and it is possible to achieve more than 90% CO_2 recovery and with a purity in the permeate above 90% CO_2 [119].

Moreover it wìhas been observed that by using the PVAm/PVA blend membrane and the 2-stage recycled process, a CH_4 recovery of 99% at a low running cost could be obtained to upgrade biogas to meet the natural gas network specification, which makes this green process more competitive compared with other conventional technologies currently used. In addition, due to the unique facilitated transport mechanism of this membrane, water vapour saturated in biogas is an advantage rather than a problem to CO_2 permeation, the pre-treatment to remove water vapor is not required [120].

The effect of heavier hydrocarbons and hydrogen sulfide has been studied considering the applicability of facilitated transport membranes based on PVAm/PVA blends in natural gas sweetening [117]. It was observed that hydrogen sulfide reduces membrane performances especially at low humidity, but it does not introduce a permanent damage in the material. Many polymers have been functionalized and also Polyacrylonitrile [20,121]. Polyacrylonitrile (PAN) is an important polymer which has many desirable properties like solvent resistance, abrasion resistance, thermal and mechanical stability, high tensile strength

and posseses good insect resistance [121]. Active nitrile groups present in polyacrylonitrile allow for the introduction of new functional groups by specific reactions [121].

2. Experimental methods

In this chapter a brief description of apparatuses and experimental technique used for the calculation of mass transport properties of gases in polymeric films are reported. In particular, togheter with the description of procedure and equipments used, the mathematics of diffusion process encountered in the different cases will be described.

2.1 Pure gas sorption

The sorption of pure gases has been studied in a self-made pressure decay apparatus, in which the amount of sorbed gas is measured as decay of pressure of the gas phase in a known volume. A sketch of the apparatus used in experiments is reported in Figure 2.1.

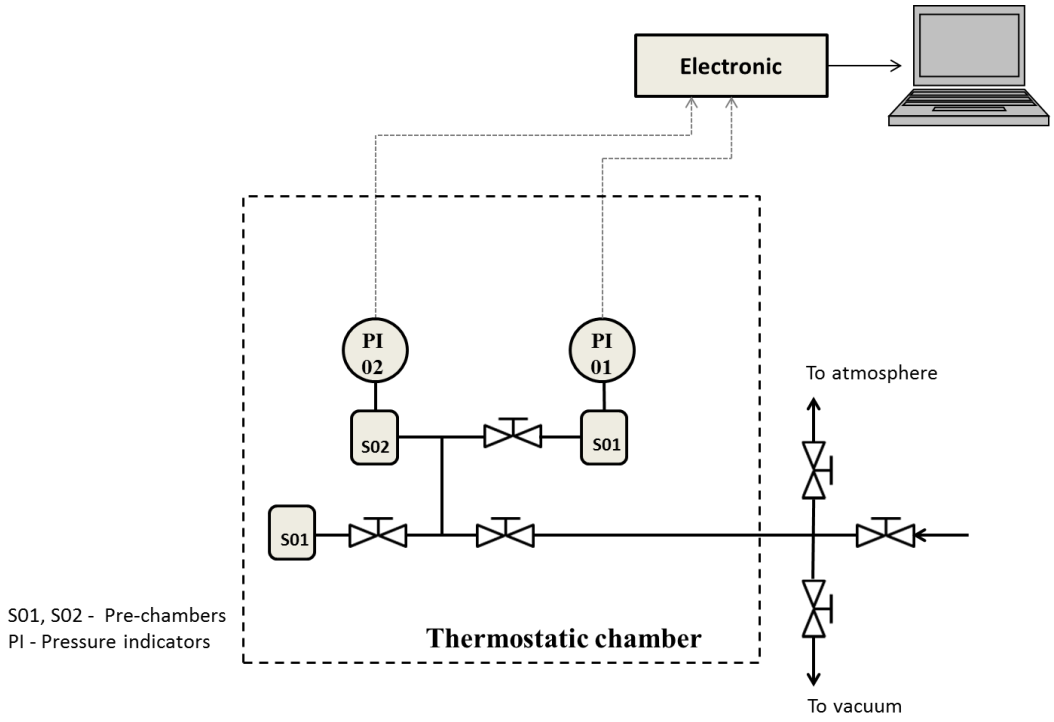

Figure 2.1: Schematic representation of pure gas pressure decay equipment.

The system, contained in a thermostatic air circulating chamber which allows constant temperature with a precision of ±0.01 °C, is characterized by two pre-chambers (S01 and S02), in which the gas is charged at the desired pressure, and a sample chamber (S01) where the polymeric film is set.

In the pre-chamber, two high precision pressure transducers, PI-01 and PI-02 (Honeywell Model STJE), with a declared accuracy ±0.05% of manometer full-scale are connected. During experiments in the range 0-15 bar the manometer with 15 bar full-scale is used, while during experiments in the range 15-30 bar the second manometer with 30 bar full-scale is considered, isolating the other one by means of valve V.

The membrane is set in the pre-chamber, after weighting with an analytical balance with a repeatability of 15 μg (Mettler Toledo Semi Micro Balance Model MS 105). In order to evacuate the apparatus and remove chemical species dissolved in the membrane, the apparatus is connected with a vacuum pump for 1 day.

The test protocol requires to fill the pre-chamber up to a certain pressure with the desired gas and to open the valve between the pre-chamber and sample chamber to start the experiment. Due to gas expansion a step decrease of pressure can be observed, followed by the sorption of penetrant in the film, which causes the pressure decay. Equilibrium or pseudo-equilibrium conditions are proved by the observation of constant pressure with time.

A sufficient number of sorption steps are required to describe accurately the sorption isotherm in the entire pressure range. By the closure of the valve, it is possible to repeat the sorption procedure, increasing the pressure in the pre-chamber for the next differential sorption step.

During each step *i*, Peng Robinson EoS is implemented in an excel sheet to calculate initial moles, n^0, and final moles, n^F, of the penetrant during the experiment, respectively in the pre-chamber and in the total volume formed by pre-chamber, sample chamber and valve,

which are connected to sorbed moles in the membrane, n_i^{sorbed}, by the following material balance:

$$n_i^{sorbed} = n_{i-1}^{sorbed} + n^0 - n^F \tag{2.1}$$

The kinetic of the process can be described by means of a variable boundary condition problem. In particular, as reported by Crank [122], if a plane sheet is suspended in a volume of gas solution so large that the amount of solute taken up by the sheet is a negligible fraction of the whole, and if the solution is well stirred, then the concentration in the solution remains constant. On the contrary, as shown if Figure 2.2, if there is only a limited volume of solution, the concentration of solute in the solution decreases as penetrant starts diffusing into the sheet, and so concentration at membrane surfaces decreases too. If the solution is well stirred the concentration in the solution depends only on time, and is determined essentially by the condition that the total amount of solute in the solution and in the sheet remains constant as diffusion proceeds.

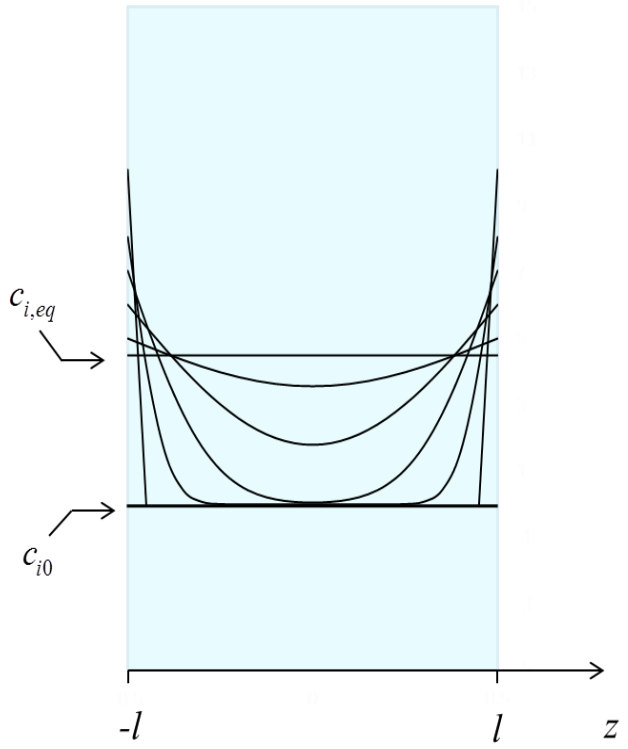

Figure 2.2: Representation of concentration profile with variable boundary condition.

On a mathematical point of view the equation to be solved is the same are reported in the system 2.2, which consist of second Fick Law with proper a initial condition and boundary conditions which express that, at any time, the rate at which the penetrant enters the membrane is the same at which it leaves the solution.

$$\begin{cases} \dfrac{\partial c_i}{\partial t} = D_i \dfrac{\partial^2 c_i}{\partial z^2} \\ t = t_{0,} \qquad c_i = c_{i0,} \qquad\qquad -l < z < +l \\ z = \pm l, \qquad \dfrac{a}{K}\dfrac{\partial c_i}{\partial t} = \mp D_i \dfrac{\partial c_i}{\partial z}, \qquad t > t_0 \end{cases} \tag{2.2}$$

Where *l* is the semithickness of the membrane sheet, *a* is volume of the solution per unit area of the sheet and *K* is the partition coefficient of the species *i* between the solution and the sheet.

The solution was given by Crank [122] by use of Laplace transform and can be written as the ratio of mass sorbed at time t over the mass sorbed at equilibrium according to equation 2.3.

$$\frac{M_t - M_{t_0}}{M_\infty - M_{t_0}} = 1 - \sum_{n=1}^{\infty} \frac{2\alpha(+\alpha)}{1+\alpha+\alpha^2 q_n^2} \exp\left(-\frac{Dq_n^2 t}{l^2}\right) \tag{2.3}$$

where M_{t_0} and M_∞ are the initial and final equilibrium mass uptake in the sorption step respectively, α is the ratio between the volume of gas phase and that of the membrane, corrected for the partition coefficient of gas between the gaseous phase and the polymeric phase and q_n variables are the positive, nonzero, solutions of the equation: $tg(q_n) = -\alpha q_n$.

From the knowledge of kinetic unsteady sorption data it is possible to calculate the diffusion coefficient during the sorption step as best fitting parameter, as reported in Figure 2.3:

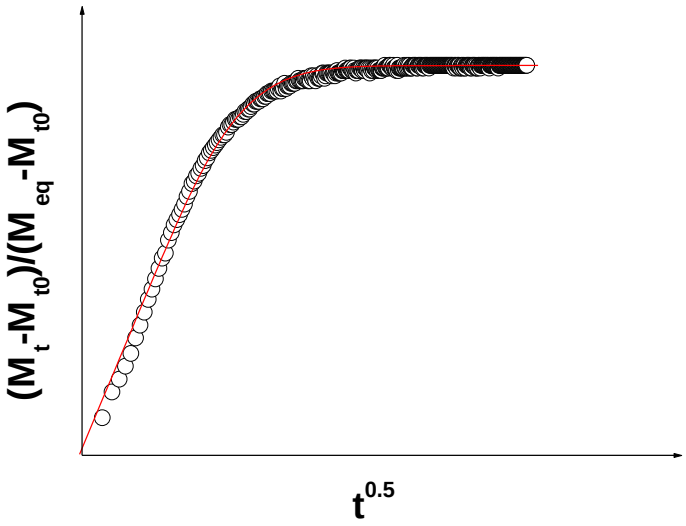

Figure 2.3: Generic kinetic result of a pressure decay sorption experiment.

2.2 Water vapor sorption

Water vapor sorption experiments have been carried out in a quartz spring microbalance (QSM). A sketch of the apparatus is reported in Figure 2.4. The system is characterized by a quartz spring (Deerslayer, sensitivity of 1 mm/mg and maximum hold of 100 mg) housed inside a water jacketed glass column for temperature control, which is connected by means of stainless steel tubing and valves to a vacuum pump (Edwards, Model RV3) and to a water vapor reservoir in which the pressure is measured with a pressure transducer (Edwards Barocell Full Scale 1000 mbar). The deionized water is stored in vapor liquid equilibrium at room temperature in the appropriate reservoir, from which the vapor is withdrawn from the head space to fill the vapor reservoir for the sorption step.

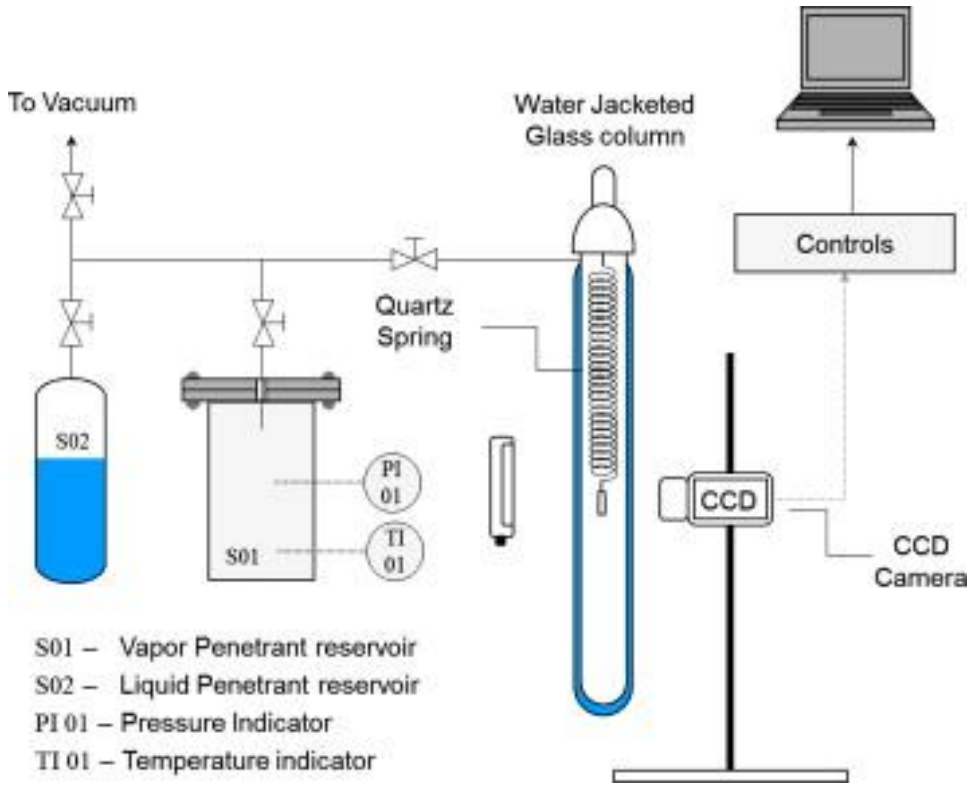

Figure 2.4: Schematic representation of QSM apparatus.

Before starting the test the sample is evacuated for long time, usually 1 day, to ensure the complete removal of penetrants within the polymeric film. Once the polymer can be considered completely dry, the vapor reservoir is filled at the desired pressure, below vapor pressure to prevent water condensation inside the tubes which in addition are wrapped with a heating tape. After the vapor has reached thermal equilibrium at test temperature, confirmed by reservoir pressure invariant with time, the experiment can start and the valve before the column is opened.

The sorption kinetic is monitored through a CCD Camera (Smartimage Sensor Series 600 Model 630) manufactured by DVT Corporation equipped with additional lenses (25 or 35 mm) and some extenders to optimize magnification and focal distance during different experiments. A strobe led array illuminator, model IDRA-6, has been placed behind the glass column to achieve the optimal illumination and the maximum image contrast [123].

Water sorption uptake during time can be calculated according to Hooke law as follow:

$$M(t) = k(x - x_0) + F_b \tag{2.4}$$

Where *k* is the constant of the spring, x and x_0 are current and initial spring extension and F_b is the buoyancy contribution, which is quite negligible in the present study, due to low pressure of water vapor.

The kinetic of the process can be described, imaging to put a flat polymeric sheet in an environment containing a pure gas or vapor at constant temperature and constant pressure, considering that at the interface fluid-membrane a constant value of concentration, $c_{i,eq}$, will be, at least in absence of relaxation phenomena of polymeric matrix with a kinetic comparable to the diffusion process one.

Inside the sample the concentration will vary with respect to spatial and time variables, due to penetrant diffusion, until equilibrium condition will be reached, with spatial and time invariant value of concentration.

On a mathematical point of view the sorption process can be described by applying Fick law, as constitutive equation for the diffusive flux, and solving the partial derivative equation, obtained under reasonable assumption that the transport of the penetrant takes place through the thickness *l* direction, with proper initial and boundary conditions:

$$\begin{cases} \dfrac{\partial c_i}{\partial t} = D_i \dfrac{\partial^2 c_i}{\partial z^2} \\ t = t_0, \quad c_i = c_{i0} \quad 0 < z < l \\ x = 0, \quad c_i = c_{i,eq} \quad t > t_0 \\ x = l, \quad c_i = c_{i,eq} \quad t > t_0 \end{cases} \tag{2.5}$$

The solution of the problem is reported as Fourier series as follow in equation 2.6 [122] and the concentration variation along the thickness is schematically reported in Figure 2.5:

$$\frac{c_i - c_{i0}}{c_{i,eq} - c_{i0}} = 1 + \frac{4}{\pi} \sum_{n=0}^{\infty} \frac{(-1)}{2n+1} \exp^{\frac{-D_i (n+1)^2 \pi^2 t}{l^2}} sen\left(\frac{(n+1)\pi z}{l} \right) \tag{2.6}$$

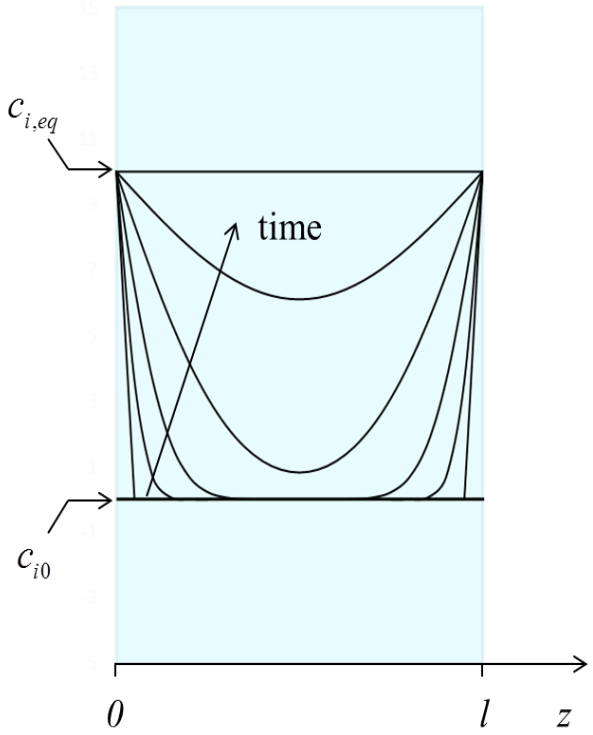

Figure 2.5: Representation of concentration variation in flat sheet with fixed boundary conditions.

From equation 2.6 it is possible to obtain the ratio of sorbed mass at time *t* and the sorbed mass at equilibrium as reported in equation 2.7:

$$\frac{M_t - M_{t_0}}{M_\infty - M_{t_0}} = 1 - \sum_{n=0}^{\infty} \frac{8}{(n+1)^2 \pi^2} \exp^{\frac{-D_i (n+1)^2 \pi^2 t}{l^2}} \tag{2.7}$$

Where M_t, M_{t_0} and M_∞ are respectively sorbed mass at time *t*, time zero and at equilibrium.

2.3 Dry gas permeation

Dry gas permeation experiments have been carried out in a closed volume variable pressure permeometer, kept in a thermostatic chamber to guarantee constant temperature, represented in Figure 2.6.

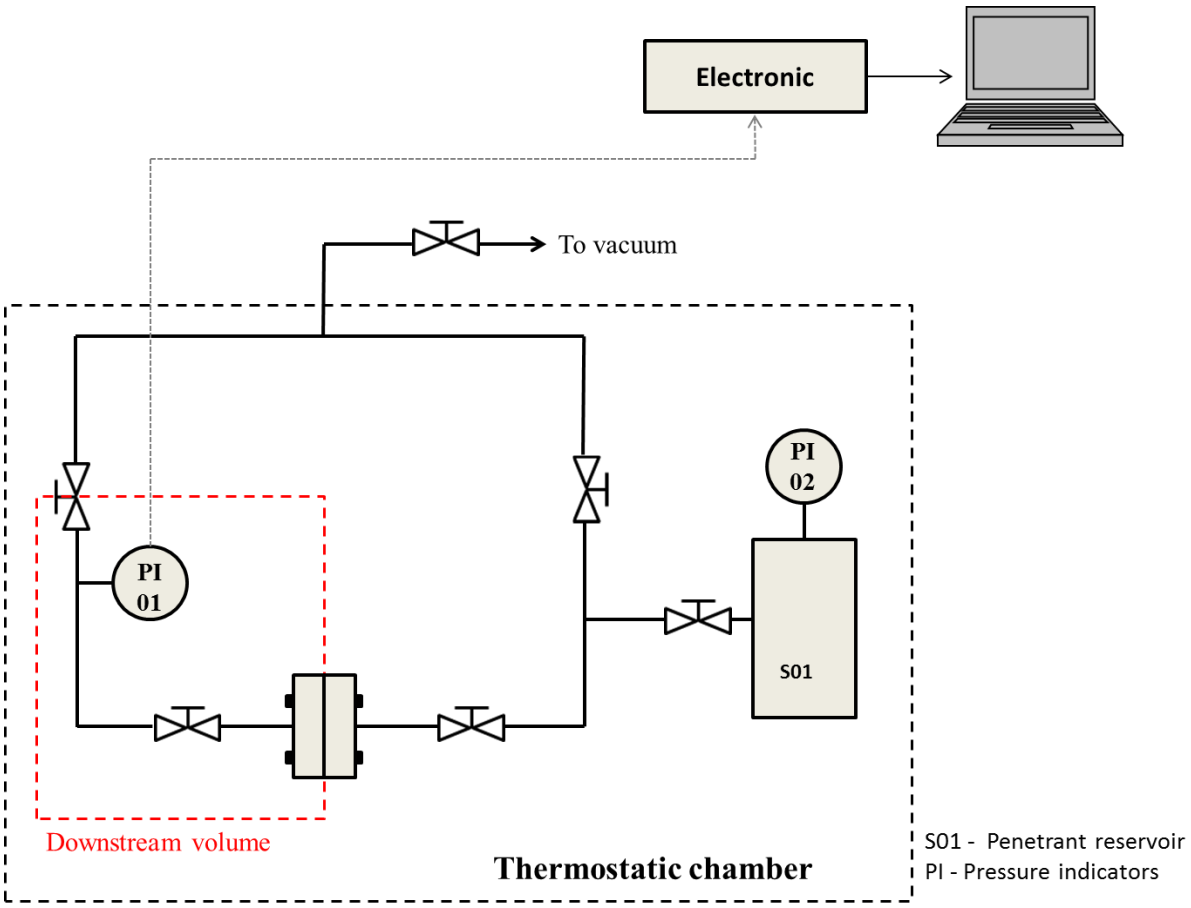

Figure 2.6: Schematic representation of pure gas permeation apparatus.

During the permeation experiments a flat sheet of membrane is put inside a permeation cell, where an O-ring guarantee good sealing. In such a way the membrane in the cell divide the apparatus in two sides: the upstream side and the downstream side. The downstream volume is known and equal to 25 ±1 cm^3 while the upstream side has a volume around 2 L and is constituted of a reservoir filled with the tested gas. During the experiments a pressure difference is kept constant across the two sides of the sample and the mass of the penetrant permeated can be calculated measuring the pressure increase in the downstream volume with a pressure transducer (Edwards Barocell Full Scale 100 mbar or 10000torr). Another manometer is placed in the upstream side to know the pressure of the reservoir and be able to calculate the pressure difference across the membrane, moreover due to high volume of this side, the pressure can be considered practically constant during the entire experiment.

The procedure requires to collocate the membrane in the permeation cell and to pull the system under vacuum to evacuate all the species dissolved in the material approximately for 1 day. After this pre-treatment, the experiment can start by isolating the downstream volume and opening the valve of the reservoir to connect it wih the upstream side of the membrane. In such a way the gas starts to diffuse in the membrane, the flux will increase during time, until steady state condition are reached and the permeability can be calculated from equation 2.8.

$$P_i = \left.\frac{dp_i}{dt}\right|_{s.s.} \frac{V_d}{RTA} \frac{l}{\left(p_i^{up} - p_i^{down}\right)} \tag{2.8}$$

During the permeation process the upstream and downstream sides of the membrane are at constant but different values of penetrant concentration, respectively $c_{i,eq}^{up}$ and $c_{i,eq}^{down}$, and the membrane is initially at uniform concentration c_{i0}. Mathematically it can be expressed as:

$$\begin{cases} \dfrac{\partial c_i}{\partial t} = D_i \dfrac{\partial^2 c_i}{\partial z^2} \\ t = t_0, \quad c_i = c_{i0} \quad 0 < z < l \\ x = 0, \quad c_i = c_{i,eq}^{up} \quad t > t_0 \\ x = l, \quad c_i = c_{i,eq}^{down} \quad t > t_0 \end{cases} \tag{2.9}$$

Applying variable separation, through Fourier series expansion, the concentration dependence on time and space can be obtained as reported in equation 2.10 [122]:

$$c_i = c_i^{up} + \left(c_i^{down} - c_i^{up}\right)\frac{x}{l} + \frac{2}{\pi}\sum_{n=1}^{\infty} \frac{c_i^{down}\cos(n\pi) - c_i^{up}}{n} \sin\left(\frac{n\pi z}{l}\right) e^{\frac{-D_i n^2 \pi^2 t}{l^2}} + \\ + \frac{4c_{i0}}{\pi}\sum_{m=0}^{\infty} \frac{1}{2m+1} \frac{\sin\left((m+1)\pi z\right)}{l} e^{\frac{-D_i (m+1)^2 \pi^2 t}{l^2}} \tag{2.10}$$

The flux exiting the downstream side of the flat sheet, at *z=l*, is given by $J_i = -D_i \left.\frac{\partial c_i}{\partial z}\right|_{z=l}$, which integrated with respect to time *t*, gives the total amount of diffusing substance Q_t which has permeated through the membrane in time t. Moreover, in general, both initial and

downstream concentration are zero, which means dry membrane at the beginning of the experiment and negligible pressure in the permeate side. In this case it can be found [122]:

$$\frac{Q_t}{lc_i^{up}} = \frac{D_i t}{l^2} - \frac{1}{6} - \frac{2}{\pi}\sum_{n=1}^{\infty}\frac{(-1)^n}{n^2} e^{\frac{-D_i n^2 \pi^2 t}{l^2}} \tag{2.11}$$

Which, as $t \to \infty$, approaches the line:

$$Q_t = \frac{D_i c_i^{up}}{l}\left(t - \frac{l^2}{6D_i}\right) \tag{2.12}$$

Equation 2.9 has an intercept in the time axis, as reported in fig, defined as time-lag, which allows the calculation of diffusion coefficient during permeation:

$$t_L = \frac{l^2}{6D_i} \tag{2.13}$$

In Figure 2.7 a general experimental output is reported.

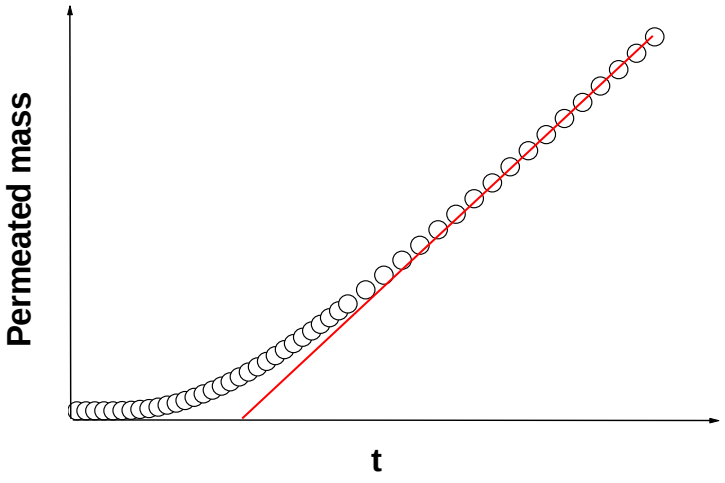

Figure 2.7: General experimental output during permeation experiments.

2.4 Humid gas permeation

Similarly to dry gas permeation experiments, also humid gas permeation experiments allow the calculation of gas permeability by means of a barometric technique, which does not require any analysis of permeate stream composition, but only a the measurement of the downstream pressure. The apparatus for the determination of humid gas permeability has been obtained by adapting a constant volume permeometer for pure gases permeation experiments, by the addition of a humidifying section in the upstream side of the membrane, of a water vapor reservoir for the initial conditioning of the membrane and of a vent flow to conduct flow-through experiments. A sketch of the apparatus is reported in Figure 2.8.

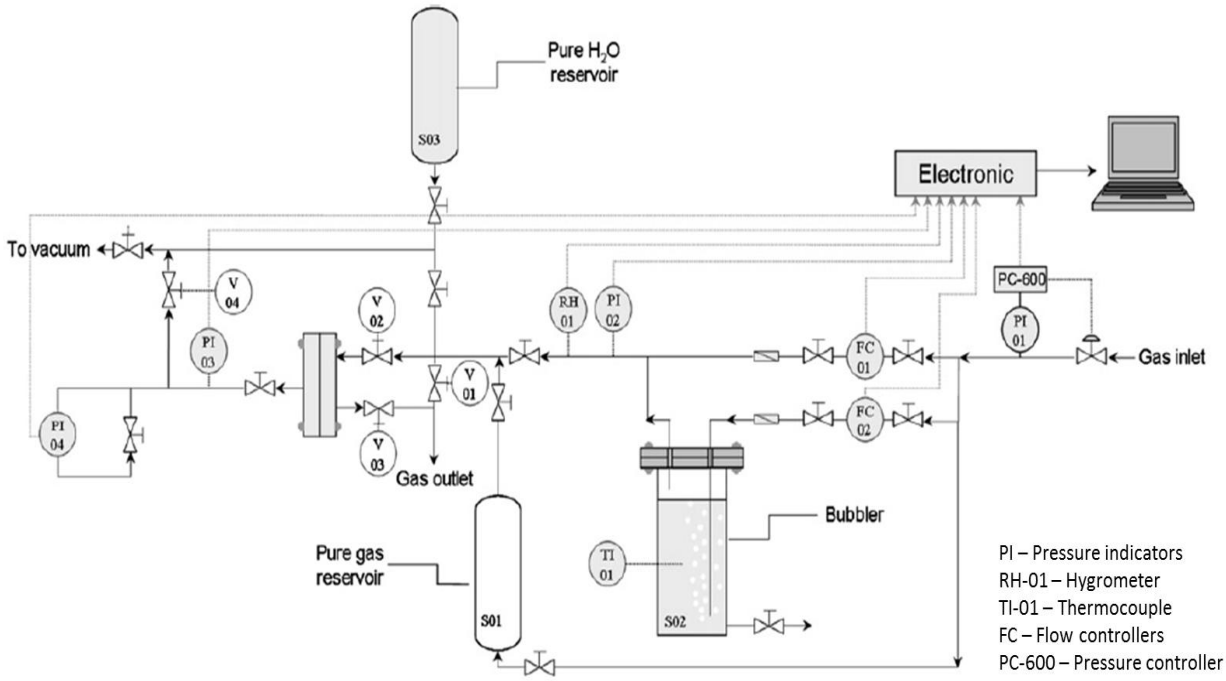

Figure 2.8: Schematic representation of humid gas permeation apparatus.

To characterize humid gas permeability, as usual, it is necessary to evacuate the sample for long time before start experiments. After evacuation is considered completed, a conditioning of the sample, which consist in equilibration with water vapor at the same activity considered in the experiment, follows, by opening the valve of pure water reservoir in vapor-liquid

equilibrium. While the membrane reaches equilibrium conditions V02, V03 and V04 are closed to isolate the sample and the humid stream is created, by splitting the gas flow coming from the cylinder in a dry stream and in a humid stream obtained by bubbling the gas in the apposite bubbler, and vented to the atmosphere. In the apparatus the humidity is measured by a humidity sensor (Vaisala HMT 330), the gas flow is adjusted by two flow meters (Bronkhorst El-Flow) and the pressure is controlled by a pressure controller (Bronkhorst El-Flow). When the sample is equilibrated with water, the humid stream is directed to the upstream side of the membrane and the permeation starts. The downstream pressure is monitored by a capacitance manometer (MKS Baratron Full Scale 100 mbar) while the upstream pressure is measured by a high pressure manometer (Druck Full Scale 60 bara). The system is collocated in a thermostatic chamber which guarantees constant temperature and an addition thermocouple is placed in the bubbler to accurately evaluate the water vapor pressure.

In these experiments the activity of the water in the upstream and downstream side is practically the same and the permeation, after an initial transient stage due to temperature fluctuations and non-equality of water activity in the humid stream activity and in the membrane, competes only to the incondensable gas. In particular the permeability at steady state can be calculated from equation 2.8, as for pure gases case.

In Figure 2.9, an illustrative example is reported:

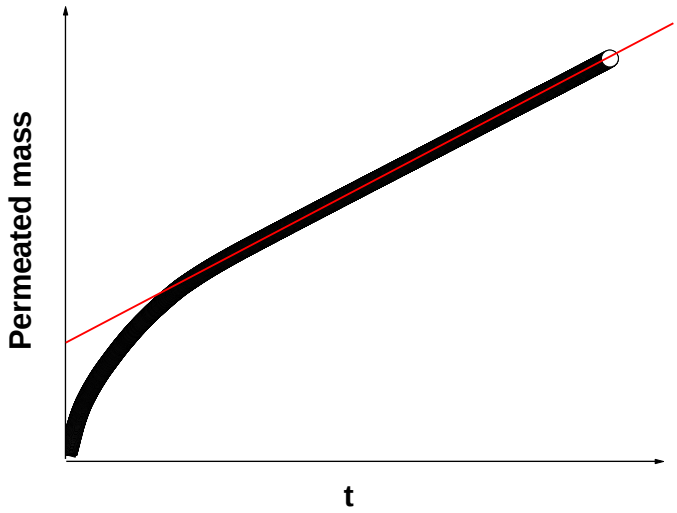

Figure 2.9: General experimental output during humid gas permeation.

3. Materials

3.1 Copolyether imides

Two series of copoly(ether imides) have been studied in this work. The first set of materials is made by 3,3',4,4′-bypheniltetracarboxyilic dianhydride (BPDA), 4,4'-oxydianiline (ODA) and bis(2-aminopropyl) poly (propylene oxide) (PPO) with nominal molecular weight of 4000 g/mol [12]. The second set of copolymers is made by 3',4,4'- Benzophenonetetracarboxylic (BKDA), 4-4' oxydianiline (ODA) and α,ω-Diamine poly(ethylene oxide) (PEO) with nominal molecular weight of 6000 g/mol (BKDA-PEO6000-ODA) [13].

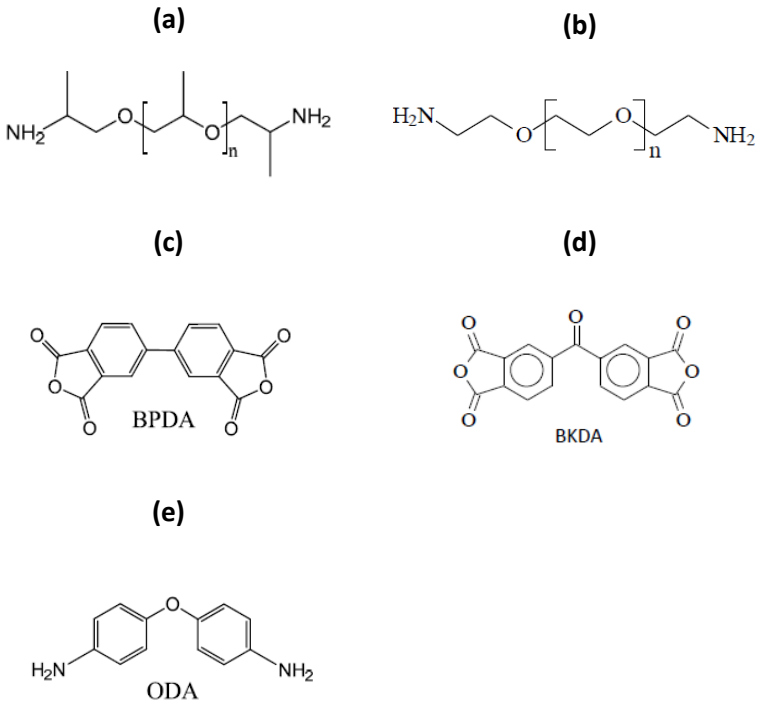

Figure 3.1: Structure of (a) diamino-terminated PPO, (b) diamino-terminated PEO, (c) BPDA, (d) BKDA and (e) ODA [12, 13].

Four samples of BPDA-PPO4000-ODA copolymers have been studied, containing 28.24%, 43.34%, 59.17% and 67.38% of PPO in weight percentage and named respectively BPDA-

PPO-ODA 1/1, 2/1, 4/1, 6/1 [12]. The samples BKDA-PEO6000-ODA 2/1 and 4/1 contain respectively 44.20% and 60.40% in mass [13] of PEO. In Fig. 3.1 chemical structures of PPO, PEO, BPDA, BKDA and ODA are reported. Polymers were synthetized by CSIC research group, in collaboration with University of Valladolid, mixing polyether with aromatic diamine in appropriate ratio in N,N'-dimethylacetamide (DMAc). Reaction mixture thus obtained was cooled down to 0°C and dianhydride was added stirring overnight at room temperature obtaining high viscosity solution, which was diluted in DMAc to the appropriate viscosity for casting. For more details we refer to previous works. [12,13]

The density of the copolymers inspected varies with the composition: an analysis of the density data can give information on the mixing volume between the two phases forming the copolymer. Densities of PPO-based copolymers and corresponding homopolymers are known from a previous work [12], while data relative to the PEO-based samples were obtained in this work by measuring the samples weight and volume. For the corresponding homopolymers density values, we refer to literature data [9,124–126].

As reported in Figure 3.2 and 3.3, interpolated data of specific volume of these samples versus the mass percentage of rubbery phase, w_R, and compared them with "ideal mixture" volume calculated from the pure rubber and pure glass specific volumes, $\hat{v}_R^0$ and $\hat{v}_G^0$, as follows:

$$\hat{v}_{ideal} = w_R \hat{v}_R^0 + (1 - w_R)\hat{v}_G^0 \qquad (3.1)$$

It can be seen in Figure 3.2 and 3.3 that for both types of copolymers, the volume is lower than the ideal mixture value, so that it seems that a contraction occurs upon phase mixing. The volume of considered materials can be interpolated with the following two equations:

$$\hat{v}_{copol} = 3.43 \cdot 10^{-1} \omega_{PPO}^3 - 3.45 \cdot 10^{-1} \omega_{PPO}^2 + 2.68 \cdot 10^{-1} \omega_{PPO} + 7.33 \cdot 10^{-1} \text{ (PPO-based)} \qquad (3.2)$$

$$\hat{v}_{copol} = 8.36 \cdot 10^{-2} \omega_{PEO}^2 + 7.80 \cdot 10^{-2} \omega_{PEO} + 7.28 \cdot 10^{-1} \qquad \text{(PEO-based)} \qquad (3.3)$$

The negative value of the mixing volume can be due to a contraction of the glassy phase, of the rubbery phase, or both of them. Usually, glassy polymers have excess free volume with respect to their equilibrium value, which can vary depending on the preparation protocol and history of the solid material. Moreover, it is known from the study of the properties of semicrystalline polymers, that the density of the rubbery amorphous regions may be lower than the equilibrium value when surrounded by crystalline domains, due to the compressive stress applied by such structures [127]. Therefore, the appearance of a negative mixing volume is not surprising. In the modeling section, when carrying out the modeling analysis of CO_2 solubility data, this aspect will be investigate in more detail.

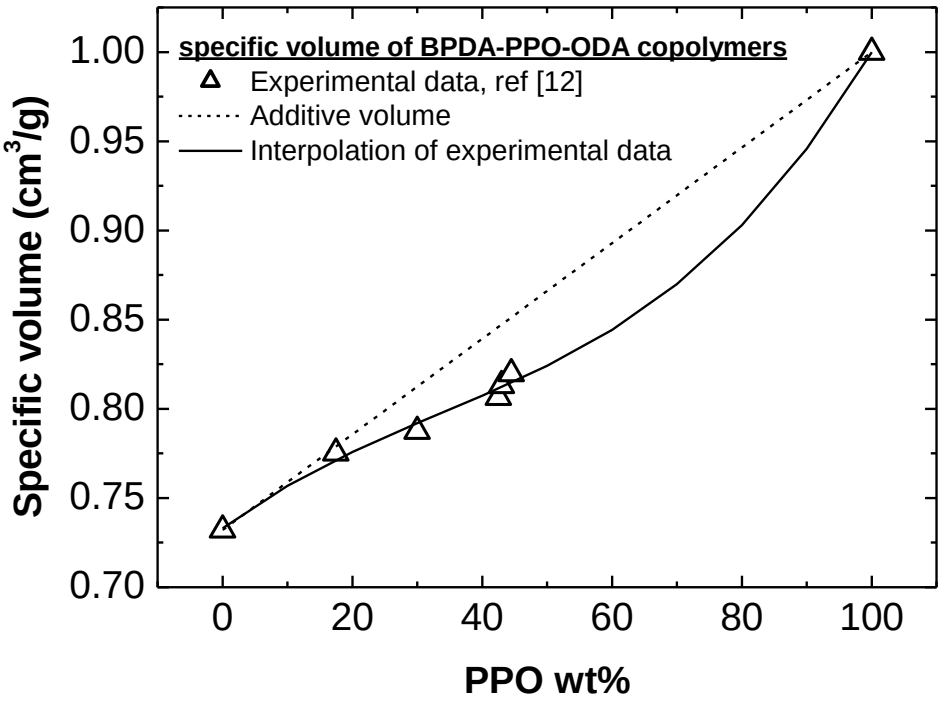

Figure 3.2: Specific volume of BPDA-PPO-ODA copolymers as a function of PPO percentage.

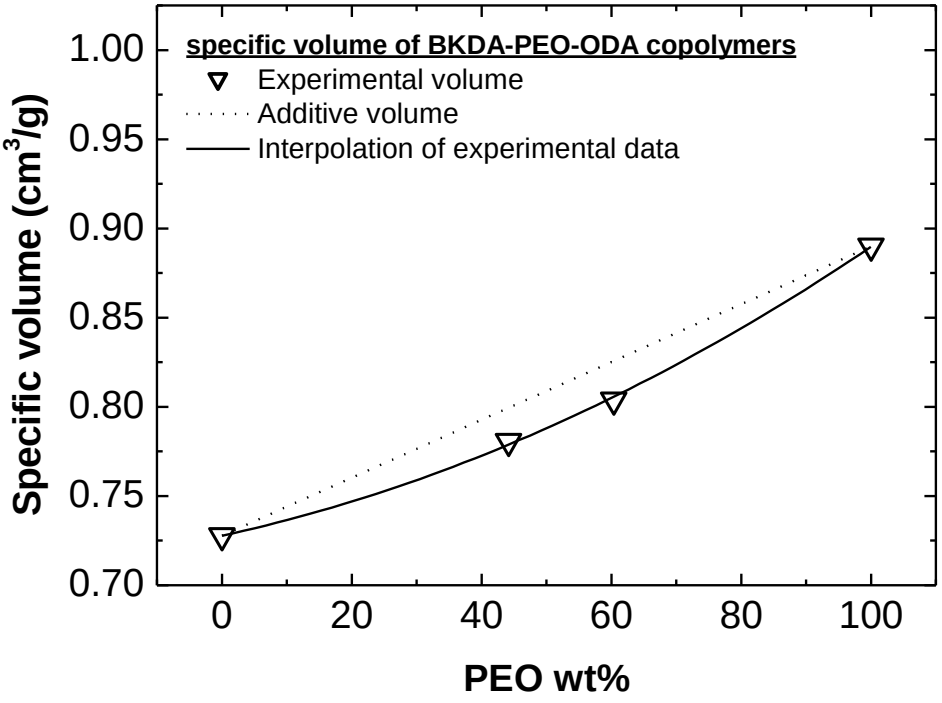

Figure 3.3: Specific volume of BKDA-PEO-ODA copolymers as a function of PEO percentage.

In Table 3.1 composition, density ρ and thickness l of all tested materials are reported:

Table 3.1: Properties of copolymer samples investigated in this work.

Sample	Rubber content	Amorphous rubber content	ρ	Thickness
	wt%	wt%	g/cm^3	μm
BPDA-PPO-ODA 1/1	28.24	28.24	1.267	161±19
BPDA-PPO-ODA 2/1	43.34	43.34	1.230	57±16
BPDA-PPO-ODA 4/1	59.17	59.17	1.187	141±8
BPDA-PPO-ODA 6/1	67.38	67.38	1.159	154±43
BKDA-PEO-ODA 2/1	44.20	43.80	1.281	116±1
BKDA-PEO-ODA 4/1	60.40	59.90	1.244	107±2

3.2 PTMSP and Graphene based Mixed Matrix Membranes

3.2.1 Polymer

PTMSP was purchased by Gelest Inc. (Morrisville, PA, USA). It is a glassy polymer which belongs to substituted polyacetylenes class. Due to the stiff main chain and bulky spherical substituents, PTMSP is characterized by high fractional free volume, up to 34%. It is a material suitable for gas separation due to its high gas and vapor permeability. It is a highly hydrophobic polymer and is soluble in many organic solvents such as toluene, cyclohexane, tetahydrofuran and chloroform.

3.2.2 Fillers

In this work fillers considered to form mixed matrix membranes are graphene and graphene oxide nanoplatelets. Graphene based materials is recently raising attention for its possible use in gas separation applications [93,128]. If free from defects, graphene is a perfect barrier to all molecules [129]; however, the production of graphene with methods such as the chemical vapor deposition (CVD) may introduce a defective microporosity, due to mechanical cleavage or oxidation of the polycrystalline structure, which make it permeable to gases. In addition, when the graphene structure is formed by multiple layers, permeable channels caused by imperfect adhesion between the layers may form. All such defects are shown to be permeable, and selective to some gases [130]; however, the highest permeability measured for a pure GO layer of 1.8 nm was found in the case of He and is much lower than that of the PTMSP for the same gas [87]. Indeed, several authors observed that the incorporation of GO to polymers leads to a reduction in gas permeability, that is generally proportional to the amount and aspect ratio of filler [88,131,132]. Such behavior indicates that the main effect of adding GO to the polymer is the increase of tortuosity of the diffusive path of gas molecules, and that its intrinsic permeability can be neglected. Based on such findings, and in view of the small

amount of filler added in this work (<1 wt%), graphene and graphene oxide platelets will be considered impermeable with respect to the polymer.

Graphene solutions were supplied by GNext in two different grades: 1) XT IND G, an industrial grade graphene with a lateral dimension of 0.2 μm and a thickness of 2-20 nm (whose AFM image is reported in Fig 3.4), 20% w/w of undisclosed dispersing agent and no oxygen species,[74,75] and 2) XT M60, a research grade graphene species with a lateral dimension of 5 μm and thickness of 2-8 nm (Fig. 3.4), 2 wt.% of undisclosed dispersing agent and around 1% oxygen content on the graphene structure. Finally GO solution contains nanoplatelets with a lateral sheet dimension of 2 μm and thickness of 1.1 nm (Figure 3.4), monolayer content higher than 95% and C/O ratio equal to 1. Additional details on the GO and Graphene XT IND G are reported in the respective technical sheets [134,135].

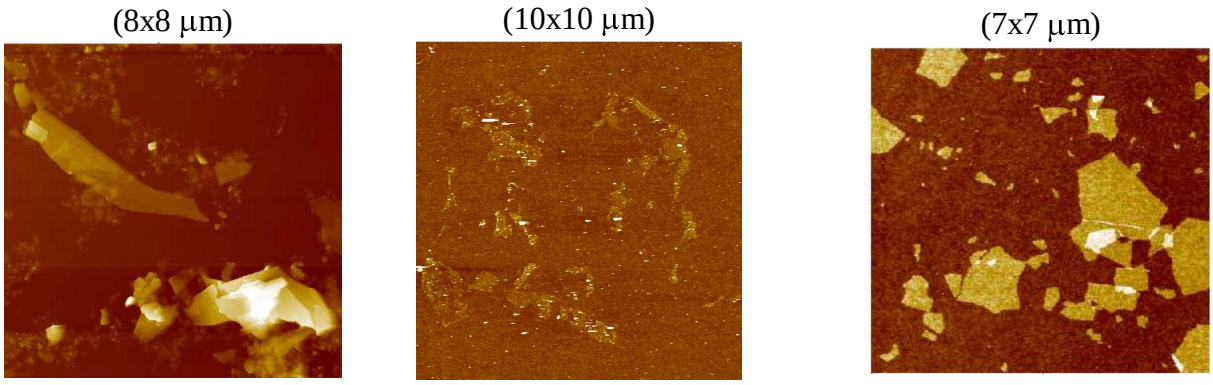

(8x8 μm)	(10x10 μm)	(7x7 μm)
Graphene XT IND G (IND G). Lateral dimension: 200 nm. Thickness: 2-20 nm Aspect ratio 10-100	Graphene XT M60 (M60). Lateral dimension: 5000 nm. Thickness: 2-8 nm Aspect ratio 625-2500	Graphene Oxide (GO). Lateral dimension: 2000 nm. Thickness: 1.1 nm Aspect ratio 1800

Figure 3.4: AFM images for graphene fillers considered in this study.

3.2.3 Thick membranes preparation

PTMSP membrane, as well as mixed matrix membranes containing G and GO were obtained through solution casting technique. The solvent chosen is chloroform (purity>99.5%, Sigma

Aldrich), because it allows to optimize the compatibility between filler and polymer according to the solubility parameters and graphene dispersibilities reported in literature [136]. The polymer has been first dissolved in chloroform to obtain 1 wt.% polymer solution, and then the filler has been added in a proper amount to reach a filler weight percentage of 1 wt% in the final membrane. After several attempts, it was found that the following protocol allows to avoid precipitation of graphene during evaporation:

i) sonication of the polymer-filler solvent solution for 2 h;

ii) evaporation of about half of the solvent from the bottled solution;

iii) casting of the solution on a covered Teflon Petri dish.

The second step allows to increase the viscosity of the solution and to avoid precipitation of solid particles during the subsequent casting step. After the casting process in a clean hood, the samples were placed in a vacuum oven at 30°C for 24 h to remove traces of solvent. In Figure 3.5 it is reported a scheme of the preparation procedure:

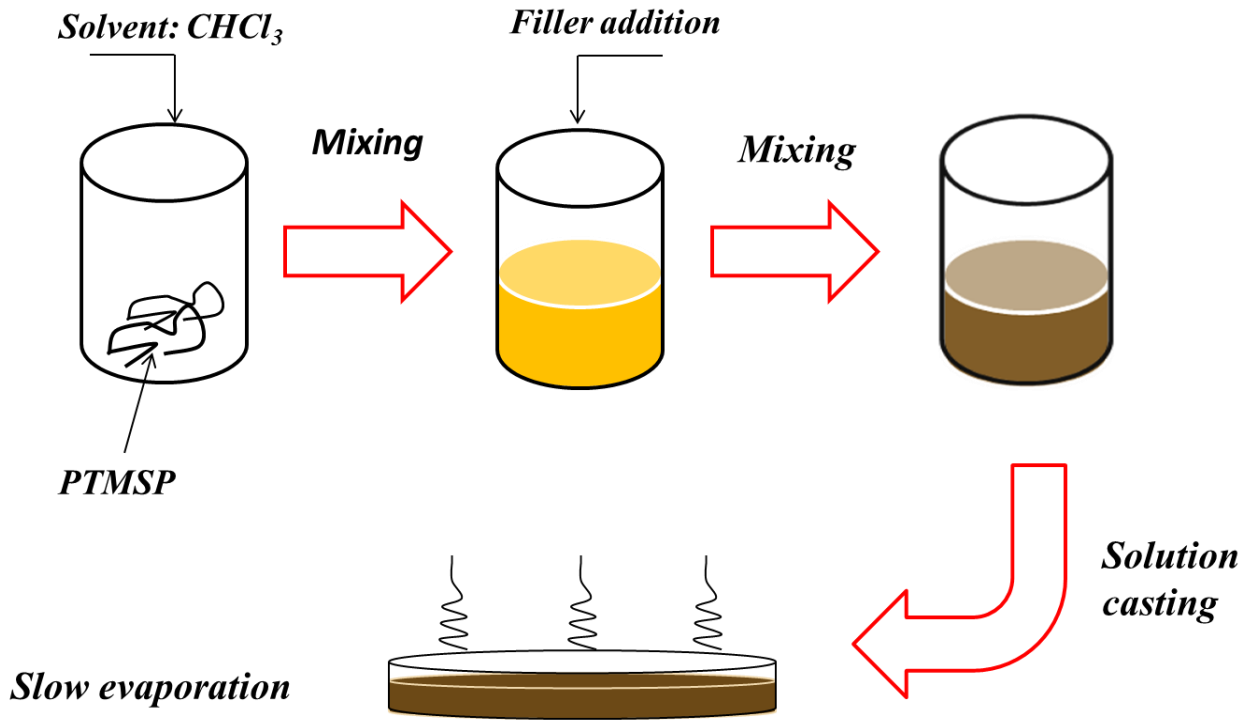

Figure 3.5: Illustrative description of the preparation protocol of thick graphene based MMM by solution casting technique.

A SEM image of the PTMSP film, as well as of the corresponding M60-MMM is shown in Figures 3.6: white circles indicate the possible location of graphene nanoplatelets. The obtained films are shown in Figure 3.7 and they exhibit macroscopic homogeneity, in particular no precipitation of platelets was observed during evaporation. The average thickness of such samples ranged between 100 and 170 μm, and the maximum percentage deviation observed for the average thickness value of each sample is equal to 10%.

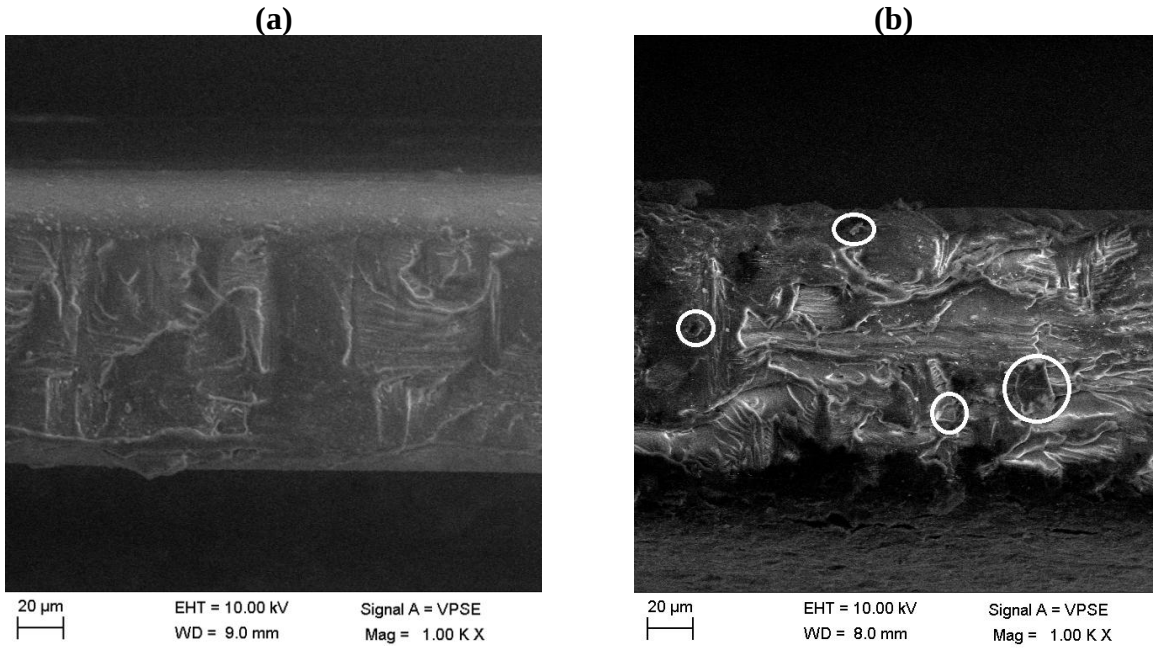

Figure 3.6: SEM images of PTMSP (a) and M60-MMM (b).

PTMSP 115±2 μm | **IND G-MMM** 169±4 μm | **M60-MMM** 132±13 μm | **GO-MMM** 120±2 μm

Figure 3.7: Images of thick films of PTMSP (I); IND G-MMM (II); M60-MMM (III) and GO-MMM (IV).

3.2.4 Thin membranes preparation

Considering that on a practical point of view 1 μm or lower of selective dense skin is usually employed in industrial application, thin films composite mixed matrix membranes have been fabricated through spin coating technique. In particular 400 μL of solutions, prepared with the same procedure as for thick membranes, have been deposed on porous Celgard® film connected to the the rotor of the spin coating apparatus. Thanks to speed in the range of 2000 rpm, the solvent quickly evaporates giving a practically dry thin membrane. To remove any trace of solvent thin membranes have been treated at 30°C under vacuum for 30 minutes.

In Figure 3.8 a scheme of preparation procedure is reported:

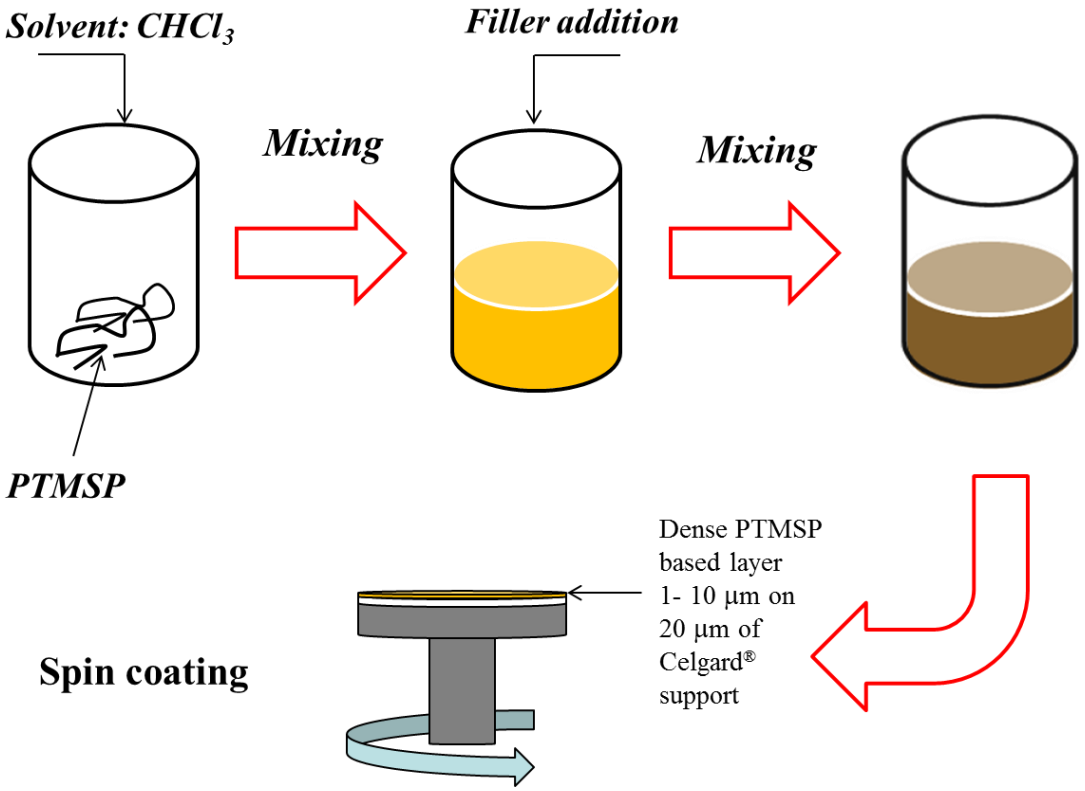

Figure 3.8: Illustrative description of the preparation protocol of thin graphene based MMM by spin coating technique.

The thickness of the thin membranes have been measured with SEM microscopy, with the help of Prof. Andrea Saccani (University of Bologna, Dept. DICAM), and it ranges between 1 and 10 μm for the membranes tested. In Figure 3.9 the SEM image of a pure PTMSP

composite membrane is reported, in which it can be observed the dense thin layer made in PTMSP and the porous support in Celgard®.

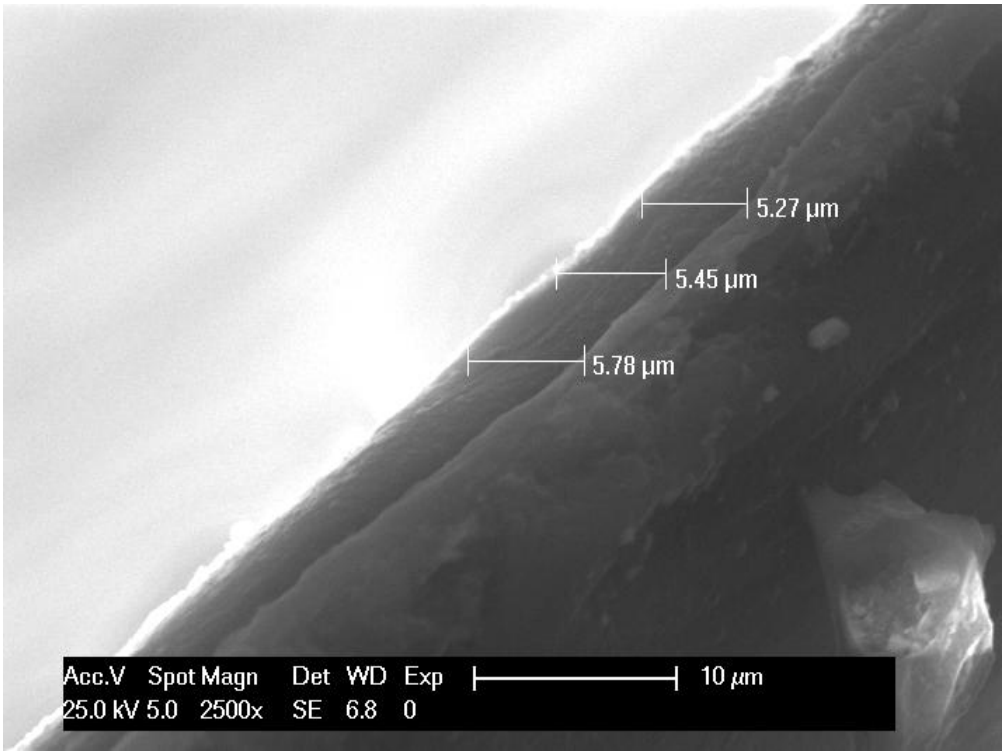

Figure 3.9: SEM image of thin PTMSP composite membrane.

3.3 Facilitated transport membranes based on Polyacrylonitrile

3.3.1 Powder functionalization

Polyacrylonitrile powder, purchased by Sigma Aldrich, has been functionalized by the research group of Prof. Alessandra Lorenzetti (University of Padova, Dept. of Industrial Engineering), following two different routes. In particular amine groups attachment to the polymer backbone has been provided by reaction with amines, hexamethylene diamine or ethylene diamine, purchased by Sigma Aldrich, or by PAN hydrolysis in aqueous NaOH 1 M basic environment. In Figure 3.10 reaction schemes considered are reported.

(a)

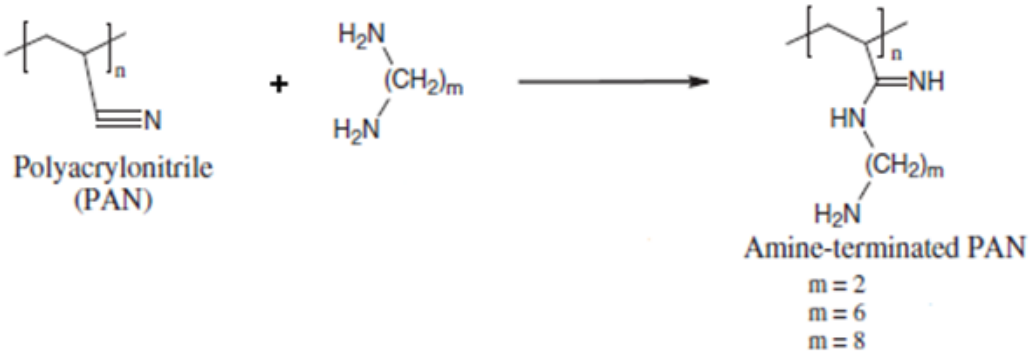

(b)

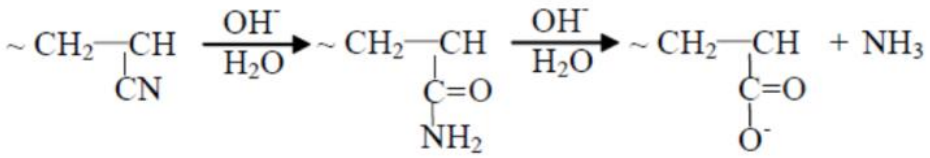

Figure 3.10: Reaction schemes for PAN functionalization with amines (a) and PAN funciotnalization via hydrolysis in basic environment (b).

The reaction of functionalization with amines has been conducted in a three neck flask, equipped with a reflux condenser, contained in a thermostatic oil bath. Amine-distilled water solution and PAN have been loaded in the reaction environment with amine excess around 10 times the stoichiometric ratio, to avoid or minimize crosslinking reactions effects. During the functionalization reaction polymer powder changes color from white to orange depending on conversion reached. The reacted powder was washed with distilled water until neutral pH and dried in an oven at 80°C.

Functionalized powders are insoluble in common solvents except Dimethyl sulfoxide, DMSO, and dimethylformamide, DMF.

The second route to functionalize PAN consists in hydrolysis of nitril groups through reaction with 1 M NaOH solution. In such a way, amine groups are formed directly on the polymer,

avoiding formation of lateral chains, which facilitate crosslinking. As first, the procedure requires to dissolve in a three neck flask balanced amounts of NaOH pellets in distilled water at 50°C. After complete dissolution, the temperature is increased up to 80°C and PAN is added in the flask, observing a very fast color transition from white to orange in few minutes, indicating a fast reaction kinetic.

3.3.2 Membrane preparation

Powder have been dissolved in DMF by the aforementioned group, obtaining a solution at 5wt% Which has been electrospun, obtaining nanostructured electrospun porous membrane which have been compacted by hydraulic press obtaining compacted dense membrane to be used in gas separation systems. Figure 3.11 shows a schematic representation of the apparatus used for electrospinning.

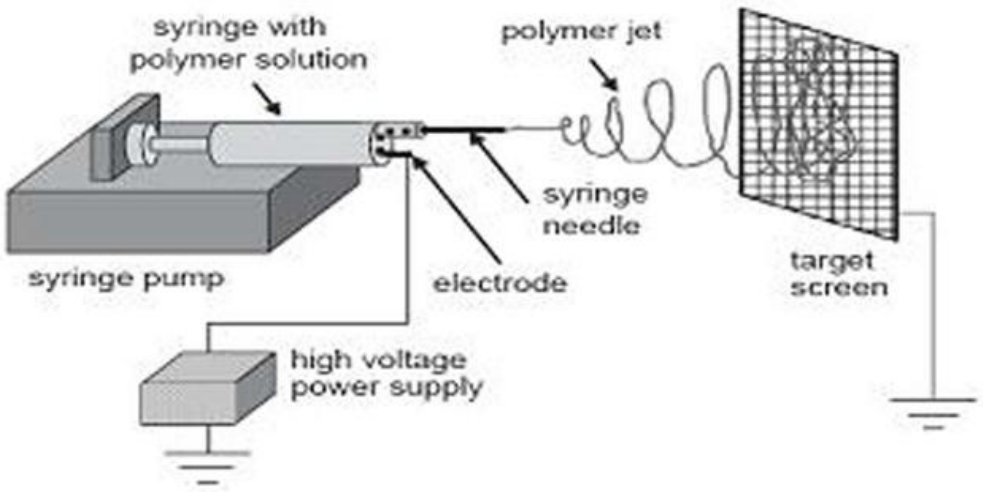

Figure 3.11: Schematic representation of electrospinning apparatus used to produce nanoporous membranes.

4. Experimental results

In this chapter experimental results obtained for materials considered in this study will be presented. In the first section it will be reported the effect of temperature and copolymers composition on CO_2 solubility, diffusivity and permeability in two series of copolyetherimides, togheter with the effect of water vapor during humid permeation. With mixed matrix membranes based on PTMSP it will be observed the ageing of the polymeric material and the effect that nanoplatelets have on its relaxation process and transport properties in thick and thin samples. Finally it will be shown the characterization of functionalized materials based on PAN to verify the effect of amine groups on solubility and permeability of CO_2. In particular FT-IR, SEM, TGA and permeation analysis have been carried out at University of Padova while CO_2 sorption experiments have been carried out at DICAM laboratories.

4.1 BPDA-PPO-ODA and BKDA-PEO-ODA copolyetherimides

The solubility of CO_2 in two series of copolyetherimides has been measured through the pressure decay technique at 30, 45 and 60°C and different pressures up to 30 bar. The value of concentration is mainly affected by uncertainties in pre-chamber and sample chamber volumes which have a relative deviation of 1% from average values. The value of diffusion coefficient is assumed to be affected by uncertainties on samples thickness, which have been measured with a digital micrometer. To take into account the effect of these uncertainties, error bars are calculated from propagation of errors.

The solubility of water in copolymers is measured with a sub-atmospheric quartz spring microbalance at 30°C. The measurement of equilibrium mass uptake is reliable to within 1%, due to the potential of the software used for image reconstruction. So it can be concluded that for QSM technique the most significant error is represented by dry polymer mass measurement.

Humid gases permeability has been measured with humid permeometer in which experimental uncertainty connected to volume calibration is lower than 2% and thus it has been assumed that the error is predominantly due to thickness measurement.

4.1.1 Solubility and diffusivity of CO_2 in BPDA-PPO4000-ODA copolymers

CO_2 sorption experiments have been carried out up to 30 bar at 30, 45 and 60°C in BPDA-PPO 4000-ODA copoly(ether-imide)s and solubility and diffusivity have evaluated at various pressures.

The solubility data in each copolymer are reported in Figures 4.1–4.4 at different temperatures. First of all one can notice that these materials show quite high CO_2 solubility, up to 40 $cm^3(STP)/cm^3$ at 20 bar, which is similar to the value found for commercial rubbery PDMS that is equal to 28 $cm^3(STP)/cm^3$ at the same pressure [137]. The solubility, as usual, decreases with increasing temperature and the data can be used to calculate sorption enthalpies, which will be shown in a subsequent section. Interestingly, by increasing the proportion of the rubbery phase in the copolymer, the shape of the solubility isotherm changes. In particular, solubility isotherms are convex to pressure axis if the rubbery phase content is higher than 43 wt.% (Fig. 4.3, 4.4). If rubbery phase percentage is lower than 30 wt.% the isotherm is concave to pressure axis (Fig. 4.1). This behavior is consistent with the fact that in glassy polymers the slope of the solubility coefficient of a gas normally decreases with increasing pressure, while in rubbery polymers the solubility coefficient may be constant with pressure or increase with it, depending on the swelling ability of the penetrant.

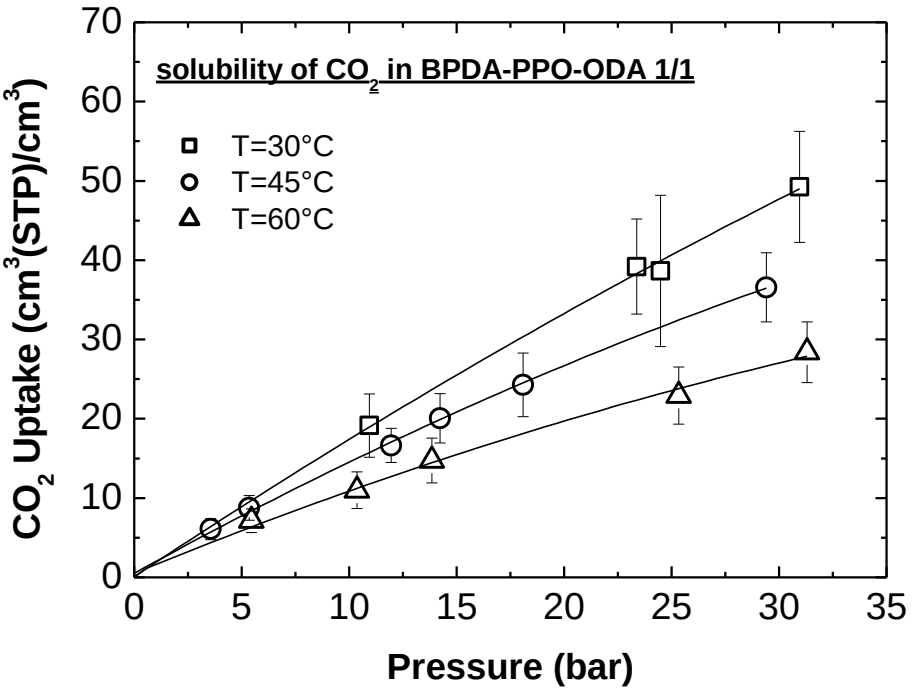

Figure 4.1: The effect of temperature on CO_2 solubility isotherms in BPDA-PPO4000-ODA 1/1. Solid lines are data interpolations.

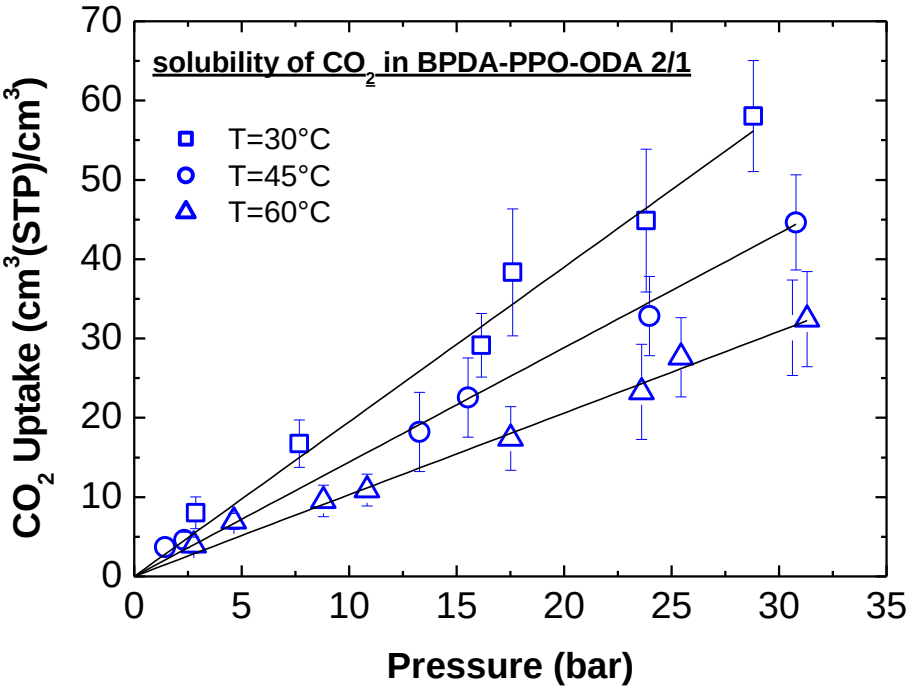

Figure 4.2: The effect of temperature on CO_2 solubility isotherms in BPDA-PPO4000-ODA 2/1. Solid lines are data interpolations.

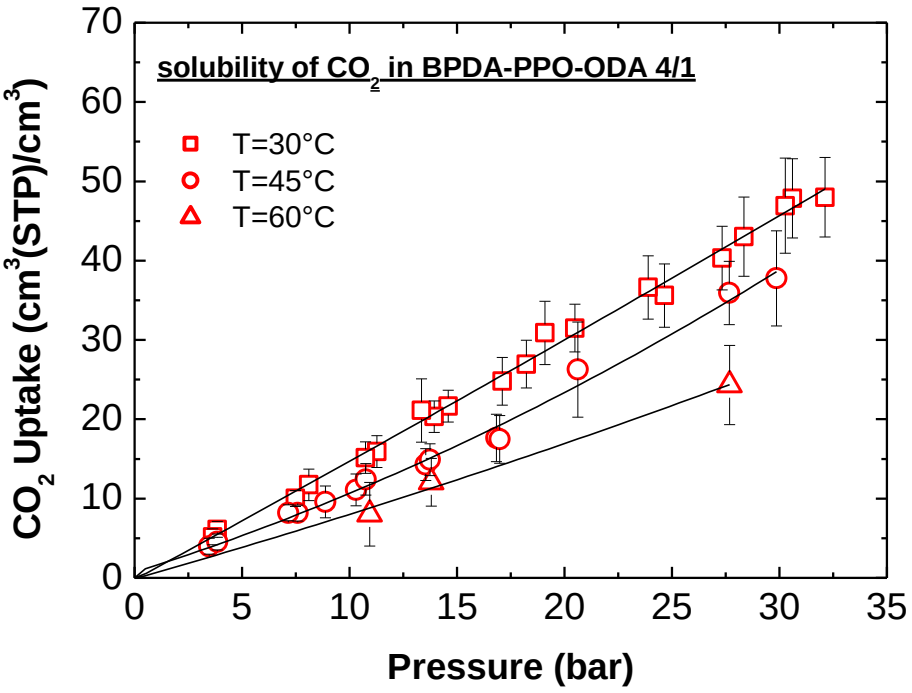

Figure 4.3: The effect of temperature on CO_2 solubility isotherms in BPDA-PPO4000-ODA 4/1. Solid lines are data interpolations.

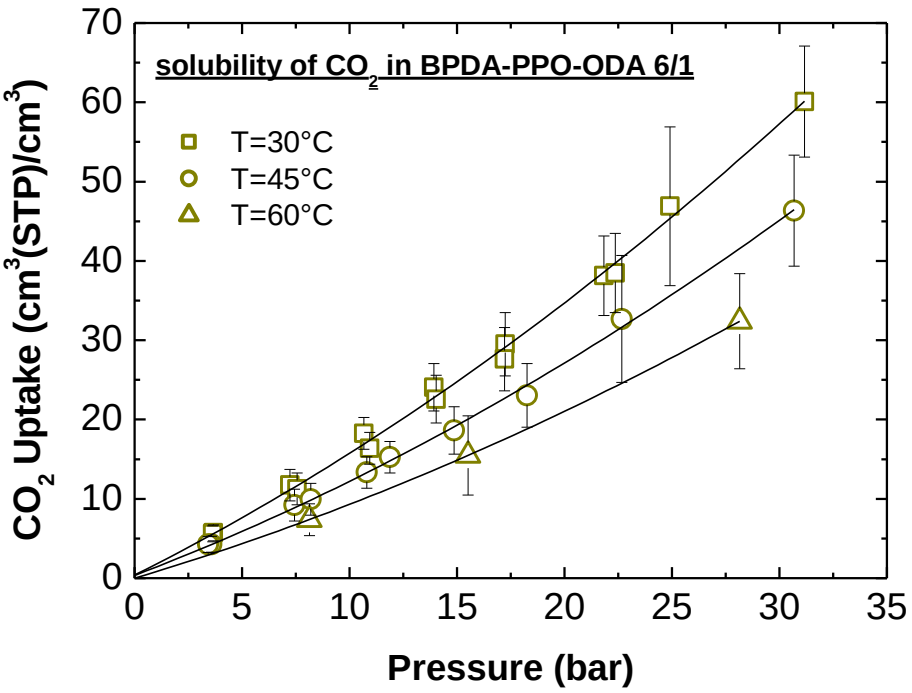

Figure 4.4: The effect of temperature on CO_2 solubility isotherms in BPDA-PPO4000-ODA 6/1. Solid lines are data interpolations.

The diffusivity values, calculated from sorption kinetics data, are reported in Figures 4.5–4.8 for the various copolymers at different temperatures. The extent of CO_2 diffusivity variation with temperature is lower for materials with higher amount of rubbery PPO, as it will be discussed more in detail in the following. More evidently, the diffusivity observes a step increase of 2 orders of magnitude for a weight percentage of PPO in the sample higher than 44% w/w, going from values between 10^{-8} and 10^{-7} cm^2/s to values around 10^{-5} cm^2/s. Such a remarkable increase indicates a strong variation of the copolymer nature with increasing amount of PPO, with a dramatic increase of polymer flexibility above a certain threshold that reflects on the average gas diffusivity. The solubility behavior, on the other hand, seems less affected by the copolymer formulation, as is discussed above.

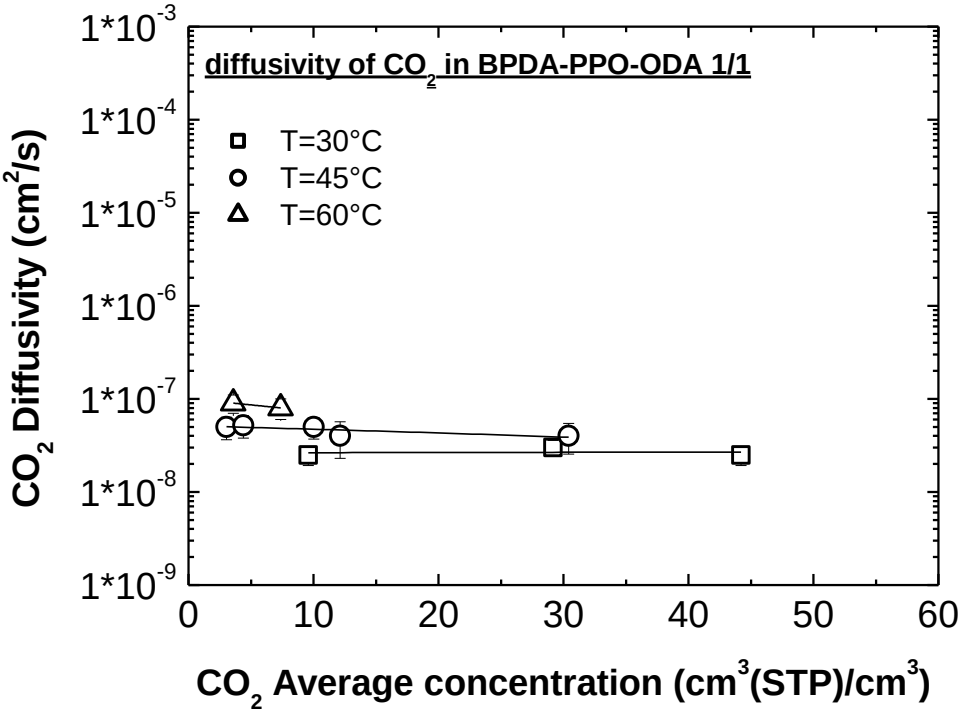

Figure 4.5: The effect of temperature on CO_2 diffusivity in BPDA-PPO4000-ODA 1/1 sample. Solid lines are data interpolations.

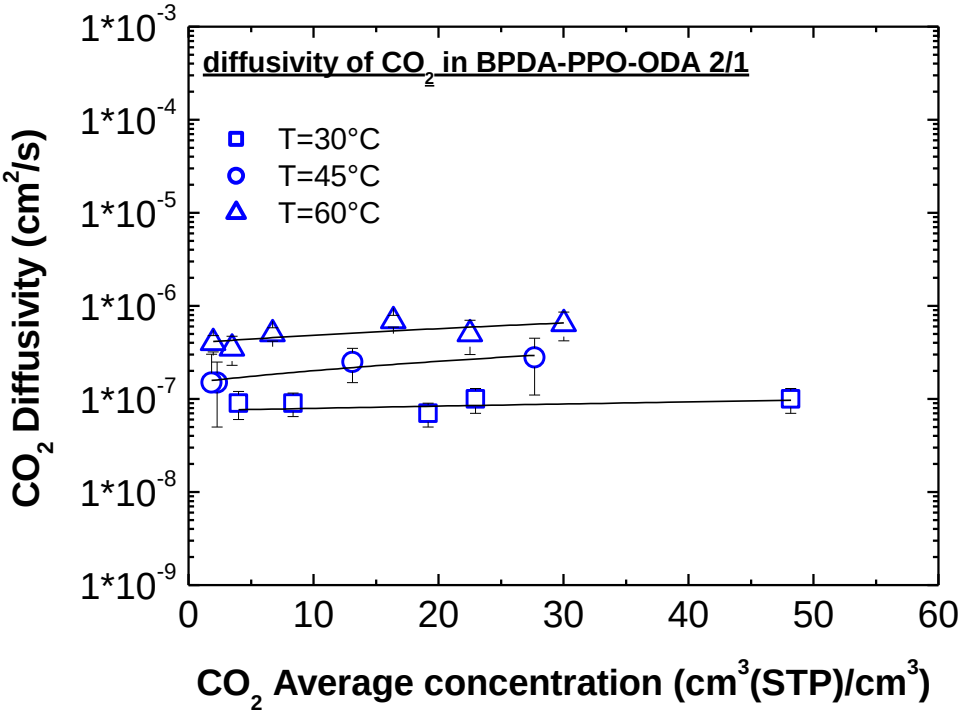

Figure 4.6: The effect of temperature on CO_2 diffusivity in BPDA-PPO4000-ODA 2/1 samples. Solid lines are data interpolations.

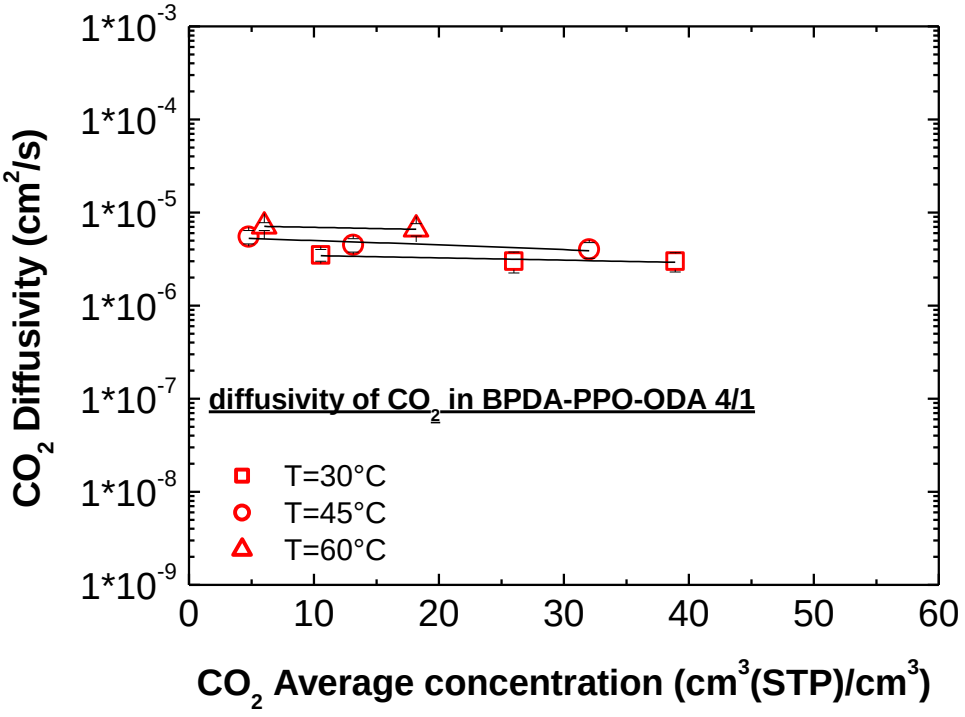

Figure 4.7: The effect of temperature on CO_2 diffusivity in BPDA-PPO4000-ODA 4/1 samples. Solid lines are data interpolations.

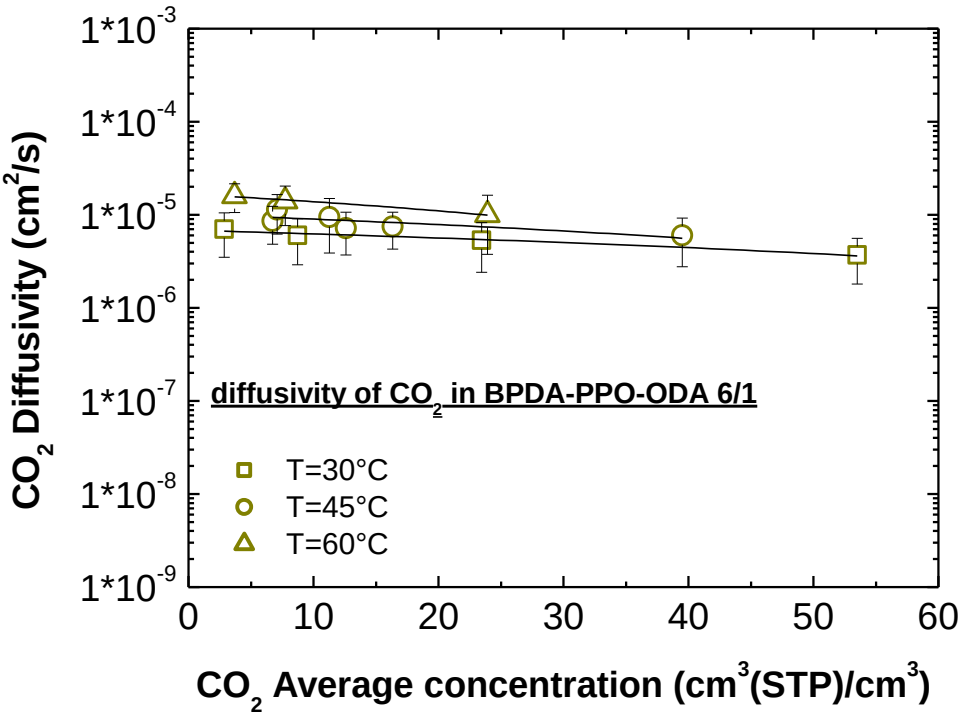

Figure 4.8: The effect of temperature on CO_2 diffusivity in BPDA-PPO4000-ODA 6/1 samples. Solid lines are data interpolations.

The influence of copolymer composition on permeability was studied in a previous work [12], and showed an enhancement of permeability with increasing PPO content in the membranes. In this work, we have the possibility of analyzing the effect that the copolymer composition has, separately, on diffusivity and solubility contribution.

Solubility of CO_2 is a very weak function of the copolymer composition in the entire range of temperature investigated, as can be seen from Figures 4.9–4.11. We can say that the ratio between two different phases in the material influences more the shape of the solubility isotherm than the actual value of solubilities.

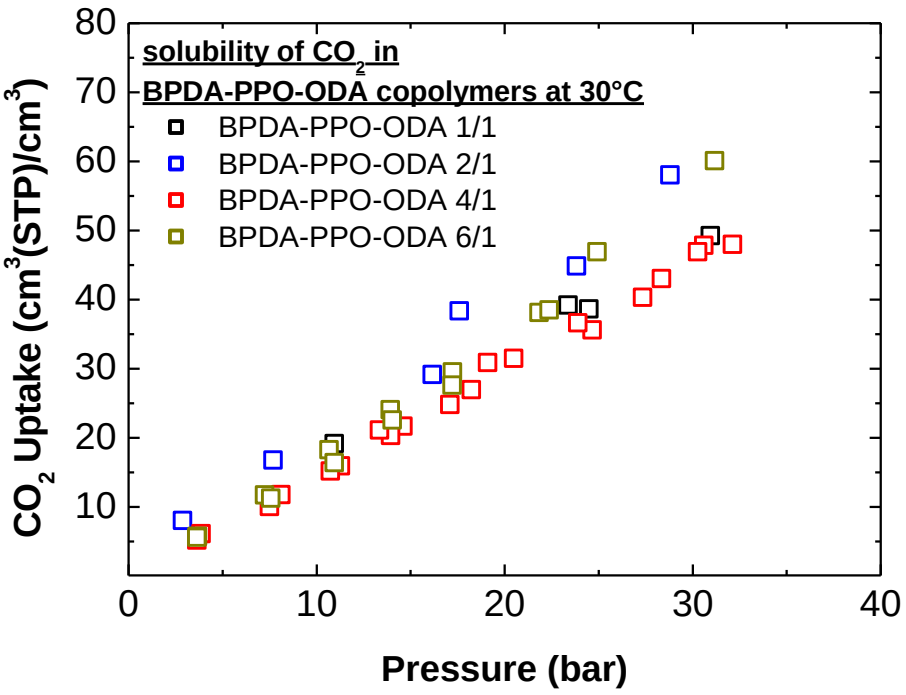

Figure 4.9: The effect of copolymer composition on CO_2 solubility isotherms in BPDA-PPO4000-ODA copolymers at 30°C.

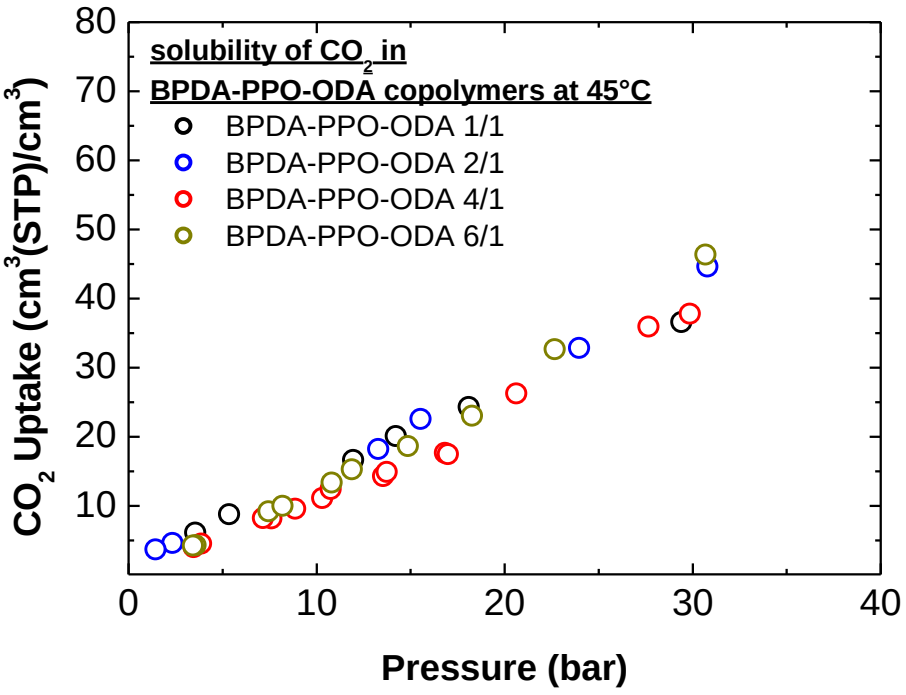

Figure 4.10: The effect of copolymer composition on CO_2 solubility isotherms in BPDA-PPO4000-ODA copolymers at 45°C.

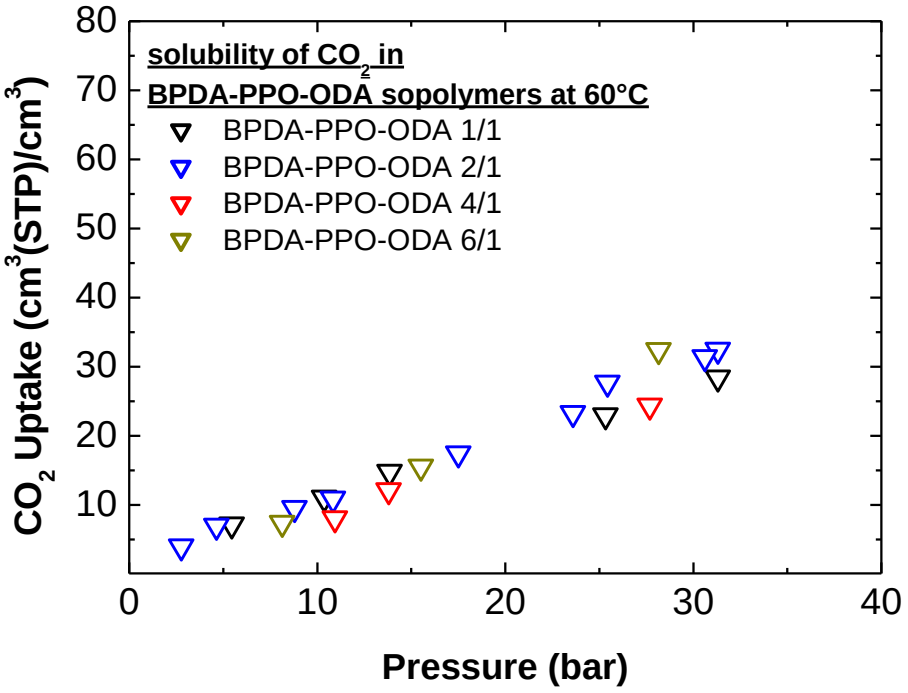

Figure 4.11: The effect of copolymer composition on CO_2 solubility isotherms in BPDA-PPO4000-ODA copolymers at 60°C.

On the other hand, it is evident from Figures 4.12–4.14 that increasing PPO percentage in the material has a strong effect on CO_2 diffusivity. Diffusivity value for the copolymer 1/1 is one order of magnitude higher with respect to the value ($3.5 \cdot 10^{-9}$ cm^2/s) of the pure polyimide [125], showing the marked effect of the rubbery phase content on average diffusivity rather than solubility. Moreover, we observe a dramatic increase of diffusivity above a certain PPO content, indicating a sharp transition from a glassy-like behavior to a rubbery-like behavior, that is also testified by changes of the shape of the solubility isotherm. Such a transition is located between a PPO weight fraction of 43% and 59%.

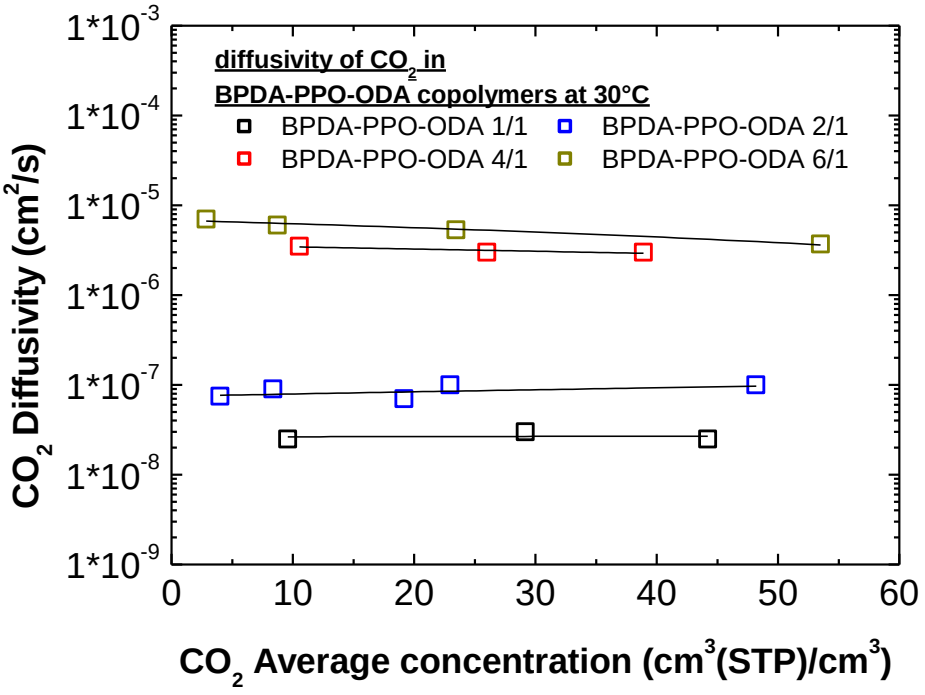

Figure 4.12: The effect of copolymers composition on CO_2 diffusivity in BPDA-PPO4000-ODA copolymers at 30°C. Solid lines are data interpolations.

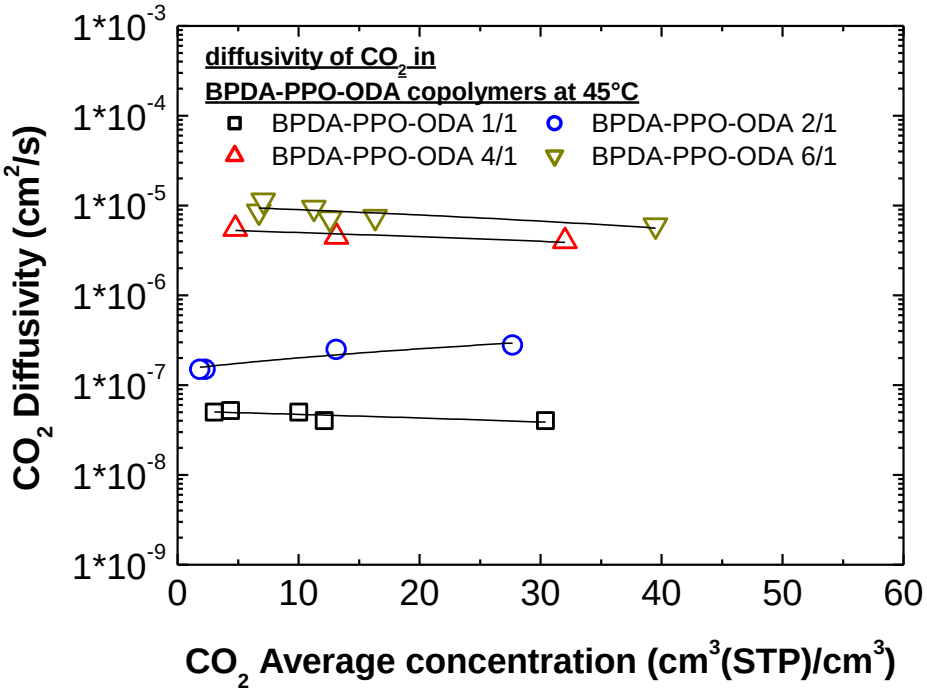

Figure 4.13: The effect of copolymers composition on CO_2 diffusivity in BPDA-PPO4000-ODA copolymers at 45°C. Solid lines are data interpolations.

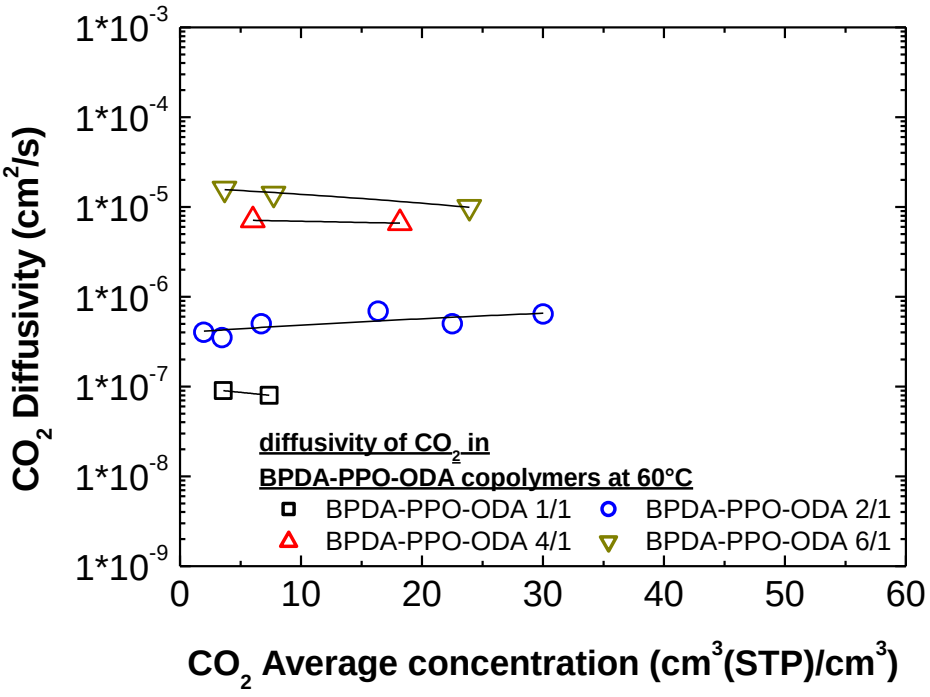

Figure 4.14: The effect of copolymers composition on CO_2 diffusivity in BPDA-PPO4000-ODA copolymers at 60°C. Solid lines are data interpolations.

4.1.2 Solubility and diffusivity of CO_2 in BKDA-PEO6000-ODA copolymers

As for the previous series of materials, also for this series we carried out sorption experiments in the temperature range 30-60 °C up to 30 bar to observe effects of operative conditions and copolymer compositions on solubility and diffusivity of CO_2. The solubility in these copolymers is lower than that observed in the copolymers based on PPO.

For BKDA-PEO-ODA 2/1 solubility decreases significantly going from 30°C to 45°C, after that, a slight variation can be observed increasing the temperature up to 60°C. On the contrary for BKDA-PEO-ODA 4/1 a gradual decrease of solubility with temperature can be observed in Figures 4.15–4.16. Diffusivity increases significantly with temperature in these membranes, as reported in Fig. 4.17 and 4.18, in particular by increasing temperature from 30°C to 60°C, *D* increases of one order of magnitude from $3 \cdot 10^{-8}$ cm^2/s up to $5 \cdot 10^{-7}$ cm^2/s in 2/1 sample, while in 4/1 sample it varies by almost 2 orders of magnitude, from $3 \cdot 10^{-8}$ cm^2/s

up to 10^{-6} cm^2/s The diffusivity value increases with CO_2 concentration due to a penetrant induced swelling, which has been calculated through LF EoS and will be shown in a subsequent section.

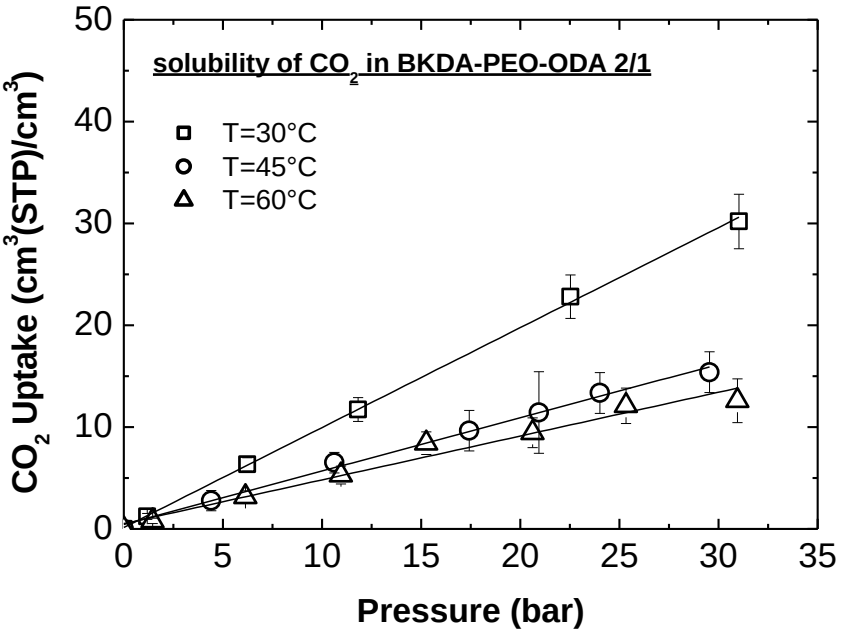

Figure 4.15: The effect of temperature on CO_2 solubility in BKDA-PEO6000-ODA 2/1. Solid lines are data interpolations.

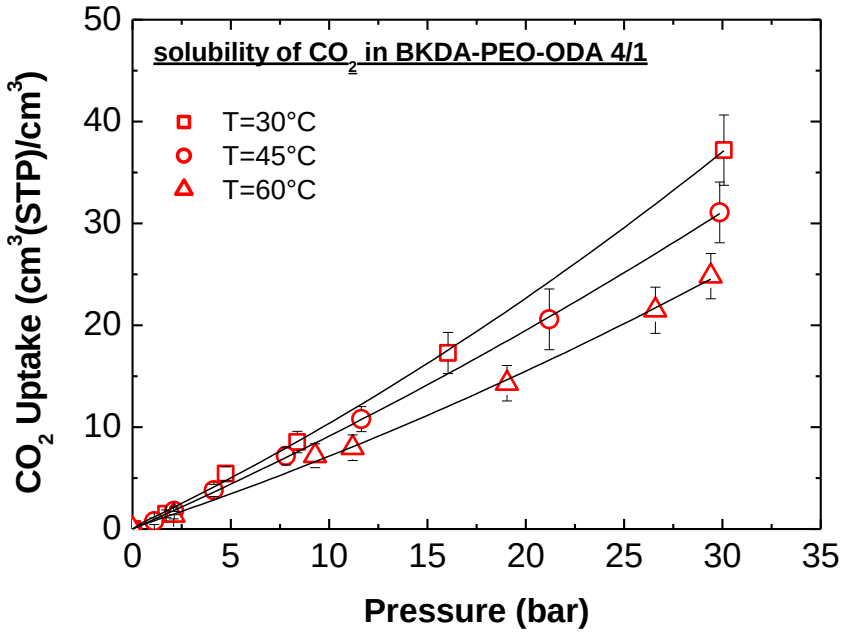

Figure 4.16: The effect of temperature on CO_2 solubility in BKDA-PEO6000-ODA 4/1. Solid lines are data interpolations.

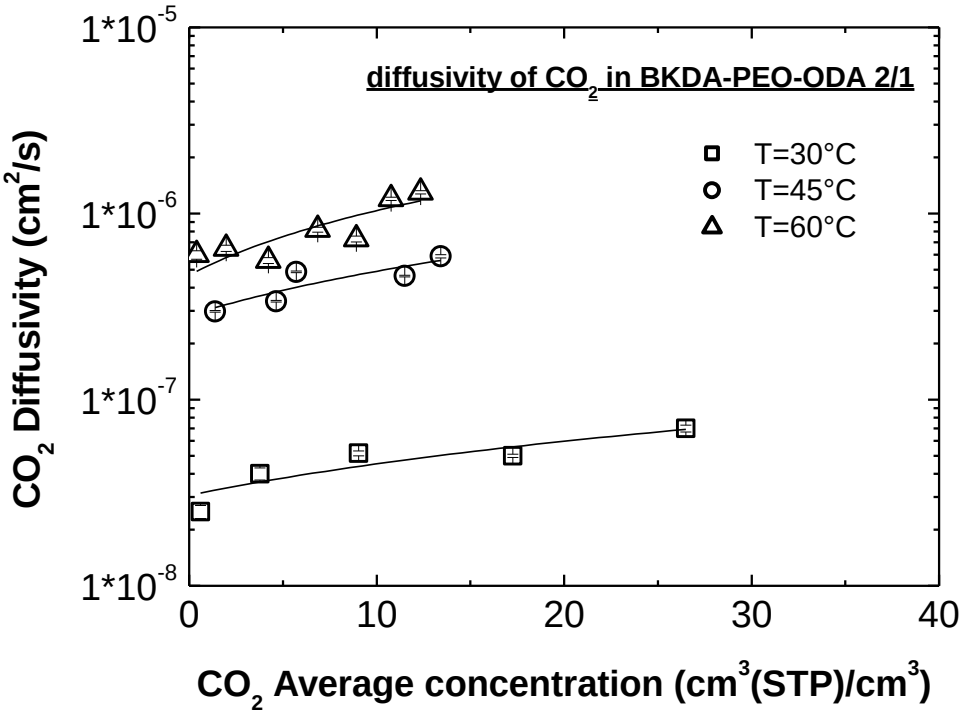

Figure 4.17: The effect of temperature on CO_2 diffusivity in BKDA-PEO6000-ODA 2/1. Solid lines are data interpolations.

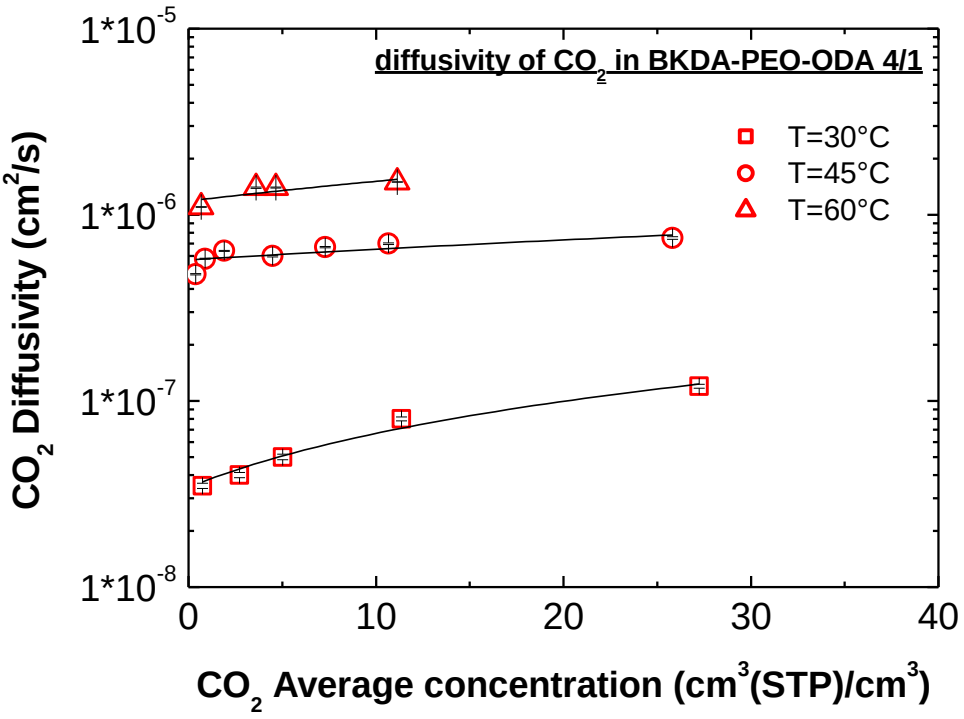

Figure 4.18: The effect of temperature on CO_2 diffusivity in BKDA-PEO6000-ODA 4/1. Solid lines are data interpolations.

Considering the variation of CO_2 solubility with membrane composition, higher effect of the rubbery PEO-phase than that observed for PPO-based copolymers is apparent from Fig. 4.19–4.21. By increasing PEO amount from 44.20 wt% to 60.40 wt% in the membrane, the solubility of CO_2 increases by 20% at 30°C, while at 45°C and 60°C solubility doubles. Moreover, the solubility isotherms of these copolymers are never concave to pressure axis, but are linear, or have positive concavity, indicating a strong effect of the PEO-based rubbery phase over the glassy one, due also to higher proportions of rubbery phase used in these copolymers.

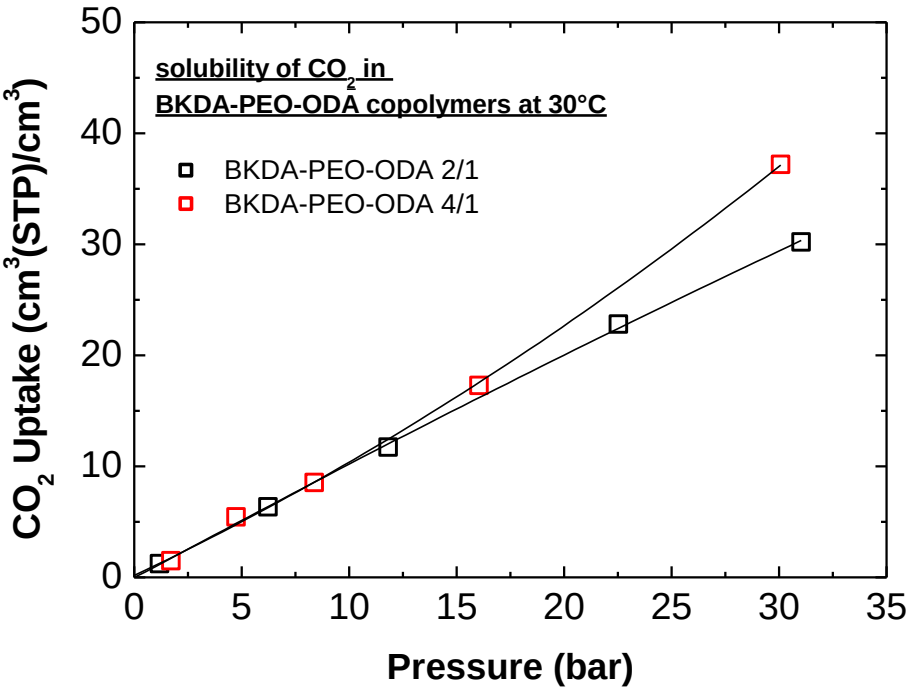

Figure 4.19: The effect of copolymer composition on CO_2 solubility in BKDA-PEO-ODA copolymers at 30°C. Solid lines are data interpolations.

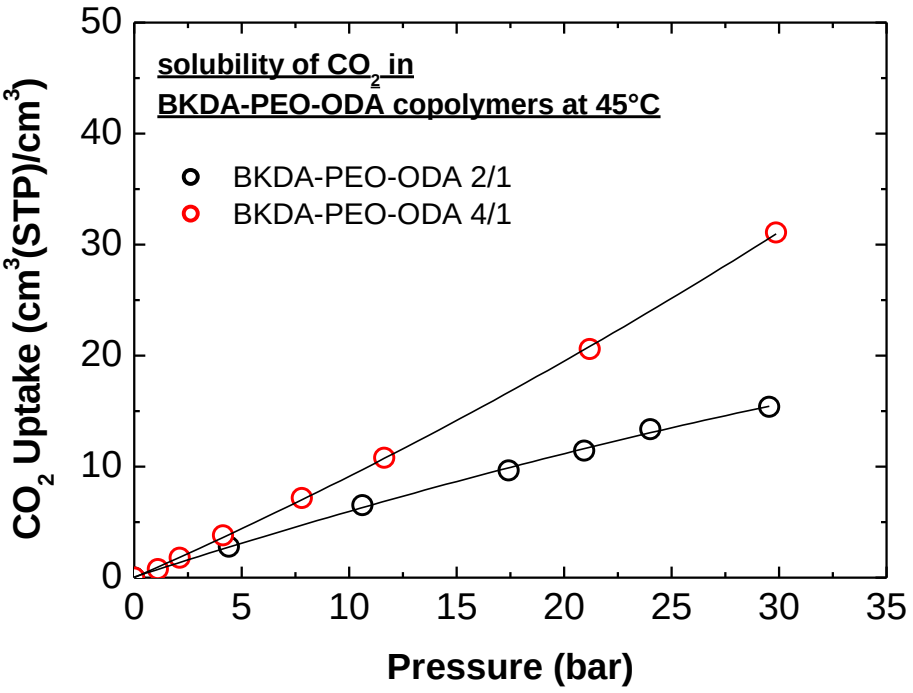

Figure 4.20: The effect of copolymer composition on CO_2 solubility in BKDA-PEO-ODA copolymers at 45°C. Solid lines are data interpolations.

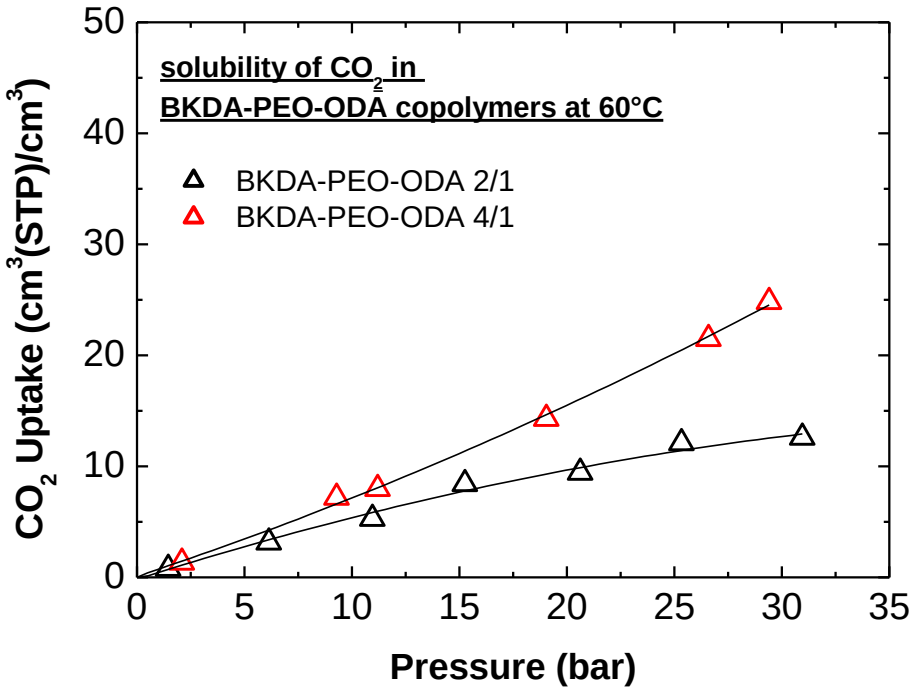

Figure 4.21: The effect of copolymer composition on CO_2 solubility in BKDA-PEO-ODA copolymers at 60°C. Solid lines are data interpolations.

The CO_2 diffusivity, reported in Figure 4.22, Figure 4.23 and Figure 4.24, increases by increasing PEO content in the membrane, although not as much as in PPO-based copolymers. In particular, all the PEO-based samples inspected have a mass fraction of PEO higher than 44 wt%, which is close to the threshold above which the PPO-based copolymers show a marked diffusivity increase.

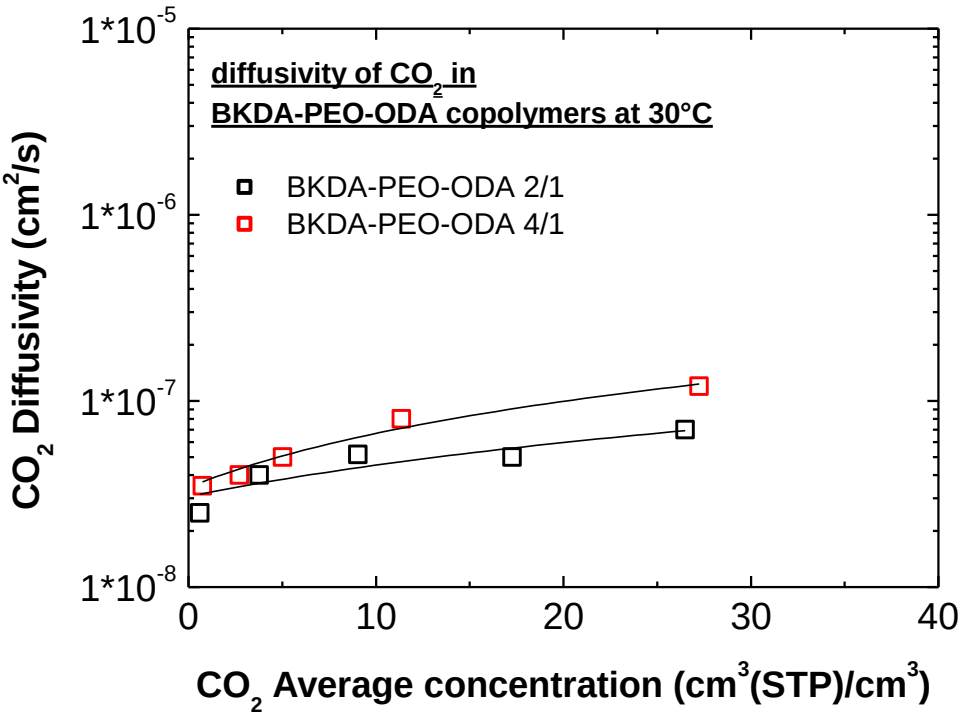

Figure 4.22: The effect of copolymers composition on CO_2 diffusivity in BKDA-PEO6000-ODA copolymers at 30°C. Solid lines are data interpolations.

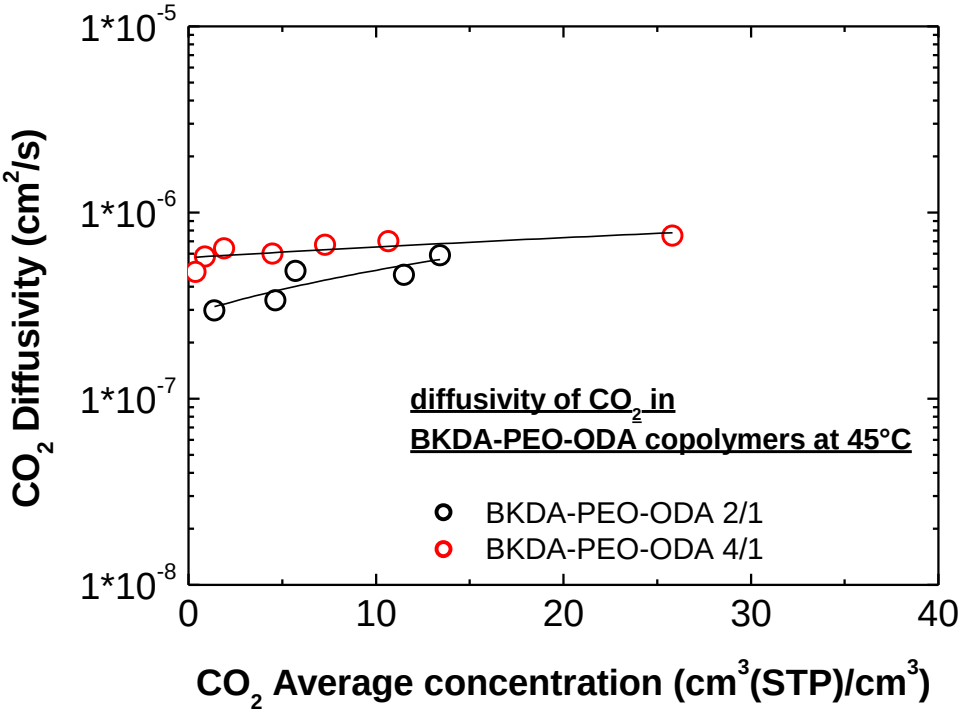

Figure 4.23: The effect of copolymers composition on CO_2 diffusivity in BKDA-PEO6000-ODA copolymers at 45°C. Solid lines are data interpolations.

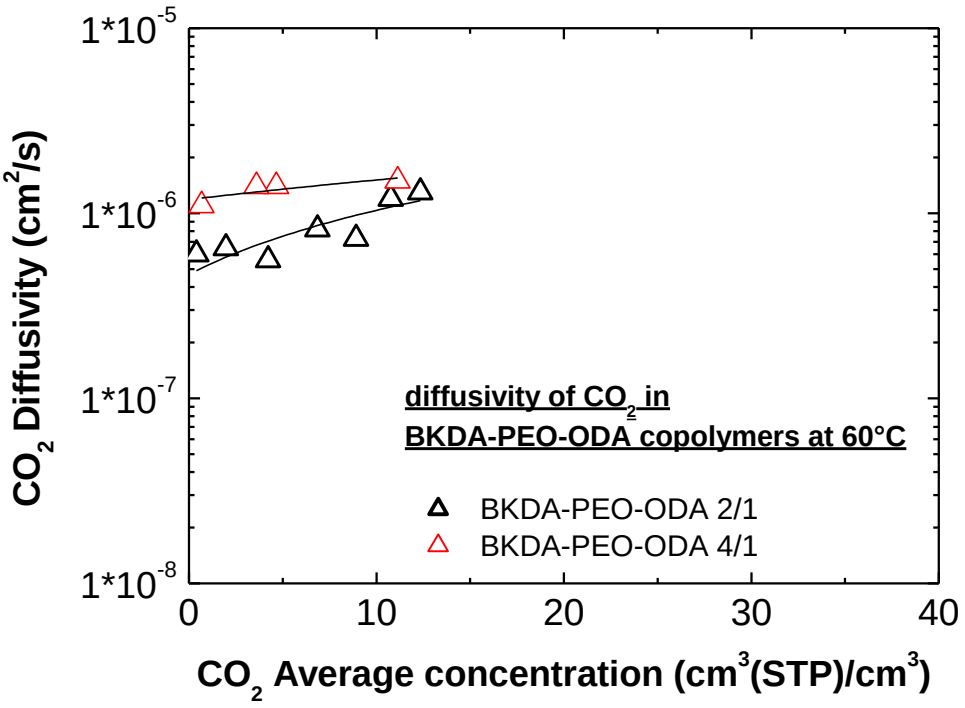

Figure 4.24: The effect of copolymers composition on CO_2 diffusivity in BKDA-PEO6000-ODA copolymers at 60°C. Solid lines are data interpolations.

Therefore in this case, the observed increase of permeability with increasing PEO content in the membrane reported in previous works is due to a simultaneous increase of solubility and diffusivity induced by the rubbery part of copolymer [13].

4.1.3 Sorption enthalpies and activation energies

The experimental data indicate that gas solubility decreases with increasing temperature in both series of copolymers, consistently with exothermic sorption. The composition of copolymers, however, affects the absolute value of the heat of absorption and consequently the dependence of solubility on temperature, as it can be seen in Figure 4.25 and Figure 4.26. For these materials sorption enthalpies increase in absolute value by increasing glassy phase content in the material, which is consistent with the higher values of sorption enthalpies normally observed in glassy phases. The values obtained are also in line with the value of -27 kJ/mol reported by Okamoto et al. [138] for pure BPDA-ODA, as well as with the value

of -16.1 kJ/mol for pure PPO calculated from the data presented in ref. [139] and with $\Delta H_S = -15$ kJ/mol for PEO, based on the data of ref. [140]. The sorption enthalpy is the sum of condensation and mixing effects: in the charts we have provided, as an indication, the condensation enthalpy of CO_2, so that the distance from this horizontal line quantifies the heat of mixing. The absolute values of sorption enthalpy decreases with increasing amount of rubbery phase on both set of copolyimides, falling approximately between the extreme values given by the sorption enthalpies of CO_2 in the two pure homopolymers. Rubbery polymers are usually characterized by lower absolute values of gas sorption enthalpy with respect to glassy polymers, due to the presence of the additional free volume in the glassy state, which does not require the deformation energy to accommodate sorbed molecules. However, CO_2 sorption in rubbery polyethers is somehow peculiar because CO_2 interacts favorably with the polymer chain, giving rise to negative mixing enthalpies, that sum with the condensation enthalpy of CO_2 [141] and produce sorption enthalpy values which are generally higher, in absolute values, than those of non polar rubbers.

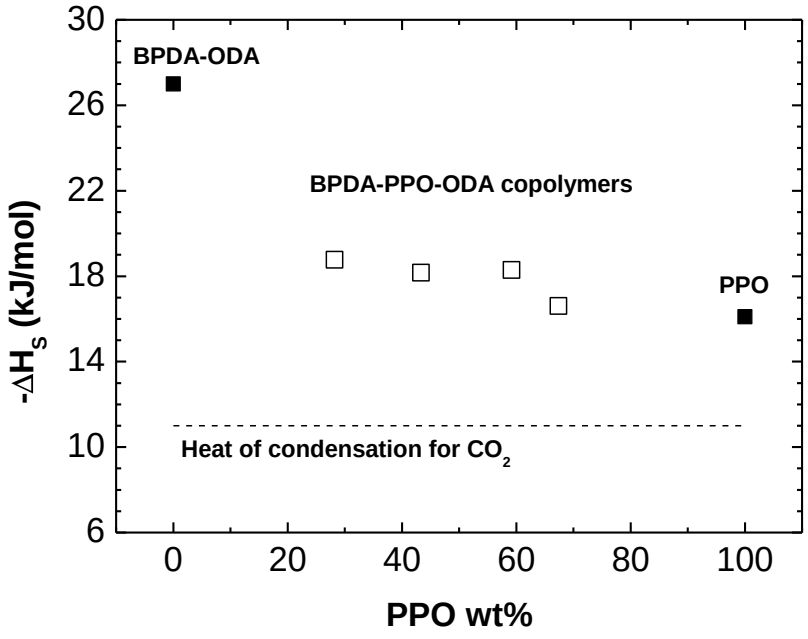

Figure 4.25: The effect of copolymer composition on sorption enthalpies in BPDA-PPO-ODA copolymers.

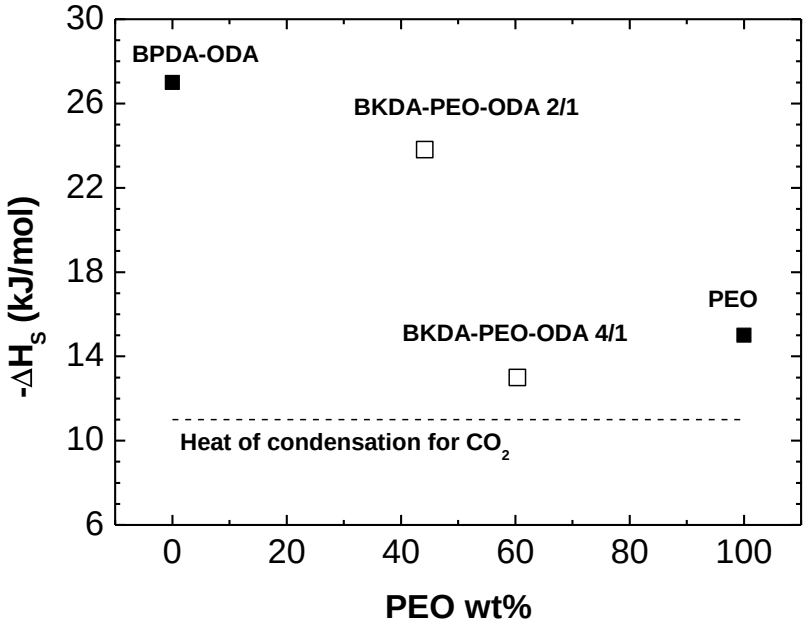

Figure 4.26: The effect of copolymer composition on sorption enthalpies in BKDA-PEO-ODA copolymers.

For PPO copolymers diffusivities follow Arrhenius type behavior in the entire range of temperature 30-60°C; on the contrary for PEO copolymers a sort of transition seems to occur between 35 and 45°C, which is consistent with data of permeability versus temperature reported in ref [13].

Activation energies for diffusion process in both series of copolymers are reported in Figure 4.27.

The value of E_D measured in PEO copolymers, is at least double than the corresponding values measured in PPO copolymers at fixed CO_2 concentration. This difference may be related to the different glass transition temperature of the polyethers (203 K for PPO [12] and 250 K for PEO [142]): according to van Krevelen [143] the value of E_D for rubbery polymers increases with their T_g, while glassy polymers show the opposite behavior. For PPO copolymers, E_D decreases with increasing rubbery phase content, consistently with the fact that the rubbery phase is more flexible and mobile than the glassy one. On the other hand, in

PEO-based copolymers the behavior with composition is reversed: however it must be said that in such case the error can be rather high, and that the crystalline content of the copolymer may increase with the amount of PEO, giving rise to higher energetic barrier for diffusion. For crosslinked PEO a value equal to 52 kJ/mol has been reported,[144] while no value for pure PPO or BKDA-ODA is available.

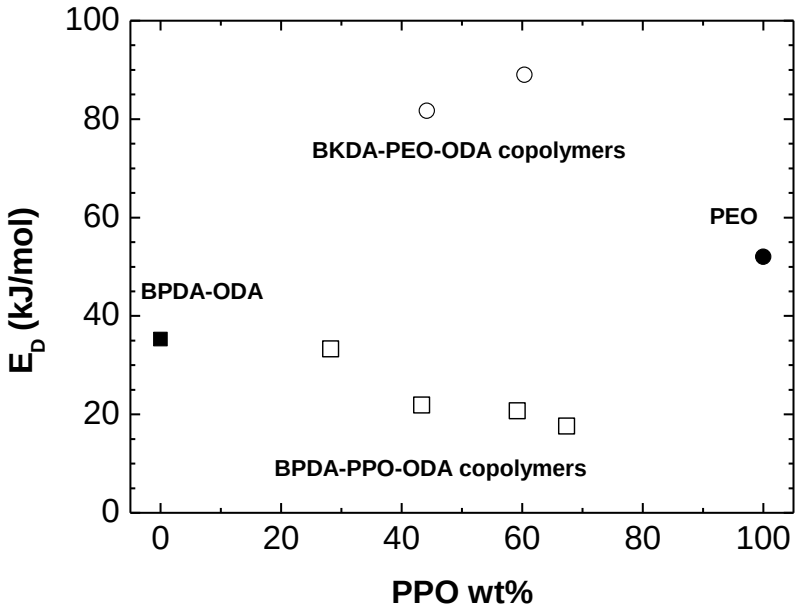

Figure 4.27: Activation energy for diffusion in BPDA-PPO-ODA and BKDA-PEO-ODA copolymers.

4.1.4 Permeability calculation

As usual the permeability of gases and vapors can be calculated from diffusivity and solubility data collected during sorption steps. The permeability of CO_2 in both series of copolymers has been calculated by the solution-diffusion model, with equation 1.3.

To this aim the permeability associated to a differential step in transmembrane pressure has been calculated; that enables to use the local diffusivity value at the local concentration prevailing in the film, and requires, on the other hand, the use of the local solubility coefficient, $\Delta c_i/\Delta p_i$, as one immediately recognizes from the definition of permeability.

Considering subsequent sorption steps k and k+1, the permeability has been calculated with equation 4.1:

$$P_i = D_i \cdot S_i = D_i \frac{c_i^{k+1} - c_i^k}{p_i^{k+1} - p_i^k} \tag{4.1}$$

In particular data are reported at constant temperature, as a function of copolymer composition, and as well as the case of diffusivity data, it can be observed a sharp transition from glassy like to rubbery like transport characteristics. For copolymers of BPDA-PPO-ODA the permeability increases with polyether content from 5 Barrer in the sample 1/1 up to 1700 Barrer in the sample 6/1 at 30°C and any plasticization seems to occur at high CO_2 pressure up to 30 bar. In particular the permeability trend at all temperatures, reproduces the trend observed for diffusivity, and the increase of diffusion coefficient, due to the increasing amount of rubbery phase, leads to the enhancement of copolymers permeability, as it can be seen in Figures 4.28–4.30.

Also in the case of BKDA-PEO-ODA copolymers the permability increases with polyether content as it is reported in Figures 4.31–4.33. In this case as explained in previous section both solubility and diffusivity seem to affect the enhancement of CO_2 permeability with PEO content. In particular lower permeabilities can be observed than in the case of PPO copolymers at high rubbery phase content, maybe because of PEO crystalline fraction which can hinder the permeation through the membrane and lower free volume of PEO copolymers as it will be observed in the modeling section.

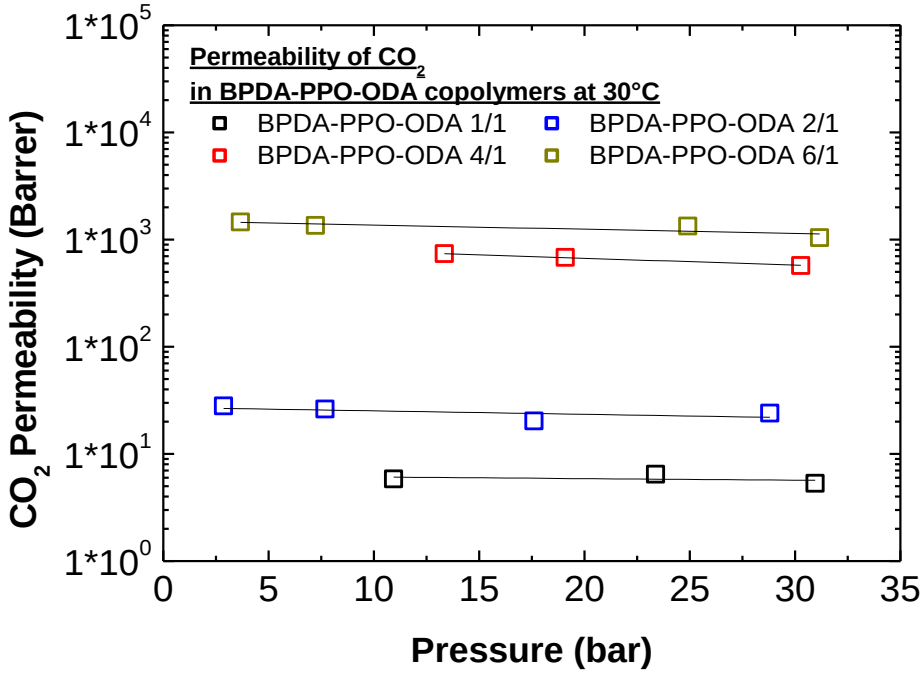

Figure 4.28: The effect of copolymer composition on CO_2 permeability in BPDA-PPO4000-ODA copolymers at 30°C.

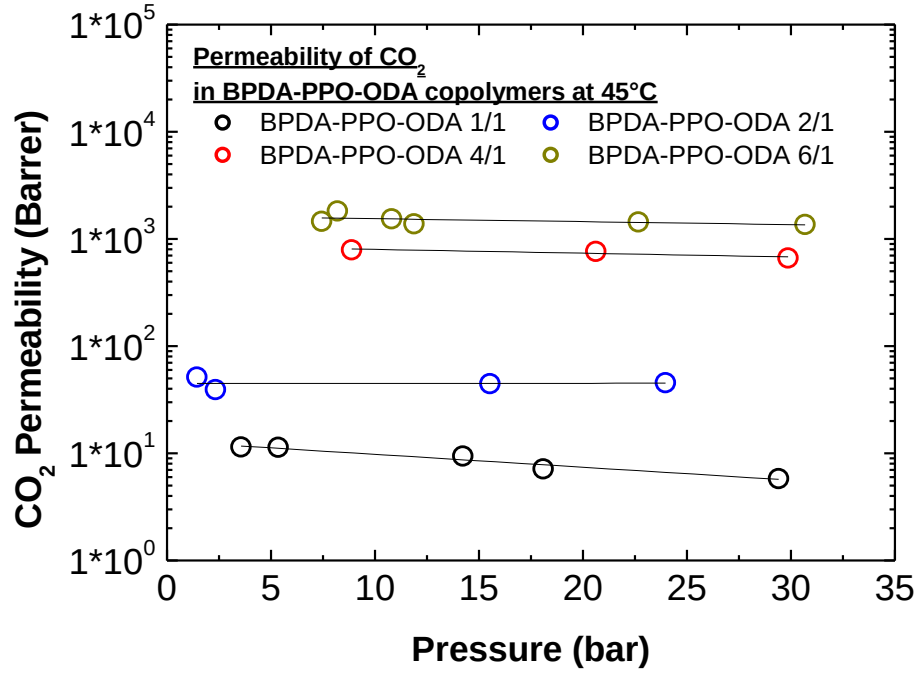

Figure 4.29: The effect of copolymer composition on CO_2 permeability in BPDA-PPO4000-ODA copolymers at 45°C.

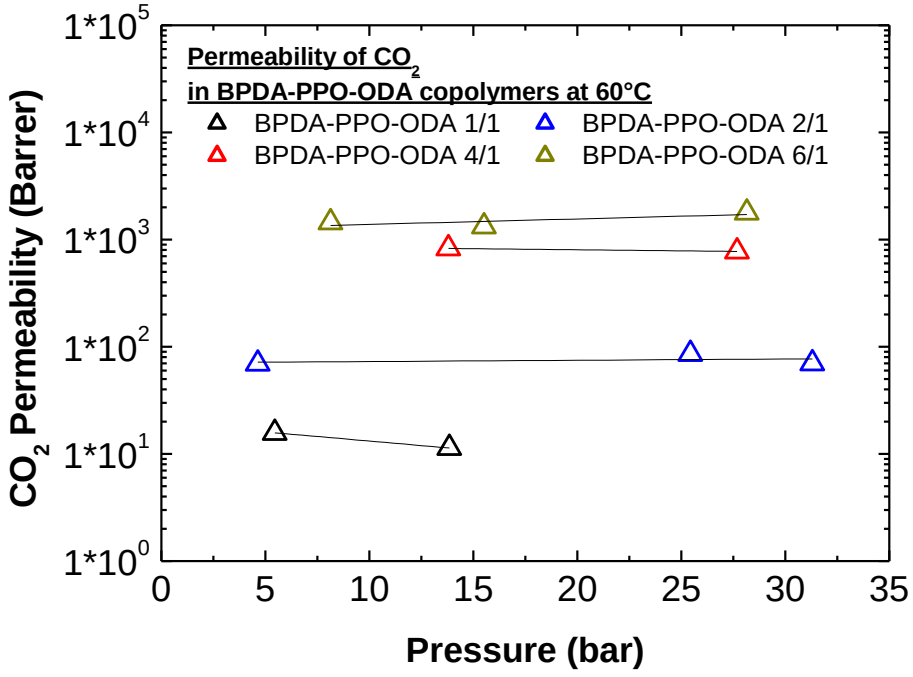

Figure 4.30: The effect of copolymer composition on CO_2 permeability in BPDA-PPO4000-ODA copolymers at 60°C.

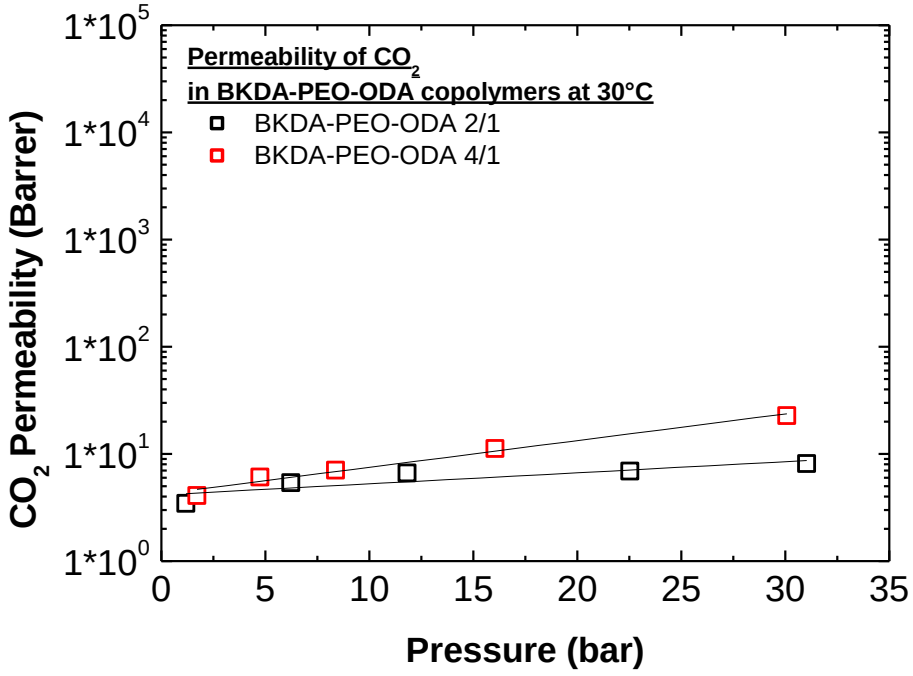

Figure 4.31: The effect of copolymer composition on CO_2 permeability in BKDA-PEO6000-ODA copolymers at 30°C.

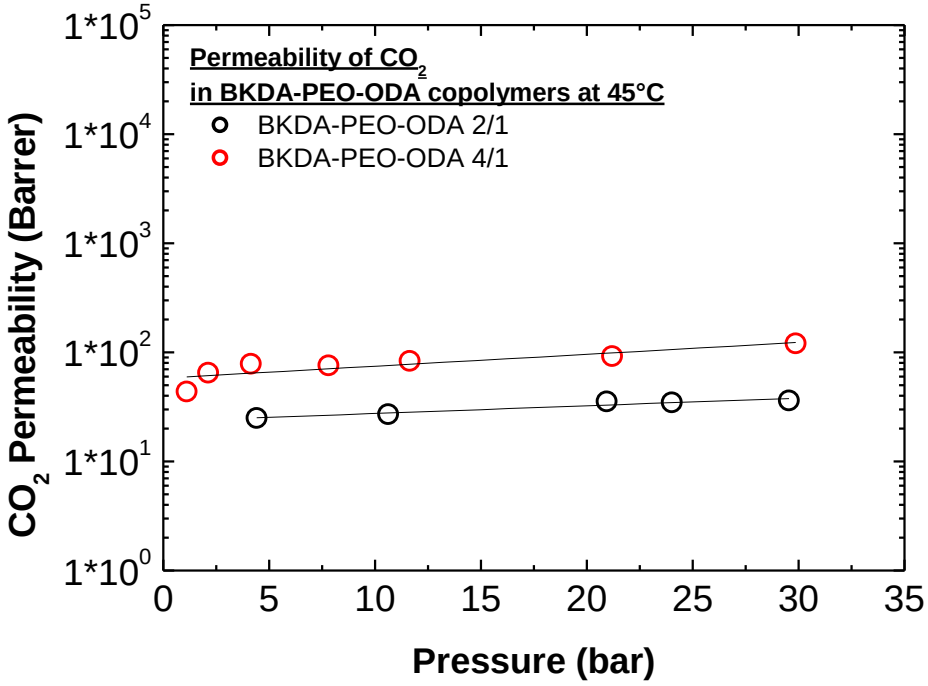

Figure 4.32: The effect of copolymer composition on CO_2 permeability in BKDA-PEO6000-ODA copolymers at 45°C.

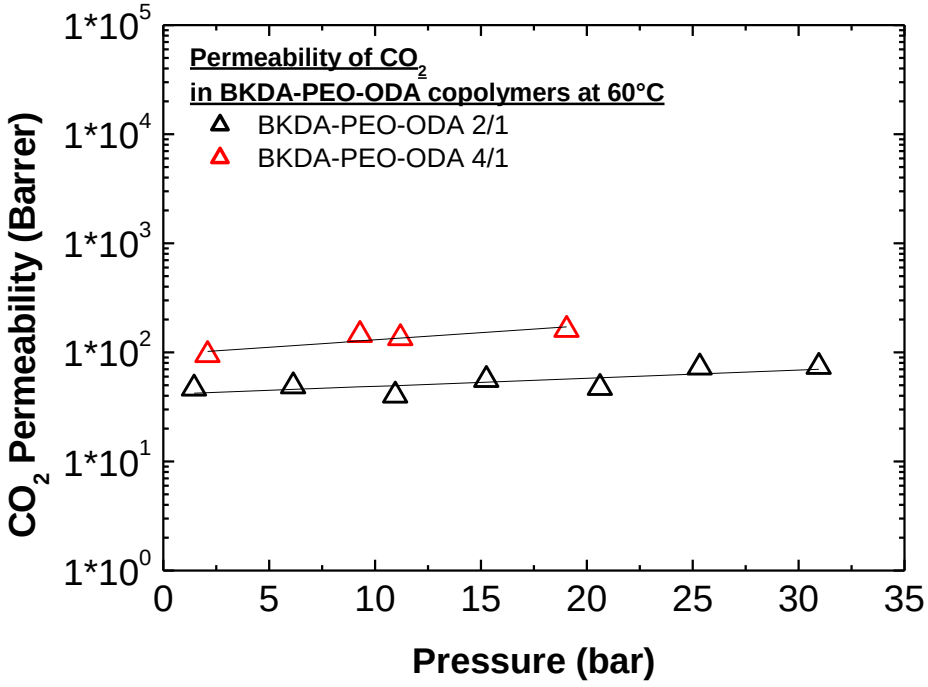

Figure 4.33: The effect of copolymer composition on CO_2 permeability in BKDA-PEO6000-ODA copolymers at 60°C.

4.1.5 Effect of water vapor

The solubility of water vapor has been studied for two samples, BPDA-PPO-ODA 2/1 and BKDA-PEO-ODA 4/1, for which solubility isotherms are reported at 30°C in Figure 4.34. These two materials contain 43.34 wt% and 60.40 wt% of polyether phase concentration respectively [12,13], and from water solubility data it is possible to observe how PEO based copolymer is more hydrophilic than PPO based one. In particular this behavior should not be addressed to polyether phase, due to similarity of their water vapor sorption isotherms at 30°C. The higher hydrophilicity of BKDA-PEO-ODA sample should be addressed to higher water uptake capacity in the glassy phase. From Figure 4.35 it is evident that PEO and PPO have practically the same sorption isotherm, ref. [145], while high differences can be observed for the two polyimides, and in particular BKDA-ODA shows solubility which is three fold the solubility of BPDA-ODA at high water activity [146,147]. This aspect was explained by Han et al. [148] considering that BKDA dyanidride shows higher affinity to water than BPDA, due to additional carbonyl group present in the backbone. In addition solubility isotherms of copolymers are slightly higher than pure polyimides, confirming the idea that both phases contribute to the total penetrant uptake.

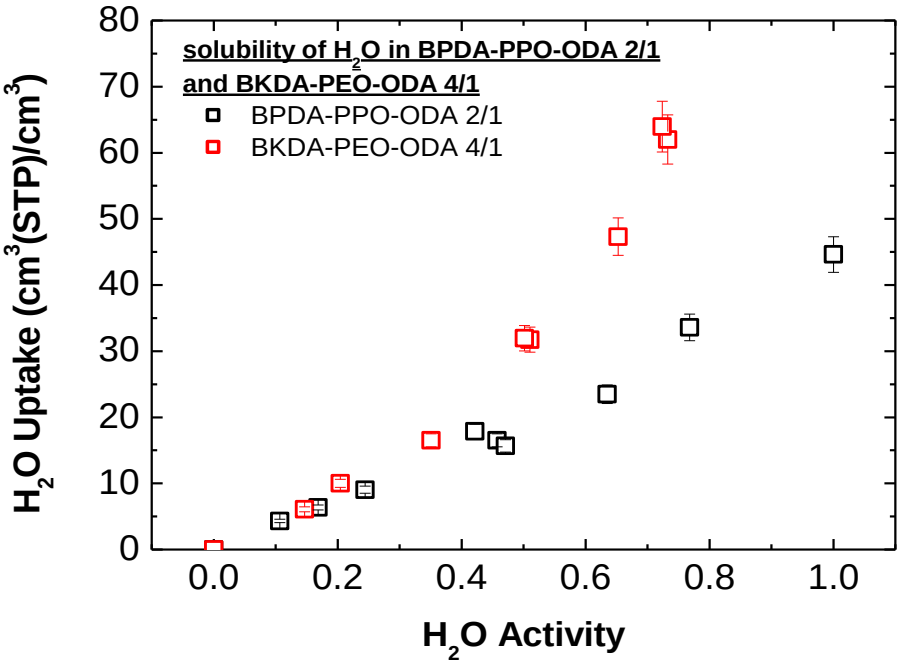

Figure 4.34: Solubility of water vapor in BPDA-PPO-ODA 2/1 and BKDA-PEO-ODA 4/1 copolymers at 30°C.

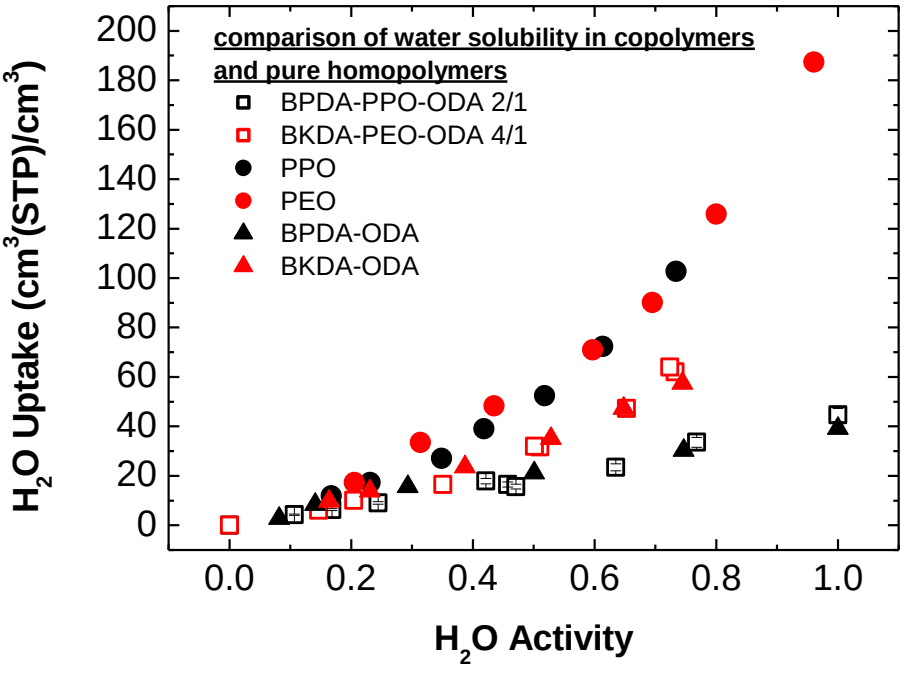

Figure 4.35: Comparison of water solubility in copolymers and pure homopolymers at 30°C. Data for pure PPO, PEO are from ref.[145], BPDA-ODA [146] and BKDA-ODA [147].

The effect of water vapor has been monitored also with humid permeation experiments with CO_2 and N_2 for BPDA-PPO-ODA 2/1 sample at 30°C and 1 bar upstream pressure, up to 75% relative humidity. In dry condition it can be said that, due to higher condensability and lower kinetic diameter than N_2, CO_2 has higher permeability, 30.1 Barrer, than N_2, whose permeability is 1.3 Barrer. As expected and already reported [12], the material is CO_2 selective and its ideal selectivity is equal to 23. The presence of water causes a decrease of the permeability with respect to pure gases values, and it can be due to competitive sorption. In particular water, which is more soluble due to higher condensability than N_2 and CO_2, competes for sorption sites in the polymeric matrix, leading to a reduction gases permeability. Anyway from results reported in Figures 4.36 and 4.37 it is evident that the polyether phase present in the copolymer reduces the negative effect of water on permeability, usually observed for glassy polyimides [70,71]. In particular the permeability decrease with respect to dry gases values is around 12% and 17% for N_2 and CO_2, respectively, at 70% relative humidity and it is a limited reduction compared with 50% reduction of dry gas permeability obtained in Matrimid films.

Finally the data of permeability of dry CO_2 obtained from permeation experiments matches with the one calculated at approximately 3 bar from the solution diffusion theory (28 Barrer), reported in Fig. 4.28. This result should confirm the validity of solution-diffusion mechanism in such kind of polymeric membranes.

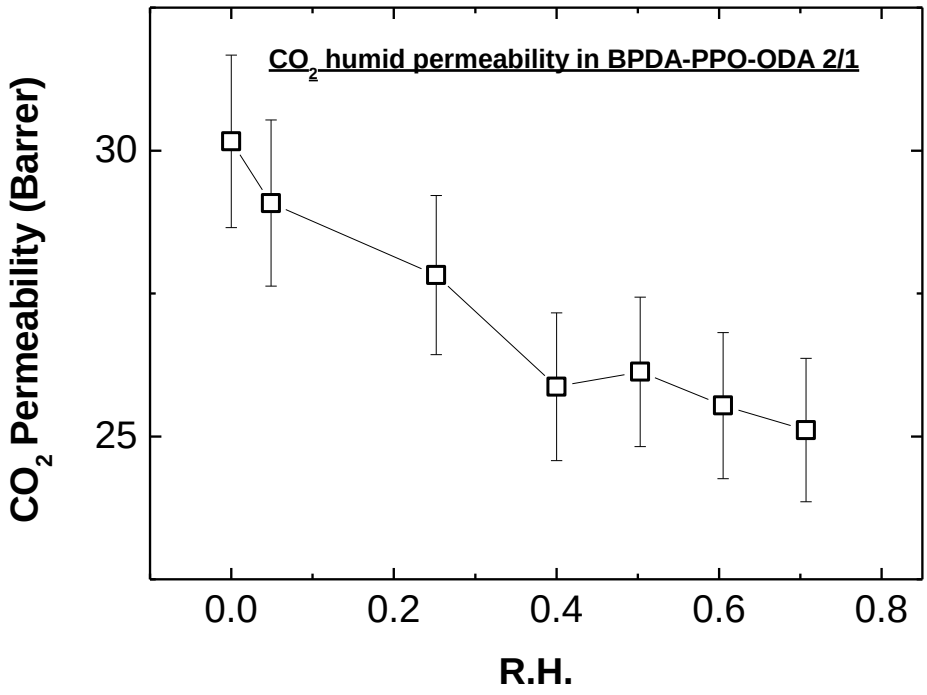

Figure 4.36: The effect of relative humidity on CO_2 permeability at 30°C and 1 bar upstream pressure in BPDA-PPO4000-ODA 2/1 copolymer.

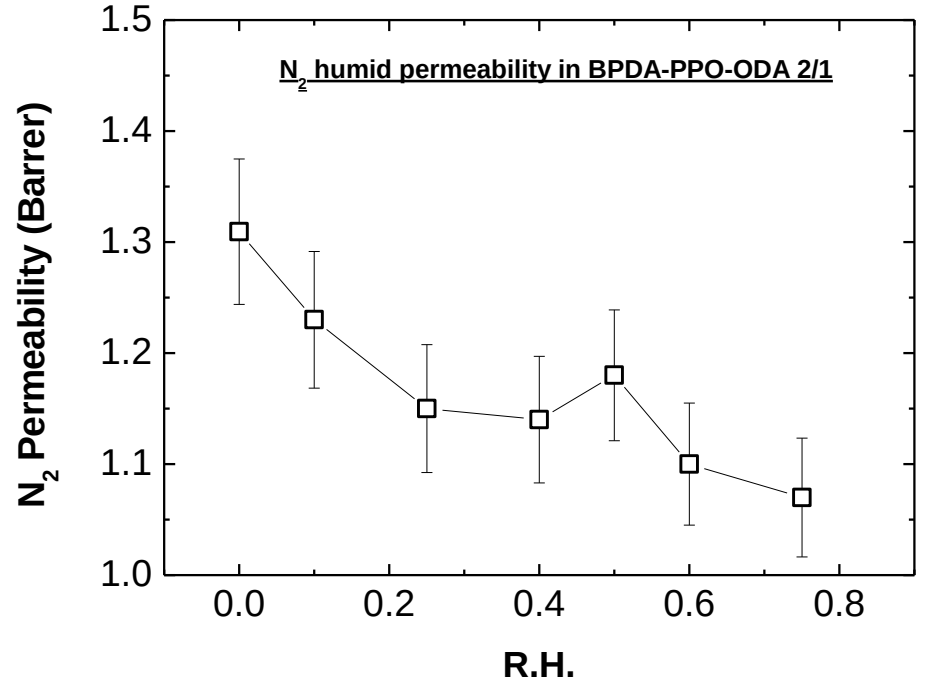

Figure 4.37: The effect of relative humidity on N_2 permeability at 30°C and 1 bar upstream pressure in BPDA-PPO4000-ODA 2/1 copolymer.

The permeability decrease of the gases considered is similar, as shown in Figure 4.38, where the ratio of the humid gas permeability and dry gas permeability is reported as a function of relative humidity. Interestingly the same behavior is observed for N_2 and CO_2, which is a plasticizer penetrant for polyimides and is more soluble in water than N_2.

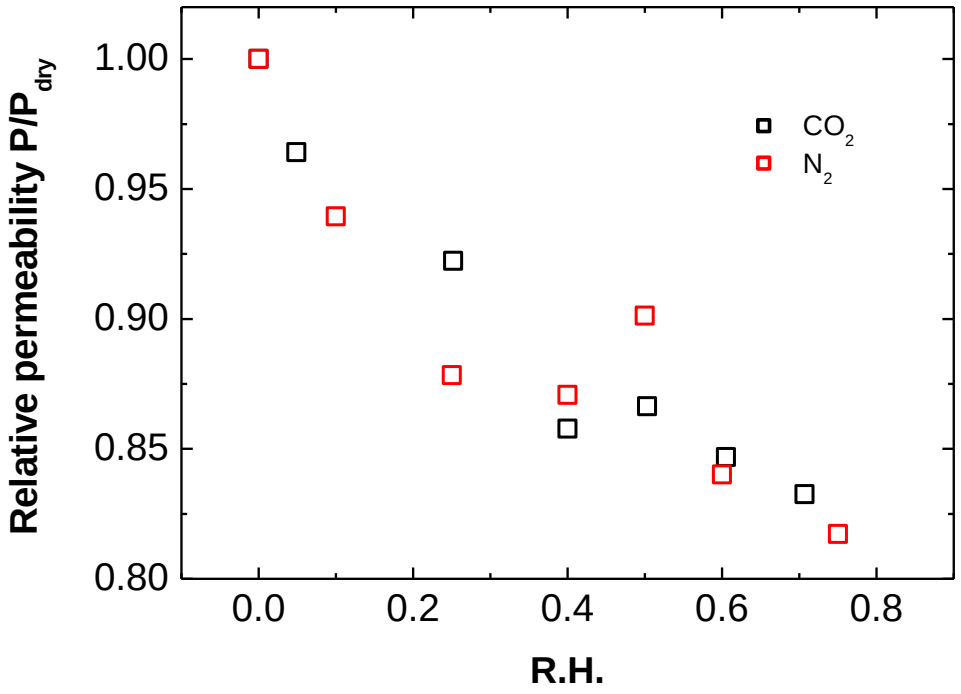

Figure 4.38: The effect of relative humidity on BDPDA-PPO4000-ODA 2/1 permeability: comparison between CO_2 and N_2 relative permeability variation.

Finally, the Robeson plot is reported for the couple of gases considered. Consistently with what observed in the previous graph, the humid gas ideal selectivity is almost constant in the range of water activity inspected while permeability of CO_2 decreases, moving to the left of the Robeson bound.

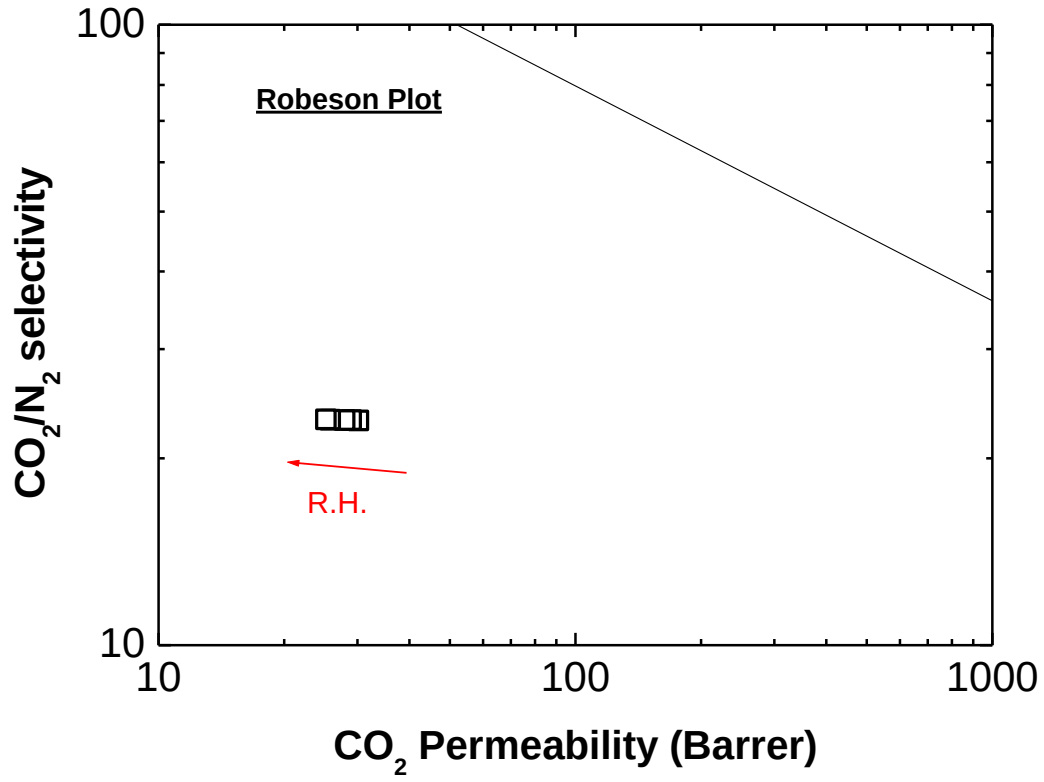

Figure 4.39: BPDA-PPO4000-ODA 2/1 in dry and humid conditions and Robeson Plot for CO_2/N_2.

4.2 PTMSP /Graphenic filler based Mixed Matrix Membranes

The gases permeabilities of the membranes were tested at 30°C with a closed volume, variable pressure permeometer, applying an upstream pressure of about 1.3 bar and vacuum on the downstream side. The permeability tests have been carried out following a chronological order that reasonably allows to avoid conditioning effects on the membranes, starting with the gas that induces lower swelling and proceeding as follows : 1) He, 2) N_2, 3) CH_4, 4) CO_2.

The value of permeance (permeability/thickness) calculated with the apparatus used in this work is affected by an error of ±5%, that is mainly due to uncertainty on the downstream volume and permeation area values, while the error on pressure is negligible. The permeability value is also affected by the uncertainty on the membrane thickness, which depends on the sample considered, as reported in Figure 1. The error on ideal selectivity of a single sample is negligible, because such value is unaffected by downstream volume, permeation area and membrane thickness values as is clear from Eq. (4). The error on the other calculated values was estimated using the laws of error propagation.

4.2.1 Characterization of thick PTMSP membrane

It is well known that preparation protocol affects history of glassy polymers and thus their excess free volume and transport properties. It is well known that the rate of solvent evaporation during film casting is an important parameter which is not easy to control.

In this work four thick film membranes of pure PTMSP have been casted and characterized with pure gases permeation experiments of He, N_2, CH_4 and CO_2. This is to verify the repeatability and reliability of pure PTSMP data, which is an important parameter to observe the effect of fillers on ageing and transport properties. In particular films with thickness ranging from 56 up to 183 μm have been obtained. They can be reasonably considered as bulky materials and thus their properties, as permeability and ageing rate, should not depend

on the value of the thickness. In particular the value of initial permeability can be affected by evaporation rate of the solvent during film casting, leading to slight differences on free volume and on permeability values. The permeability of the four gases has been measured repeatedly for 3 days for the sample with 66 μm thick, for 5 days for the sample 56 μm thick, for 7 days for the sample 183 μm thick and for 9 months for the sample 115 μm thick. In table data of average solvent evaporation rate are reported for each PTMSP sample considered. Results of permeabilities of fresh PTMSP samples are reported in Figures 4.40–4.43 and it can be observed that a trend can be established between initial permeability value and solvent evaporation rate. In particular for all the gases considered the permeability of PTMSP increases monotonously with the rate of evaporation, and it is reasonable because increasing the velocity, the material will be characterized by higher number of voids characterized by bigger dimension with respect to the case of slow evaporation.

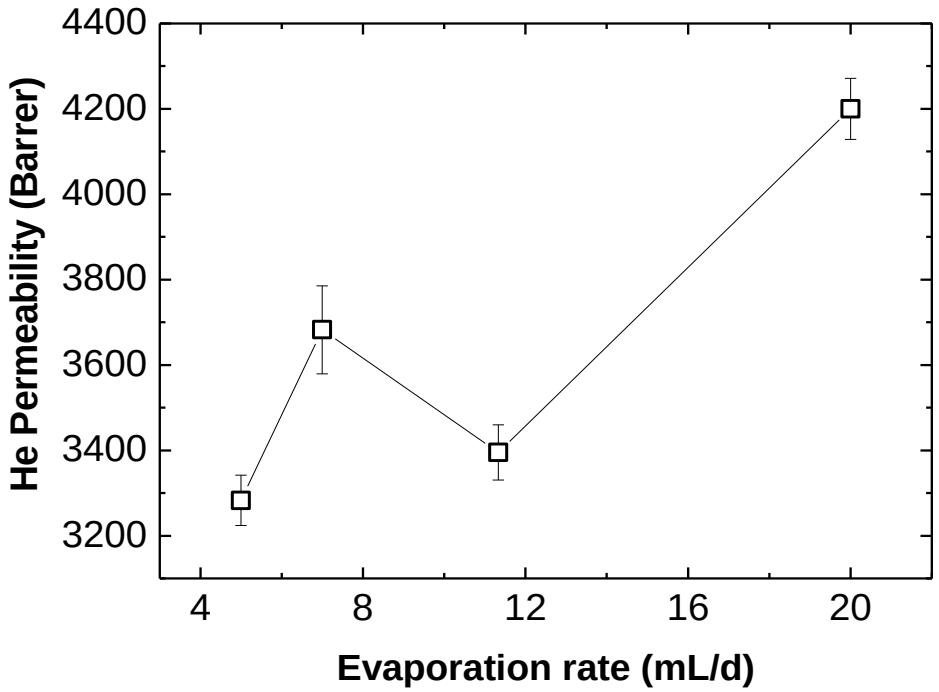

Figure 4.40: The effect of solvent evaporation rate on He fresh PTMSP permeability at 30°C.

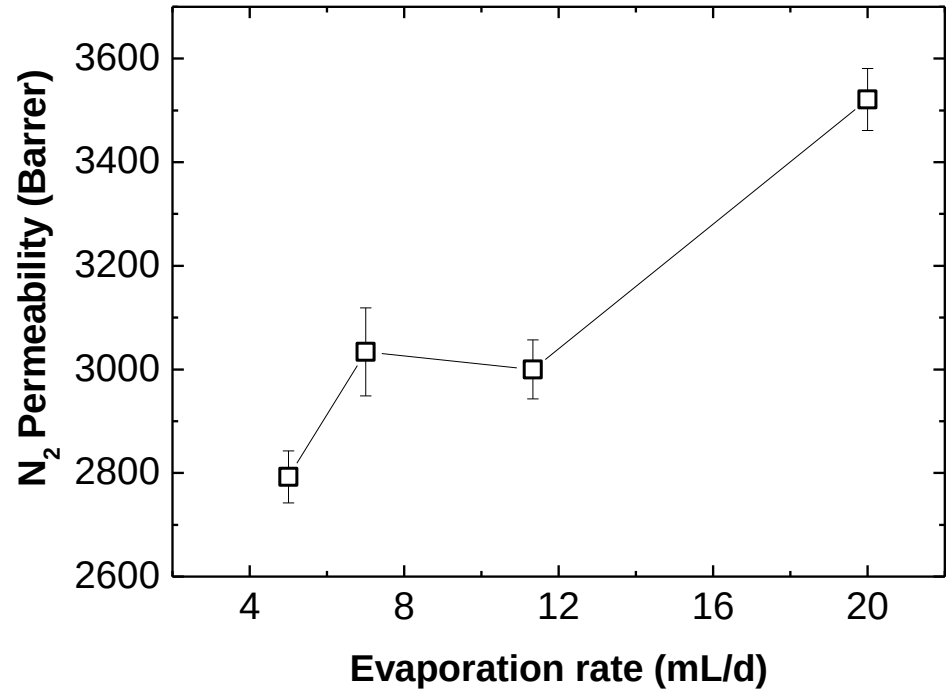

Figure 4.41: The effect of solvent evaporation rate on N_2 fresh PTMSP permeability at 30°C.

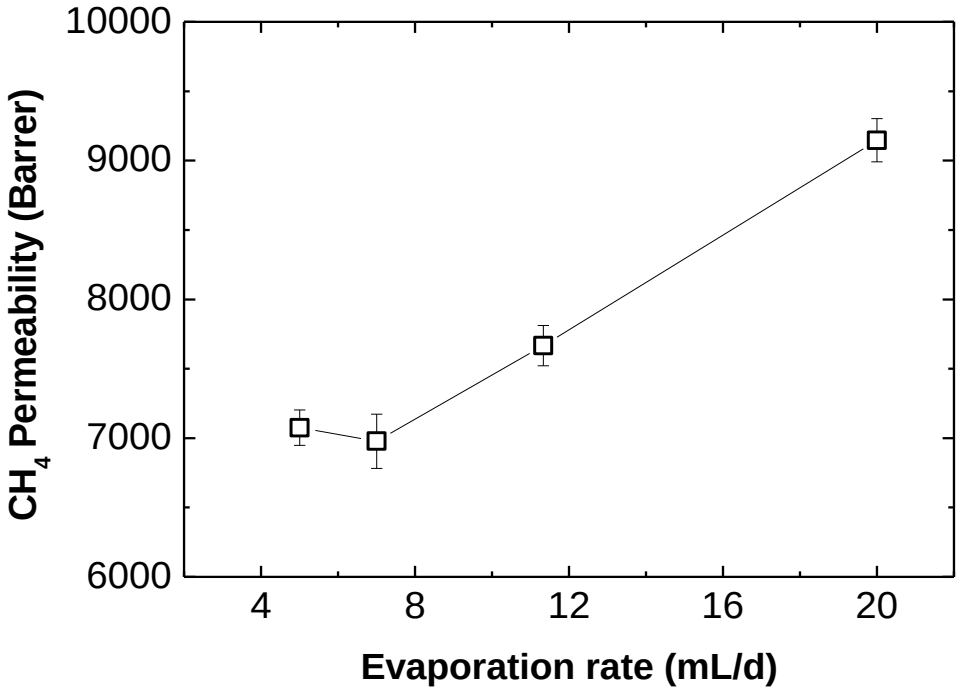

Figure 4.42: The effect of solvent evaporation rate on CH_4 fresh PTMSP permeability at 30°C.

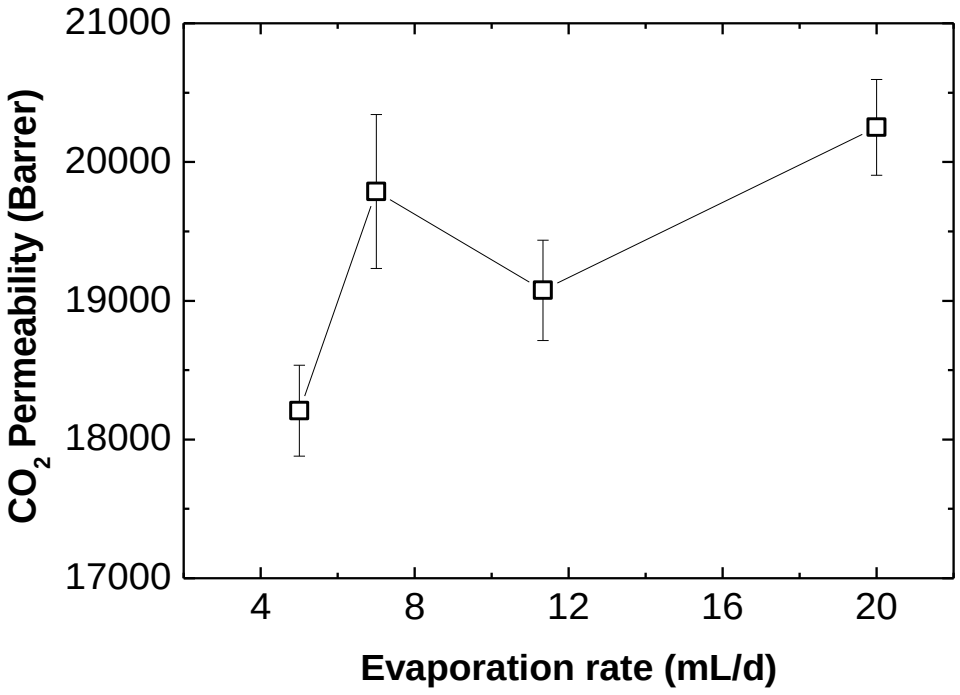

Figure 4.43: The effect of solvent evaporation rate on CO_2 fresh PTMSP permeability at 30°C.

For all the membranes inspected it has been observed that $P_{CO_2} > P_{CH_4} > P_{He} > P_{N_2}$, i.e. that, with the exception of Helium, the permeability increases systematically with the gas critical temperature. Such behavior indicates that the gas permeability in PTMSP-based membranes is strongly affected by the solubility value. In Figure 4.44 the gas permeability data of the sample with 115 μm of thickness versus the penetrant critical temperature T_C, that is a measure of penetrant condensability. The trend is not followed by Helium because such gas is much smaller than the other ones and compensates its low condensability with an extremely high diffusivity value.

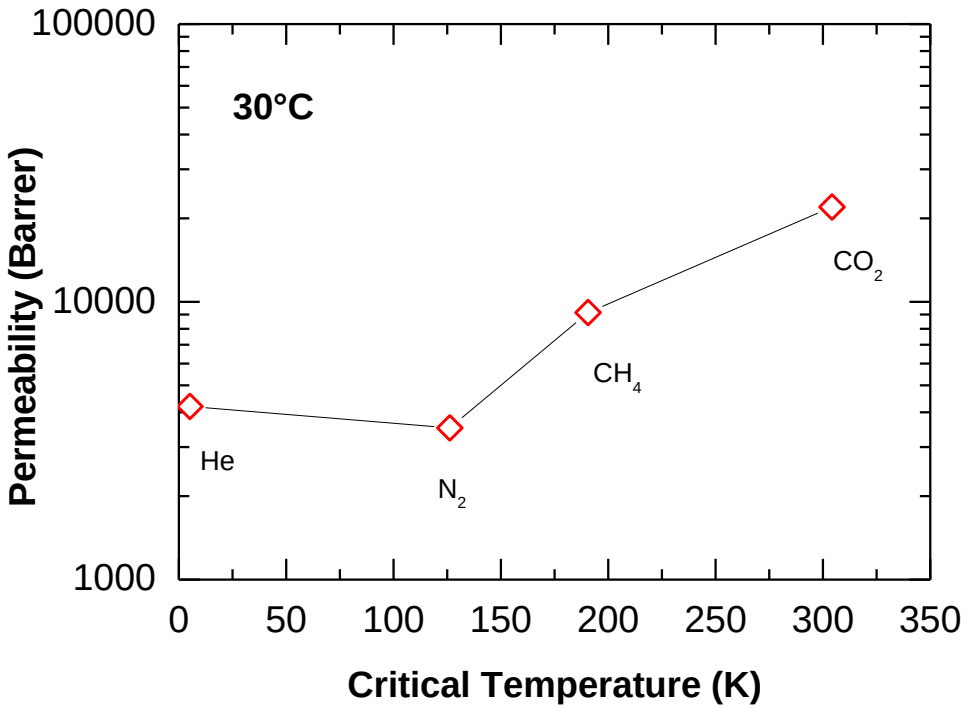

Figure 4.44: Correlation of PTMSP permeability with penetrant critical temperature for the sample with 115μm thickness.

The reproducibility of the results obtained is testified by ageing data. In particular it can be observed from Figures 4.45–4.48 that all the four PTMSP film shows similar behavior during ageing for the gases considered, and it testify that small variation of initial permeability does not change the ageing behavior of thick PTMSP membranes, whose relaxation time is higher than the observation one.

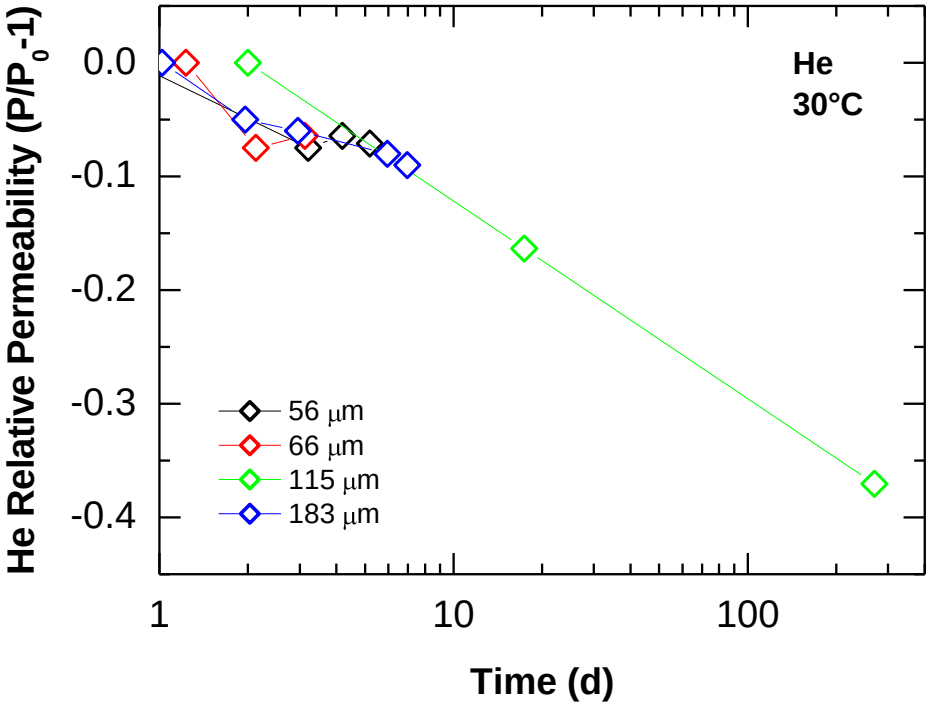

Figure 4.45: He relative permeability variation with time for different PTMSP thick samples.

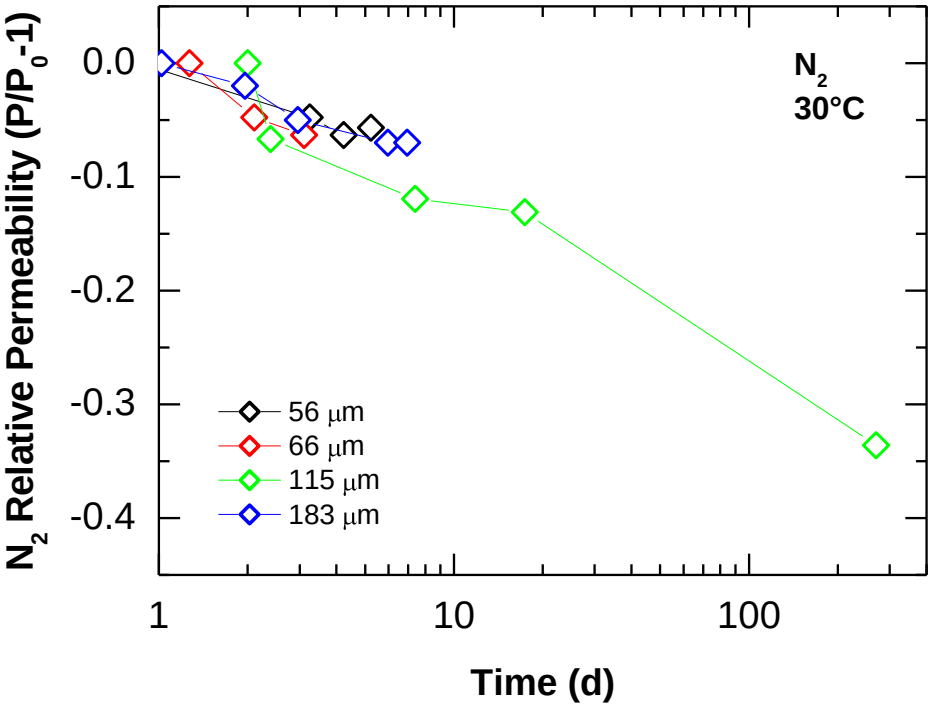

Figure 4.46: N_2 relative permeability variation with time for different PTMSP thick samples.

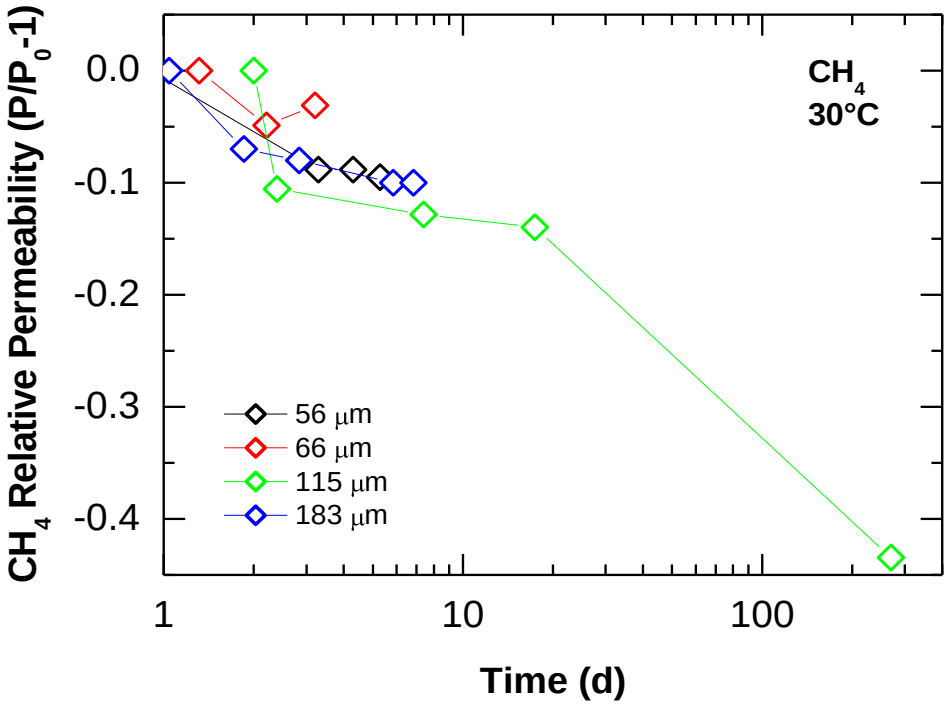

Figure 4.47: CH_4 relative permeability variation with time for different PTMSP thick samples.

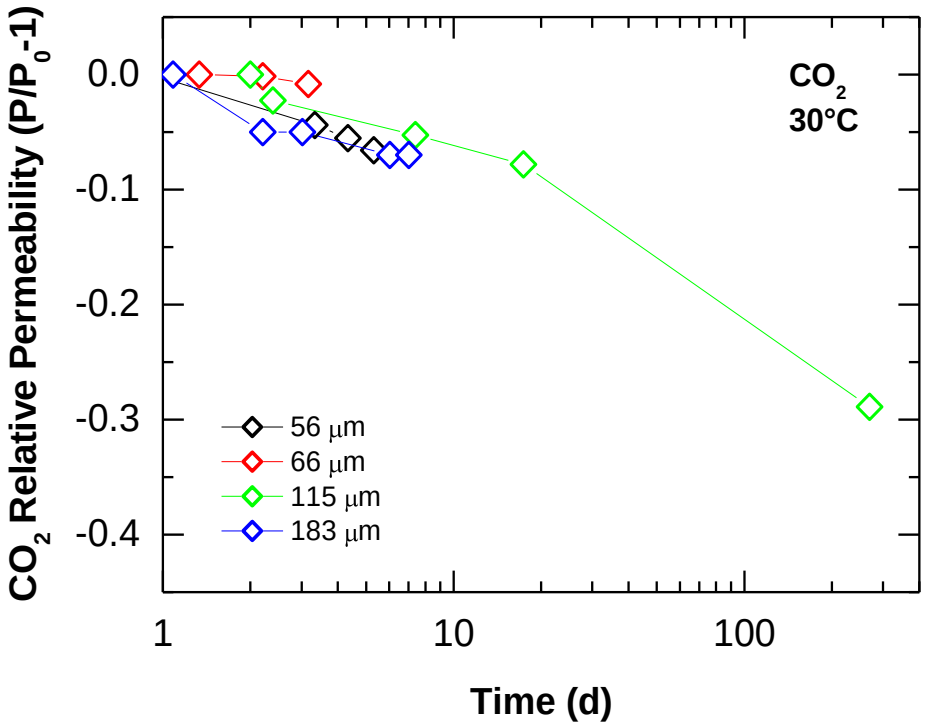

Figure 4.48: CO_2 relative permeability variation with time for different PTMSP thick samples.

Considering the ageing response for the different gases tested, it can be observed that PTMSP shows different behavior with different gases. This aspect is interesting and is in line with results reported by Consolati et al. [149] who experimentally monitored ageing in PTMSP through PALS analysis in 100 μm thick membranes films. They observed that PTMSP is characterized by a bimodal distribution of free volume and that the mean radius of small holes is 0.45 nm and the mean radius of large holes population is 0.75 nm. After 60 days of physical ageing they observed that the size of the small volume population is subject to a slight reduction of the number of voids and a big variation, around 19% (from 0.45 nm to 0.37 nm) of mean radius of the holes, on the other hand number of holes of the large volume population decreases of 20% while its size remain practically constant. In light of this, data of fig. can be explained. The CO_2 permeability decrease in PTMSP after 9 months is equal to -29% while N_2, He and CH_4 permeability decrease is about -34%, -37% and -44% respectively. The permeability of CO_2 is more affected by solubility than diffusivity, and consequently less influenced by free volume reductions due to ageing. He and N_2, with kinetic diameter of 2.6 and 3.4 Å respectively, have sizes which are lower than the aged mean radius of small holes reported by Consolati et al. [149], and show similar physical ageing. Finally, CH_4 is the bigger penetrant considered and more affected by free volume variation. For the sake of clarity and because it has been deeply investigated during time, only data obtained for the sample with thickness of 115 μm are reported but similar behavior can be observed for all the samples.

4.1.2 The effect of fillers on Permeability and selectivity of fresh PTMSP

Mixed matrix membranes based on PTMSP and graphene fillers have been obtained practically with the same evaporation rate of the sample with 115 μm. The average solvent evaporation rate for these membranes is 20 mL/d and their results have to be compared with a

membrane characterized by the same drying velocity, to see the effect of fillers on permeability and selectivity.

In Figure 4.49 it is reported the effect that the fillers addition has on the fresh membrane permeability. In particular, it can be observed that the addition of GO enhances the permeability of PTMSP to all gases, even if the variation induced is within the confidence interval of the measured PTMSP permeability. On the other hand, the addition of graphene fillers lowers the gas permeability of PTMSP: while the variations induced by the graphene with higher aspect ratio (M60) lie within the confidence interval of the measured values, the reduction measured when platelets with lower aspect ratio (IND G) are added is more significant. The addition of impermeable fillers to glassy polymers in solution can affect the gas permeability in two ways: *i*) it increases the tortuosity of the diffusive path of gas molecules inside the membrane, thus lowering the permeability by a factor that is usually gas-independent; *ii*) it affects the distribution of polymeric chains, modifying the free volume. The latter effect can cause negative or positive variations of permeability, and the extent of permeability variation can depend on the gas nature, especially for those polymers which show a bimodal distribution of free volume sizes like PTMSP.

In particular the addition of GO leads to an increase of permeability ranging from 6 %, for He, to 7%, for CO_2, and to 10% for N_2 and CH_4 is obtained when adding GO to PTMSP.

The addition of M60 graphene to PTMSP, which has a different chemical structure with respect to GO, but a comparable aspect ratio and higher thickness, results in a decrease of permeability, ranging from -5%, for CH_4, to -10%, for N_2, and to -14% for CO_2 and -20% for He. According to those values, the addition of M60 lowers more significantly the permeability of smaller penetrants like He. Usually, such a size-dependent variation of permeability can be attributed to the fact that PTMSP has a bimodal distribution of voids, which can be affected in different ways by the addition of fillers. If such results are

confirmed, the effect on selectivity is extremely promising because M60 allow to enhance the selectivity of PTMSP for the couple CO_2/He, CH_4/N_2 and CH_4/He.

The addition of graphene nanoplatelets with low aspect ratio, (IND G), lowers appreciably, around 24/30%, the permeability of PTMSP to all gases, and the effect seems to be independent on the gas size.

It is interesting to point out that the, if we compare the results obtained by adding two types of graphene fillers with different aspect ratios (M60 and IND G) to PTMSP, we notice that the highest permeability reduction is induced by the filler with the lower aspect ratio (IND G): this is somehow unexpected because the tortuosity should increase with aspect ratio of particles. Such behavior may indicate that the most significant effect of graphene fillers addition, in a high free volume glassy polymer like PTMSP, is the modification of polymer chain distribution and free volume rather than the increase of tortuosity.

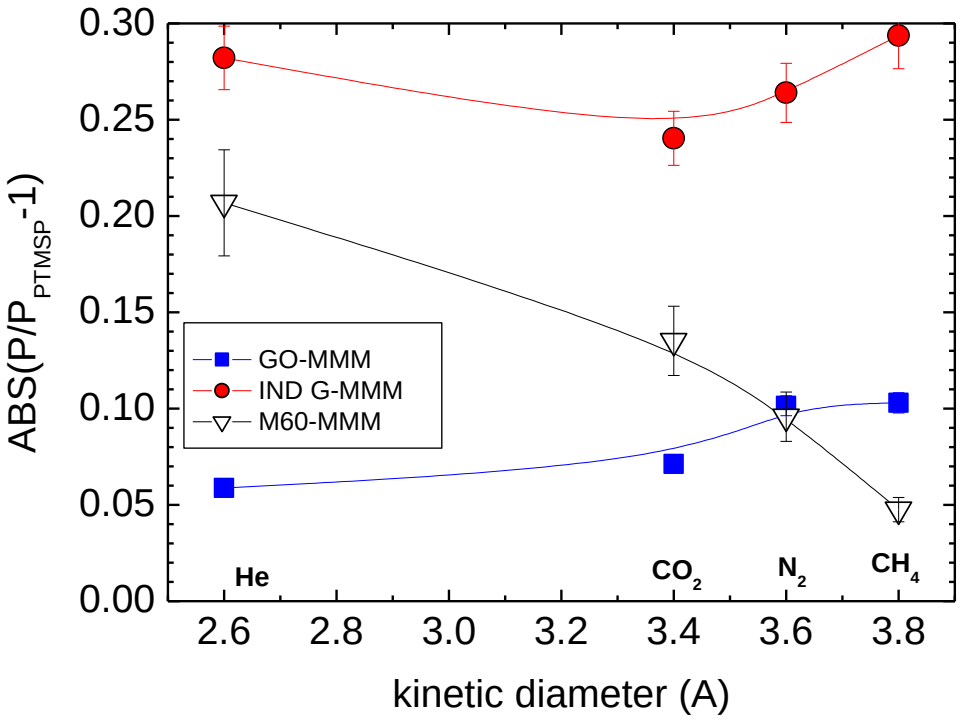

Figure 4.49: The effect of fillers on fresh PTMSP permeability.

Also in composite membranes the permeability of gases inspected is well correlated to penetrant critical temperature. This aspect testifies that MMM based and graphene fillers maintain the same solubility selective behavior of the polymeric matrix. Results are reported in Figure 4.50.

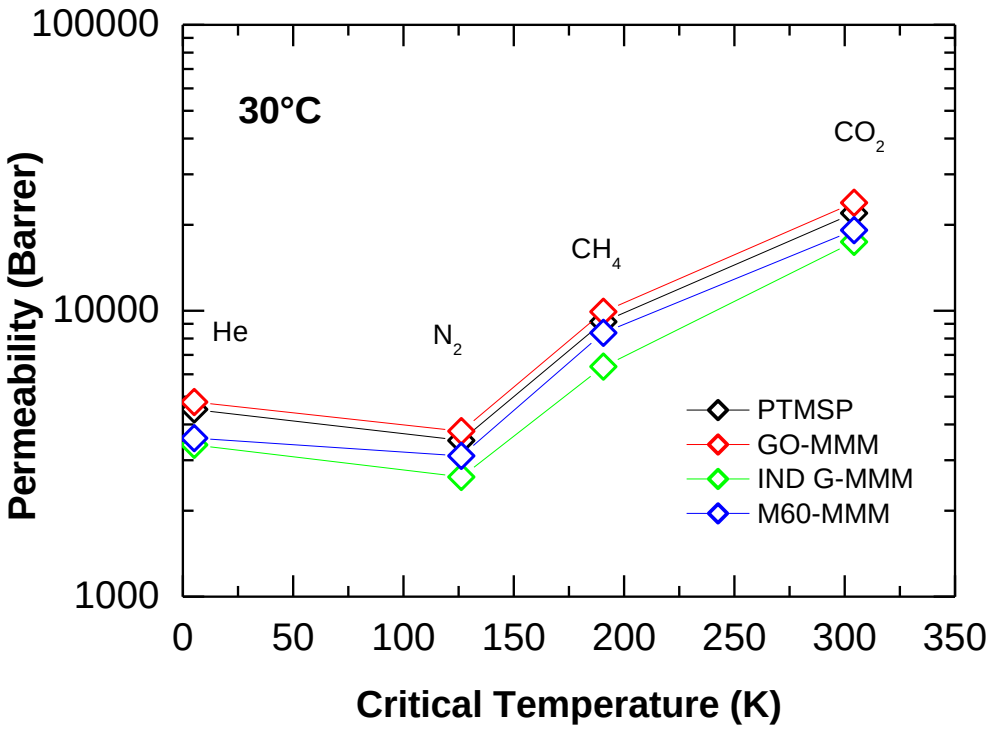

Figure 4.50: The correlation of PTMSP and graphene based MMM permeability with penetrant critical temperature at 30°C.

The ideal selectivity of the membranes, after 2d from casting, is reported in Figure 4.51: for almost all gas mixtures, the filler addition enhances the selectivity of pure PTMSP. It is a small effect due to small amount of filler in the membrane. In particular, the M60-MMM has the highest selectivity for the CO_2/He, CH_4/N_2, CH_4/He gas couples, while IND G-MMM is the most selective membrane for CO_2/N_2 and CO_2/CH_4 mixtures. Such results are interesting

because indicate that the CO_2-selective nature of PTMSP can be enhanced by the addition of graphene-based fillers.

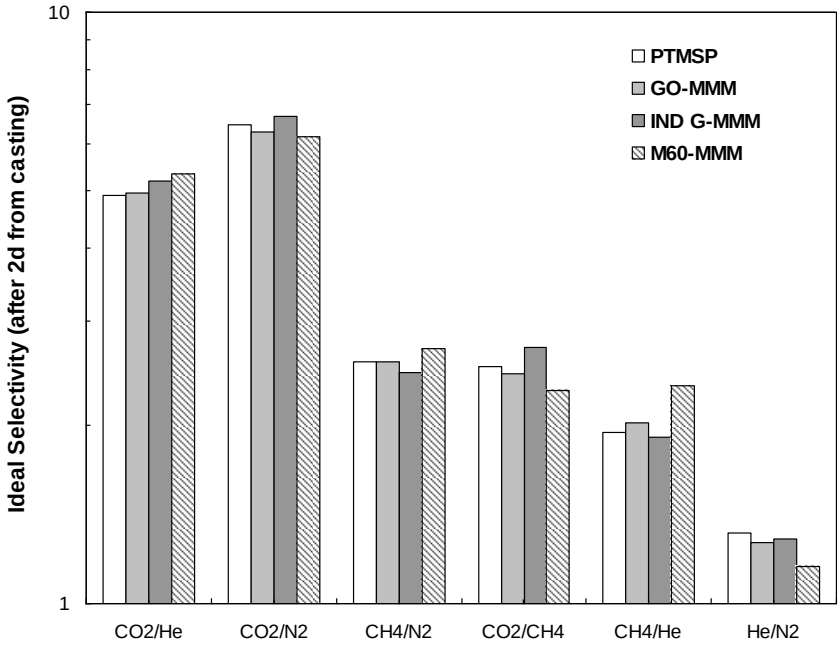

Figure 4.51: Ideal selectivity of fresh PTMSP and Mixed matrix membranes.

4.2.3 CO_2 solubility and diffusivity in fresh samples of PTMSP and M60-MMM at different pressures

In order to analyze in more detail the effect that the filler has on the different contributions to permeability, and to study the effect of pressure, which can be an important parameter in the case of CO_2 transport, especially in glassy polymers, the solubility and diffusivity of CO_2 and CH_4 in PTMSP and the M60-MMM have been analyzed, at 35°C and up to 30 bar. It is possible to observe from Figures 4.52 and 4.53 that CO_2 and CH_4 solubility isotherms in PTMSP are almost unaffected by addition of M60: this behavior can be attributed to the relatively small amount of filler added, and to the small impact on gas-membrane interactions that such filler has.

On the other hand, the CO_2 diffusivity reported in Fig. 4.54 in both PTMSP and M60-MMM shows the typical behavior recorded in high free volume glassy membranes: diffusivity

decreases with concentration of gas absorbed, because the matrix volume occupied by the absorbed gas is not replaced by a significant dilation of the polymer, which is very rigid in these operative conditions. The diffusivity of CO_2 is initially lower in the composite matrix than in the polymer, indicating that the reduction of permeability measured in such mixed matrix membrane with respect to the value obtained in PTMSP, at low pressure, is to be attributed mainly to the diffusivity reduction. However, the diffusivity of CO_2 in the M60-MMM decreases slowly with pressure. Such behavior can be explained in this way: at infinite dilution of gas the composite membrane, characterized by lower free volume than PTMSP, has also a lower diffusivity (-40%). Eventually, when the concentration of CO_2 in the membranes is sufficiently high, the extra free volume of PTMSP with respect to the M60-MMM becomes saturated and smaller differences (-16%) are observed between the diffusivities of the two matrices.

The CH_4 diffusivity in PTMSP, shown in Fig. 4.55 is constant with concentration, as usual for such penetrant in polymeric membranes; as for the case of CO_2 the M60-MMM exhibits lower values of diffusion coefficients, as expected due to its lower free volume, and also almost constant with concentration.

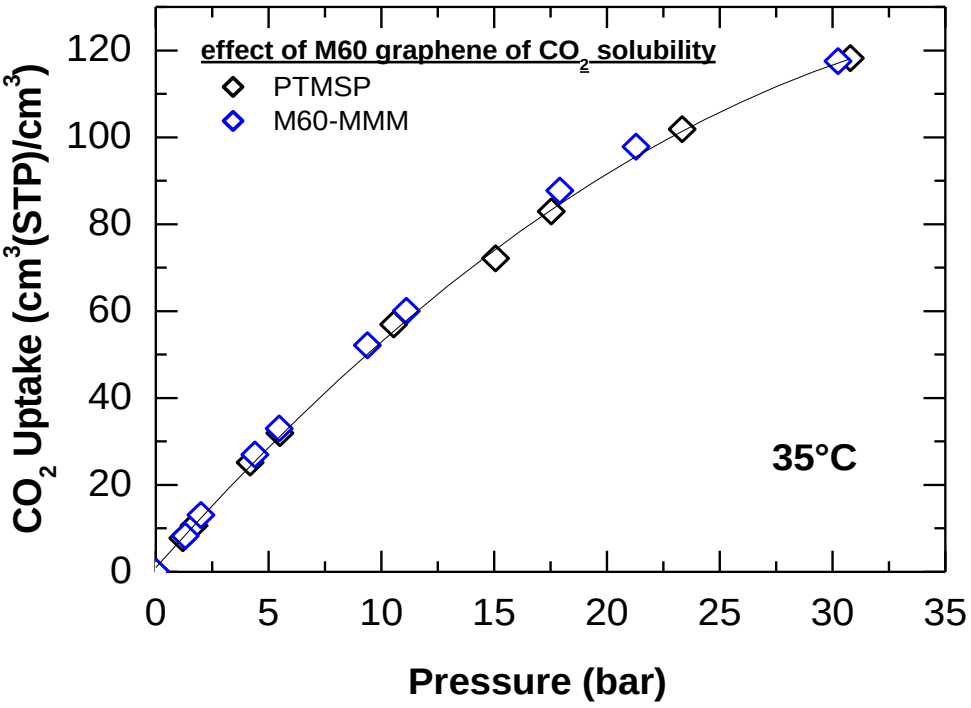

Figure 4.52: The effect of graphene M60 filler on CO_2 solubility in PTMSP at 35°C.

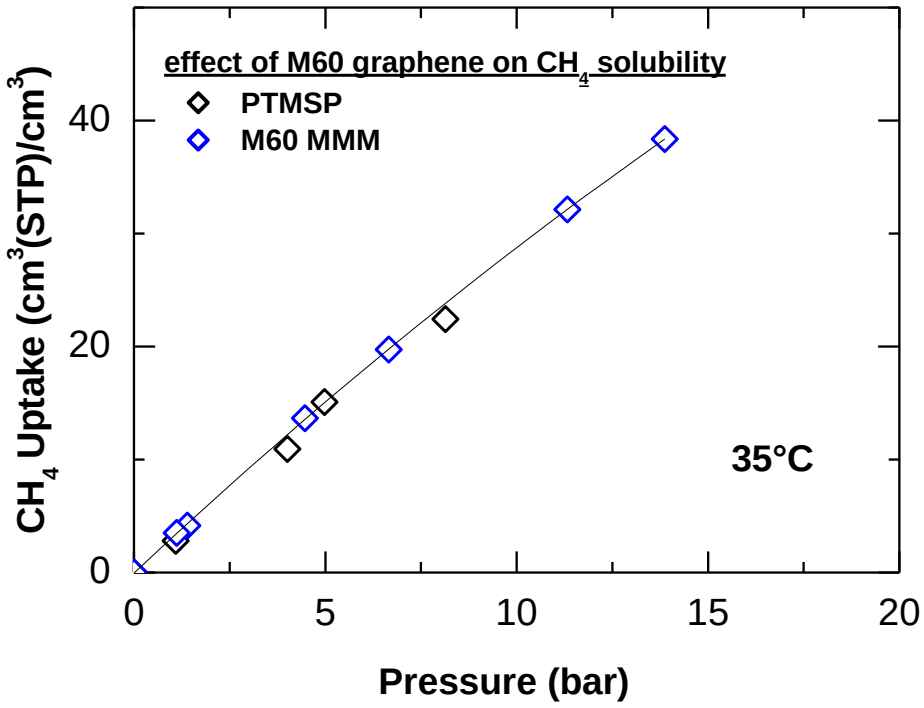

Figure 4.53: The effect of graphene M60 filler on CH_4 solubility in PTMSP at 35°C.

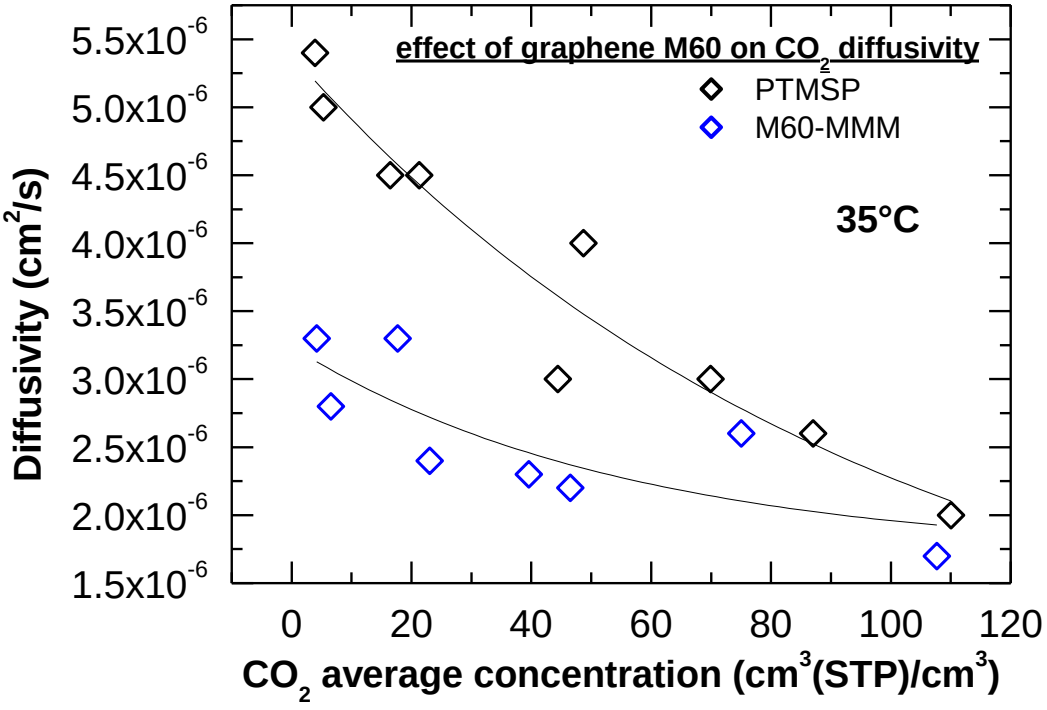

Figure 4.54: The effect of graphene M60 filler on CO_2 diffusivity in PTMSP at 35°C.

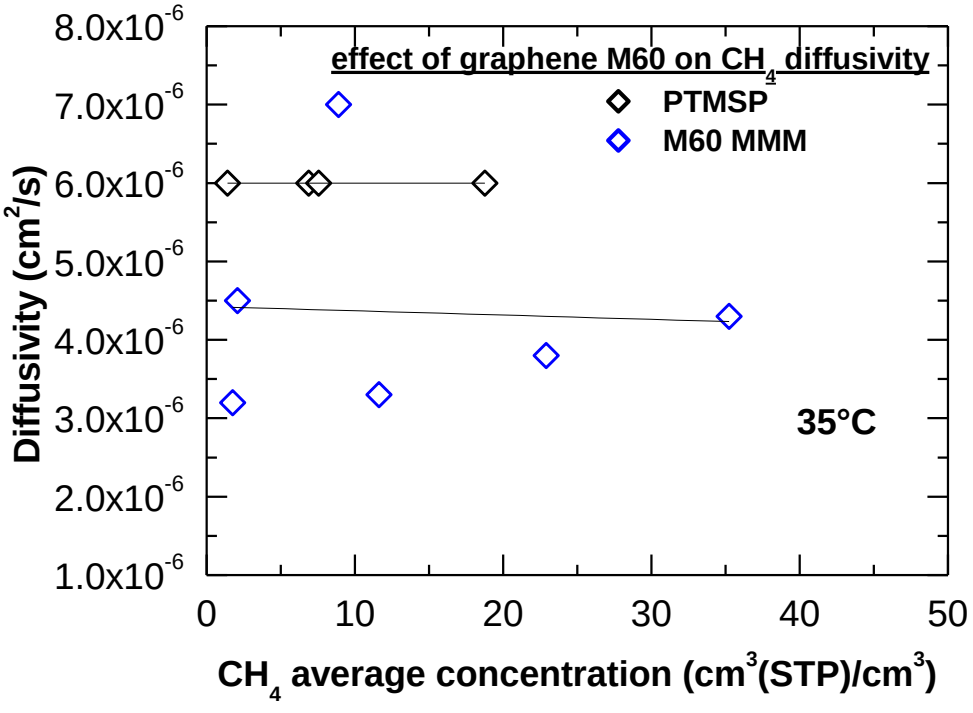

Figure 4.55: The effect of graphene M60 filler on CH_4 diffusivity in PTMSP at 35°C.

4.2.4 Effect of fillers on physical ageing

At this point it is interesting to consider the effect of fillers on PTMSP ageing behavior. To this end a comparison between ageing in PTMSP tested repeatedly over 9 months (i.e. membrane 115 mm thick) and filled membranes will be reported. GO-MMM samples have been tested over 9 months while the IND G-MMM and M60-MMM ones have been monitored over 4 months. The membranes were stored in room conditions between every measurement.

The permeability decreases with time, according to a logarithmic law, for practically all gases and all membranes inspected, as it can be seen in Figures 4.56–4.59 for PTMSP, GO-MMM, IND G-MMM and M60-MMM respectively. It can be noticed that all membranes exhibit ageing for the permeability of all gases; in particular, the CO_2 permeability decrease in PTMSP after 9 months is equal to -29% while N_2, CH_4 and He permeability decrease is about -44%, -34% and -37% respectively. In GO-MMM membranes, the permeability decreases is less significant, especially for CO_2, and it is equal to -17%, -25%, -38% and -36% for CO_2, N_2, CH_4 and He permeability respectively after 9 months.

For the graphene-based MMMs the time interval inspected is smaller and equal to about 4 months. In IND G-MMM membranes the decreases of permeability after 4 months is equal to -28%, -31%, -39% and -21% for CO_2, N_2, CH_4 and He respectively; in M60-MMM for the same set of gases we measures a permeability loss of -14%, -13%, -21% and -21% respectively.

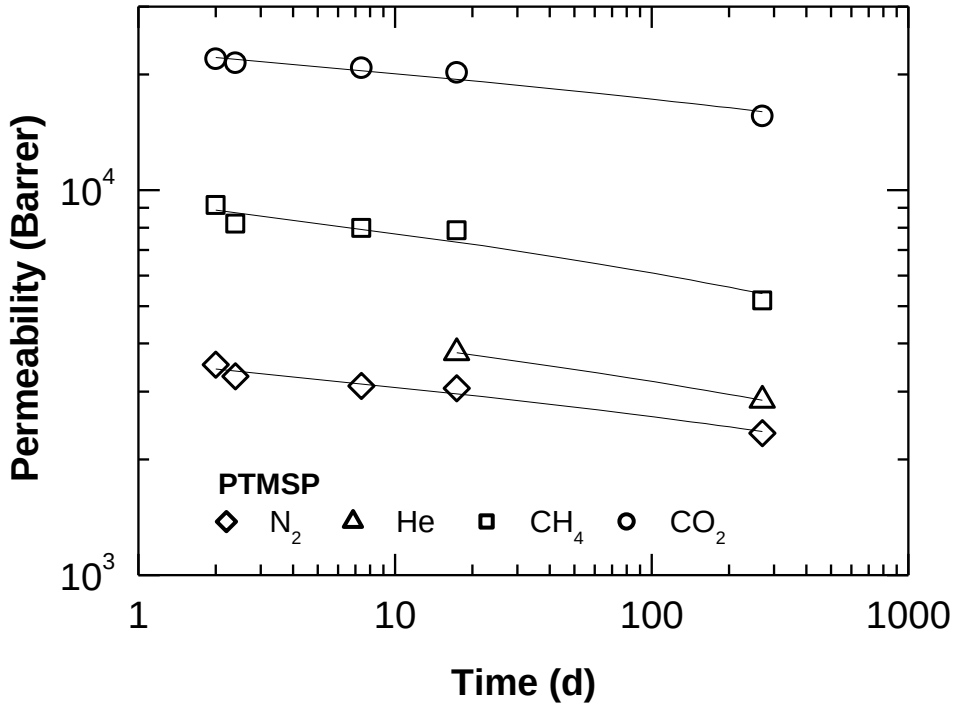

Figure 4.56: The effect of ageing on permeability of PTMSP.

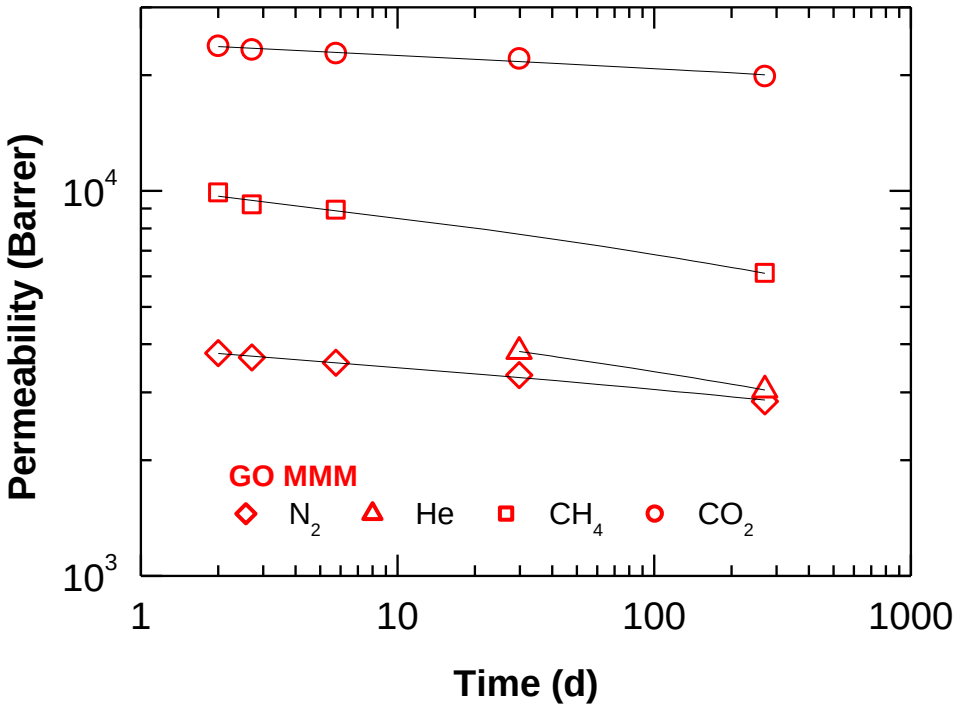

Figure 4.57: The effect of ageing on permeability of GO-MMM.

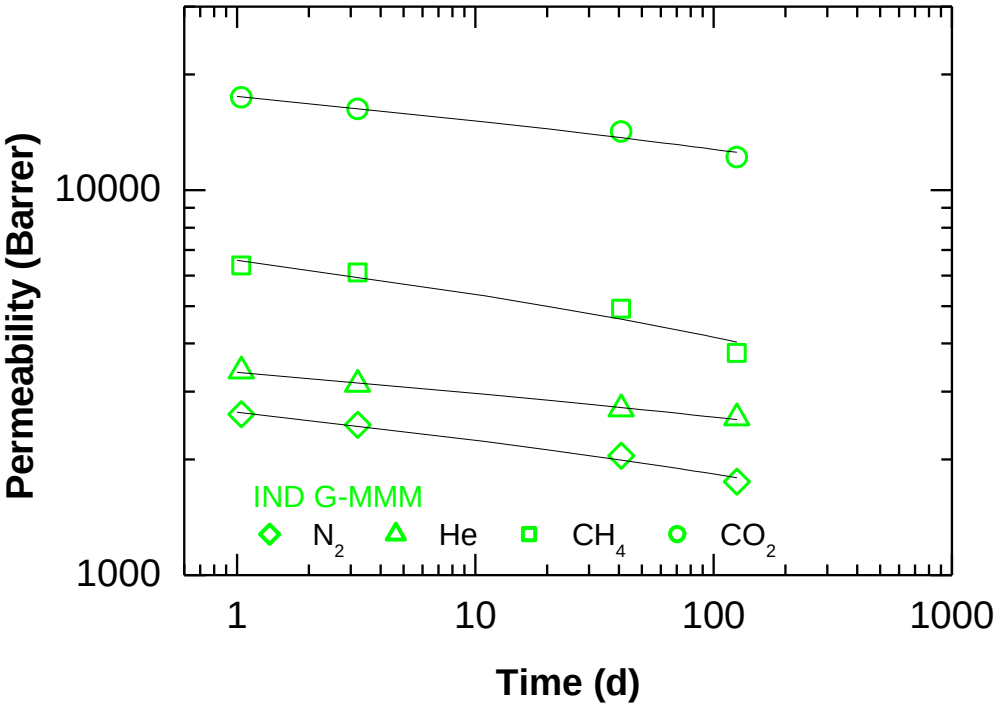

Figure 4.58: The effect of ageing on permeability of ING G-MMM.

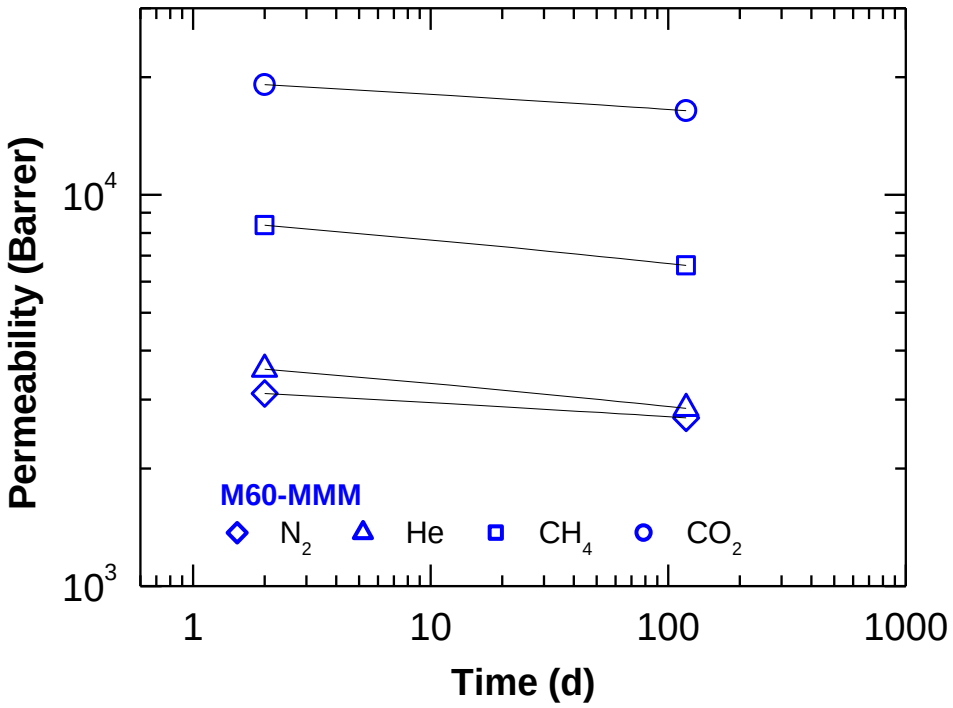

Figure 4.59: The effect of ageing on permeability of M60-MMM.

The ageing permeability data indicate that no stable permeability value is reached after 9 months; in order to inspect the long-time behavior of such membranes we thermally treated them at 200°C, so to accelerate the ageing. The treatment was performed on pure PTMSP and on GO-MMM, and their gas permeability inspected after 1 and 9 months since casting.

In Figures 5.60–5.63 relative decreases of gases permeability with time are reported, evaluated as the relative difference between the permeability measured at time t, ($P(t)$) and the permeability measured after 2 d from casting ($P(2d)$). In Figure 4.60, the higher permeability losses can be observed for PTMSP and GO-MMM, that reach values of about -40% after 9 months of natural ageing. On the other hand, the samples containing graphene fillers, IND G-MMM and M60-MMM, are more stable, in terms of He permeability, with a -20% decrease after 4 months of ageing. The thermal treatment of PTMSP and GO-MMM samples drastically lowers their permeability, by a factor equal to about -40% for GO-MMM. Such value can be assumed as a pseudo-equilibrium permeability for He in such membrane. The PTMSP permeability is more drastically reduced by thermal treatment than that of GO-MMM (-50%). Therefore, as far as the He permeability is concerned, it seems that the pseudoequilibrium state for GO-MMM and for PTMSP can be reached after 9 months of natural ageing or, equivalently, with a short thermal treatment at 200°C. Also, samples containing graphene filler show a slower ageing with respect to PTMSP and GO-MMM samples.

The decrease of N_2 permeability with time, reported in Figure 4.61 is comparable to that of He; the permeability decreases by -35% after 9 months, for pure PTMSP, and by -25%, for the GO-MMM membrane. On the other hand, the ageing behavior of IND G-MMM membrane is similar to that of PTMSP, while the M60-MMM permeability only decreases by about -15% after 4 months. Therefore, the N_2 permeability loss in PTMSP due to ageing is reduced by adding GO and M60 fillers.

Considering the thermally treated samples it can be noticed that, unlike the case of He permeability, the N_2 permeability reduction obtained by thermal treatment is higher, in absolute value, than that obtained by natural ageing over 9 months. In particular the permeability reductions observed in PTMSP and GO-MMM are both equal to about -53% and they seem stable with time.

The CH_4 permeability, reported in Figure 4.62, shows reductions which are somehow higher than those observed for the case of N_2, and they range around -40%, for PTMSP and GO-MMM samples after 9 months, while they are equal to -40% and -20% for IND G-MMM and M60-MMM after 4 months, respectively. Therefore, also in this case the addition of graphene M60 seems to slow down the ageing process observed in PTMSP.

When the ageing is accelerated via a thermal treatment at 200°C, the CH_4 permeability reduction is higher than what obtained after 9 months of natural ageing: PTMSP permeability goes down by more than 60%, although it regains a part of its initial permeability at the end of the time interval inspected. The reduction of CH_4 permeability in GO-MMM membranes seems to be initially less marked than that observed in PTMSP, but eventually the two membranes exhibit the same value of relative permeability reduction.

In Figure 4.63 it can be seen that the CO_2 permeability is less affected than that of other gases by natural ageing, for all membranes. In particular the PTMSP and GO-MMM permeability reduction after 9 months are equal to -30% and -15% respectively. The IND G-MMM follows the same ageing trend as PTMSP, while the M60-MMM is the more stable sample, with a reduction of CO_2 permeability equal to -14% after 4 months.

In this case the thermal treatment induces a different permeability change in the two membranes: the CO_2 permeability drop after annealing is equal to -50% for PTMSP and -40% for the GO-MM membrane. This situation seems stable with time, and indicates that, in the long run, the loss of CO_2 permeability is definitely mitigated by the addition of GO.

Furthermore, one can conclude that GO-MMM samples are resistant to thermal treatments which can partly reduce GO.

The higher stability of CO_2 permeability with time, with respect to the permeability of other gases, is probably due to the fact that the (high) CO_2 permeability in PTMSP-based matrices is largely based on solubility; the solubility is a sum of entropic factors (related to free volume) and energetic factors (related to penetrant condensability and gas-polymer interactions). Therefore, when the free volume of the matrix is reduced due to ageing, the reduction is more marked for diffusivity than for solubility, as the first quantity is much more strongly related to the free volume, and the permeability reduction less marked for the more soluble penetrants like CO_2.

The addition of IND G nanoplatelets to PTMSP does not modify significantly the ageing behavior in almost all cases, indicating that such filler has only the effect to reduce PTMSP permeability, without modifying its relaxation time, and ageing behavior.

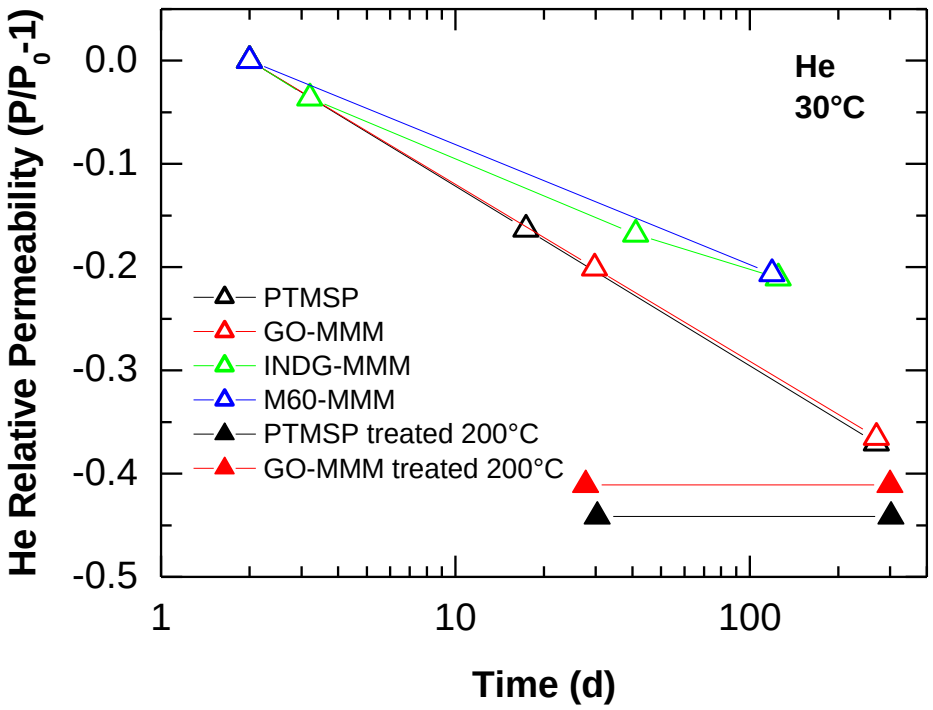

Figure 4.60: The effect of fillers on PTMSP ageing monitored by He permeability loss with time.

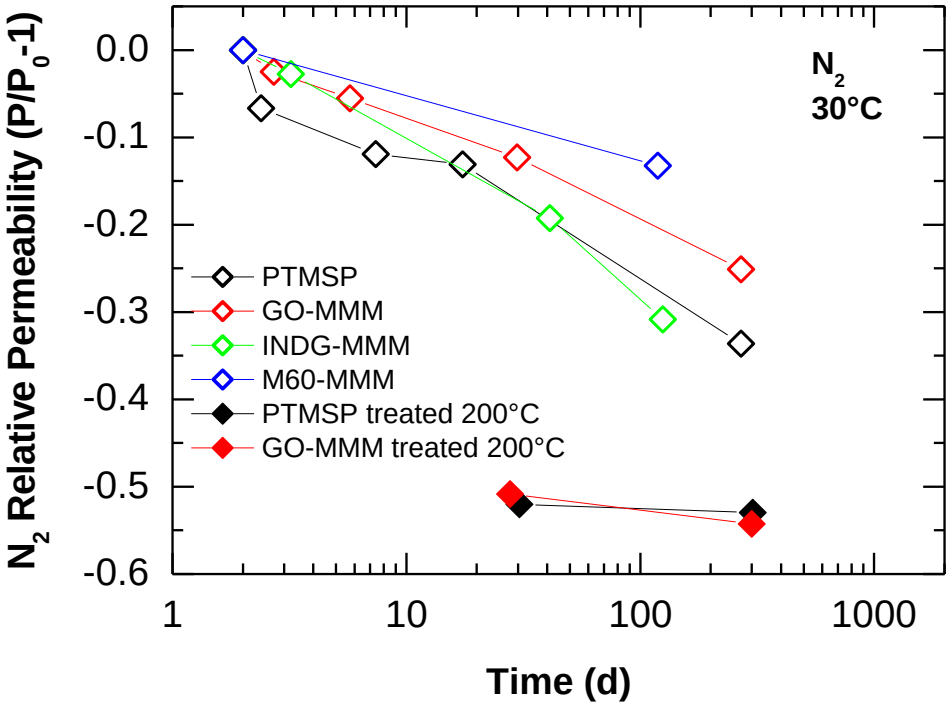

Figure 4.61: The effect of fillers on PTMSP ageing monitored by N_2 permeability loss with time.

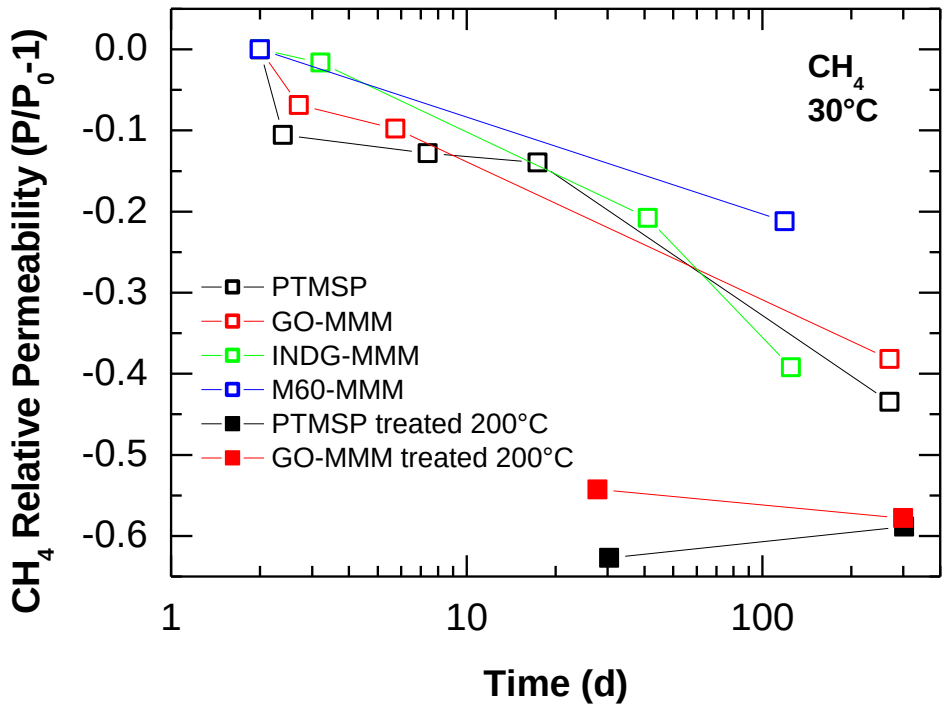

Figure 4.62: The effect of fillers on PTMSP ageing monitored by CH_4 permeability loss with time.

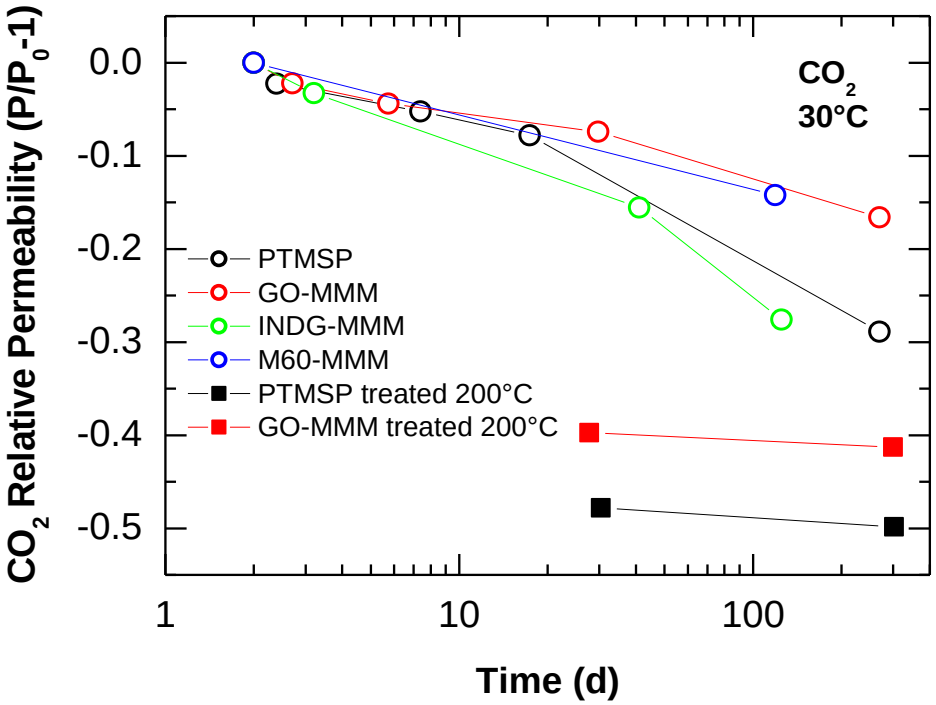

Figure 4.63: The effect of fillers on PTMSP ageing monitored by CO_2 permeability loss with time.

The addition of M60 filler, albeit its effect was inspected over a shorter time interval than the other samples, slows down the ageing process, as tested through the permeability of all gases. This aspect, combined to the fact that the addition of M60 reduces the permeability to a limited extent and often enhances the selectivity, is promising for the use of such filler as additive to reduce the physical ageing of PTMSP without compromising the permeability.

It can be noticed that CO_2 permeability is more stable with time after GO incorporation, while the permeability of other gases does not change significantly. Such a selective ageing behavior, combined to the enhancement of permeability induced by GO addition, demonstrates the potential of such additive in CO_2 capture applications. Indeed, while the permeability reduction measured after the thermal treatment is essentially the same for PTMSP and GO-MMM in the case of He, N_2 and CH_4, it is lower for the GO-MMM sample than for PTMSP in the case of CO_2. The treatment at 200°C induces a partial reduction of

GO, which can lower its ability to interact with CO_2 molecules, but apparently such phenomena do not affect gas transport, consistently with the fact that the amount of GO added is small.

Results indicate that a correlation exists between filler dimension and effect on polymer relaxation. In particular, the fillers with larger lateral dimension (GO and M60) can reduce PTMSP ageing, while nanoplatelets with smaller lateral size (IND G) do not affect it remarkably, as if the filler acts as mechanical constraint only if its size is big enough to limit chains rearrangement.

Figure 4.64 reports selectivity towards several gas couples, at different ages of the sample (2d, 100 d, 300 d); the arrows represent the evolution of selectivity with samples age. It can be observed that, for gas mixtures exhibiting a tradeoff between selectivity and permeability according to Robeson, namely the CO_2/N_2, CO_2/CH_4 couples, the selectivity increases with sample age. Coupled to the fact that the permeability generally decreases with age, such behavior indicates that, as time elapses, the performance of such membranes in a Robeson's plot evolves in a direction parallel to the trade off line, towards lower permeabilities and higher selectivities. This aspect is clearer in the Fig. 7b and c that report CO_2/N_2 and CO_2/CH_4 selectivity versus CO_2 permeability, for the different membranes at different times, where arrows indicate the time evolution of the membrane performance.

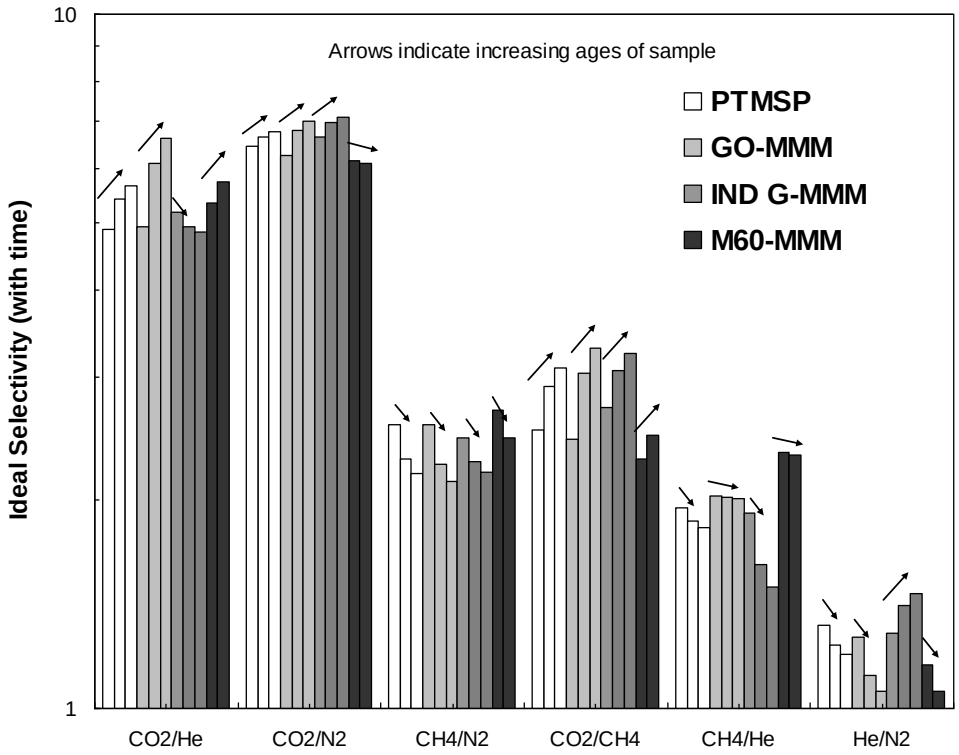

Figure 4.64: Selectivity of PTMSP and MMM for different gas couples at at different ages of the samples (2d, 100 d, 300 d).

4.2.5 Thin samples results and comparisons

In this section it will be shown the results obtained for thin film composite membranes based on PTMSP and graphene fillers, comparing them with results of thick membranes. It is well known from literature [65–68] that glassy polymer ageing is strictly connected to film thickness. In particular the ageing in thin film membranes is accelerated with respect to bulky films and in some cases the permeability drop due to relaxation is higher in thin films than thick ones [68]. In light of this, it is important to start and characterize thin sample at a time which approach a virtual zero time after complete solvent removal. In particular in this work, according to other works related to physical ageing in thin films found in literature, the zero time is around 30 minutes. This choice is also driven by the fact that it is necessary to pull the samples under vacuum for a fixed time to ensure complete solvent removal.

It is interesting to notice that the permeability of neat PTMSP measured in samples with 7 μm thickness, at a time within 30 minutes, practically reproduces the values found for thick membranes previously reported in Fig. 4.65.

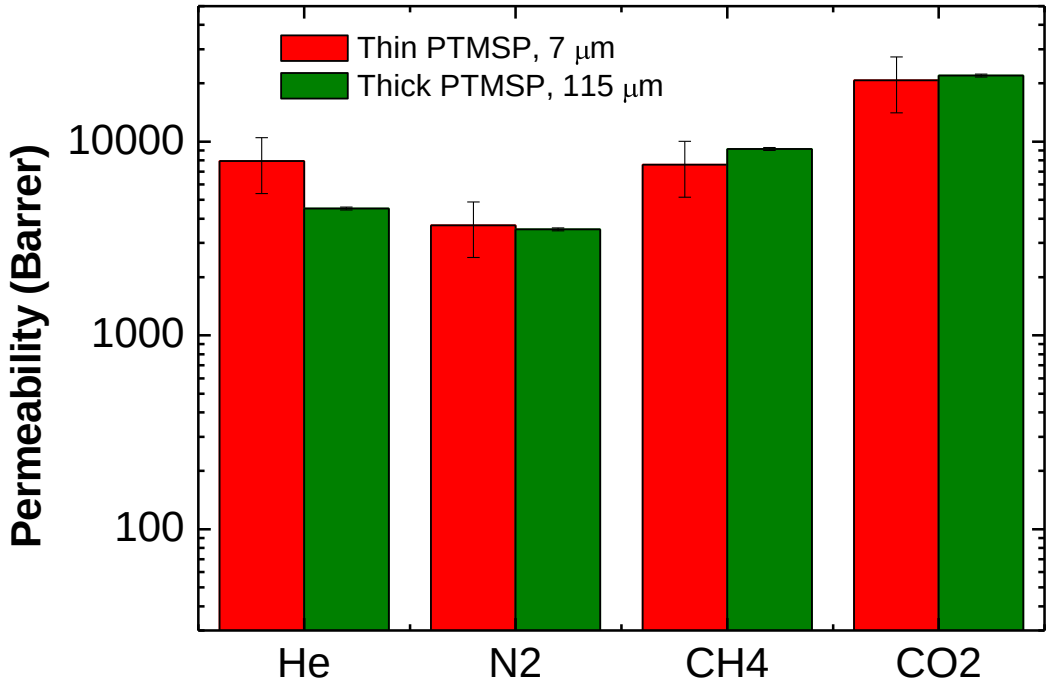

Figure 4.65: Comparison of fresh permeability in fresh thick and thin PTMSP films.

In particular from this data it is possible to observe that the permeability of He in the thin membrane is 70% higher than the one obtained in self-standing thick membranes. Such a behaviour could be due the higher evaporation rate of the solvent during sample spin coating than solvent casting, which lead to obtain membranes with more open structures, characterized by higher free volume. Considering that the permeability increases exponentially with free fractional volume, according to Paul et al. [150], the higher permeability in thin sample can be attributed to higher free volume. Moreover He is the smallest gas considered in this work and thus its permeability value is the more affected by free volume variations. On the contrary the permeability of larger penetrants such as CH_4, N_2

and CO_2 seems to be less affected by preparation method (i.e. spin coating/solvent casting) and are more similar to values observed in the thick membrane. In particular N_2 and CO_2 permeabilities differ of 5%, and CH_4 of 16% with respect to thick PTMSP. In any case differences between thick and thin membranes are in the order of experimental uncertainties on thin film thickness.

Now it is interesting to observe the effect of thickness on ageing rate of samples. From Figures 4.66–4.69 it is possible to observe that in thin samples ageing is much faster than thick one. In particular, for instance, for Helium a permeability loss of 40% has been measured after 9 months of ageing. In thin materials the same variation can be observed after 1 day for a membrane 7 mm thick, after 2 hours for a sample 5 mm thick and after 1 hour for a sample 4 mm thick. Similar results have been obtained for all the penetrants and are reported in the following.

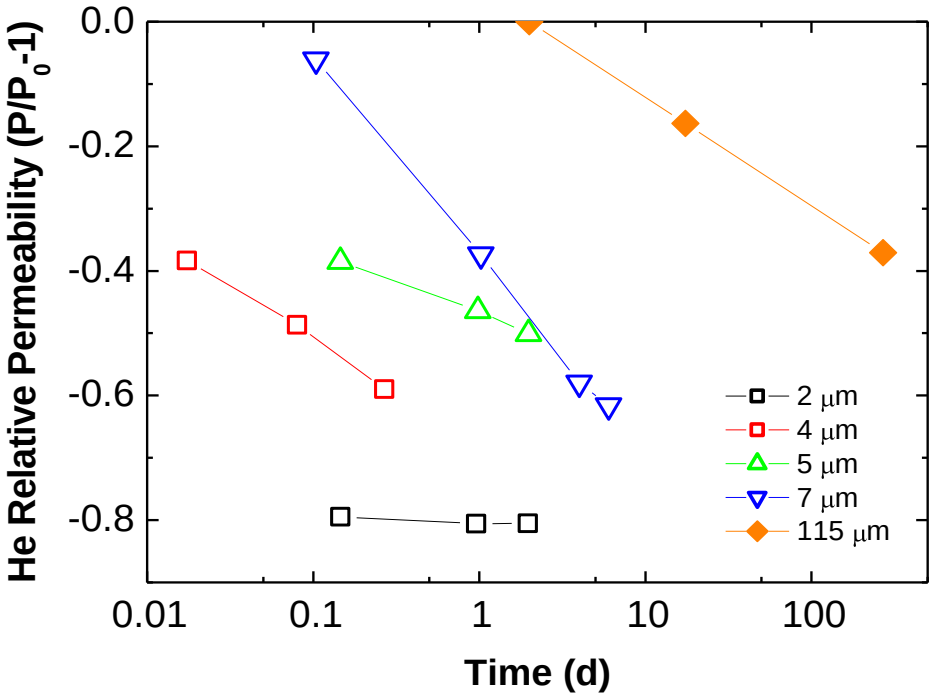

Figure 4.66: The effect of thickness on He permeability loss in PTMSP at 35°C.

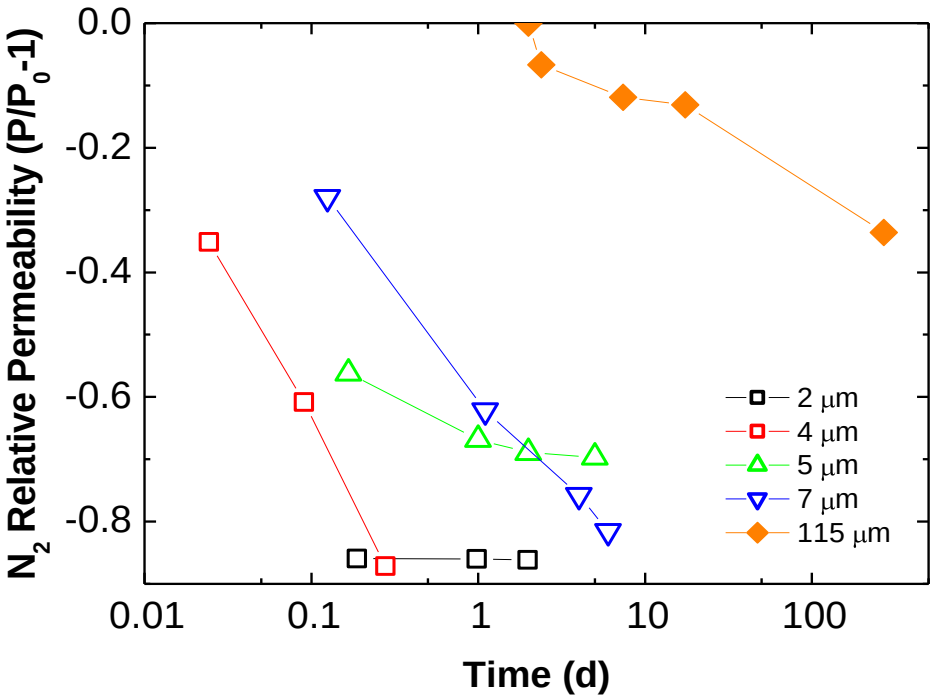

Figure 4.67: The effect of thickness on N_2 permeability loss in PTMSP at 35°C.

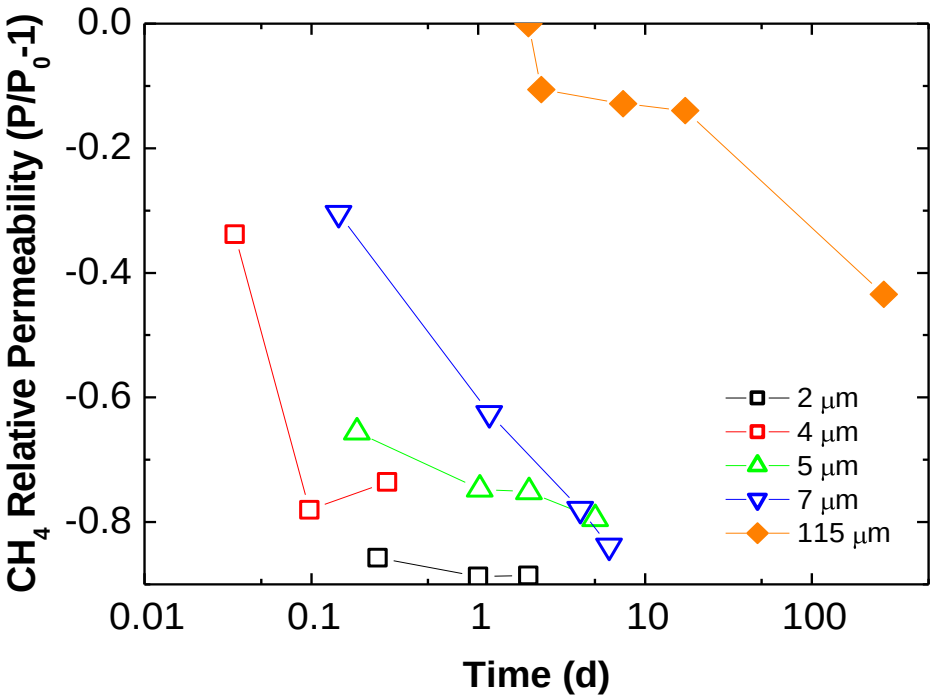

Figure 4.68: The effect of thickness on CH_4 permeability loss in PTMSP at 35°C.

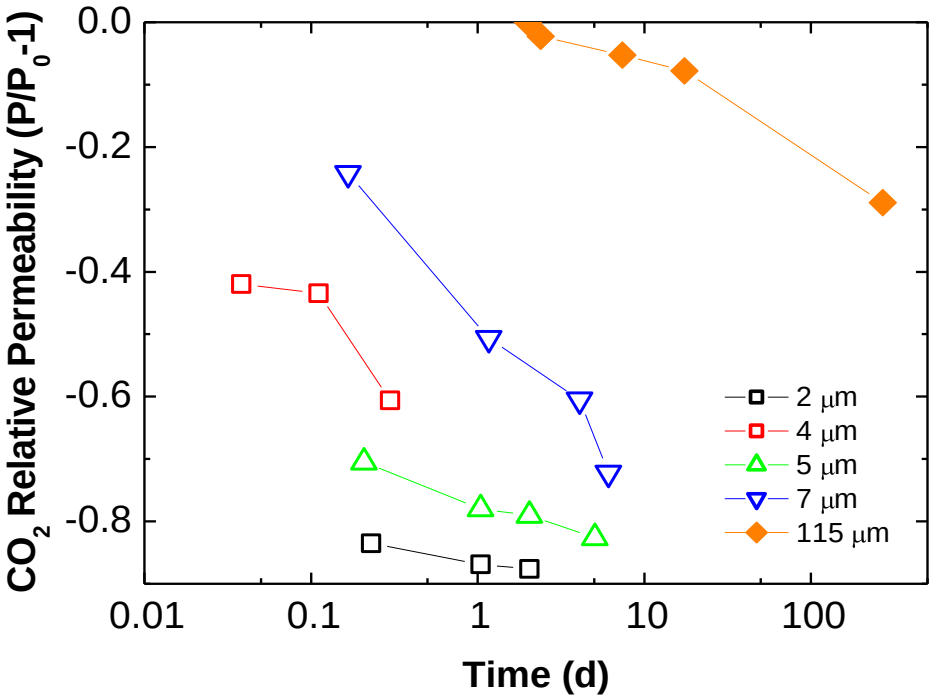

Figure 4.69: The effect of thickness on CO_2 permeability loss in PTMSP at 35°C.

The effect of fillers on fresh PTMSP permeability in thin films is reported in Figures 4.70 and 4.71, in which also data for thick membranes are included. From this comparison it can be clearly observed that the effect of fillers on gases permeability is at least reproduced. In particular the effect of fillers, related to penetrant size, observed in thick membranes, is encountered also in thin films. With GO it can be observed in Fig. that gases permeability is enhanced by the presence of the filler. In very similar results have been obtained in the case of CO_2 and CH_4 permeabilities, on the contrary deviations from thick membranes results can be observed for He and N_2. M60 filler, as observed in thick samples, reduces gases permeability. In particular the reduction is more pronounced in thin films, as it can be observed in Fig. 4.77 that the effect on PTMSP permeability is systematically lower than in thick samples. This aspect may be explained considering that in thin membrane the permeability reduction due to

tortuosity becomes relevant. In particular the lateral dimension of the graphene M60 nanoplatelets is reported to be 5 μm [ref. data sheet], and assuming that, during spin coating, graphene filler disposes parallel to the basis of porous support (assumption validated by absence of pinhole in the thin skin), they constrict gas molecules to move in a more tortuous pathway, which reduces gas diffusivity and permeability.

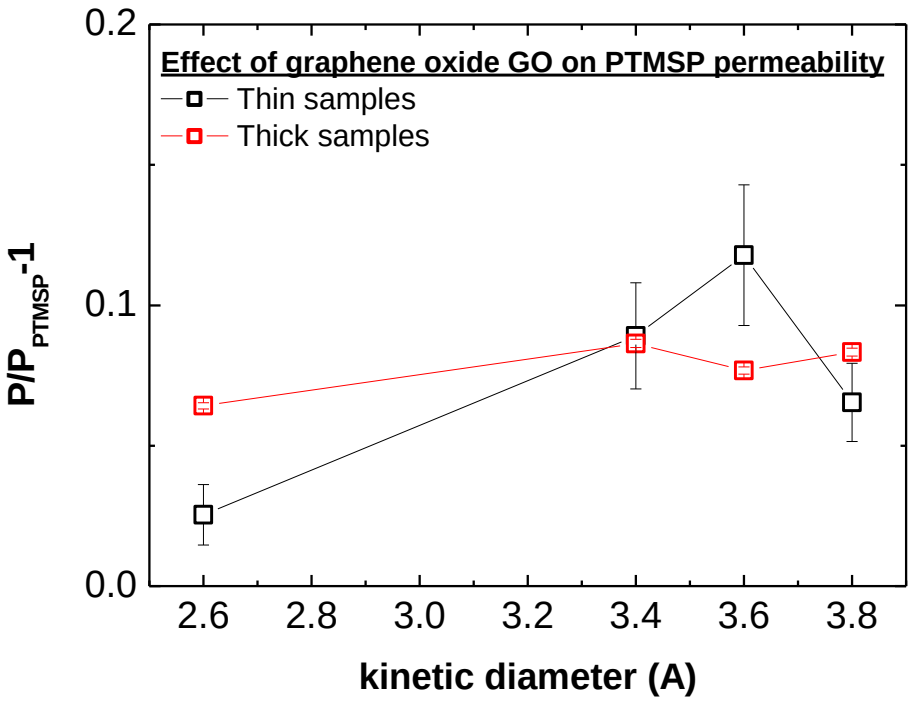

Figure 4.70: Comparison of the effect of GO in thick and thin fresh samples.

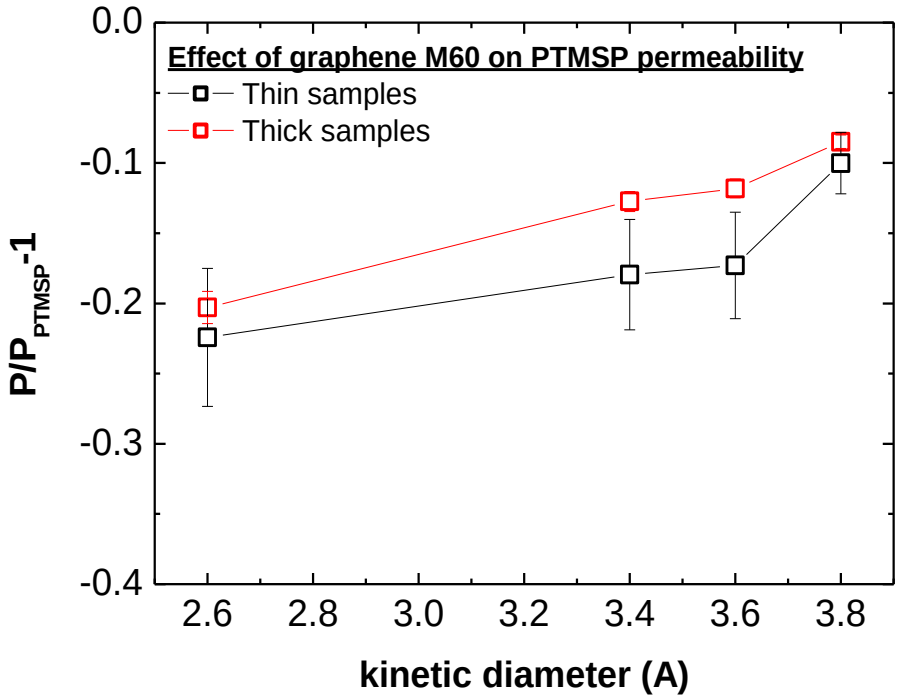

Figure 4.71: Comparison of the effect of GO in thick and thin fresh samples.

Finally the effect of graphene based nanoplatelets on physical ageing can be considered. As observed in thick membranes, also in thin samples ageing is slow down by addition of small amount of GO and graphene M60. In particular results of ageing in MMM for 3 μm thin membranes have been compared with a pure PTMSP thin film with the same average thickness. Although samples have been characterized for a shorter time interval with respect to thick membranes the effect of reduction of physical ageing phenomenon is reported in Figures 4.72–4.75. For He and CO_2 it is clear that the permeability reduction in GO-MMM is lower than pure PTMSP as observed in thick membranes after 200°C thermal treatment. On the contrary, as reported for thick ones, N_2 and CH_4 permeability loss seems to be similar in both PTMSP and GO composite membrane after 100 hours.

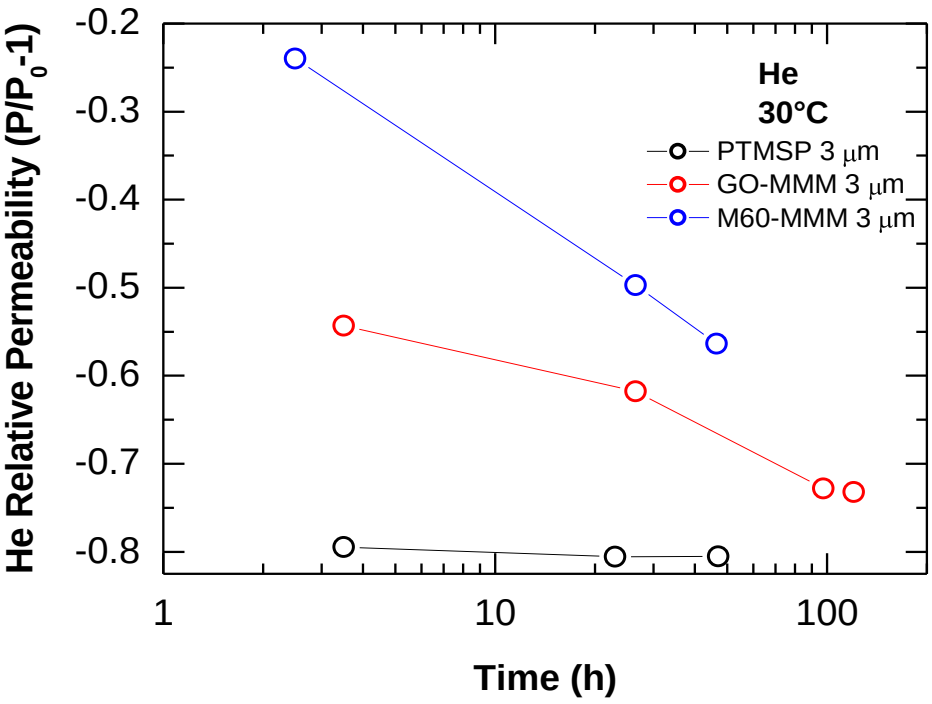

Figure 4.72: The effect of fillers on thin PTMSP ageing monitored by He permeability loss with time.

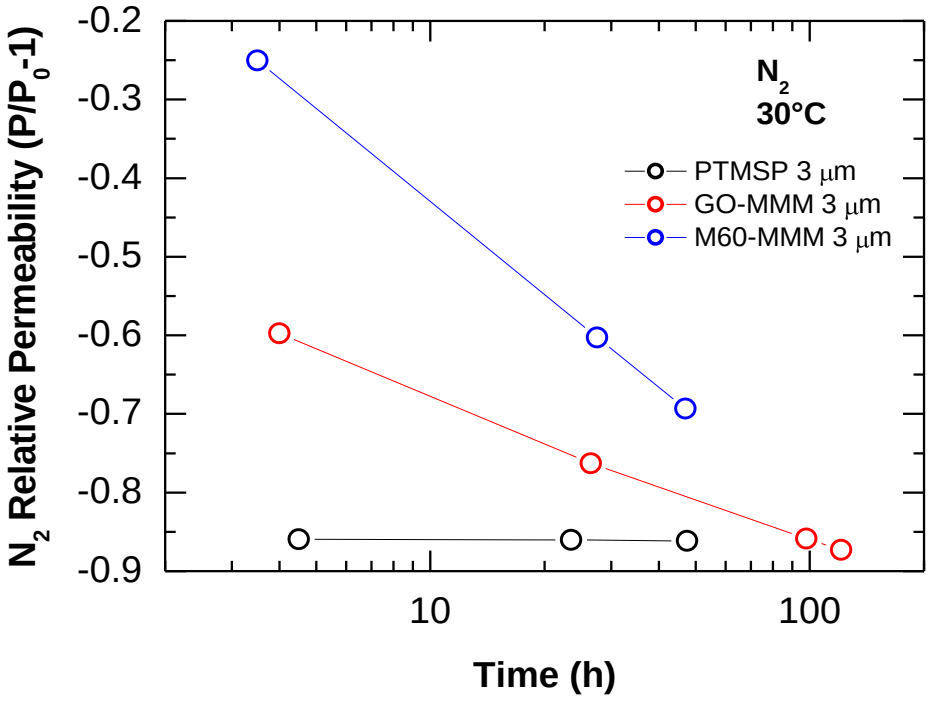

Figure 4.73: The effect of fillers on thin PTMSP ageing monitored by N_2 permeability loss with time.

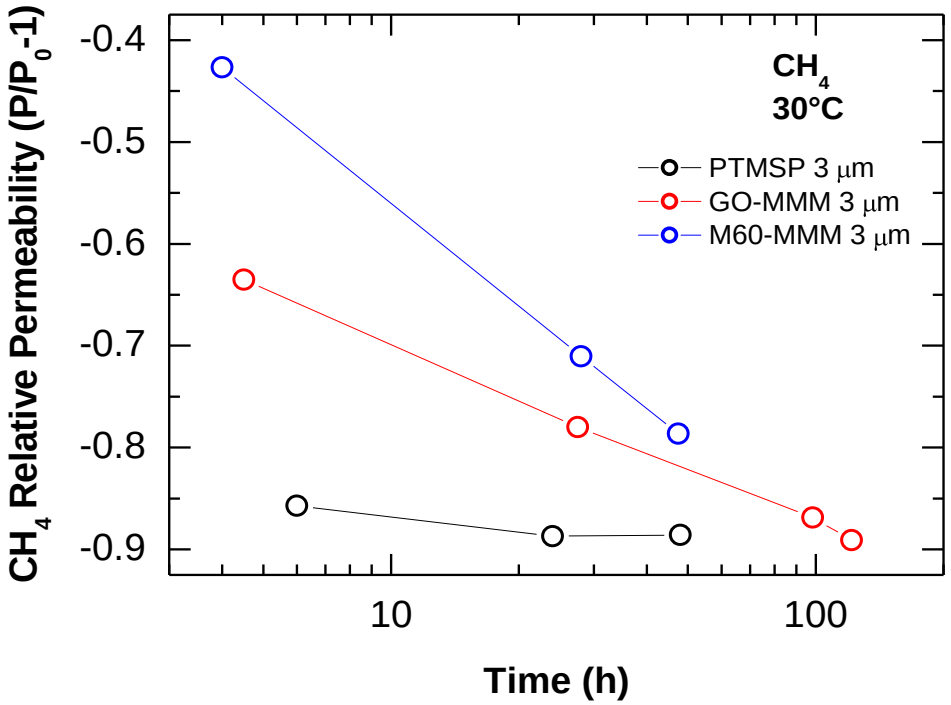

Figure 4.74: The effect of fillers on thin PTMSP ageing monitored by CH_4 permeability loss with time.

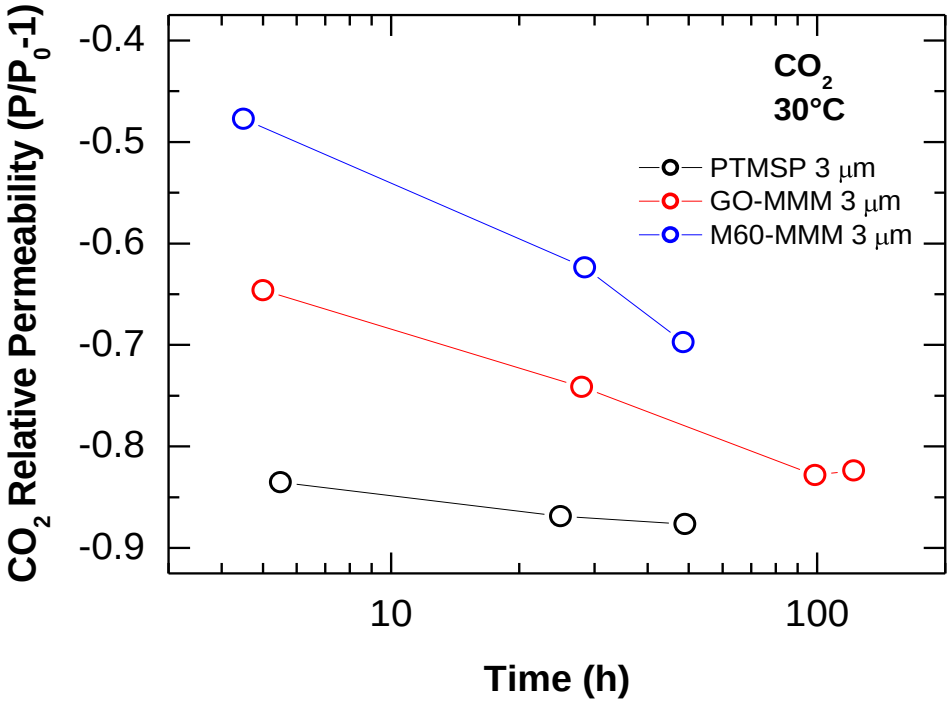

Figure 4.75: The effect of fillers on thin PTMSP ageing monitored by CO_2 permeability loss with time.

4.2.6. Robeson plots

In Figures 4.76–4.78 selectivity versus permeability data are reported for CO_2/N_2, CO_2/CH_4, and CO_2/He systems at different ages of the sample up to 300 days; the arrows represent the evolution of selectivity with samples age. It can be observed that, for gas mixtures exhibiting a tradeoff between selectivity and permeability according to Robeson, namely the CO_2/N_2, CO_2/CH_4 couples, the selectivity increases with sample age both in thick and in thin samples. Coupled to the fact that the permeability generally decreases with age, such behavior indicates that, as time elapses, the performance of such membranes in a Robeson's plot evolves parallel to the trade off line, in the direction of lower permeabilities and higher selectivities. This aspect is clearer in the Figures 4.77 and 4.78 that report CO_2/N_2 and CO_2/CH_4 selectivity versus CO_2 permeability, for the different membranes at different times. Arrows indicate the time evolution of the membrane performance and is clearly evident that, as time elapses, membrane performances evolve following a direction parallel to the tradeoff curve.

A different behavior is observed in the case of the CO_2/He couple, reported in Fig. 4.76. Robeson reported a tradeoff between He/CO_2 selectivity and He permeability for this curve, while PTMSP and associated mixed matrix membranes show a CO_2-selective behavior. However, even after reporting the performance of the membranes in a He/CO_2 performance plot, the ageing takes the membranes closer to the tradeoff line; in other words the ageing mechanism does not follow a direction parallel to the tradeoff curve, but perpendicular to it. The only exception is represented by the membrane IND G-MMM and by thin membranes. Such behavior can be due to the bimodal distribution of free volume domains in PTMSP and to the fact that the small free volume domains available for He collapse more rapidly than the large ones so that reduction of He permeability is faster than CO_2 one for thick membranes.

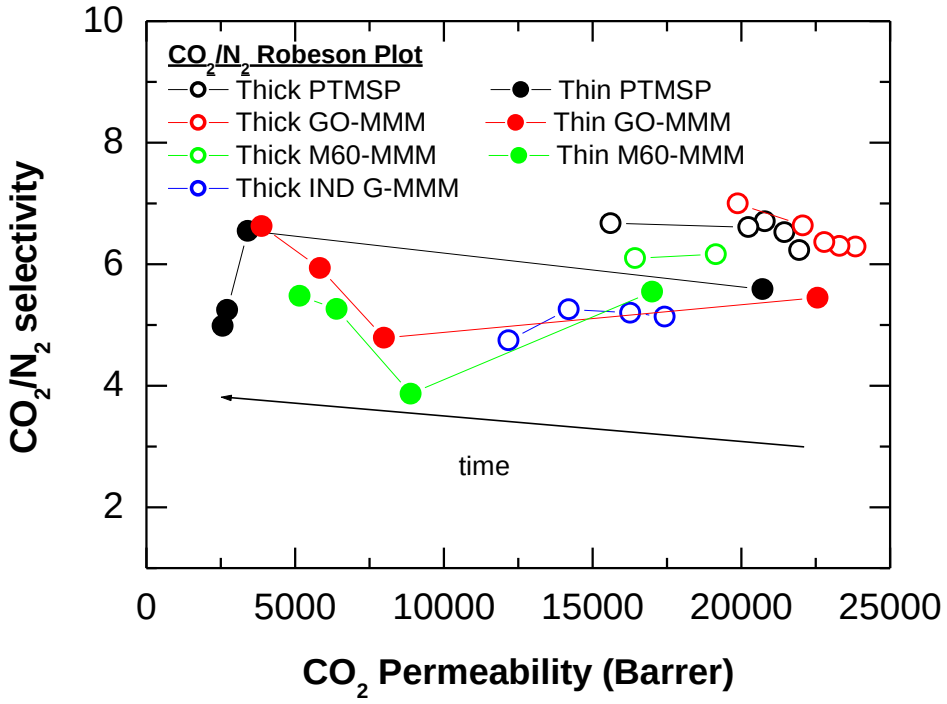

Figure 4.76: CO_2/N_2 Robeson plot for thin and thick PTMSP and Mixed Matrix Membranes.

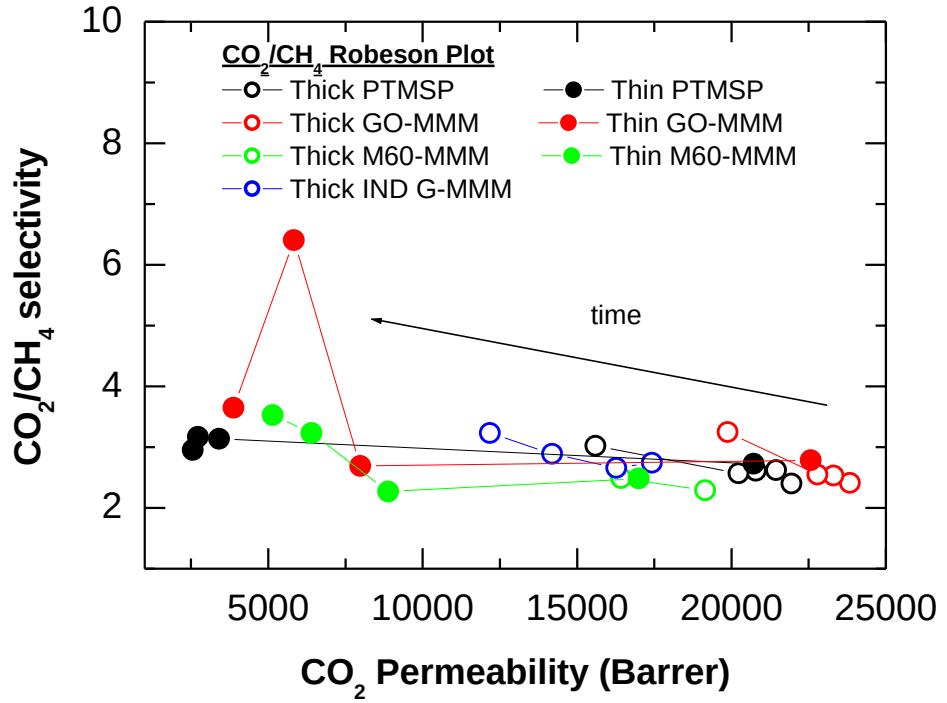

Figure 4.77: CO_2/CH_4 Robeson plot for thin and thick PTMSP and Mixed Matrix Membranes.

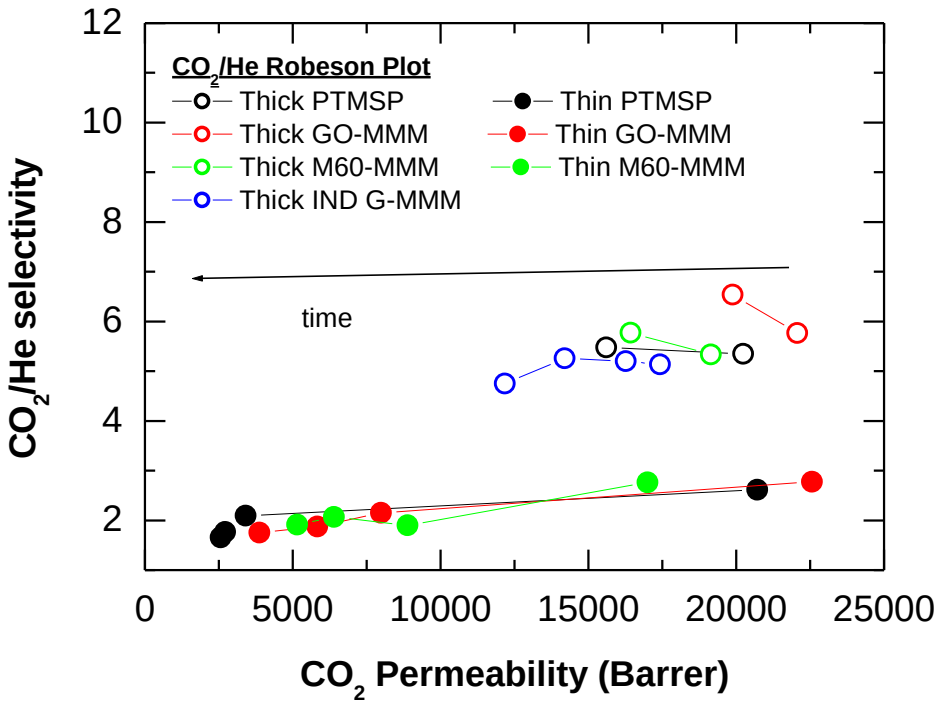

Figure 4.78: CO_2/He Robeson plot for thin and thick PTMSP and Mixed Matrix Membranes.

4.3 Experimental results in functionalized materials

Different powder samples obtained have been analyzed by FT-IR spectroscopy to recognize amine peaks, verify the attachment to the polymer and quantify the amount of amine groups bound to polymeric chains. To quantify the degree of functionalization we can calculate the ratio between nitrile groups, C≡N, and methyl groups, CH_3, in functionalized and pure PAN. In particular during the reaction nitrile groups decrease due to formation of imine groups, while methyl groups, inert during the reaction are constant in both functionalized and pure polymer. The conversion of PAN can be calculated as follow:

$$\chi_{PAN} = 1 - \frac{\left.\frac{C \equiv N}{CH_3}\right|_{functional izedPAN}}{\left.\frac{C \equiv N}{CH_3}\right|_{PAN}} \tag{4.2}$$

Membranes morphology has been observed by scanning electron microscopy.

CO_2 transport properties have been measured by sorption experiment at 35°C up to 30 bar in a pressure decay apparatus and permeation experiments have been conducted in a commercial MultiPerm permeometer equipped with composition detector by the University of Padova .

4.3.1 FTIR analysis

The final end of FT-IR analysis is to evaluate and compare conversion of nitrile groups in fabricated powders. Figure 4.79 pure PAN FT-IR spectra are reported, obtained and provided by the University of Padova, in which different groups can be recognized for the characteristic absorption peak; among them we have CH_3 groups characterized by a peak around 2935 cm^{-1} [151], CH_2 groups with a peak at 2860 cm^{-1}, the peak at 2240 cm^{-1} [151], corresponding to nitrile groups while any peak is visible at 3359 cm^{-1} [151], where amines absorb [151].

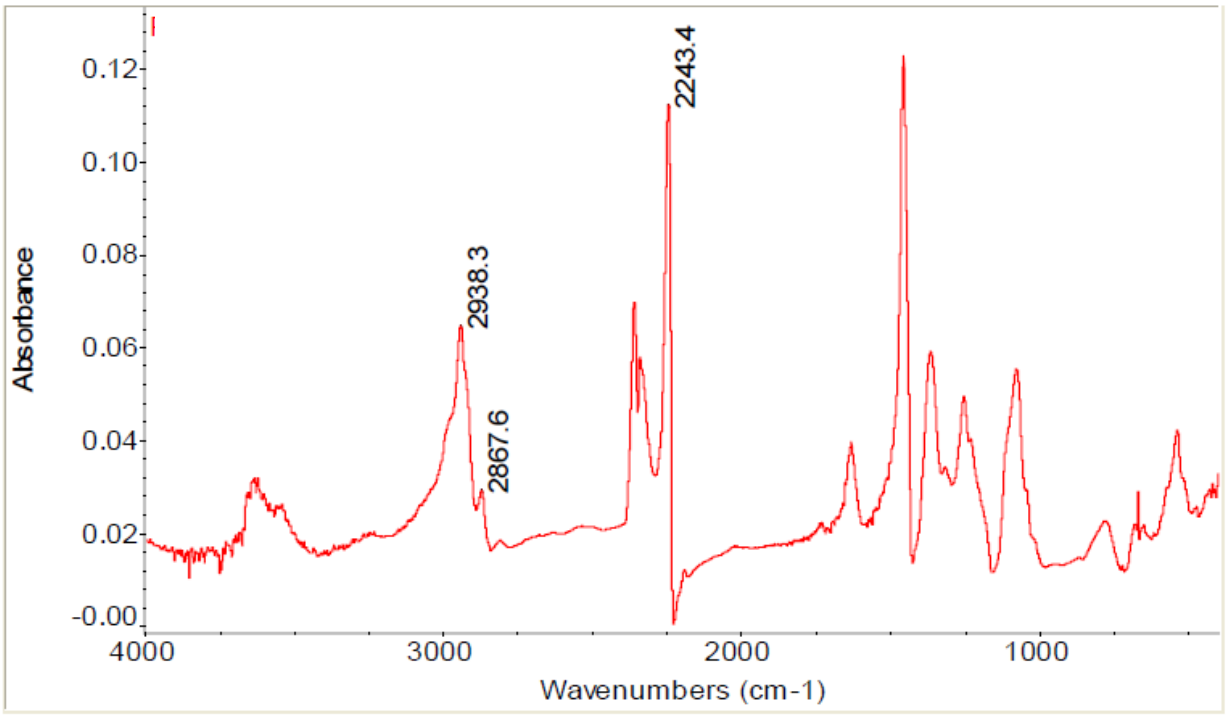

Figure 4.79: Pure PAN FT-IR spectra.

In Figure 4.80 results for powder functionalized with HMDA for different reaction time, respectively are reported. What can be observed is the appearance of additional peaks, in the range 3500-3200 cm^{-1} with respect to pure PAN. Moreover it can be clearly seen the increase of peaks heights at 1700-1500 cm^{-1} with the increase of reaction time, which denotes that increasing reaction time leads to increase of secondary amines and crosslinking of the polymer.

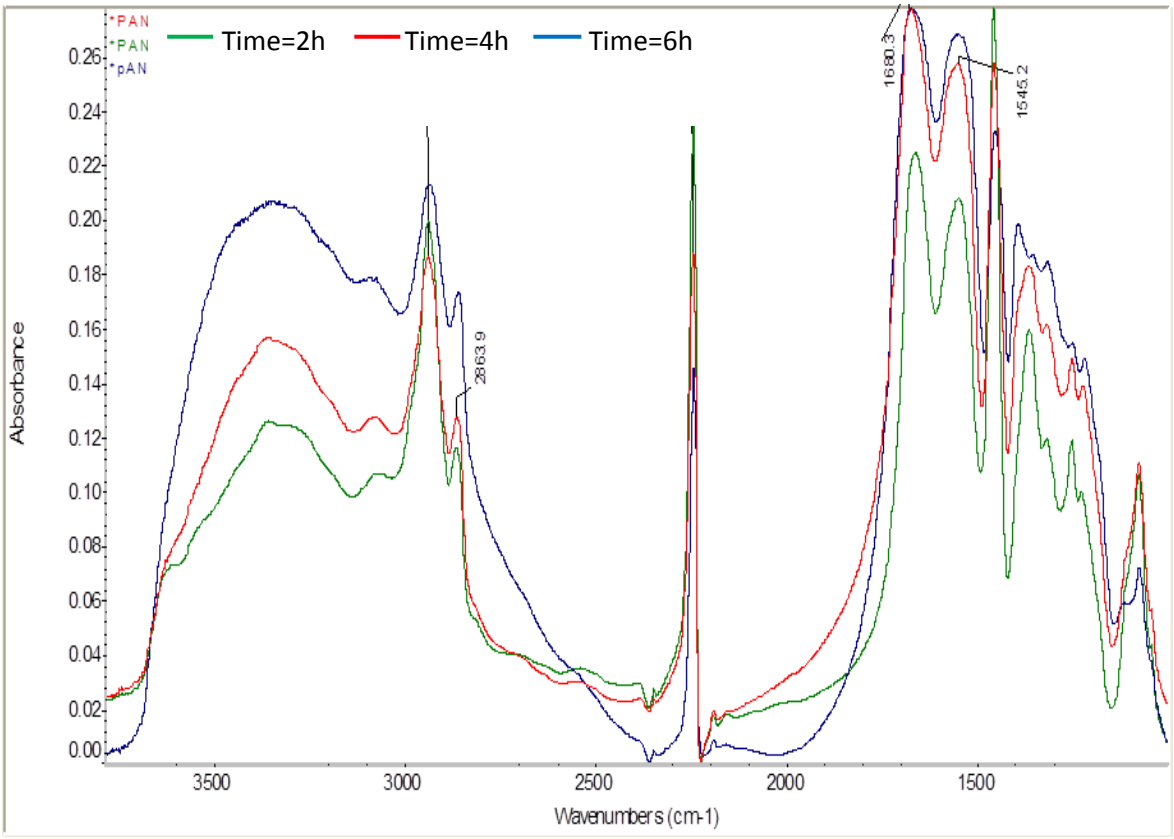

Figure 4.80: FT-IR spectra of functionalized powders with HMDA with a excess 2 times stoichiometric ratio at 110°C for 2, 4 e 6.

Considering fixed reaction time of 3 hours and PAN/EDA ratio of 1/5, increasing the system temperature from 80 up to 100°C it can be observed an increase of both primary and secondary amines, as reported in Figure 4.81. In particular for the reaction conducted at 100°C we have a too high increase of the latter which underlines crosslinking of the polymer, consequently the powder result non soluble in the proper solvent and cannot be electrospun.

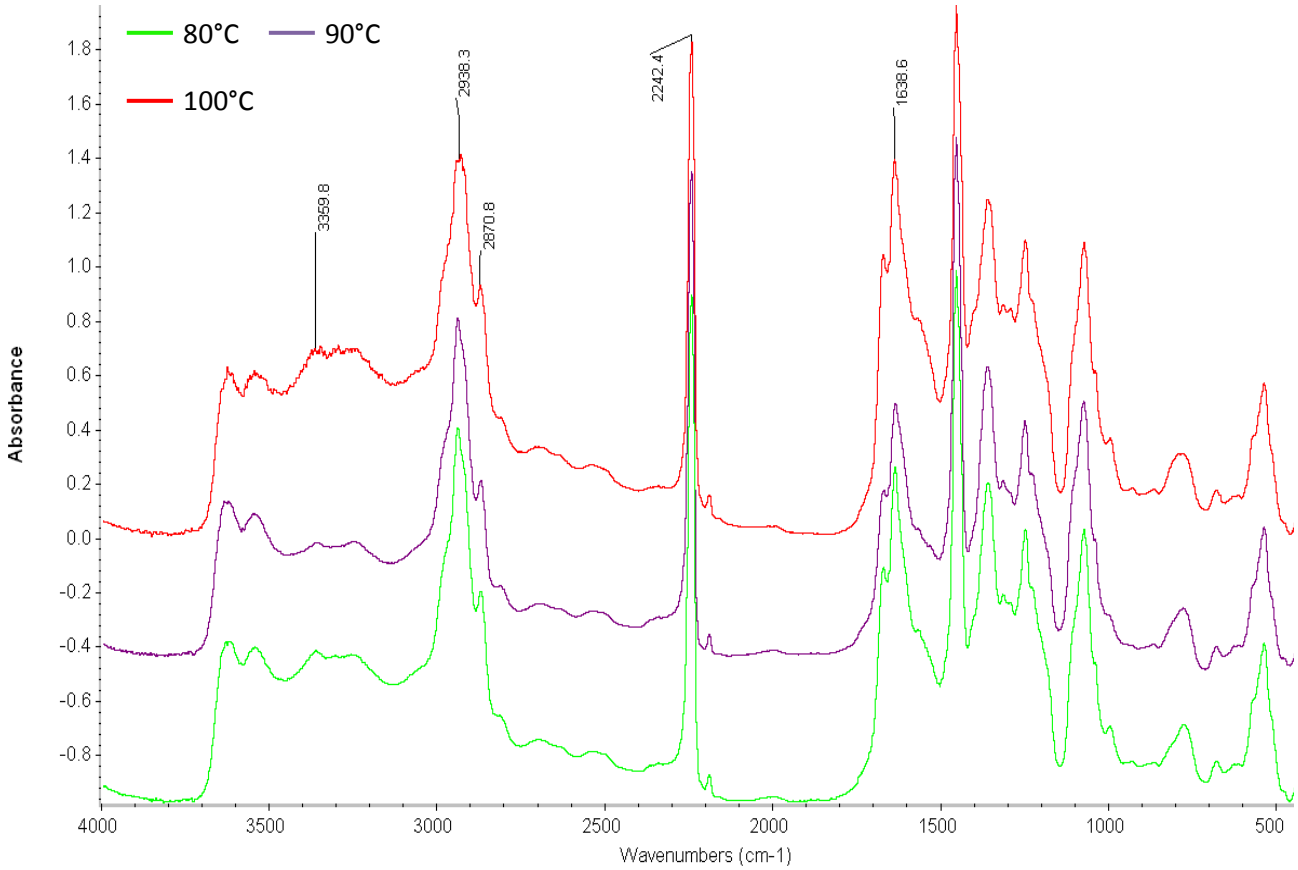

Figure 4.81: FT-IR spectra of functionalized powders with EDA with a amine excess 5 times the stoichiometric ratio for 3 hours at 80, 90 and 100 °C.

Considering the effect of reactant ratio, what is expected is that the increasing of amine excess favors the functionalization, reducing crosslinking [121]. From Fig. 4.82 it can be observed an increase of nitrile groups reacted but also a decrease of amines bound to the polymer. This aspect is due to the basicity of reaction environment which leads to hydrolysis of the polymer as confirmed by the appearance of $-COO^-$ peak at 1580 cm^{-1}.

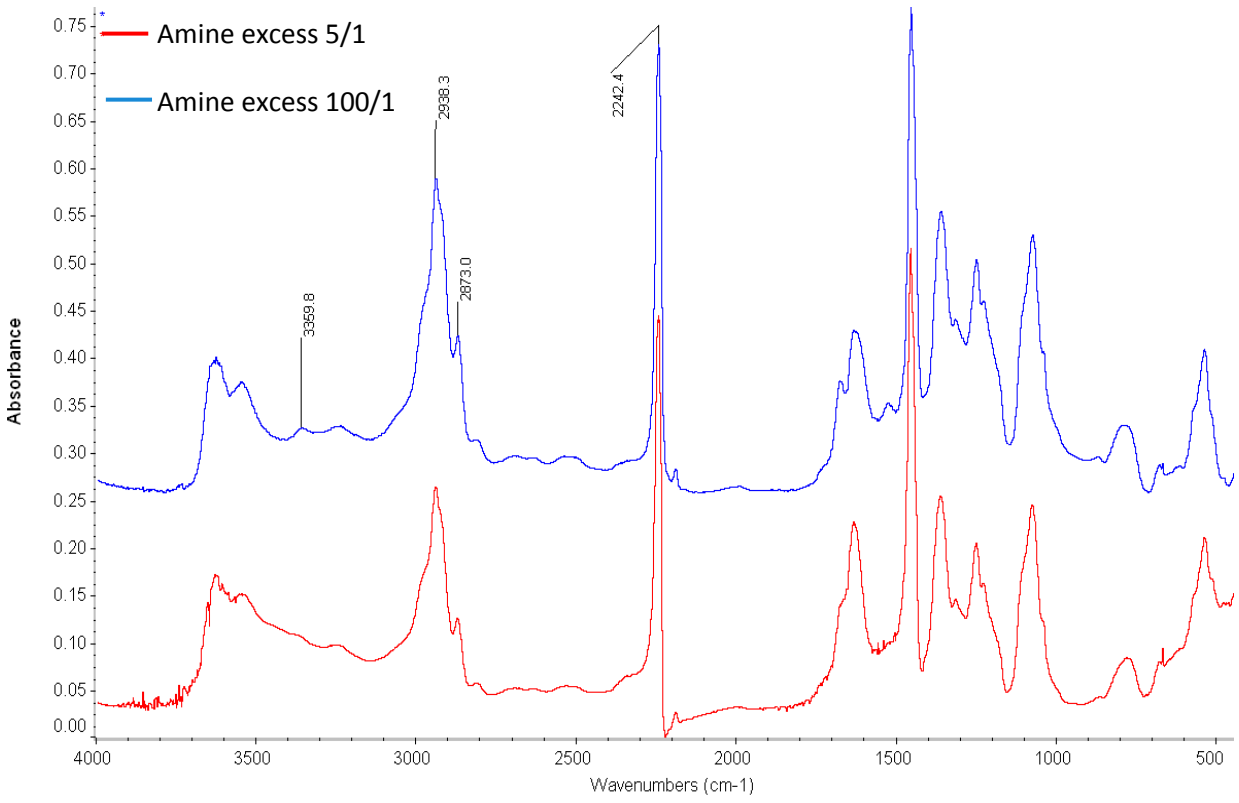

Figure 4.82: FT-IR spectra of functionalized powders with EDA for 1 hour at 80°C, with amine excess 5 and 100 times the stoichiometric ratio.

FT-IR results for hydrolyzed PAN are now reported. Also in this case, as shown in Fig. 4.83, an increase in time is followed by an increase in nirtrile conversion and primary and secondary amines formation, respectively 1570 and 1640 cm^{-1}, moreover it can be observed the appearance of other groups at 1400 and 1680 cm^{-1} justified by formation of groups $–COO^-$ and –CO. In conclusion the optimal operative condition is to conduct the reaction for 5 min, because all the other powders could not be dissolved in DMF.

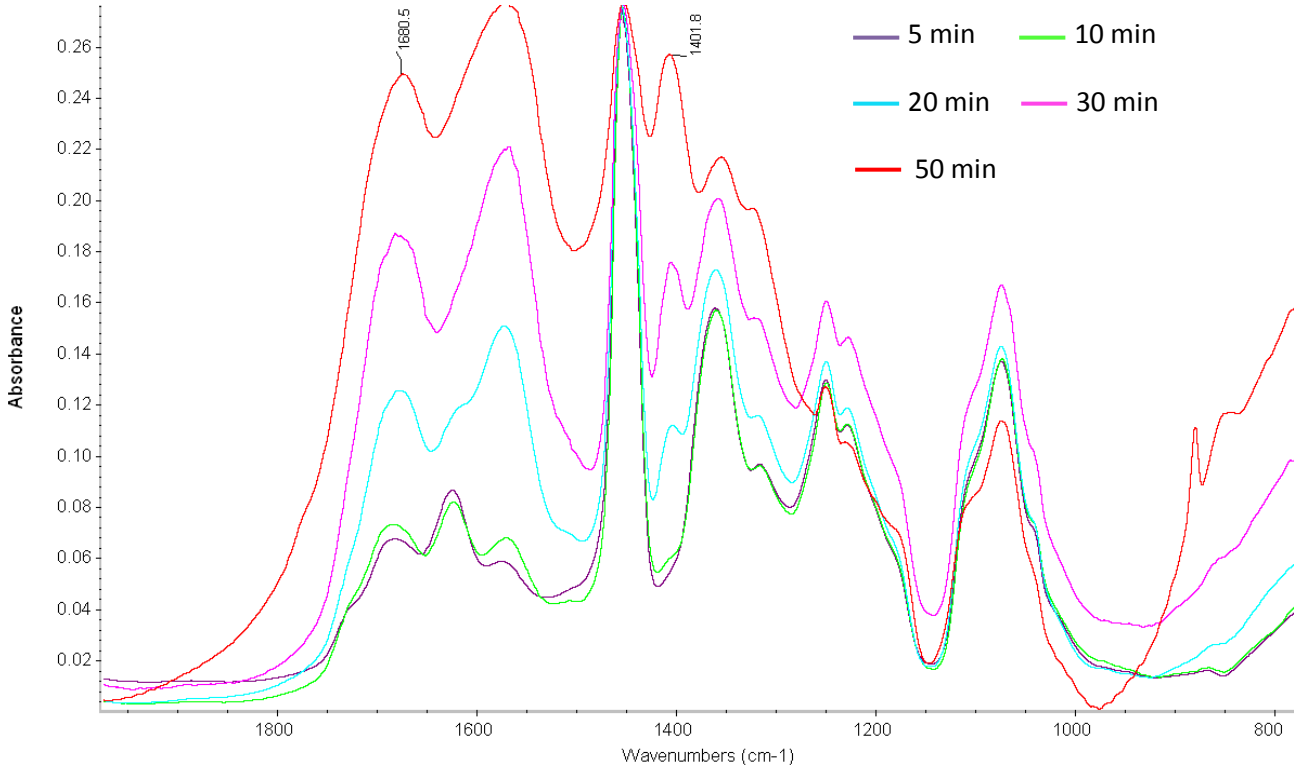

Figure 4.83: FT-IR spectra of hydrolyzed PAN with 1M NaOH aqueous solution at 80°C and different reaction times.

4.3.2 SEM analysis

From Fig. 4.84 it can be observed that electrospun PAN membrane arises as a tangle of defectless polymeric fibers, randomly distributed without any preferential orientation; moreover it can be said that the reaction of functionalization does not implicate variation in the porous structure of membranes. After compaction at hydraulic press, as reported in Fig. 4.90, it can be observed the formation of a compacted layer with no pores, and the disappearance of nanofibers.

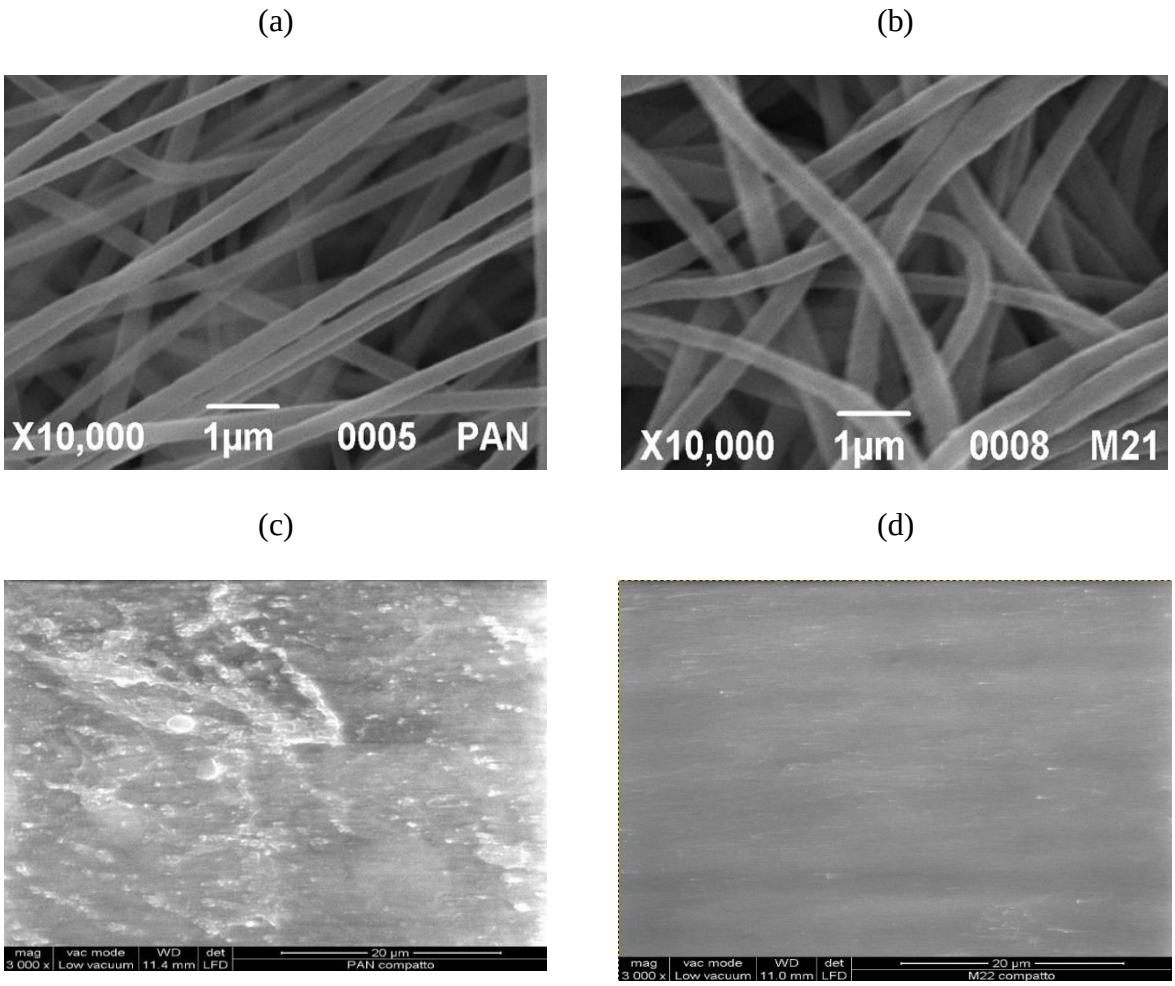

Figure 4.84: SEM images of electrospun (a) and compacted (b) PAN, and electrospun (b) and compacted (d) functionalized PAN with EDA at 90°C fo 3 hours and amine excess equal to 5.

4.3.3 TGA analysis

Thermal stability of fabricated membranes has been analyzed by TGA. In Figure 4.85 TGA curves are reported for different membranes produced. In all cases it is possible to individuate two steps: in the first one we assist to humidity loss, the second one is due to degradation of nitrile groups and amine groups present in the membranes [120]. Moreover it can be observed that functionalized membranes are less stable than pure PAN, in fact their curves are on the left of pure PAN, but variations are very small with respect to polymer and we can conclude that functionalization has no particular negative effects on membranes thermal stability.

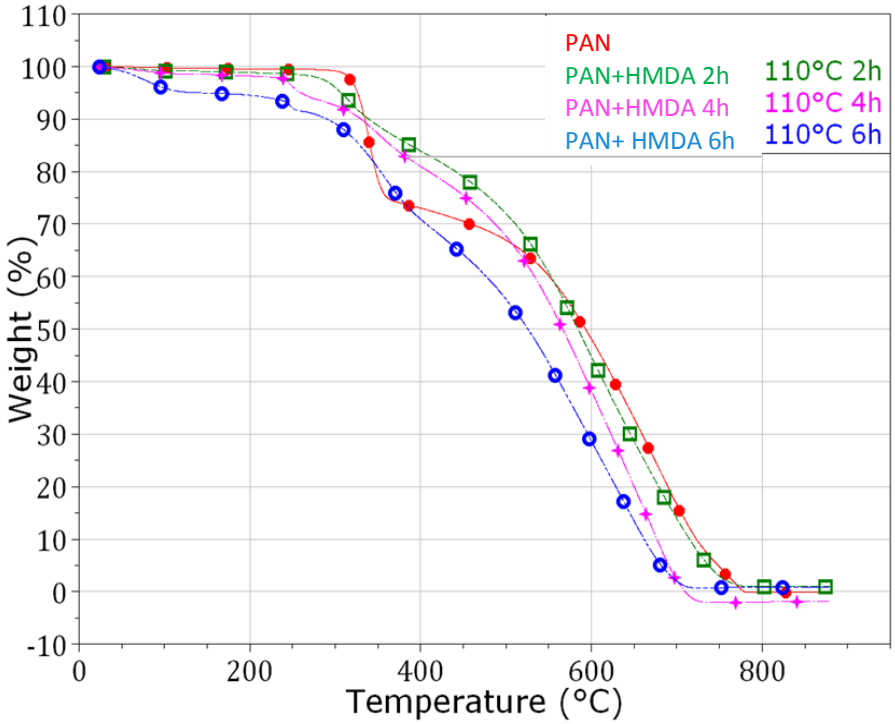

Figure 4.85: TGA results for PAN and functionalized PAN with HMDA.

4.3.4 Transport properties

4.3.4.1 CO_2 solubility in powders and membranes

CO_2 solubility has been measured at 35°C up to 30 bar equilibrium pressure. As reported in literature [152] PAN shows a dependence of CO_2 uptake on material morphology. In particular as can be seen from Fig. 4.86 the solubility increases with surface area contained in the material, high surface area morphologies have higher CO_2 uptake. It is evident that in porous and compacted materials we have to consider an adsorption contribution together with the sorption in bulk of the polymer. It is the same conclusion adduct by Huvard et al. [152], who observed that the solubility of CO_2 in PAN microspheres of 100 nm was higher around three time the one in membrane film, due to surface adsorption of the penetrant molecules.

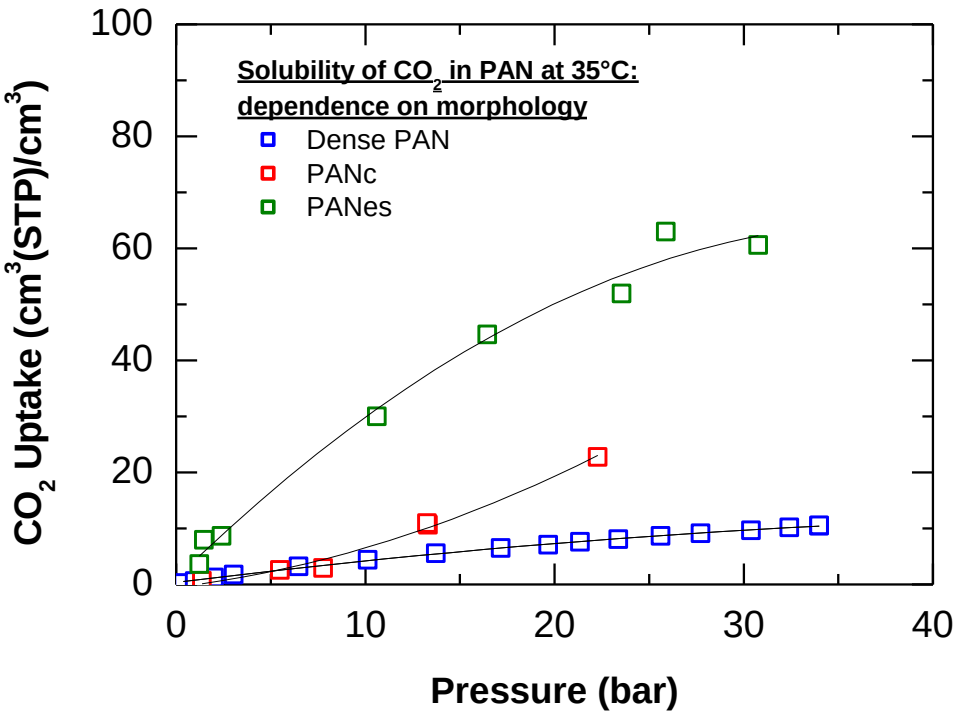

Figure 4.86: Effect of morphology on CO_2 solubility in PAN. Lines are data interpolations.

Functionalization effect on solubility can be observed from Fig. 4.87 where CO_2 solubility results in pure and functionalized PAN with HMDA are reported. Amine content in the tested powders and membranes and preparation route are reported in Table 4.1. It can be observed that solubility increases with amine groups contained in the materials even in dry condition, which suggests higher CO_2 affinity and interactions due to the presence of amines bound to the polymer backbone. In particular solubility increases up to 4 times with respect to pure PAN by increasing amine content up to 63%, which has to be related to higher sorbent capacity of amine sites as already reported by many authors [153–157].

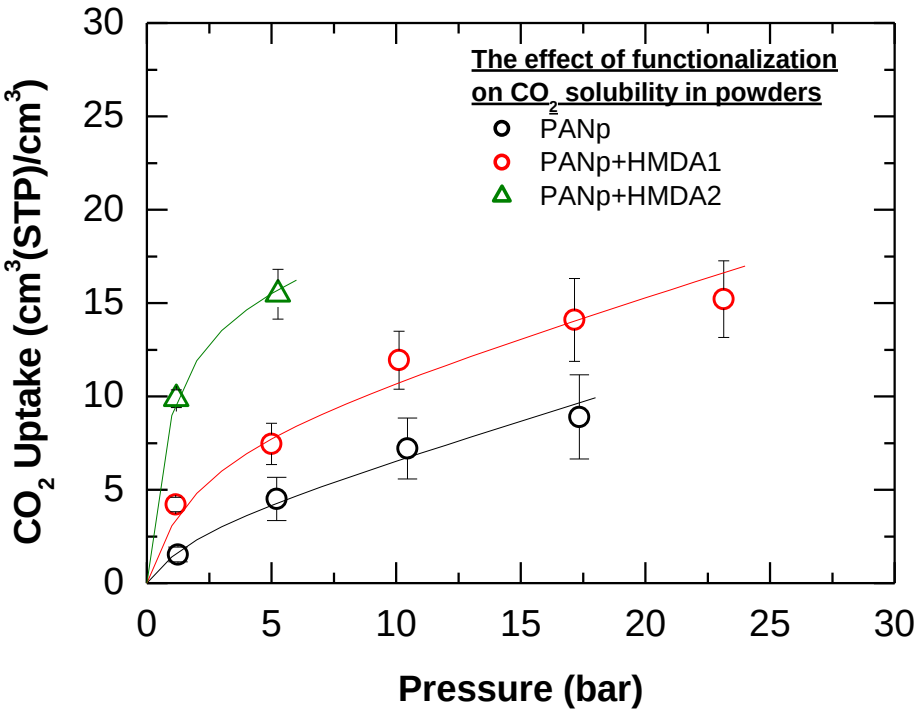

Figure 4.87: Effect of functionalization on CO_2 solubility. Lines are Dual mode model interpolations.

Table 4.1: Materials characterized for CO_2 transport properties.

Material	Reactant	PAN/ Reactant	Reaction	Nitrile groups conversion (%)	Morphology
PANp	-	1/0	-	-	Powder
PANes	-	1/0	-	-	Electrospun membrane
PANc	-	1/0	-	-	Electrospun membrane, compacted
PANp-HMDA1	HMDA	1/2	1	32	Powder
PANp-HMDA2	HMDA	1/2	1	63	Powder

PANc-EDA	EDA	1/5	1	45	Electrospun Membrane, compacted
PANc-HMDA1	HMDA	1/5	1	32	Electrospun Membrane, compacted
PANc-Hydro	Basic solution, NaOH 1M	1/50	2	34	Electrospun Membrane, compacted

4.3.4.2. CO_2 permeability

CO_2 permeability dependence on relative humidity of PAN is reported in Figure 4.88. It can be observed a slight decrease of permeability, around 15% at 75% RH, which could be due to a capacity of water vapor to cluster in existing microcavities in PAN [158].

Considering functionalized membranes, in dry condition, it can be observed from Fig. 4.88 and 4.89 the effect of crosslink during functionalization reaction. In particular in the case of hexamethylene diamine the permeability decreases up to 94%, with ethylene diamine the permeability decreases up to 82%, while with hydrolyzed PAN the permeability loss is smaller, around 69% thanks to the reduction of lateral chain formation during the reaction and consequent crosslinking. Moreover even if PANc-EDA membrane shows higher content of amine sites than PANc-HMDA1, it has a less crosslinked , due to a lower length of EDA chain than HMDA, and has the highest permeability in dry conditions.

Increasing the relative humidity of the feed stream up to 75%, hydrolyzed PAN maintains a pretty constant permeability around 20 Barrer, which suggests that the material is probably not adequately functionalized for the instauration of facilitated transport mechanism in humid conditions. While materials functionalized with HMDA and EDA show increase of permeability up to 20% and 70%, respectively, with respect to pure PAN, which underline

that facilitated transport takes place and is induced in presence of water as reported by many authors [105–110].

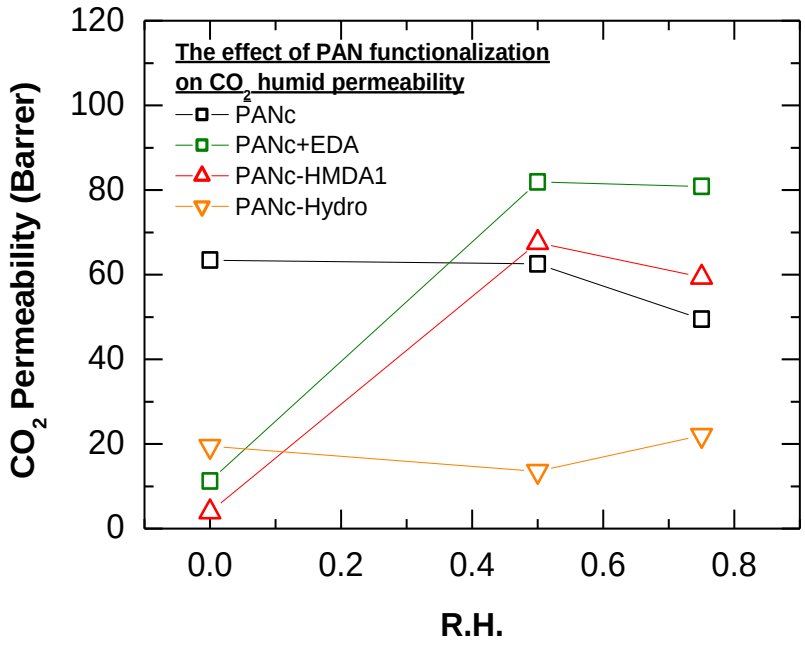

Figure 4.88: Effect of relative humidity on CO_2 permeability in PAN and functionalized PAN with HMDA, EDA and hydrolyzed PAN.

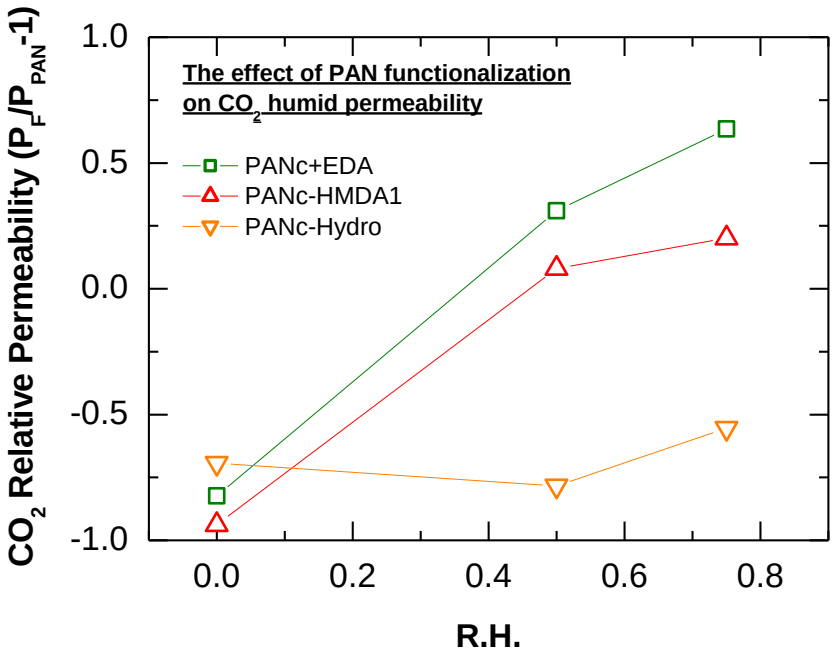

Figure 4.89: Effect of functionalization route on CO_2 permeability in PAN in dry and humid conditions at 35°C and 1 bar.

5. Models

In this chapter the experimental data obtained for copoly(ether imides), shown in the previous section have been modelled, aiming to the rationalization of the effect of copolymer composition and operative conditions one transport mechanism in these kind of materials.
Models used for the theoretical representation of the diffusivity, solubility and permeability will be briefly presented and afterward they will be applied to give the theoretical representation of these physical quantities involved in the transport process.

5.1 Free volume theory

The utilization of polymeric materials as separation membranes requires the necessity of the estimation of the diffusivity of different gases in the polymeric film. A widely used model for the description of the diffusion of low molecular weight species in polymeric systems is the well-known free volume theory of diffusion [150,159,160].
As first presented by Cohen and Turnbull [161], the diffusion of gases in the polymeric matrix can be considered as a series of diffusive jumps in the free volume available for the penetrants. Cohen and Turnbull in particular reported a theoretical description of the diffusion coefficient in a liquid formed of hard spheres, dividing the volume of the liquid in the one occupied by the spheres and the free volume, which can be approximated and considered as voids created by density fluctuations. The fluctuation in density opens a hole within a cage large enough to permit a considerable displacement of the molecules contained by it. Such a displacement gives rise to diffusive motion only if another molecule jumps into the hole before the first returns its original position. So diffusion is treated as translation of a molecule

across the void within its cage, which occurs as a result of redistribution of the free volume within the liquid. Cohen e Turnbull results for free volume are derived within the hypothesis the entire free volume is available to be distributed among molecules without limitations [161]; in free volume theory development by Vrentas e Duda [162,163] two distinct contributions are recognized: the interstitial free volume and the hole free volume. In particular interstitial free volume, function of temperature, corresponds to the fraction of free volume around the molecule which can be exchanged with other molecules only at high energy costs and that, in practice, do not participate to mechanism promoting mass transport, while hole free volume is assumed to be redistributed without energy increase, can be exchanged between molecules without limitations and so is the one available for diffusional transport. In their work, Vrentas and Duda, developed a complex mathematical framework able to describe the self diffusion coefficient of different penetrants in polymer systems. The model can describe the diffusion process both above and below the glass transition temperature of the pure polymer, considering that it seems appropriate to assume that the same type of transport mechanism describes diffusion both in the rubbery and in the glassy state [164].

After the original formulation, many other simplified versions of the free volume theory have been considered. In particular simpler correlation of the diffusion coefficient have been obtained as a function of fractional free volume, *FFV*, as reported in equation 5.1, which recalls Doolittle equation for the viscosity of liquids [165]:

$$D_i = A_i \exp\left(-\frac{B_i}{FFV}\right) \tag{5.1}$$

Where the constants A and B depend on the particular penetrant considered. The constant *A* depends on the system's temperature and the gas molecule's volume and shape and *B*, while

originally labelled as a material constant, was later found to depend on the gas molecule's kinetic diameter [18].

The fractional free volume is defined as the ratio of the polymer average free volume, $\hat{v}_F$, and the specific volume of the polymer, $\hat{v}$, and the free volume is defined as the difference between the specific volume of the polymer and the volume occupied by polymer macromolecules $\hat{v}_O$.

$$FFV = \frac{\hat{v}_F}{\hat{v}} = \frac{\hat{v} - \hat{v}_O}{\hat{v}} \tag{5.2}$$

The definition of occupied volume $\hat{v}_O$ is different throughout the literature. As stated earlier, Doolittle defined occupied volume as the volume of 1 g of liquid extrapolated to absolute zero without a change of phase. Over time the most popular definition of occupied volume for polymers has come from using Bondi's group contribution method which is based on the packing densities of molecular crystals at absolute zero and the van der Waals volume of each of the various groups in the polymer structure:

$$\hat{v}_O = 1.3\sum_{k=1}^{K} \hat{v}_{W,k} \tag{5.3}$$

Where *K* is the total number of groups into which the repeat unit structure of the polymer is divided and $\hat{v}_{W,k}$ is the van der Waals volume of each group *k*. The factor of 1.3 was estimated by Bondi from packing density considerations, taking into account also the volume of the polymer inaccessible to gas molecules, and is assumed to be applicable to all groups and structures.

5.1.1 Modeling diffusivity in copolymers

In the case of copoly(ether imides), materials are formed by two segregated phases which are randomly distributed and as reported in literature [15], for practical purpose, the free volume can be expressed with an additive rule as follow:

$$FFV_{copolymer} = \frac{\hat{v}_{copolymer} - 1.3\left(\omega_R \hat{v}_{w,R} + \omega_G \hat{v}_{w,G}\right)}{\hat{v}_{copolymer}} \tag{5.4}$$

Where $\hat{v}_{copolymer}$ is the specific volume of the copolymer, ω_R and ω_G are the mass fraction of rubbery and glassy phase respectively, $\hat{v}_{w,R}$ and $\hat{v}_{w,G}$ are the van der Waals volume of the rubbery and glassy pure homopolymer taken from [143] and reported in Table 5.1.

Table 5.1: Van der Waals volumes for pure homopolymers.

Polymer	Van der Waals volume (cm^3/g)
PPO	0.592
PEO	0.673
BPDA-ODA	0.495
BKDA-ODA	0.490

Having the knowledge of experimental diffusion activation energies, the constant A_i in equation 5.1 has been expressed as:

$$A_i = D_{i,0} \exp\left(-\frac{E_D}{RT}\right) \tag{5.5}$$

Where the parameter $D_{i,0}$ is a specific gas-polymer pair, temperature independent, which is assumed to be independent with copolymer formulation, and E_D is the activation energy for diffusion process in the copolymer. The parameters $D_{i,0}$ and B_i for the two series of

copolymers have been optimized on CO_2 diffusivity data reported in the experimental results section.

5.2 Equilibrium and Non Equilibrium Lattice Fluid Models

The theoretical representation of the solubility of gases and vapors in polymeric matrices is a crucial aspect to estimate the separation performances offered by the membrane and to deeply understand the connection between polymer structure and morphology with its sorption capacity.

Rubbery amorphous polymers-penetrant mixtures can be described by the well known Flory Huggins model, which is meant to apply to mixtures of molecules of different sizes. Unlike the Flory-Huggins model, the Sanchez-Lacombe model [167] considers configurations with empty sites in the lattice, so free volume exists in the polymer-penetrant mixture, and volume changes upon mixing penetrant and polymer molecules are allowed. The Sanchez-Lacombe model treats polymer chains as a set of beads on a lattice, in which polymer chains are mixed randomly with penetrant molecules. Each component of the mixture is completely characterized by three independent parameters: the characteristic pressure p_i^*, which is the hypothetical cohesive energy density of component *i* in the closed-packed state, the corresponding mass density ρ_i^*, and the characteristic temperature T_i^*, related to the closed-packed lattice site energy. These parameters can be obtained by the best fit of the LF equation of state to pressure-volume-temperature data, PVT, above glass transition temperature for the polymer, and to vapor liquid equilibrium data for penetrants. Statistical analysis of the corresponding picture for polymer−penetrant binary mixtures allows to derive an expression for the Helmholtz free energy in the equilibrium states as a function of temperature *T*, polymer mass density, $\rho_{Polymer}$, and solute mass fraction, ω_i, of the following form:

$$a_{LF}^{EQ,mix} = a(T, \rho_{Polymer}, \omega_i) \tag{5.6}$$

By using well-known results from classical thermodynamics, an equation of state (EoS) for equilibrium pressure describing the behavior of the polymer−solute system is derived:

$$p = -a_{LF}^{EQ,mix}(T, \rho_{Polymer}, \omega_i) + \rho_{Polymer}\left(\frac{\partial a_{LF}^{EQ,mix}}{\partial \rho_{Polymer}}\right)_{T,\omega_i} \tag{5.7}$$

The models developed for the description of rubbery polymer, such as LF EoS, fails in the description of the glassy state, due to the out of equilibrium of glassy polymers. Empirical or semi-empirical approaches have been proposed for the description of gases and vapors dissolution in glasses. The widely used model remains the Dual Mode Sorption Model [168], DMSM, which has found extensive and successful applications over the years. The model is very easy to apply, with its three adjustable parameters, which have to be calculated from a data-fitting procedure based on experimental data available for each penetrant-polymer couple. So the model has no predictive ability, and in addition, usually parameters depends on the pressure range examined for the fitting procedure.

In 1996 Doghieri and Sarti [169] developed a modeling approach for the prediction of penetrant solubility in glassy polymer, called as Non Equilibrium Thermodynamics for Glassy Polymers (NET-GP), which adopts an equation of state approach for the description of polymeric systems. In fact, based on a thermodynamic approach, they demonstrated the extension to the glassy state of equilibrium models, adopting the density of the polymer as an internal state variable capable to describe the non-equilibrium state of the system, as it can not evolve toward equilibrium conditions due to kinetic constraints, which hinders polymers relaxation below glass transition temperature. In particular, the Non Equilibrium Lattice Fluid model adopts the same thermodynamics representation of Sanchez-Lacombe LF theory and extends its validity to the glassy state by the use of the density as internal state variable, which cannot be calculated as usual for rubbery polymers with the LF equation of state, but has to be

experimentally determinate, and depends on the previous sorptive and thermal history of the glassy polymer.

The NELF model moves from the results of LF theory indicated above, extending the mapping of free energy density to the glassy states of the polymer−penetrant systems. The simple conclusion is finally drawn for Helmholtz free energy in non-equilibrium states of the system indicated in the following relation:

$$a_{LF}^{EQ,mix}(T,\rho_{Polymer},\omega_i) = a_{NELF}^{NE,mix}(T,p,\omega_i,\rho_{Polymer}) \tag{5.8}$$

Adopting rigorous thermodynamics arguments, they demonstrated that the expression of the chemical potential is formally the same as LF theory. It must be stressed that while in equilibrium conditions the mass density of polymeric species is related to temperature, pressure, and composition by means of equation 5.7, in non-equilibrium glassy states, the mass density of polymeric species is not unequivocally related to the same set of variables, and it needs to be independently estimated in corresponding NELF formulations of phase equilibrium problems.

So, as described in detail in previous papers [167,168,170] the solubility of a gas in a rubbery or glassy polymer can be modelled and predicted with lattice fluid models, considering equilibrium and non-equilibrium conditions respectively, applying the equality of chemical potential of penetrant between the gaseous phase and the polymeric one.

We report in Table 5.2 the main equations and parameters of lattice fluid models:

Table 5.2: Main equation of LF models.

	Symbol	Name	Definition/property
Pure component *i*	ρ_i^*, p_i^*, T_i^*	Characteristic density, pressure and temperature	
	$\tilde{\rho}_i, \tilde{p}_i, \tilde{T}_i$	Reduced density, pressure and temperature	$\tilde{\rho}_i = \rho_i / \rho_i^* ; \tilde{p}_i = p / p_i^* \ ; \tilde{T}_i = T / T_i^*$
	v_i^*	Volume occupied by a mole of lattice sites	$v_i^* = \frac{R T_i^*}{p_i^*}$
	r_i^0	Number of lattice sites occupied by a molecule	$r_i^0 = \frac{M_i}{r_i^* v_i^*}$
	ω_i	Mass fraction	
	ϕ_i	Volume fraction	$\phi_i = \frac{\omega_i / \rho_i^*}{\sum_{i=1}^{N_P+1} \omega_i / \rho_i^*}$
Mixtures	ρ^*	Characteristic density	$1/\rho^* = \sum_{i=1}^{N_P+1} \omega_i / \rho_i^*$
	p^*	Characteristic pressure	$p^* = \sum_{i=1}^{N_P+1} \phi_i p_i^* - \frac{1}{2} \sum_{i=1}^{N_P+1} \phi_i \sum_{i \neq j} \phi_j \Delta p_{ij}^*$
	Δp_{ij}^*	Binary parameter	$\Delta p_{ij}^* = p_i^* + p_j^* - 2(1-k_{ij})\sqrt{p_i^* \cdot p_j^*}$
	k_{ij} , Ψ_{ij}	Binary parameter	$\Psi_{ij} = 1 - k_{ij}$
	r_i	Number of lattice sites occupied by a molecule	$r_i^0 v_i^* = r_i v^*$
	r	Molar average number of lattice sites occupied by a molecule	$r = \sum_{i=1}^{N_P+1} x_i r_i$
	T^*, v^*	Characteristic temperature, average close-packed mer molar volume	$T^* = \frac{p^*}{r} \sum_{i=1}^{N_P+1} x_i r_i^0 \frac{T_i^*}{p_i^*} = \frac{p^* v^*}{R}$
	$\tilde{\rho}, \tilde{p}, \tilde{T}$	Reduced density, pressure and temperature	$\tilde{\rho} = \rho / \rho^* ; \ \tilde{p} = p / p^* \ ; \ \tilde{T} = T / T^*$
		Equation of state for the fluid-polymer mixture ($\phi_i = 1$ for pure *i*)	$\tilde{\rho}^2 + \tilde{p} + \tilde{T}\left[\ln(1-\tilde{\rho}) + \tilde{\rho}\left(1 - \sum_{i=1}^{N_P+1} \frac{\phi_i}{r_i}\right)\right] = 0$

	$\mu_i^{(S)}$	Chemical potential of *i* in the polymer mixture ($\phi_i = 1$ for pure *i*)	$\mu_i = \ln\phi_i + (1-\phi_i) + \tilde{\rho}\frac{M_i}{\rho_i^*}\frac{\Delta p^*}{RT}(1-\phi_i)^2 + r_i^0\left[-\frac{\tilde{\rho}}{\tilde{T}_i} + \frac{\tilde{p}_i}{\tilde{T}_i\tilde{\rho}} + \frac{(1-\tilde{\rho})\ln(1-\tilde{\rho})}{\tilde{\rho}} + \frac{\ln\tilde{\rho}}{r_i}\right]$
	$\frac{\Delta V}{V_0}$	Volume dilation induced by penetrant sorption (V_0 is dry polymer volume)	$\frac{\Delta V}{V_0} = \frac{1}{\tilde{\rho}\rho^*(1-\omega_i)\hat{v}^0_{Polymer}} - 1$

The models also contain a binary gas-polymer interaction parameter, k_{ij}, which affects the characteristic pressure of the gas-polymer mixture and can be set equal to zero, in first approximation, or adjusted on solubility data.

The gas solubility at each temperature and pressure can be obtained by solving the phase equilibrium condition, using the expression of the chemical potential reported in Table 5.2. In particular in the case of the rubbery polymer, phase equilibrium is represented by equation 5.9 and the density of polymeric mixture is calculated by LF EoS, that must be solved together with the phase equilibrium condition between gas (G) and solid (S) phase:

$$\mu_i^G(T,p) = \mu_i^S(T,p,\omega_i) \tag{5.9}$$

For the glassy phase, due to its non-equilibrium state, the polymer density is an internal state variable that should be provided to the model from experimental data, or adjusted on solubility data:

$$\mu_i^G(T,p) = \mu_i^S(T,p,\omega_i,\rho_{POL}) \tag{5.10}$$

It must be also specified that, during sorption of swelling penetrants such as CO_2, the glassy polymer density may not stay constant to its dry value, but can change due to swelling. In case no swelling data are available for the gas-polymer mixture inspected, as in the present case, one can rely on the assumption that density varies linearly with gas pressure, as reported by many authors [171–174], and thus introduce only one additional adjustable parameter to represent its value in the entire pressure range. The value of the slope of density

versus pressure is called swelling coefficient, $k_{sw,}$ and relates density to pressure and dry polymer density ρ_{POL}^{0} according to the following equation:

$$\rho_{POL} = \rho_{POL}^{0} \left(- k_{sw} p_i \right) \tag{5.11}$$

5.2.1 Model for gas solubility in copolymers

The NELF model has been used, over the years, to model the solubility of pure and mixed fluids in many complex polymeric systems such as the polymer blends [175], crosslinked polymers [176], semicrystalline structures [127] and composite materials [177,178]. Different types of approaches are possible when we deal with the estimation of the gas solubility in a complex system such as a copolymer formed by a rubbery phase, at equilibrium, and a glassy phase, that is not at equilibrium.

In general, both phases are active during the sorption process and the gas concentration can be expressed assuming additivity of the solubility contributions due to the rubbery and to the glassy phase, named c_R and c_G respectively:

$$c_{copol} = w_R c_R + (1 - w_R) c_G \tag{5.12}$$

In the above equation, the concentration of gas absorbed by the rubbery phase is estimated at each pressure with the LF EoS model, while the concentration of gas absorbed by the glassy phase is estimated with the NELF model. Different assumptions can be made for the degree of interaction and interpenetration between the two phases, which affect the choice of the parameters required by the equilibrium and non equilibrium models in order to calculate the solubility.

In particular, the estimation of the concentration of a gas in a rubbery polymer by the LF EoS requires for the values of the pure gas and pure polymer parameters, as explained above, and of a binary energetic parameter k_{ij} (gas-polymer). In this work we assumed that the rubbery pure polymer phase parameters are equal to those obtained on the corresponding pure

rubbery homopolymer. The binary parameter k_{ij} was taken equal to the one obtained based on the solubility of the gas in the pure homopolymer.

When it comes to the density of the polymeric phases to be used in the modeling, one has to account for the fact that the copolymers volume is lower than the sum of the homopolymers volumes, considering the negative mixing volume observed experimentally, and thus that one, or both phases assumes a density value higher than that of the corresponding pure homopolymer. Indeed the glassy phase, by nature, can assume rather different density values at fixed pressure, temperature, and gas composition; however, also the rubbery phase present in the copolymer may be not free to expand and to assume the equilibrium value of the volume, as it would be in its pure state. In order to reduce the number of adjustable parameters of the model, and following physical considerations and model assumptions, we attributed the negative mixing volume entirely to the glassy phase, and assumed that the rubbery density value is equal to that of the pure homopolymer $\hat{v}_R = \hat{v}_R^0$. The glassy density value indeed is not a unique value because it can vary due to different sample history; the NELF model is thus already set to account for such variations and to include arbitrary values of polymer density, decoupled from the prevailing temperature, pressure and composition values. Moreover, some previous results indicate that some of the excess free volume of the glassy domains are penetrated by soft segments in these copolymers. The value of glassy phase density in each copolymer, $\hat{v}_G$ according to the previous considerations, can be calculated from experimental data for the copolymer volume with the following equation

$$\hat{v}_{copol} = w_R \hat{v}_R^0 + (1 - w_R)\hat{v}_G \tag{5.13}$$

5.3 Permeability modeling

Considering the validity of solution-diffusion model, confirmed by experimental evidences, in this work the permeability has been modeled by calculating the solubility coefficient with LF

models, as reported in the previous section, and diffusion coefficient with free volume theory, as reported in equation 5.7.

$$P_i = D_i \cdot S_i = D_{i,0} \exp\left(-\frac{E_D}{RT}\right) \exp\left(-\frac{B_i}{FFV}\right) \cdot S_i \tag{5.14}$$

5.4 Evaluation of pure component LF parameters

As said before to model solubility data with NELF model, we need the lattice fluid parameters, T^*, p^*, ρ^*, for CO_2 and the different polymeric phases forming the copolymer. Normally such data are retrieved by fitting the LF EoS parameters on PVT data above T_g for the polymers, and on LV data for the gases. This was the procedure followed for the polymer PPO and we report in Figure 5.1 comparison of experimental data of specific volume [124] with prediction of LF model. The maximum error in the estimated polymer volume in the entire range of pressure and temperature considered is below 1%.

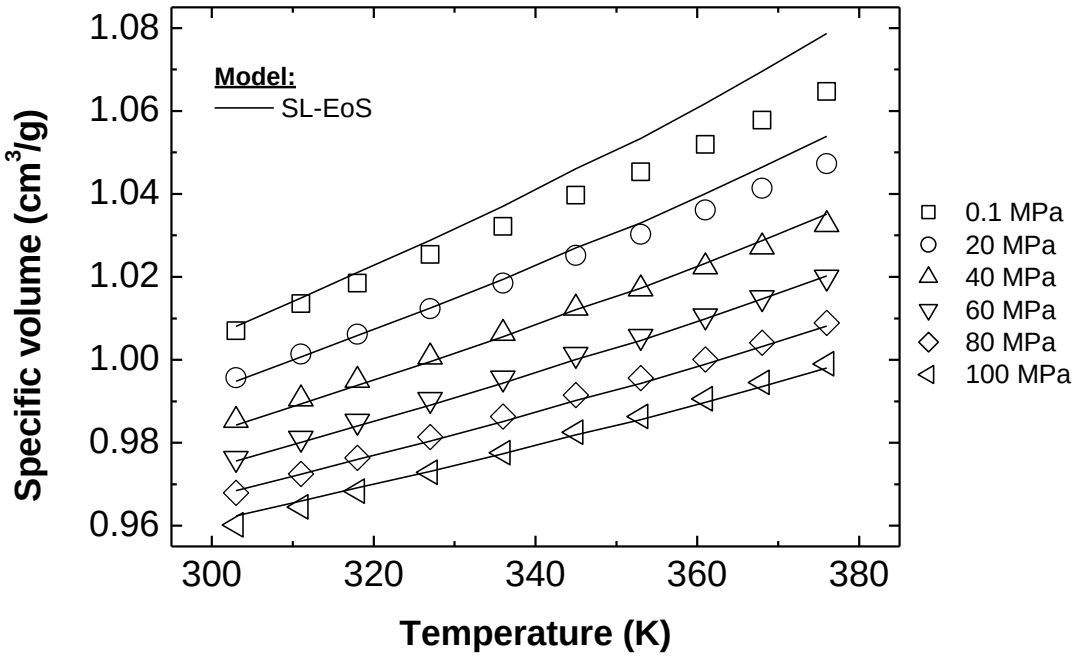

Figure 5.1: Comparison of Sanchez and Lacombe LF-EoS and experimental data of specific volume of PPO at different temperature and pressure.

For BPDA-ODA and BKDA-ODA pure component PVT data above T_g are not available and different procedure has been followed, as it can be seen in Figure 5.2 and Figure 5.3, that fits the LF parameters using the NELF model for the solubility in the glassy state and the gas solubility data in the glassy polymers taken from ref [180,181]. It is important to underline that LF parameters were optimized considering for all gases zero value for k_{ij} and k_{sw}. The set of parameters thus obtained is listed in Table 5.3 together with those of PPO, CO_2 taken from ref [124] and PEO taken from ref.[178].

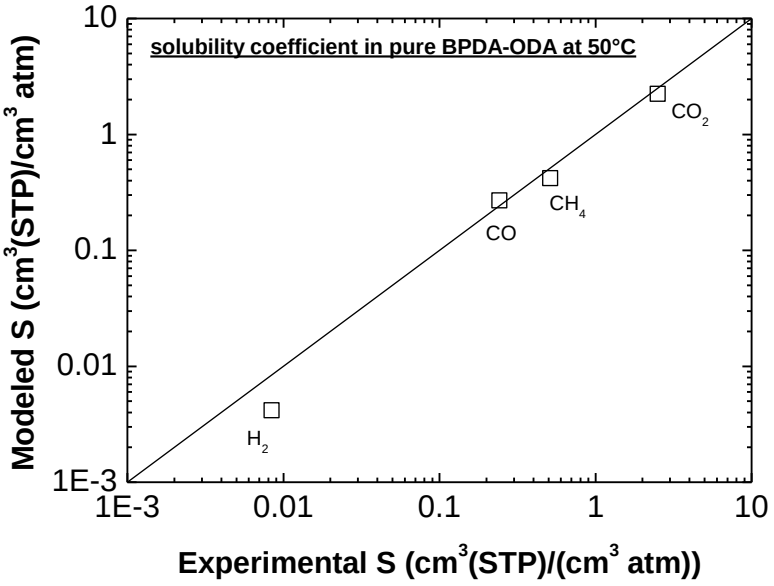

Figure 5.2: Parity plot for comparison of NELF model and experimental solubility data in BPDA-ODA.

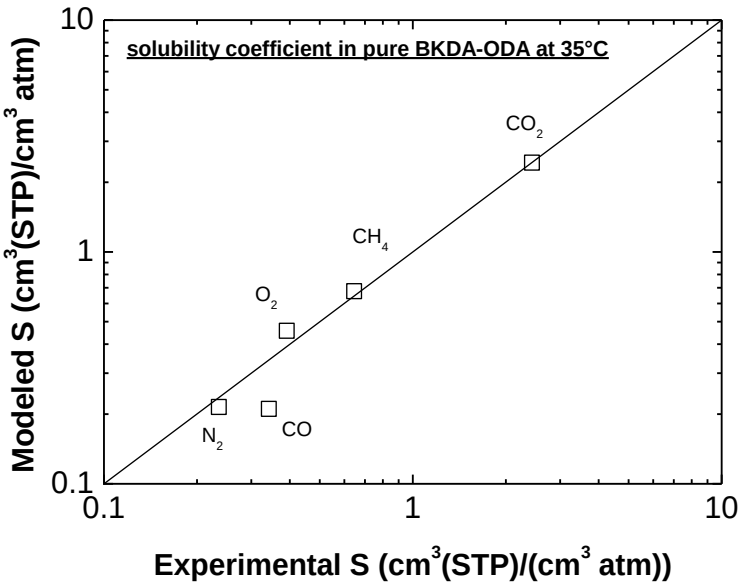

Figure 5.3: Parity plot for comparison of NELF model and experimental solubility in BKDA-ODA.

Table 5.3: Sanchez and Lacombe pure component LF parameters.

Component	T*	p*	ρ*	Reference
	K	MPa	g/cm^3	
PPO	542	420	1.096	This work, modelling p-v-T data taken from ref. 124 with LF EoS
PEO	590	620	1.218	Taken from ref. 178
BPDA-ODA	570	480	1.610	This work, based on NELF model fitting of solubility data of CO_2, CH_4, CO, H_2 taken from ref. 179
BKDA-ODA	670	600	1.530	This work, based on NELF model fitting of solubility data of CO_2, CH_4, CO, O_2, N_2 taken from ref. 180
CO_2	300	630	1.515	Taken from ref. 169

5.5 Modeling CO_2 sorption in pure PPO, BPDA-ODA, PEO and BKDA-ODA

The binary parameters k_{ij}, and k_{sw}, have been calculated from literature CO_2 induced dilation and CO_2 solubility data in the pure homopolymers using LF EoS for PPO [181] and PEO [181,182] and NELF model for polyimide membrane BPDA-ODA [179]. For polyimide BKDA-ODA we considered the value of k_{ij} equal to zero, as imposed for LF parameters estimation. These parameters are listed in Table 5.3. In particular for rubbery phases, which

are in thermodynamic equilibrium, the only adjustable parameter is k_{ij}, while for glassy phases one needs to estimate also k_{sw}. However, for all the glassy homopolymers considered, the swelling coefficient has been set equal to zero obtaining good fits of the sorption isotherms both for homopolymers and copolymers, thus indicating that such polyimides are rather rigid. This result also indicates that, in the copolymers considered, the only phase responsible for swelling is the rubbery one.

The same is true for all binary energetic parameters k_{ij}, that are equal to zero in practically all cases except that of pure PEO, that is in line with the value reported in a previous work for a different molecular weight and experimental temperature [127]. The value of zero indicates a good compatibility between gas and polymer phase. The fact that k_{ij} is constant with copolymer composition is consistent with the fact that such parameter represents interactions between CO_2 and repeating units (monomers) of the polymeric phases.

In Figures 5.4–5.8 comparisons of experimental solubility isotherms and modeled data for CO_2 in PPO, PEO and BPDA-ODA are reported. One can observe that experimental data for PPO seem not to have the classical behavior of gas sorption in a rubbery polymer and they are underestimated by the model particularly in the low pressure range. On the other hand dilation data are well represented by LF model.

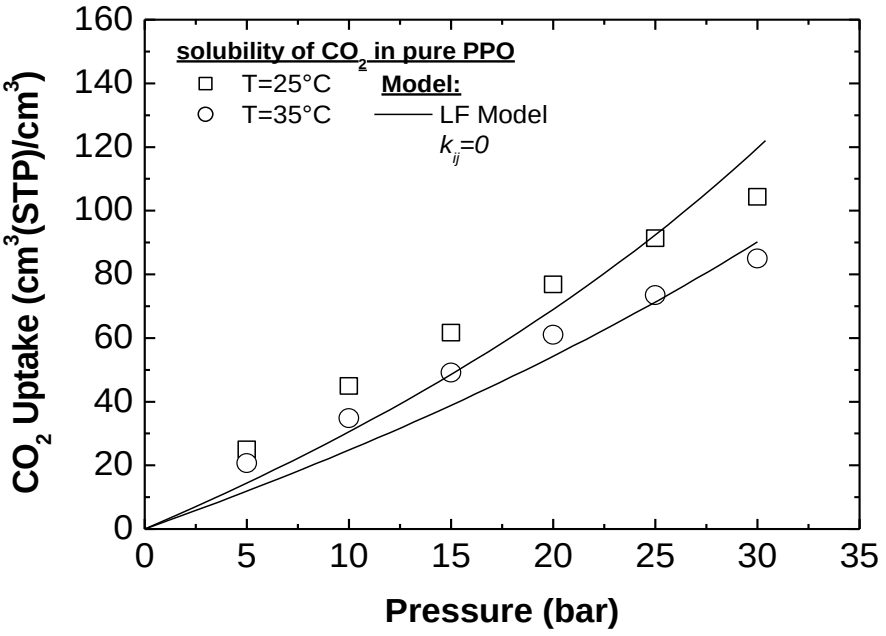

Figure 5.4: Comparison of LF model with data of CO_2 sorption in PPO at different temperature and pressure.

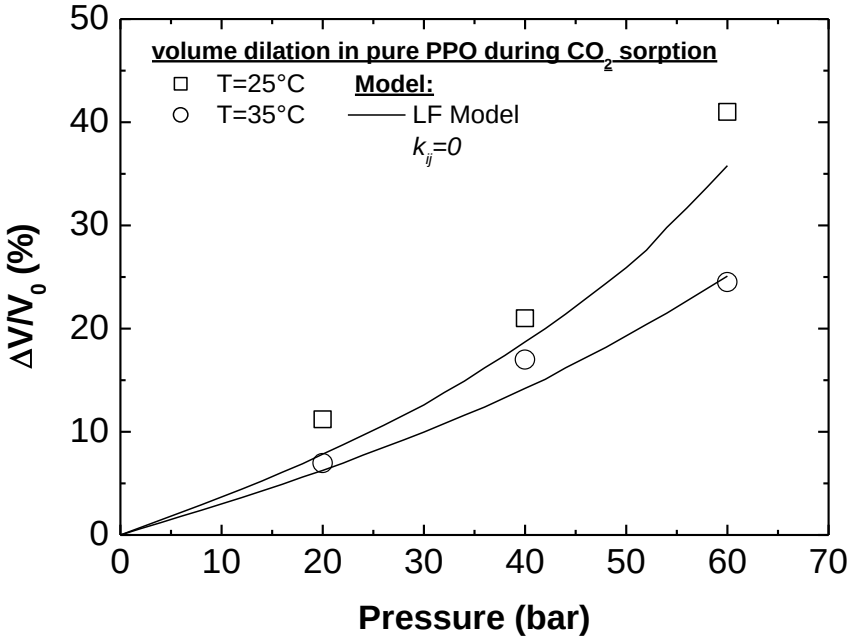

Figure 5.5: Comparison of LF model with data of CO_2 induced dilation in PPO at different temperature and pressure.

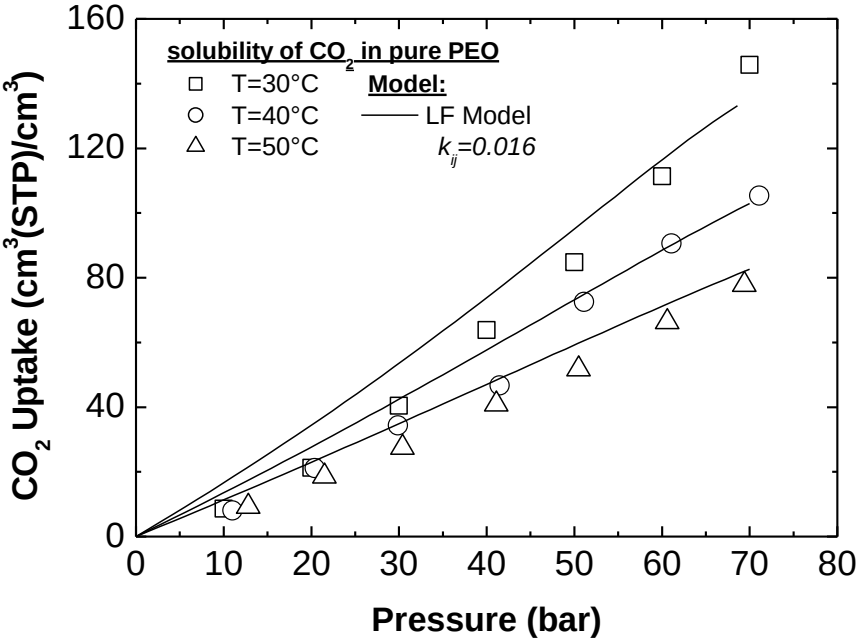

Figure 5.6: Comparison of LF model with data of CO_2 sorption in PEO at different temperature and pressures.

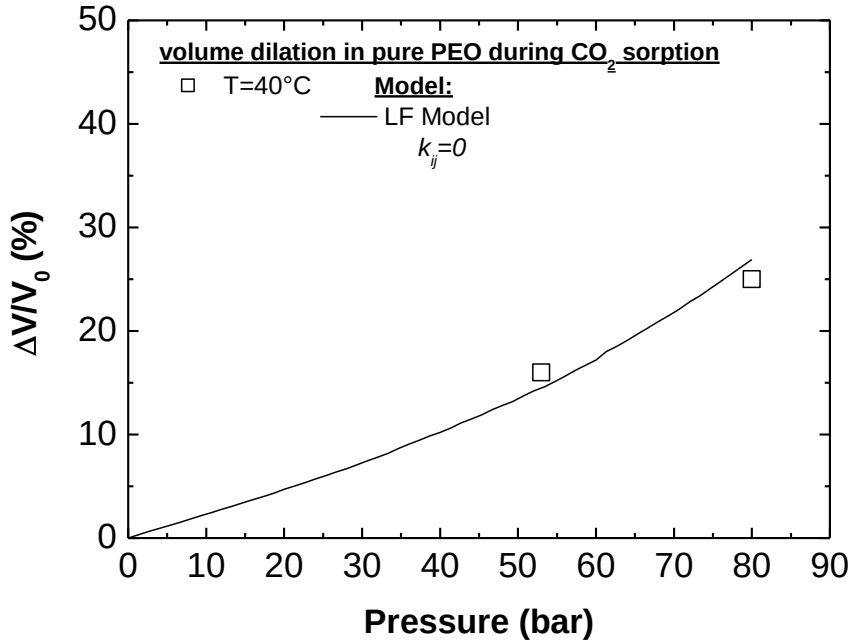

Figure 5.7: Comparison of LF model with data of CO_2 induced dilation in PEO at different pressures.

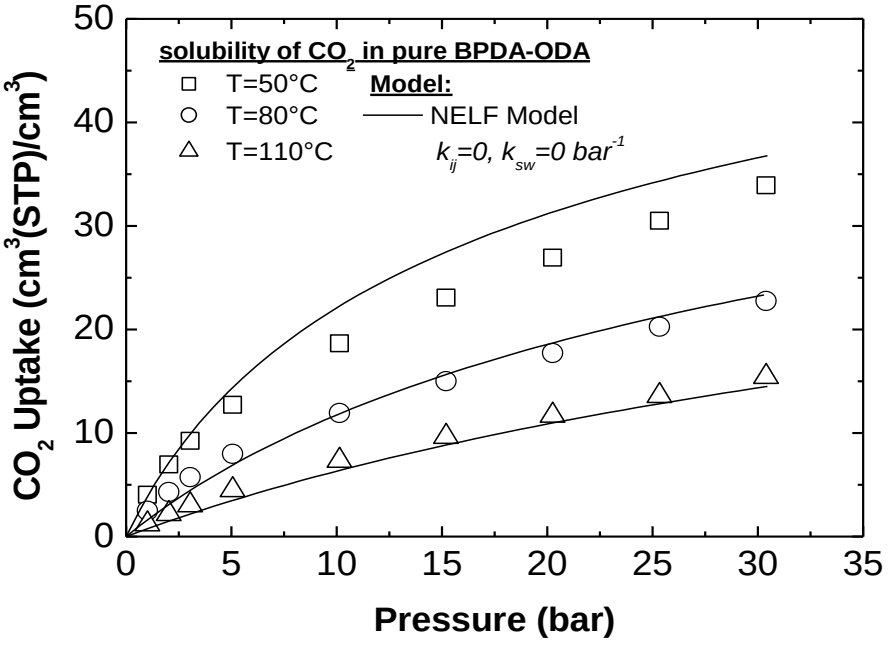

Figure 5.8: Comparison of NELF model and experimental data of CO_2 sorption in BPDA-ODA at different temperatures and pressures.

Table 5.4: Adjustable parameters for LF and NELF models.

	CO_2 - PPO	**CO_2 - BPDA-ODA**		**CO_2 – PEO**	**CO_2 - BKDA-ODA**	
T	**k_{ij}**	**k_{ij}**	**k_{sw}**	**k_{ij}**	**k_{ij}**	**k_{sw}**
°C			**bar^1**			**bar^{-1}**
30	0	0	0	0.016	0	0
45	0	0	0	0.016	0	0
60	0	0	0	0.016	0	0

5.5 Modeling CO_2 sorption in copolyetherimides

As it can be seen in Figures 5.9–5.14, using the proposed model with reported parameters, we see that we obtain a good representation of the experimental data within the experimental error. It must be pointed out that no adjustable parameters were used in the model. The energetic interactions between CO_2 and the two different phases, represented by the k_{ij} value, are equal to those observed between CO_2 and the respective homopolymers, as it is

reasonable, and are in almost all cases equal to the default value of zero. The same is true for swelling coefficient.

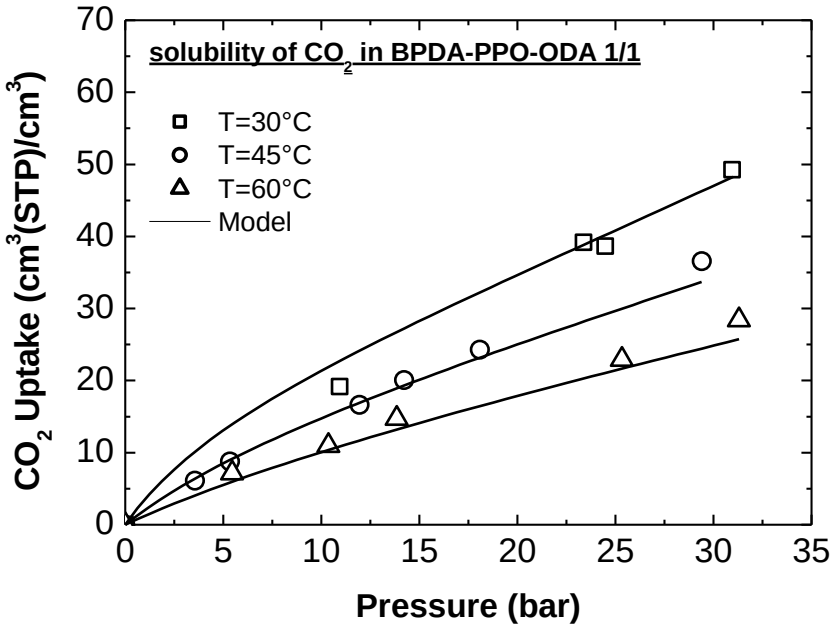

Figure 5.9: Comparison between experimental CO_2 solubility data and modeled solubility data with LF and NELF Models in BPDA-PPO-ODA 1/1 at 30°C, 45°C and 60°C.

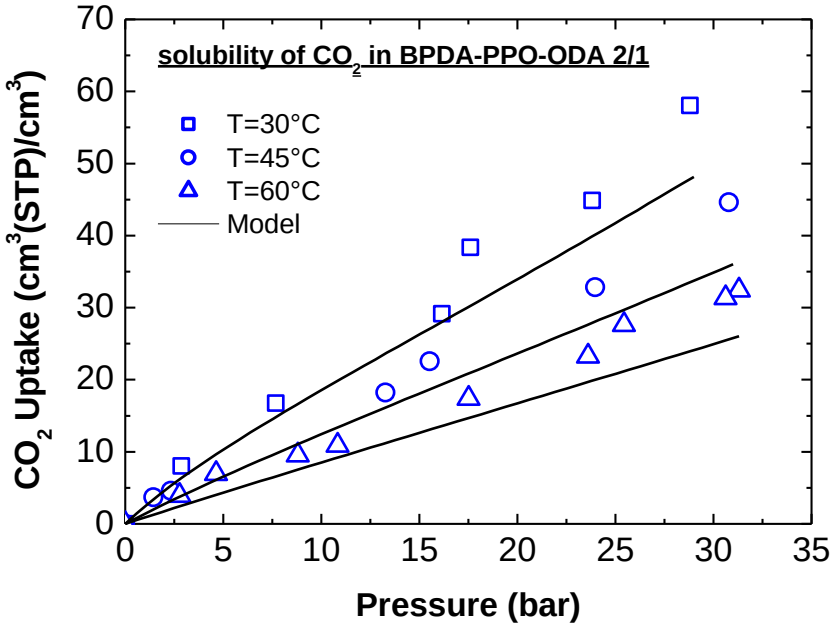

Figure 5.10: Comparison between experimental CO_2 solubility data and modeled solubility data with LF and NELF Models in BPDA-PPO-ODA 2/1 at 30°C, 45°C and 60°C.

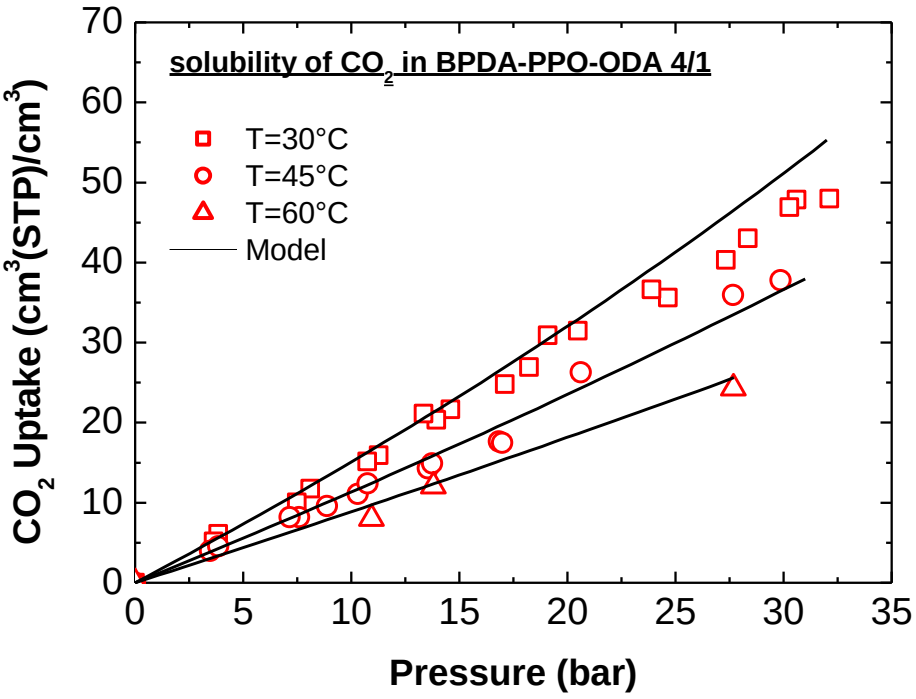

Figure 5.11: Comparison between experimental CO_2 solubility data and modeled solubility data with LF and NELF Models in BPDA-PPO-ODA 4/1 at 30°C, 45°C and 60°C.

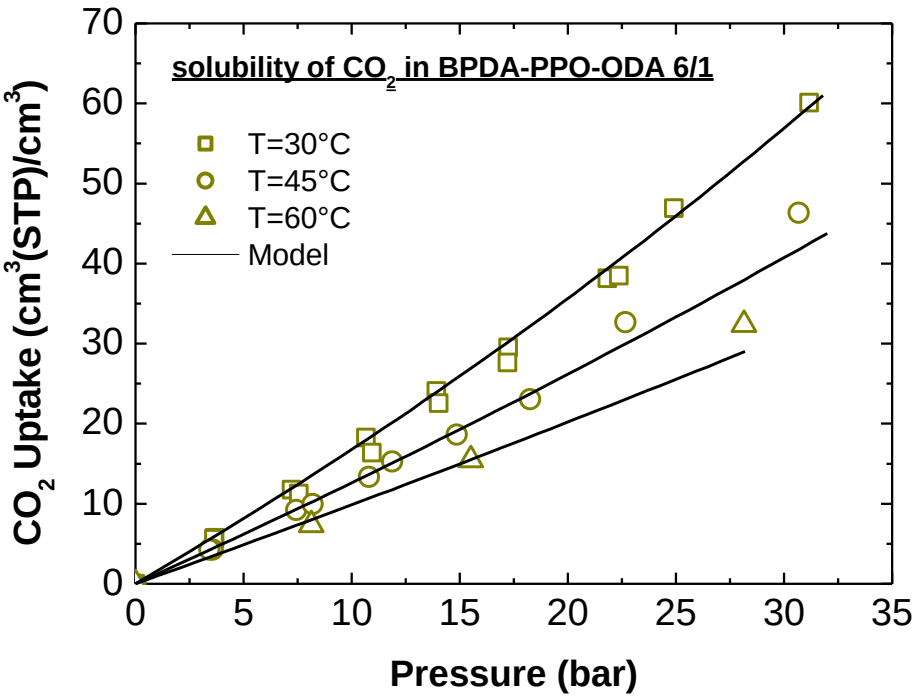

Figure 5.12: Comparison between experimental CO_2 solubility data and modeled solubility data with LF and NELF Models in BPDA-PPO-ODA 6/1 at 30°C, 45°C and 60°C.

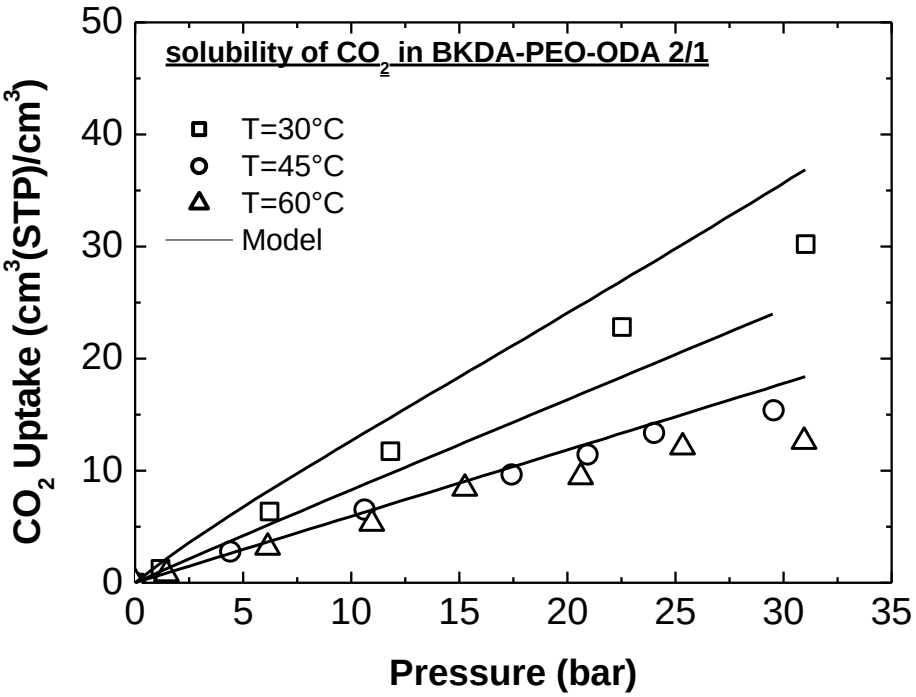

Figure 5.13: Comparison between experimental CO_2 solubility data and modeled solubility data with LF and NELF Models in BKDA-PEO-ODA 2/1 at 30°C, 45°C and 60°C.

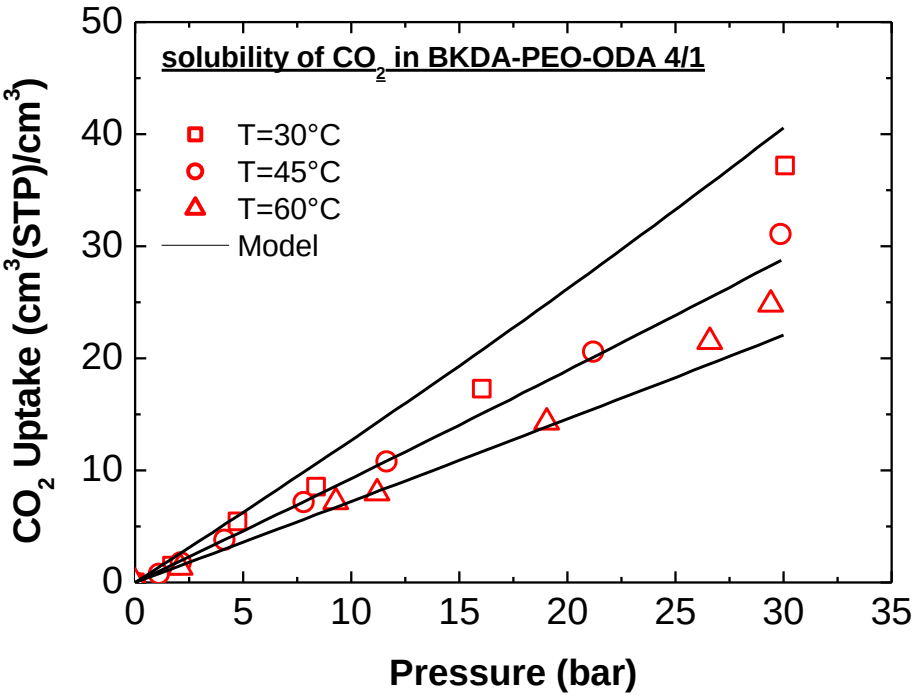

Figure 5.14: Comparison between experimental CO_2 solubility data and modeled solubility data with LF and NELF Models in BKDA-PEO-ODA 4/1 at 30°C, 45°C and 60°C.

Considering the additive rules for solubility and copolymers volume used by the model, equations 5.12 and 5.13, these results confirm the hypothesis that both phases are active during the sorption process. In particular increasing the rubbery phase content, the solubility in the glassy phase becomes less relevant and the model is able to predict the higher swelling capacity of CO_2 in polymer matrix, reproducing qualitatively and quantitatively experimental data. Moreover from the model it is clearly evident that the rubbery phase is not influenced by the copolymerization and membrane formation, as it maintains its equilibrium condition and is free to expand as it would be in its pure state, on the contrary it is necessary to take in consideration volume variation of the glassy phase, which vary as a function of copolymer composition, increasing with rubbery content from 1% up to 30% with respect to the pure glassy polyimide volume. In Figure 5.15 are reported, as an example, the curves representing the solubility isotherms calculated with the model, using, for the glassy phase, the volume estimated with equation 5.13, represented by the solid line, and pure homopolymer glassy volume (dashed line). As it can be seen, assuming that the glassy phase volume is not affected by presence of the rubbery phase yields an overestimation of the solubility in the copolymers.

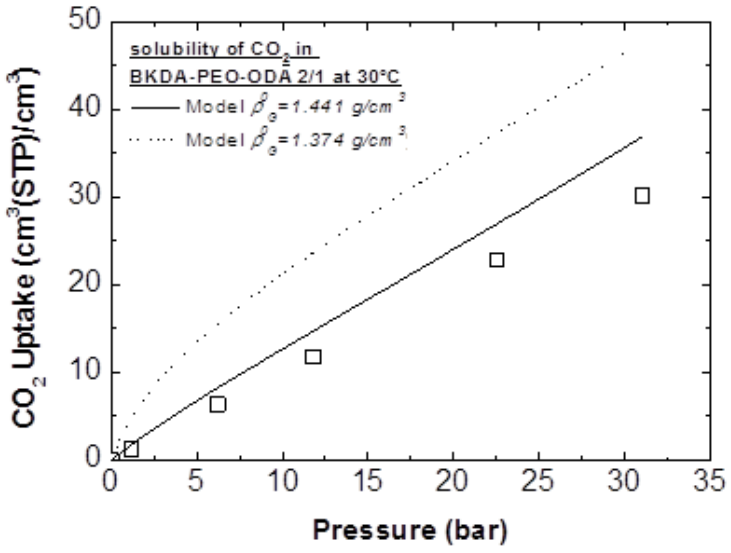

Figure 5.15: Comparison of CO_2 solubility modeling results in BKDA-PEO-ODA 2/1 at 30°C with (solid line) and without (dashed line) density adjustment of glassy phase.

5.6 Estimation of volume dilation during CO_2 sorption in copolyetherimides

According to previous work [183] and volume additivity equation 5.13, volume dilation during sorption in copoly(ether imides) can be predicted a priori as follows:

$$\frac{\Delta V}{V_0} = \frac{\omega_R\left(\frac{1}{\tilde{\rho}^R \rho^{*R}(1-\omega_{CO_2}^R)\hat{v}_R^0} - 1\right)\hat{v}_R^0 + \omega_G\left(\frac{1}{\tilde{\rho}^G \rho^{*G}(1-\omega_{CO_2}^G)\hat{v}_G^0} - 1\right)\hat{v}_G^0}{v_{copolymer}} \tag{5.15}$$

Where $\tilde{\rho}^R$, $\tilde{\rho}^G$, ρ^{*R}, ρ^{*G} are respectively reduced density and characteristic density of rubbery and glassy phase during CO_2 sorption, calculated according to equations reported in Table 5.1.

According to our calculations it can be observed in Figures 5.16–5.17 that in both series of materials increasing CO_2 content in copolymer mixture volume dilation does, up to 10%, due to high ability of the penetrant to swell polymer matrices. It can be seen that increasing rubbery phase content, volume dilation increase at constant temperature. Moreover in PPO series, for which a wide range of composition has been inspected, volume dilation reaches a maximum value, not varying going from sample 4/1 to 6/1. So it seems that rubber mass fraction higher than 60% does not affect material swelling.

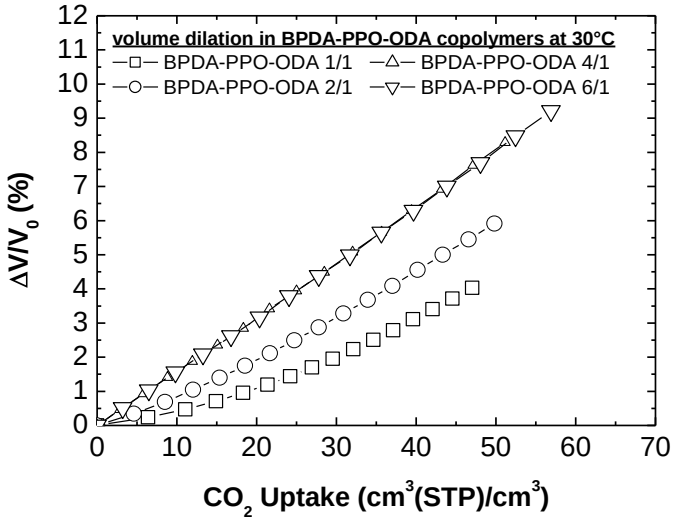

Figure 5.16: Calculation of volume dilation in BPDA-PPO-ODA copolymers at 30°C with LF models.

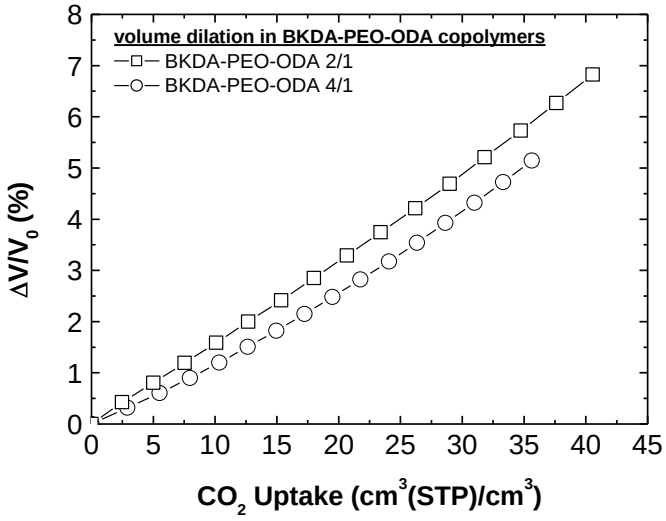

Figure 5.17: Calculation of volume dilation in BKDA-PEO-ODA copolymers at 30°C with LF models.

5.7 Modeling CO_2 diffusivity and permeability in copolymers

The free volume theory, equations 5.1 and 5.5, has been used to model diffusivity data of CO_2 in PPO and PEO based copolymers. In particular free volume values for dry copolymers, calculated by means of equation 5.4, are reported in Table 5.5.

Table 5.5: Estimation of dry copolymers fractional free volume, FFV.

Sample	Rubber content	ρ	FFV
	wt%	g/cm^3	%
BPDA-PPO-ODA 1/1	28.24	1.267	13.9
BPDA-PPO-ODA 2/1	43.34	1.230	14.1
BPDA-PPO-ODA 4/1	59.17	1.187	14.7
BPDA-PPO-ODA 6/1	67.38	1.159	15.6
BKDA-PEO-ODA 2/1	44.20	1.281	13.8
BKDA-PEO-ODA 4/1	60.40	1.244	14.6

So it seems that fractional free volume in the materials analyzed is comprised in the range between 14% and 16%, and it is reasonable considering the high content of rubbery phase in

copolymers. In addition during, CO_2 sorption and diffusion, free volume has been calculated by means of equation 5.15, taking into account swelling of copolymer matrix

This procedure allows for the representation of diffusivity data as reported in Figures 5.18–5.23 with the following adjustable parameters reported in Table 5.6:

Table 5.6: Free volume theory adjustable parameters.

Copolymers	$D_{i,0}$ **cm²/s**	***B***
BPDA-PPO-ODA	$5 \cdot 10^{-3}$	0.08
BKDA-PEO-ODA	$2.5 \cdot 10^{-1}$	0.09

The model represents well experimental data unless for the case of PEO copolymers for which the maximum deviation is around 70% at 30°C. Permeability modeling data, reported in Figures 5.24–5.29, have been calculated with equation 5.14 and they reproduce accurately experimental results.

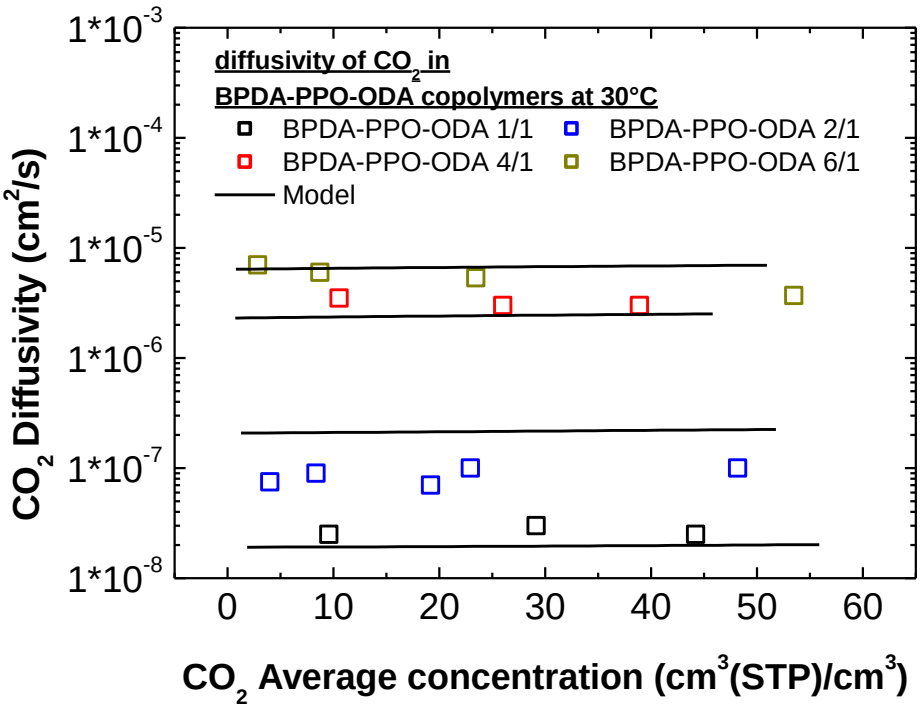

Figure 5.18: Comparison between experimental CO_2 diffusivity data and data modeled with free volume theory for BPDA-PPO-ODA copolymers at 30°C.

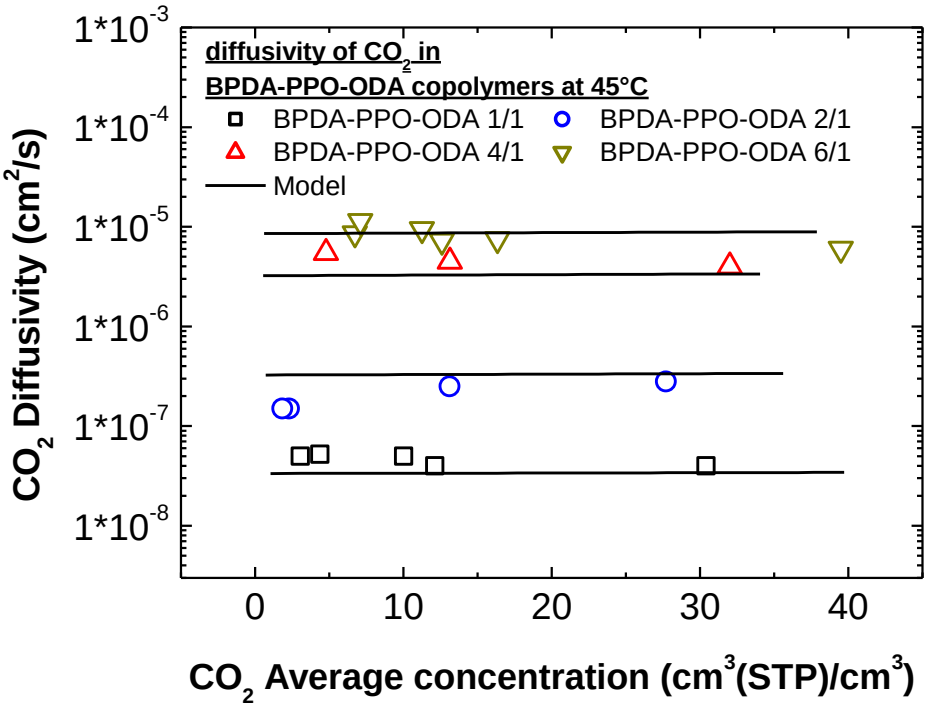

Figure 5.19: Comparison between experimental CO_2 diffusivity data and data modeled with free volume theory for BPDA-PPO-ODA copolymers at 45°C.

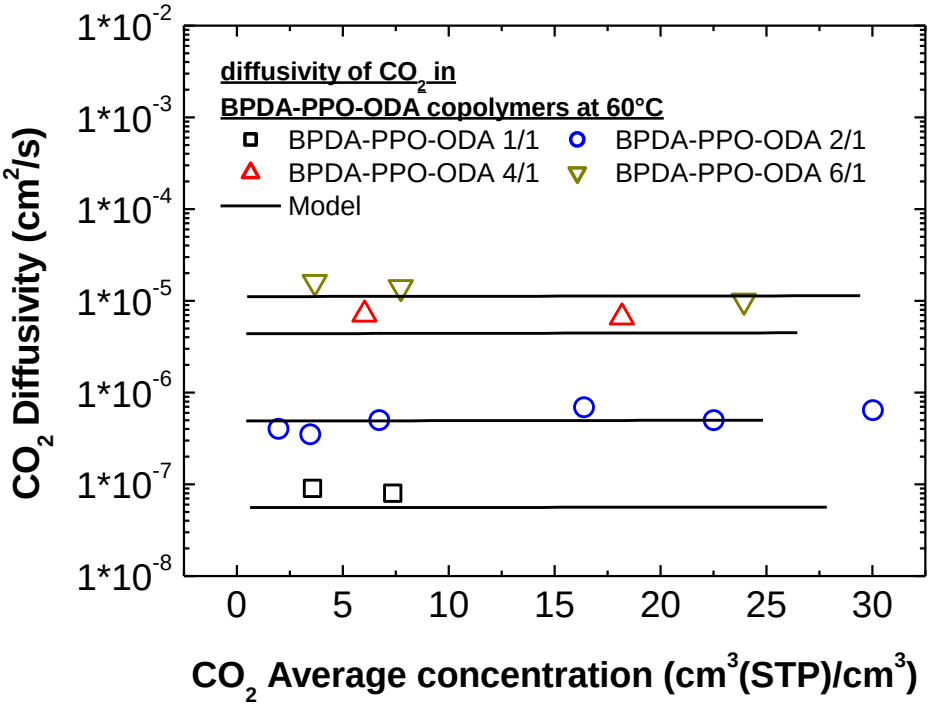

Figure 5.20: Comparison between experimental CO_2 diffusivity data and data modeled with free volume theory for BPDA-PPO-ODA copolymers at 60°C.

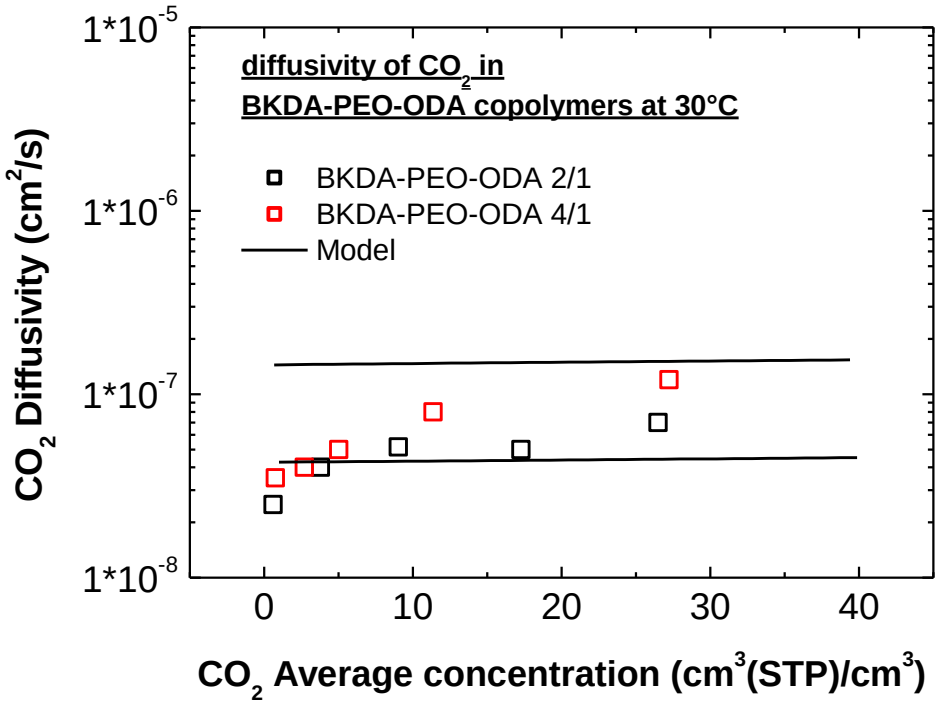

Figure 5.21: Comparison between experimental CO_2 diffusivity data and data modeled with free volume theory for BKDA-PEO-ODA copolymers at 30°C.

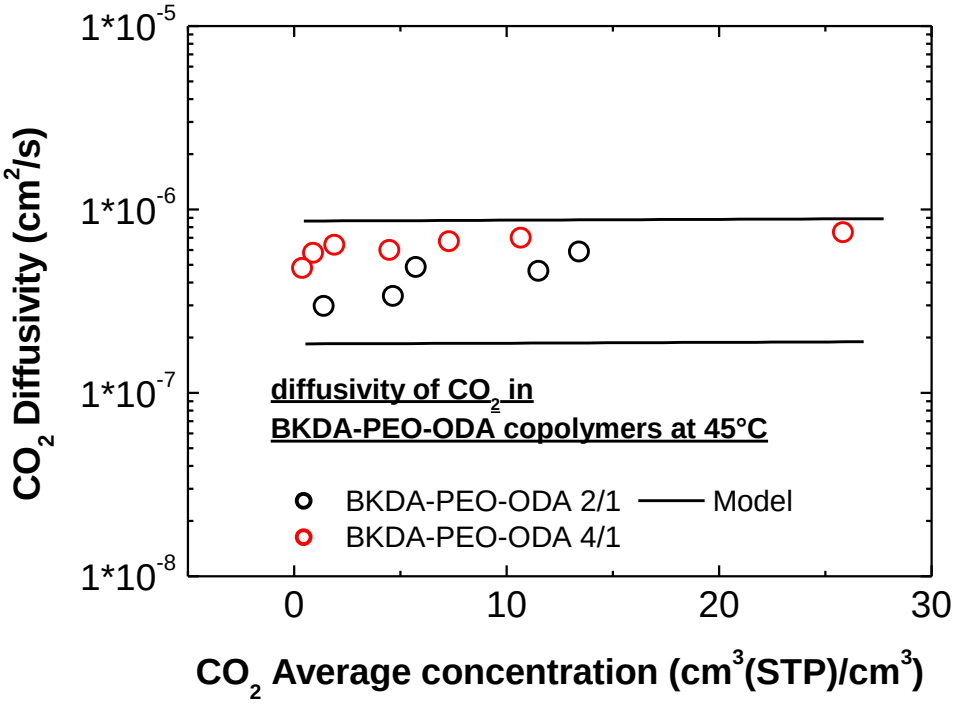

Figure 5.22: Comparison between experimental CO_2 diffusivity data and data modeled with free volume theory for BKDA-PEO-ODA copolymers at 45°C.

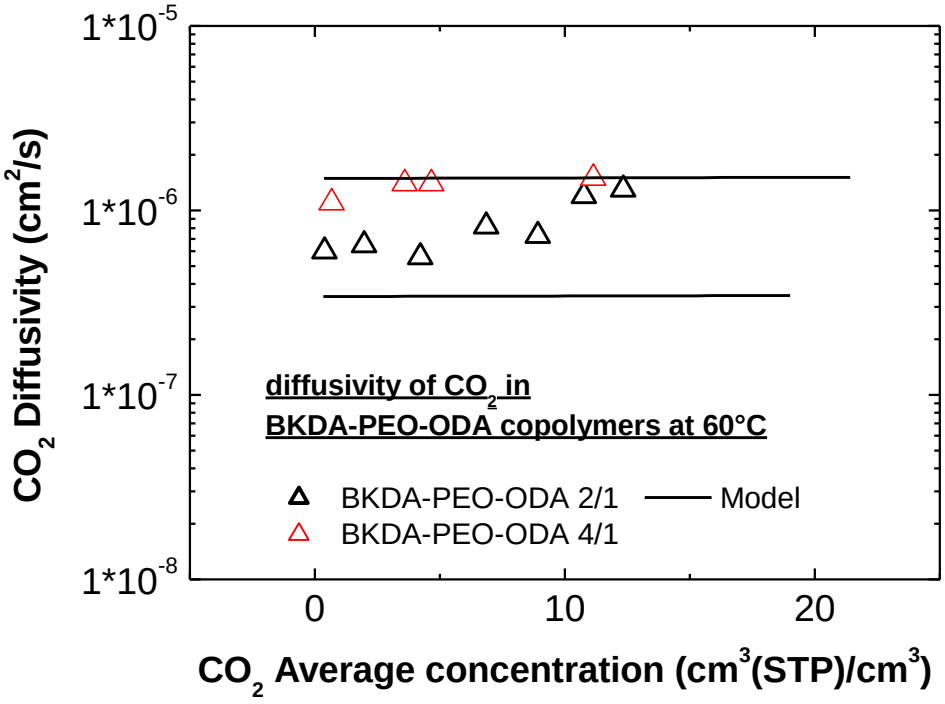

Figure 5.23: Comparison between experimental CO_2 diffusivity data and data modeled with free volume theory for BKDA-PEO-ODA copolymers at 60°C.

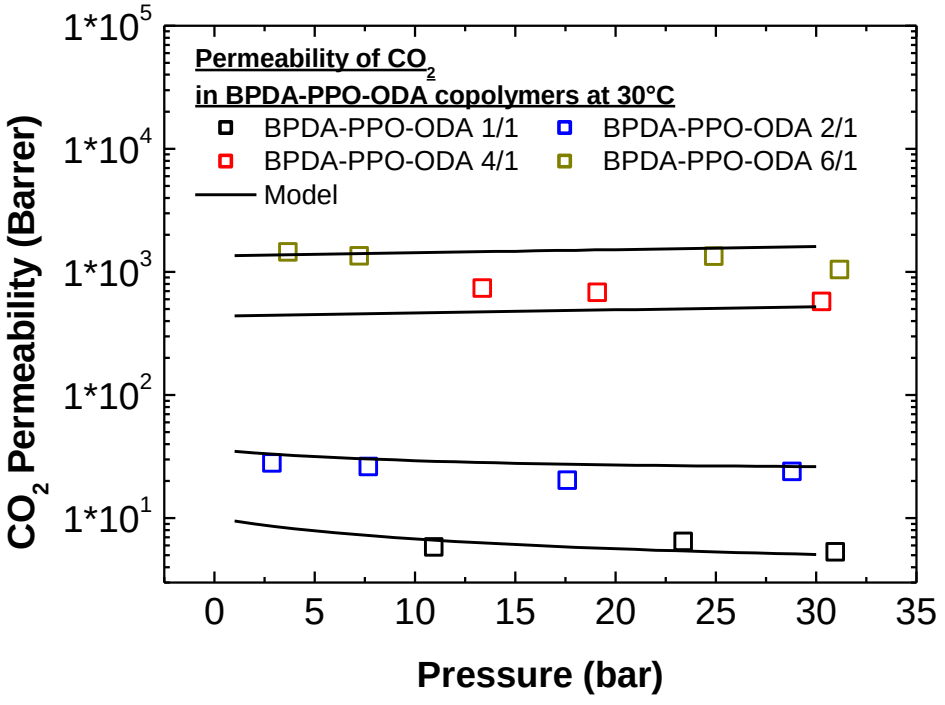

Figure 5.24: Comparison between experimental CO_2 permeability data and data modeled with LF models and free volume theory for BPDA-PPO-ODA copolymers at 30°C.

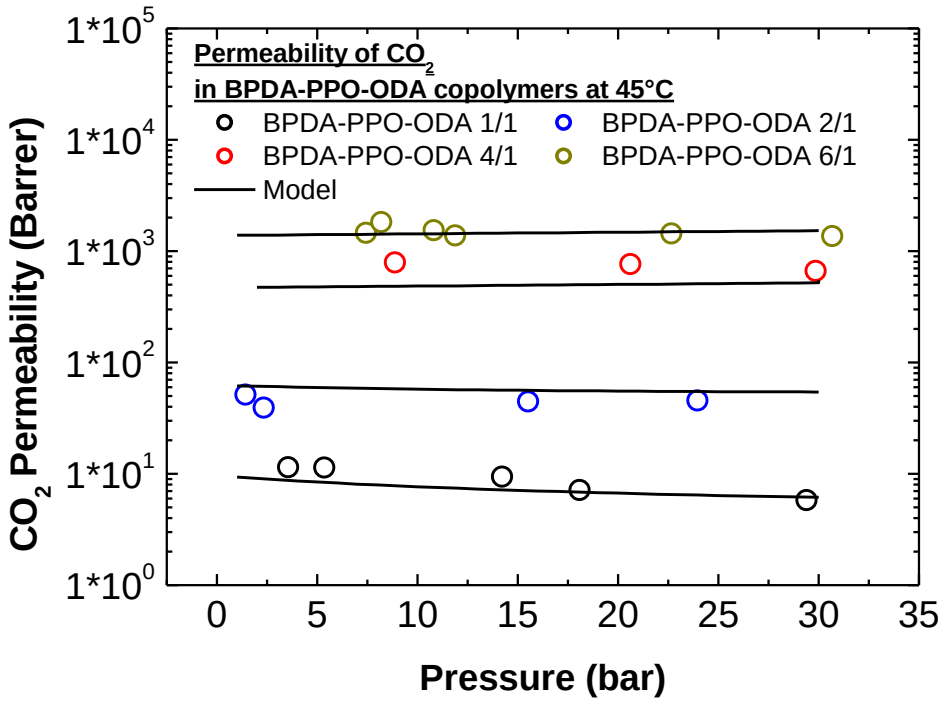

Figure 5.25: Comparison between experimental CO_2 permeability data and data modeled with LF models and free volume theory for BPDA-PPO-ODA copolymers at 45°C.

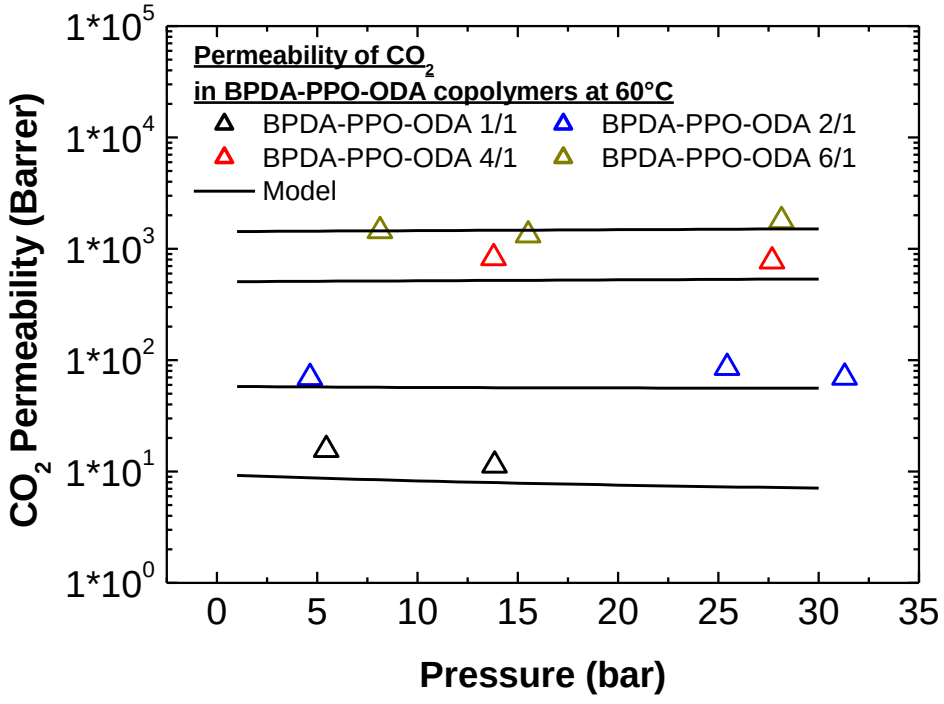

Figure 5.26: Comparison between experimental CO_2 permeability data and data modeled with LF models and free volume theory for BPDA-PPO-ODA copolymers at 60°C.

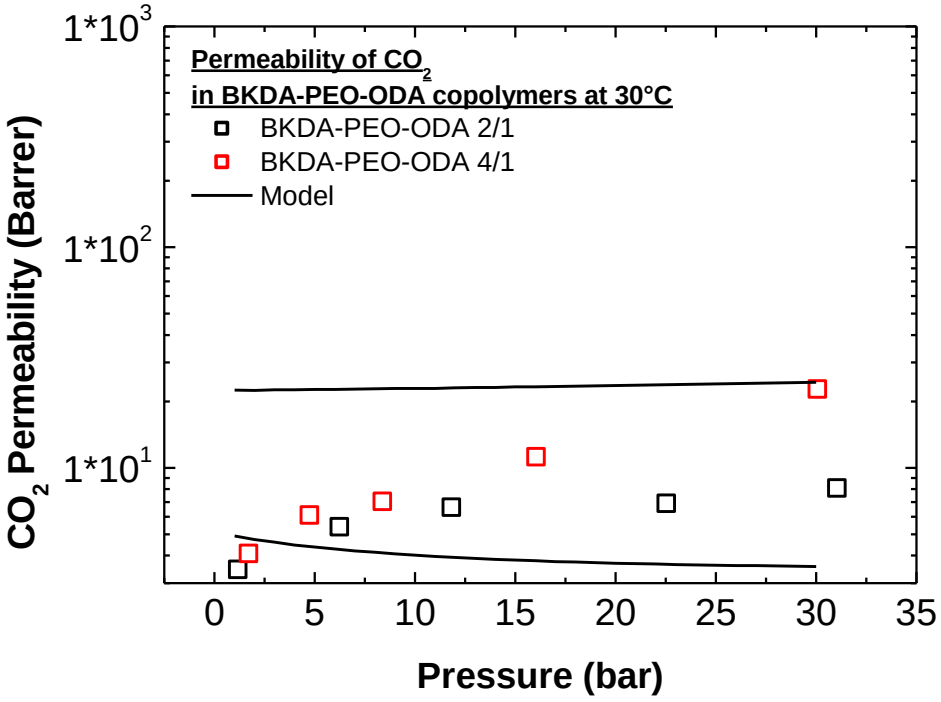

Figure 5.27: Comparison between experimental CO_2 permeability data and data modeled with LF models and free volume theory for BKDA-PEO-ODA copolymers at 30°C.

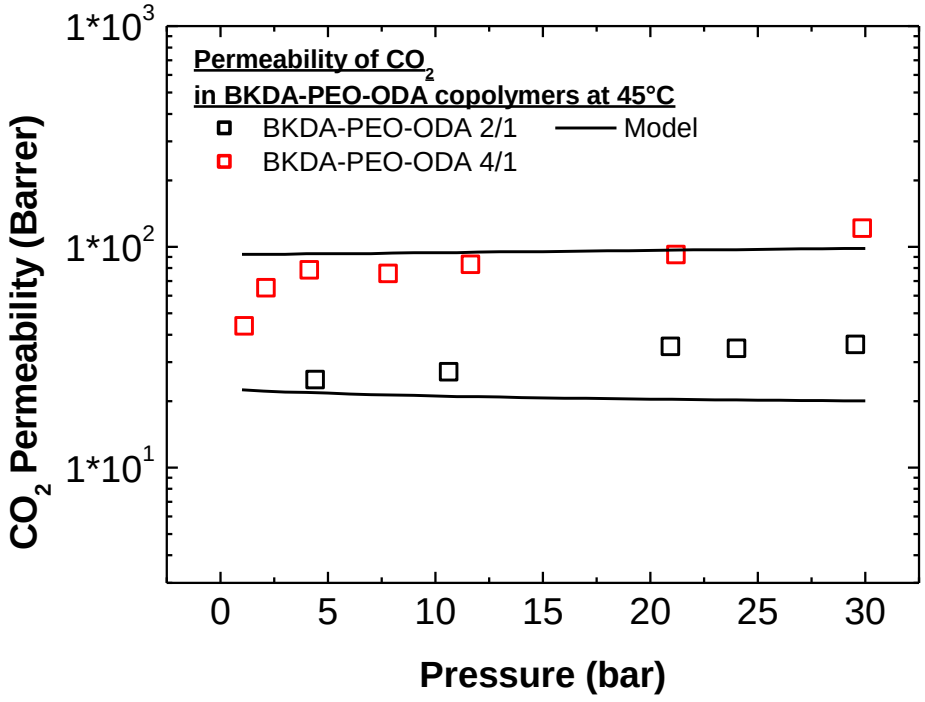

Figure 5.28: Comparison between experimental CO_2 permeability data and data modeled with LF models and free volume theory for BKDA-PEO-ODA copolymers at 45°C.

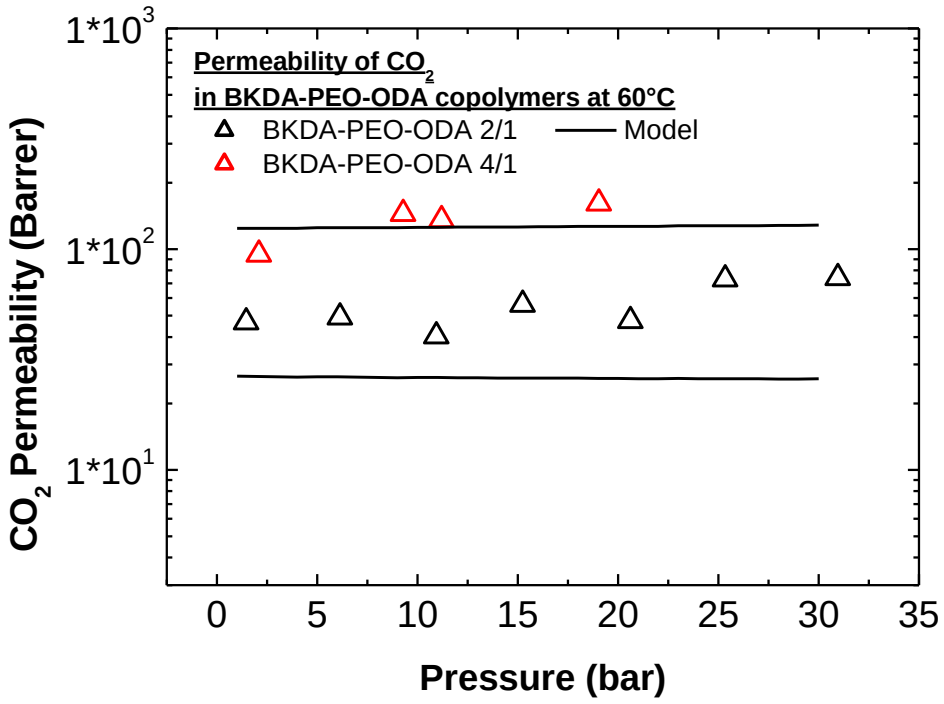

Figure 5.29: Comparison between experimental CO_2 permeability data and data modeled with LF models and free volume theory for BKDA-PEO-ODA copolymers at 60°C.

Conclusions

In this work the investigation of transport properties of innovative materials for the separation and capture of carbon dioxide has been conducted by means of different experimental techniques.

The effect of temperature, pressure and copolymer composition on solubility and diffusivity of CO_2 in two series of copoly(ether-imides) made by hard (BPDA-ODA or BKDA-ODA) and soft (PPO or PEO) segments has been observed. In the case of BPDA-PPO-ODA copolymers the solubility is not dependent on material composition, while on the contrary diffusivity strongly depends on rubbery phase content, increasing with it due to higher mobility of PPO with respect to rigid BPDA-ODA. A dramatic increase of diffusivity is observed when the fraction of PPO is between 40 and 60wt%, which can indicate a transition from a glassy-like to a rubbery-like behavior, as also indicated by the variation of the shape of the solubility isotherms. On the other hand in BKDA-PEO-ODA materials, which show a rubber-like behavior in almost all situations, both solubility and diffusivity increase by increasing PEO content in the membrane, and it is due to higher affinity with CO_2 of PEO rather than BKDA-ODA. The effect of temperature has been studied both for solubility and diffusivity, giving sorption enthalpies and diffusion activation energy as a function of copolymer composition. According to the solution diffusion mechanism of transport permeability has been calculated, obtaining results which reproduce the qualitative behavior of the diffusion coefficient with operative conditions. Finally, LF models have been used to model CO_2 solubility in copolymers. In spite of its simplicity, the model has proved accuracy in representing thermodynamic behavior of mixture formed by CO_2 and both series of

copolymers. The success of the approach seems to confirm the physical assumptions underlying it, and in particular that both phases absorb CO_2; the rubbery phase maintains the same volumetric and sorption behavior as in the respective pure homopolymer, while the glassy phase volume is reduced by the presence of the rubbery phase, and consequently its ability to absorb CO_2. It can be concluded that the model developed allows to represent the effect of composition on CO_2 solubility and that the non ideality of the rubbery/glassy copolymers is due to a reduction of the glassy phase free volume induced by the presence of the rubber. In addition the diffusivity of carbon dioxide has been modeled with the well known free volume theory, taking into account volume variation due to swelling and dilation. In such a way it has been possible to describe the dependence of diffusivity on CO_2 uptake and according to the solution diffusion model permeability has been modeled obtaining good results which reproduce experimental data with two adjustable parameters.

In this work it has been studied MMMs based on PTMSP and 1 wt% of different types of graphene-based nanoplatelets: two graphenes (IND G and M60), and one GO. The membrane preparation procedure was carefully optimized to avoid filler precipitation and obtain good homogeneity and flexibility.

The films have been analyzed for He, N_2, CH_4 and CO_2 permeability and, in some cases, also for the solubility and diffusivity contributions. Gas permeability have been studied over 9 months, in order to monitor the ageing, and after a mild (200°C) thermal treatment, that accelerates ageing. In particular, as far as the permeability and ideal selectivity are concerned one can observe that:

- the addition of GO nanoplatelets (lateral dimension 2 μm, thickness 1.1 nm) to PTMSP enhances slightly the permeability of all gases, and enhances the selectivity for the couple CO_2/He and CH_4/He. The solubility and diffusivity are both enhanced by addition of GO filler. Such effects are attributed to a modification of the polymeric chain packing induced by

the presence of nanoplatelets during casting, that creates additional free volume, similarly to what happens in the case of nanosilica-based membranes.

-The addition of a research grade of graphene (M 60) (lateral dimension 5 □m, thickness 2-8 nm) to PTMSP lowers slightly the gas permeability, with factors that increase with decreasing molecule size, and enhance the ideal selectivity for the couples CO_2/He and CH_4/N_2, CH_4/He. Such effects can be attributed to a reduction of the polymer free volume due to the presence of nanoplatelets during solvent evaporation. The phenomenon seem to affect more the small free volume domains than the large ones, and to enhance the vapor-selective behavior of PMTSP, that is more permeable to large and more condensable molecules. Permeability variations are mainly due to diffusivity changes, as it was tested with separate solubility and diffusivity experiments on CH_4 and CO_2 which show that solubility is almost unvaried, while the diffusivity is slightly reduced by addition of M60 to PTMSP.

- the addition of graphene IND G (lateral dimension 0.2 □m, thickness 2-20 nm) to PTMSP lowers the permeability by a factor equal to about -24÷-30% for all gases. The selectivity for the couple CO_2/He, CO_2/N_2, CO_2/CH_4 is enhanced with respect to pure PTMSP. Such results may be due to a substantial reduction of free volume induced by IND G addition to PTMSP-based membranes.

The most interesting findings are those related to the effect of filler addition on the ageing behavior of PTMSP, which can be summarized as follows:

-Addition of GO slows down the ageing process: the initial loss of N_2, CH_4 and CO_2 permeability is reduced with respect to pure PTMSP. For CO_2, also the final, equilibrium permeability loss is mitigated by addition of GO, as verified by accelerating ageing via a thermal treatment at 200°C. Moreover, the response of the GO-MMM to a thermal treatment at 200°C, that partially reduces GO, is comparable or even better than that of the PTMSP

membrane subject to the same treatment, indicating a good chemical stability of such composite structure.

-Addition of M60 slows down the ageing process of PTMSP, reducing the permeability loss with time for all gases. Addition of IND G, characterized by different morphology, does not affect the ageing of PTMSP, with the exception of He permeability, that decreases more slowly with respect to pure PTMSP .

The reduction of PTMSP ageing observed when adding GO and M60 nanoplatelets is significantly higher than that obtained in the literature with the use of other inorganic fillers like TiO_2 and MgO, even though the amount of filler added in this case is much smaller.

Therefore, GO and M60 fillers modify the relaxation time of the polymer chains, by reducing their mobility and mitigating the ageing process. In some cases, such effect is gas-selective and can be exploited to tune the selectivity. Therefore, we can conclude that the addition of certain types of graphene nanoplatelets to PTMSP in small amounts is a promising strategy to reduce ageing, without sacrificing the permeability.

Finally a feasibility study for the fabrication of innovative membranes based on poly acrylonitrile has been done. Polymeric powders have been functionalized following two different routes and have been analyzed by FT-IR to quantify the amount of amine groups contained in the materials and the presence of secondary amines which lead to the creation of lateral chains and crosslinking. Nanoporous membranes have been obtained by elecrospinning technique and have been compacted to obtain dense sheet to be used as separation membranes. Materials functionalized with amines, HMDA and EDA, and compacted show facilitated transport mechanism induced by the presence of water vapor in the feed stream. Moreover, as previously reported, a dependence on material morphology of CO_2 solubility has been observed. Finally these functionalized materials still need to be optimized, but the

approach seems promising for the development of new membranes or adsorbent materials for CO_2 capture

References

[1] H. Yang, Z. Xu, M. Fan, R. Gupta, R. B. Slimane, A. E. Bland, I. Wright, 2008, Progress in carbon dioxide separation and capture: a review, Journal of Environmental Sciences, 20, 14.

[2] J. K. Adewole, A. L. Ahmad, S. Isamail, C. P. Leo, 2013, Current challenges in membrane separation of CO_2 from natural gas: a review, International Journal of Greenhouse Gas Control, 17, 46.

[3] IEA, CO_2 Emissions from Fuel Combustion, 2015.

[4] C. Fu, T. Gundersen, 2012, Carbon Capture and Storage in the power industry: challenges and oppurtunities, Energy Procedia, 16, 1806.

[5] A. A.Olajire, 2010, CO_2 capture and separation technologies for end-of-pipe application – A review, Energy, 35, 2610.

[6] R. Bounaceur, N. Lape, D. Roizard, C. Vallieres, E. Favre, 2006, Energy, 31, 2556.

[7] P. Bernardo, E.Drioli, G. Golemme, 2009, Membrane Gas Separation: A Review/State of the Art, Industrial and Engineering Chemistry Research, 48, 4638.

[8] R. W. Baker, K. Lokhanwala, 2008, Natural Gas Processing with Membranes: An Overview, Industrial and Engineering Chemistry Research, 47, 2109.

[9] H. Ohya, V. V. Kudryavtsev, S. I. Semenova, Polyimide Membranes - applications, fabrications and properties, Kodansha LTD and Gordon and Breach Science Publishers S. A, 1996.

[10] L. M. Robeson, 1991, Correlation of separation factor versus permeability for polymeric membranes, Journal of Membrane Science, 62, 165.

[11] L. M. Robeson, 2008, The upper bound revisited, Journal of Membrane Science, 320, 390.

[12] A. Tena, A. M. Fernandez, A. E. Lozano, J. C. De La Campa, J. de Abajo, L. Palacio, P. Pradanos, A. Hernandez, 2013, Industrial and Engineering Chemistry Research, 52, 4312.

[13] A. Tena, A. E. Lozano, L. Palacio, A. M. Fernandez, P. Pradanos, J. de Abajo, A. Hernandez, 2013, International Journal of Greenhouse Gas Control, 12, 146.

[14] T. Masuda, E. Isobe, T. Higashimura, 1983, Poly[l-(trimethylsily1)-1-propyne]: A New High Polymer Synthesized with Transition-Metal Catalysts and Characterized by Extremely High Gas Permeability, Journal of American Chemical Society, 105, 7473.

[15] I. Pinnau, L. G. Toy, 1996, Gas and vapor transport properties of amorphous perfluorinated copolymer membranes based on 2,2-bistrifluoromethyl-4,5-difluoro-l,3-dioxole/tetrafluoroethylene, Journal of Membrane Science, 109, 125.

[16] Y. Huang, X.Wang, D. R. Paul, 2006, Physical aging of thin glassy polymer films: Free volume interpretation. Jourana of Membrane Science, 277, 219.

[17] J. M. Hutchinson, 1995, Physical aging of polymers. Progress in Polymer Science, 20, 703.

[18] L. C. E. Struik, Physical Ageing in Amorphous Polymers and Other Materials; Elsevier: New York, 1978.

[19] K. D. Dorkenoo, P. H. Pfromm, 2000, Accelerated Physical Aging of Thin Poly(1-(trimethylsilyl)-1-propyne) Films, Macromolecules, 33, 3747.

[20] G. Li, J. Xiao, W. Zhang, 2012, Efficient and reusable amine-functionalized polyacrylonitrile fiber catalysts for Knoevenageli condensation in water, Green Chemistry, 14, 2234.

[21] S. Rapagnà, N. Jand, P. U. Foscolo, 1998, Catalytic gasification of biomass to produce hydrogen rich gas, International Journal of Hydrogen Energy, 23, 551.

[22] Zhi-Ming Xia, Xiao-Sen Li, Zhao-Yang Chen, Gang Li, Ke-Feng Yan, Chun-Gang Xu, Qiu-Nan Lv, Jing Cai, 2016, Hydrate-based CO_2 capture and CH_4 purification from simulated biogas with synergic additives based on gas solvent, Applied Energy, 162, 1153.

[23] Z. Bacsik, O. Cheung, P. Vasiliev, N. Hedin, 2016, Selective separation of CO_2 and CH_4 for biogas upgrading on zeolite NaKA and SAPO-56, Applied Energy, 162, 613.

[24] V. Vakharia, K. Ramasubramanian, W. Ho, 2015, An experimental and modeling study of CO_2-selective membranes for IGCC syngas purification, Journal of Membrane Science, 488, 56.

[25] A. Makaruk, M. Miltner, M. Harasek, 2010, Membrane biogas upgrading processes for the production of natural gas Substitute, Separation and Purification Technology, 74, 83.

[26] C.Yu, C. Huang, C. Tan, 2012, A Review of CO_2 capture by absorption and adsorption, Aerosol and Air Quality Research, 12, 745.

[27] M. T. Ho, G. W. Allinson, D. E.Wiley, 2008, Reducing the cost of CO_2 capture from flue gasesusing pressure swing adsorption, Industrial and Engineering Chemistry Research, 47, 4883.

[28] S. Wong, R. Bioletti, 2002, Carbon dioxide separation technology, Carbon and Energy Management, Alberta Research Council.

[29] A. Brunetti, F. Scura, G. Barbieri, E. Drioli, 2010, Membrane technology for CO_2 separation, Journal of Membrane Science, 359, 115.

[30] R.W. Baker, 2002, Future directions of membrane gas separation technology, Industrial and Engineering Chemistry Research, 41, 1343.

[31] L. Wang, Y. Cao, M. Zhou, S. J. Zhou, Q. Yuan, 2007, Novel copolyimide membranes for gas separation, Journal of Membrane Science, 305, 338.

[32] M. Al-Masri, H. R. Kricheldorf, D. Fritsch, 1999, New polyimides for gas separation, Macromolecules, 32, 7853.

[33] A. Bos, I. G. M. Punt, M. Wessling, H. Strathmann, 1998, Plasticization resistant glassy polyimide membranes for CO_2/CH_4 separations, Separation Purification Technology, 14, 27.

[34] W. Koros, R. Mahajan, 2000, Pushing the limits for large scale gas separation: which strategies?, Journal of Membrane Science, 175, 181.

[35] L. Jiang, T. Chung, D. F. Li, C. Cao, S. Kulprathipanja, 2004, Fabrication of Matrimid/polyethersulfone dual layer hollow fiber membranes for gas separation, Journal of Membrane Science, 240, 91.

[36] S. Sridhar, R. S. Veerapur, M. B. Patil, K. B. Gudasi, T. M. Aminabhavi, 2007, Matrimid polyimide membranes for the separation of carbon dioxide from methane, Journal of Applied Polymer Science, 106, 1585.

[37] H. B. Park, S. H. Han, C. H. Jung, Y. M. Lee, A. J. Hill, 2010, Thermally rearranged (TR) polymer membranes for CO_2 separation, Journal of Membrane Science, 359, 11.

[38] S. Kim, Y. M. Lee, 2012, Thermally rearranged (TR) polymer membranes with nanoengineered cavities tuned for CO_2 separation, Journal of Nanoparticle Research, 14, 949.

[39] S. H. Han, J. E. Lee, K. J. Lee, H. B. Park, Y. M. Lee, 2010, Highly gas permeable and microporous polybenzimidazole membrane by thermal rearrangement, Journal of Membrane Science, 357, 143.

[40] Ruilan Guo, David F. Sanders, Zachary P. Smith, Benny D. Freeman, Donald R. Paul, James E. McGrath, 2013, Synthesis and characterization of Thermally Rearranged (TR) polymers: influence of ortho-positioned functional groups of polyimide precursors on TR process and gas transport properties, Journal of Materials Chemistry A, 1, 262.

[41] B. C. Gandara, J. G. de La Campa, A. Hérnandez, H. J. Jo, Y. M. Lee, J. de Abajo, A. E. Lozano, 2015, Gas separation membranes made through thermal rearrangement of ortho-methoxypolyimides, Journal of Materials Chemistry, 5, 102261.

[42] Y. Ichiraku, S. A. Stern, T. Nakagawa, 1987, An investigation of the high gas permeability of poly(1-trimethylsylil-1-propyne), Journal of Membrane Science, 34, 5.

[43] R. Srinivasan, S. R. Auvil, P.M. Burban, 1994, Elucidating the mechanism(s) of gas transport in poly(1-trimethylsylil-1-propyne) (PTMSP) membranes, Journal of Membrane Science, 86, 67.

[44] N. A Platé, A.K Bokarev, N.E Kaliuzhnyi, E.G Litvinova, V.S Khotimskii, V.V Volkov, Y. Yampol'skii, 1991, Gas and vapor permeation and sorption in poly (trimetylsilylpropyne), Journal of Membrane Science, 60, 13.

[45] J. Schultz, K. V. Peinemann, 1996, Membranes for separation of higher hydrocarbons from methane, Journal of Membrane Science, 110, 37.

[46] I. Pinnau, L.G. Toy, 1996, Transport of organic vapors through poly(1-trimethylsilyl-1-propyne), Journal of Membrane Science, 116, 199.

[47] V. V. Teplyakova, D. Roizarda, E. Favre, V.S. Khotimsky, 2003, Investigations on the peculiar permeation properties of volatile organic compounds and permanent gases through PTMSP, Journal of Membrane Science, 220, 165.

[48] L. G. Toy, K. Nagai, B. D. Freeman, 2000, Pure-Gas and Vapor Permeation and Sorption Properties of Poly[1-phenyl-2-[p-(trimethylsilyl)phenyl]acetylene](PTMSDPA), Macromolecules, 33, 2516.

[49] A. Morisato, I. Pinnau, 1996, Synthesis and gas permeation properties of poly(4-methyl-2-pentyne), Journal of Membrane Science, 121, 243.

[50] V. P. Shantarovich, I. B. Kevdina, Yu. P. Yampolskii, A. Yu. Alentiev, 2000, Positron Annihilation Lifetime Study of High and Low Free Volume Glassy Polymers: Effects of Free Volume Sizes on the Permeability and Permselectivity, Macromolecules, 33, 7453.

[51] P. M. Budd, K. J. Msayi, C. E. Tattershall, B. S. Ghanem, K. J. Reynolds, N. B. McKeown, Detlev Fritsch, 2005, Gas separation membranes from polymers of intrinsic microporosity, Journal of Membrane Science, 251, 263.

[55] S. Zhou, S. A. Stern, 1989, The effect of plasticization on the transport of gases in and through glassy polymers, Journal of Polymer Science | Part B Polymer Physics, 27, 205.

[53] M. Wessling, S. Schooeman, Th. Van der Boomgaard, C. A. Smolders, 1991, Plasticization of gas separation membranes, Gas separation and purification, 5, 222.

[54] G. C.Kapantaidakis, G. H. Koops, M. Wessling, 2003, CO_2 plasticization of polyethersulfone/polyimide gas-separation membranes, AIChe Journal, 49, 1702.

[55] A. F. Ismail, W. Lorna, 2002, Penetrant-induced plasticization phenomena in glassy polymers for gas separation membrane, Separation and purification technology, 27, 173.

[56] C. S. K. Achoundong, N. Bhuwania, S. K. Burgees, O. Karvan, J. R. Johnson, W. J. Koros, 2013, Silane modification of Cellulose Acetate dense films as material for acid gas removal, Macromolecules, 46, 5584.

[57] G. George, N. Bhoria, S. AlHallaq, A. Abdala, V. Mittal, 2016, Polymer membranes for acid gas removal from natural gas, Separation and Purification Technology, 158, 333.

[58] B. Kraftschik, W. J. Koros, J. R. Johnson, O. Karvan, 2013, Dense film polyimide membranes for aggressive sour gas feed separations, Journal of Membranes Science, 428, 608.

[59] S.Yi, X. Ma, I. Pinnau, W. J. Koros, 2015, A high performance hydroxyl functionalized polymer of intrinsic microporosity for an environmentally attractive membrane based approach to decontamination of sour natural gas, Journal of Materials Chemistry, 3, 22794.

[60] J. D. Wind, C. Staudt-Bickel, D. R. Paul, W. J. Koros, 2002, The Effects of Crosslinking chemistry on CO_2 plasticization of polyimide gas separation membranes, Industrial and Engineering Chemistry Research, 41, 6139.

[61] J. D. Wind, C. Staudt-Bickel, D. R. Paul, W. J. Koros, 2003, Solid-State covalent cross-linking of polyimide membranes for carbon dioxide plasticization reduction, Mcromolecules, 36, 1882.

[62] A. M. W. Hillock, W. J. Koros, 2000, Cross-linkable polyimide membrane for natural gas purification and carbon dioxide plasticiazation reduction, Macromolecules, 40, 583.

[63] W. Qiu, C. Chen, L. Xu, L. Cui, D. R. Paul, W. J. Koros, 2011, Sub-Tg cross-linking of a polyimide membrane for enhanced CO2 plasticization resistance for natural gas separation, Mcromolecules, 44, 6046.

[64] T. C. Merkel, L. G. Toy, 2006, Comparison of Hydrogen sulfide transport in fluorinated and nonfluorinated polymers, Macromolecules, 39, 7591.

[65] Y. Huang, D. R. Paul, 2007, Effect of film thickness on the Gas-Permeation Characteristics of Glassy Polymer Membranes, Industrial and Engineering Chemistry Research, 46, 2342.

[66] L. Cui, W. Qi, D.R. Paul, W.J. Koros, 2011, Physical aging of 6FDA-based polyimide membranes monitored by gas permeability, Polymer, 52, 3374.

[67] Wen-Hui Lin, Tai-Shung Chunga, 2001, Gas permeability, diffusivity, solubility, and aging characteristics of 6FDA-durene polyimide membranes, Journal of Membrane Science, 186, 183.

[68] X. Wang, F. T. Willmore, R. D. Raharjo, X. Wang, B. D. Freeman, A. J. Hill, 2006, Molecular simulations of physical ageing in polymer membrane materials, The Journal of Physical Chemistry B, 110, 16685.

[69] J. D. Wind, S. M. Sirard, D. R. Paul, P. F. Green, Keith P. Johnston, W. J. Koros, 2003, Carbon Dioxide-Induced Plasticization of Polyimide Membranes: Pseudo-Equilibrium Relationships of Diffusion, Sorption, and Swelling, Macromolecules, 36, 6433.

[70] G. Q. Chen, C. A. Scholes, G. G. Qiao, S. E. Kentish, 2011, Water vapor permeation in polyimide membranes, Journal of Membrane Science, 379, 479.

[71] L. Ansaloni, M. Minelli, M. Giacinti Baschetti, G. C.Sarti, 2014, Effect of relative humidity and temperature on gas transport in Matrimid: Experimental study and modelling, Journal of Membrane Science, 471, 392.

[72] S. L. Liu, L. Shao, M. L. Chua, C. H. Lau, H. Wang, S. Quan, 2013, Recent progress in the design of advanced PEO-containing membranes for CO_2 removal, Progress in Polymer Science, 38, 1089.

[73] K. Okamoto, M. Fujii, S. Okamyo, H. Suzuki, K. Tanaka, H. Kita, 1995, Gas permeation properties of poly(ether imide) segmented copolymers, Macromolecules, 28, 6950.

[74] T. C. Merkel, Z. He, I. Pinnau, B. D. Freeman, P. Meakin, A. J. Hill, Effect of Nanoparticles on Gas Sorption and Transport in Poly(1-trimethylsilyl-1-propyne). Macromolecules 2003, 36, 6844.

[75] T. C. Merkel, Z. He, I. Pinnau, B. D. Freeman, P. Meakin, A. J. Hill, 2003, Sorption and Transport in Poly (2,2-bis(trifluoromethyl)-4,5-difluoro-1,3-dioxole-co-tetrafluoroethylene) Containing Nanoscale Fumed Silica, Macromolecules, 36, 8406.

[76] T. C. Merkel, B. D. Freeman, R. J. Spontak, Z. He, I. Pinnau, P. Meakin, A. J. Hill, 2003, Sorption, Transport, and Structural Evidence for Enhanced Free Volume in Poly(4-methyl-2-pentyne)/Fumed Silica Nanocomposite Membranes, Chemistry of Materials, 15, 109.

[77] T. C. Merkel, B. D. Freeman, R. J. Spontak, Z. He, I. Pinnau, P. Meakin, A. J. Hill, Ultrapermeable, Reverse-Selective Nanocomposite Membranes, Science, 2002, 296, 519.

[78] J. Ahn, W-J. Chung, I. Pinnau, J. Song, N. Du, G. P. Robertson, M. D. Guiver, 2010, Gas transport behavior of mixed-matrix membranes composed of silica nanoparticles in a polymer of intrinsic microporosity (PIM-1), Journal of Membrane Science, 346, 280.

[79]] J. Ahn, W-J. Chung, I. Pinnau, M. D. Guiver, 2008, Polysulfone/silica nanoparticle mixed-matrix membranes for gas separation, Journal of Membrane Science, 314, 123.

[80] M. C. Ferrari, M. Galizia, M. G. De Angelis, G. C. Sarti, 2010, Gas and Vapor Transport in Mixed Matrix Membranes Based on Amorphous Teflon AF1600 and AF2400 and Fumed Silica. Industrial and Engineering Chemistry Research, 49, 11920.

[81] M. Galizia, M. G. De Angelis, M. Messori, G. C. Sarti, 2014, Mass transport in hybrid PTMSP/Silica membranes, Industrial and Engineering Chemistry Research, 53, 9243.

[82] M. G. De Angelis, R. Gaddoni, G. C. Sarti, Gas Solubility, 2013, Diffusivity, Permeability, and Selectivity in Mixed Matrix Membranes Based on PIM-1 and Fumed Silica, Industrial and Engineering Chemistry Research, 52,10506.

[83] M. G. De Angelis, G.C. Sarti, 2008, Solubility and Diffusivity of Gases in Mixed Matrix Membranes Containing Hydrophobic Fumed Silica: Correlations and Predictions Based on the NELF Model, Industrial and Engineering Chemistry Research, 47, 5214.

[84] De Angelis M.G., Sarti G.C., Gas sorption and permeation in mixed matrix membranes based on glassy polymers and silica nanoparticles, Current Opinion in Chemical Engineering, 2012, 1, 148.

[85] B. M. Yoo, H. J. Shin, H. W. Yoon, H. B. Park, 2013, Graphene and graphene oxide and their uses in barrier polymers, Journal of Applied Polymer Science, 1.

[86] J. Zhu, J. Lim, C.-Ho Lee, H.-Ik Joh, H. Chul Kim, B. Park, N.-Ho You, S. Lee, 2013, Multifunctional polyimide/graphene oxide composites via in situ polymerization, Journal of Applied Polymer Science, 11, 1.

[87] J.-T. Chen, Y.-J. Fu, Q.-F. An, S.-C. Lo, Y.-Z. Zhong, C.-C. Hu, K.-R. Lee, J.-Y. Lai, 2014, Enhancing polymer/graphene oxide gas barrier film properties by introducing new crystals, Carbon, Elsevier, 27, 443.

[88] H. M. Kim, J. K. Lee, H. S. Lee, 2011, Transparent and high gas barrier films based on poly(vinyl alcohol)/graphene oxide composites, Thin Solid Films, Elsevier, 5, 7766.

[89] C. Liu, B. McCulloch, S. T. Wilson, A. I. Benin and M. E. Schott, US Patent, 7637983, 2009.

[90] A. K. Geim, K. S. Novoselov, 1997, The rise of graphene, Nature, 6, 183.

[91] V. Singh, D. Joung, L. Zha, S. Das, 2011, Graphene based materials: Past, present and future, Progress in material science, 56, 1178.

[92] H. Kim, A. A. Abdala, C. W. Macosko, 2010, Graphene/polymer nanocomposites, Macromolecules, 43, 6515.

[93] H. W. Kim, H. W. Yoon, S. M. Yoon, B. M. Yoo, B. K. Ahn, Y. H. Cho, H. J. Shin, H. Yang, U. Paik, S. Kwon, J. Y. Choi, H. B. Park, 2013, Selective Gas Transport Through Few-Layered Graphene and Graphene Oxide Membranes, Science, 342, 91.

[94] H. Kim, H. Yoon, B. Yoo, J. Park, K. Gleason, B. D. Freeman, H. Park, 2014, High performance CO_2-phylic graphene oxide membranes under wet conditions, Chem. Communications, 13563.

[95] H. Li, Z. Song, X. Zhang, Y. Huang, S. Li, Y. Mao, H. J. Ploehn, Y. Bao, M. Yu, 2013, Ultrathin, Molecular-Sieving Graphene Oxide Membranes for Selective Hydrogen Separation. Science, 342, 95.

[96] J. Shen, G. Liu, K. Huang, W. Jin, K.-R. Lee, N. Xu, 2015, Membranes with Fast and Selective Gas-Transport Channels of Laminar Graphene Oxide for Efficient CO_2 Capture, Angenwadte Chemie, 127, 588.

[97] X. Li, L. Ma, H. Zhang, S. Wang, Z. Jiang, R. Guo, H. Wu, X. Z. Cao, J. Yang, B. Wang, 2015, Synergistic effect of combining carbon nanotubes and graphene oxide in mixed matrix membranes for efficient CO_2 separation, Journal of Membrane Science, 479, 1.

[98] L. Zhao, C. Cheng, Yu-Fei Chen, T. Wang, Chun-Hui Du, Li-Guang Wu, 2015, Enhancement on the permeation performance of polyimide mixed matrix membranes by incorporation of graphene oxide with different oxidation degrees, Polymers advanced technologies, 26, 330.

[99] T. Koschine, K. Rätzke1, F. Faupel, M. Munir Khan, T. Emmler, V. Filiz, V. Abetz, L. Ravelli, W. Egger, 2015, Correlation of Gas Permeation and Free Volume in New and used High Free Volume Thin Film Composite Membranes. Journal of Polymer Science Part B: Polym. Phys., 53, 213.

[100] C. Hon Lau, P. Tien Nguyen, M. R. Hill, A. W. Thornton, K. Konstas, C. M. Doherty, R. J. Mulder, L. Bourgeois, A. C. Y. Liu, D. J. Sprouster, J. P. Sullivan, T. J. Bastow, A. J. Hill, D. L. Gin, R. D. Noble, 2014, Ending Aging in Super Glassy Polymer Membranes. Angew. Chem. Int. Ed., 53, 5322.

[101] S. D. Kelman, B. W. Rowe, C. W. Bielawski, C. W.; S. J. Pas, A. J. Hill, D. R. Paul, B. D. Freeman, Crosslinking poly(1-(trimethylsilyl)-1-propyne) and its effect on physical stability, Journal of Membrane Science, 2008, 320, 123.

[102] S. Matteucci, V. A. Kusuma, D. Sanders, S. Swinnea, B. D. Freeman, 2008, Gas transport in TiO_2 nanoparticle-filled poly (1-trimethylsilyl-1-propyne), Journal of Membrane Science, 307, 196.

[103] S. Matteucci, V. A. Kusuma, S. D. Kelman, B. D. Freeman, 2008, Gas transport properties of MgO filled poly(1-trimethylsilyl-1-propyne) nanocomposites, Polymer, 49, 1659.

[104] P. F. Scholander, Oxygen transport through hemoglobin solution, Science, 131, 1960, 585.

[105] Hans H. Funke, Richard D. Noble, Separation of gaseous olefin isomers using facilitated transport membranes, Journal of Membrane Science, 82, 1993, 229.

[106] Jin Huang, Jian Zou, W. S. Winston Ho, Carbon dioxide capture using a CO_2 selective facilitated transport membrane, Industrial and Engineering Chemistry Research, 47, 2008, 1261.

[107] Liyuan Deng, Taek-Joong Kim, May-Britt Hagg, 2009, Facilitated transport of CO_2 in novel PVAm/PVA blend membrane, Journal of Membrane Science, 340, 154.

[108] Richard D. Noble, Generalized microscopic mechanism of facilitated transport in fixed site carrier membranes, Journal of Membrane Science, 75, 1992, 121.

[109] Luca Ansaloni, Yanan Zhao, Benson T. Jung, Kartik Ramasubramanian, Marco Giacinti Baschetti, W.S. Winston Ho, 2015, Facilitated transport membranes containing amino-functionalized multi-walled carbon nanotubes for high-pressure CO_2 separations, Journal of Membrane Science, 490, 18.

[110] Y. Zhao, W. S. W. Ho, 2012, CO_2-Selective Membranes Containing Sterically Hindered Amines for CO_2/H_2 Separation, Industrial and Engineering Chemistry Research, 52, 8774.

[111] J. D. Way, R. D. Noble, T. M. Flynn, E.D. Sloan, 1982, Liquid membrane transport: a survey, Journal of Membrane Science, 12, 239.

[112] R. Quinn, J. R. Aplleby, G. P. Pez, 1995, New facilitated transport membranes for the separation of carbon dioxide from hydrogen and methane, Journal of Membrane Science, 104, 139.

[113] Y. Zhang, Z. Wang, S. C. Wang, 2002, Selective permeation of CO_2 through new facilitated transport membranes, Desalination, 385.

[114] C. Yi, Z. Wang, M. Li, J. Wang, S. Wang, 2006, Facilitated transport of CO_2 through polyvinylamine/polyethleneglycol blend membranes Desalination, 193, 90.

[115] J. Shen, L. Wu, D. Wang, C. Gao, 2008, Sorption behavior and separation performances of novel facilitated transport membrane for CO2/CH4 mixtures, Desalination, 223, 425.

[116] T. J. Kim, B. Li, M. B. Hagg, 2004, Novel Fixed-Site–Carrier Polyvinylamine Membrane for Carbon Dioxide Capture Journal of Polymer Science, Part B, Polymer Physics, 42, 4326.

[117] M. W. Uddin, M. B. Hagg, 2012, Natural gas sweetening-the effect on CO_2/CH_4 separation after exposing a facilitated transport membrane to hydrogen sulfide and heavier hydrocarbons, Journal of Membrane Science, 143, 423.

[118] M. B. Hagg, R. Quinn, 2006, Polymeric facilitated transport membranes for hydrogen purification, MRS Bullettin, 31, 750.

[119] A. Hussain, M. B. Hagg, 2010, A feasibility study of CO_2 capture from flue gas by a facilitated transport membrane, Journal of Membrane Science, 359, 140.

[120] L. Deng, M. B. Hagg, 2010, Techno-economic evaluation of biogas upgrading process using CO_2 facilitated transport membrane, International Journal of Greenhouse gas control, 4, 638.

[121] Mohamed H. El-Newehy, Abdullah Alamri, Salem S. Al-Deyab, Optimization of amine-terminated polyacrylonitrile synthesis and characterization, Arabian Journal of Chemistry, 7, 2014, 235.

[122] J. Crank, The Mathematics of Diffusion, 2nd Ed., Oxford University Press, Oxford, 1975.

[123] E. Piccinini, M. G. Baschetti, G.C. Sarti, 2004, Use of an automated spring balance for the simultaneous measurements of sorption and swelling in polymeric films, Journal of Membrane Science, 234, 95.

[124] P. Zoller, D. Walsh, Standard Pressure-Volume-Temperature Data for Polymers, Technomic, Lancaster, PA, 1995.

[125] K. Okamoto, K. Tanaka, H. Kita, A. Nakamura, Y. Kusuki, 1989, The effect of morphology on sorption and transport of carbon dioxide in a polyimide from 3,3′,4,4′-biphenyltetracarboxylic dianhydride and 4,4′-oxydianiline, Journal of Polymer Science, 27, 1221.

[126] K. Tanaka, H. Kita, M. Okano, K. Okamoto, 1992, Permeability and permselectivity in fluorinated and non-fluorinated polyimides, Polymer, 33, 585.

[127] M. Minelli, M. G. De Angelis, 2014, An equation of state (EoS) based model for the fluid solubility in semicrystalline polymers, Fluid Phase Equilibria, 367, 173-181.

[128] J. Schrier, 2010, Helium separation using porous graphene membranes, Journal of Physical Chemistry Letters, 1, 2284.

[129] B. M. Yoo, H. J. Shin, H. W. Yoon, H. B. Park, 2013, Graphene and graphene oxide and their uses in barrier polymers, Journal of Applied Polymer Science, 131, 39628.

[130] J. Zhu, J. Lim, C. Ho Lee, H. Joh, H. Chul Kim, B. Park, N.-HoYou, S. Lee, 2014, Multifunctional polyimide/graphene oxide composites via in situ polymerization, Journal of Applied Polymer Science, 131, 40177.

[131] X. Yang, L. Li, S. Shang, X.-M. Tao, 2010, Synthesis and characterization of layer-aligned poly(vinyl alcohol)/graphene nanocomposites, Polymer, 3, 3431.

[132] H.-D. Huang, P. G. Ren, J. Z. Xu, L. Xu, G. J. Zhong, B. S. Hsiao, Z. M. Li, 2014, Improved Barrier properties of poly(lactic acid) with randomly dispersed graphene oxide nanosheets, Journal of Membrane Science, 23,110.

[133] http://www.graphene.it/workinprogress/wp-content/uploads/GNext-XT-Ink-15.pdf

[134] http://www.graphene.it/workinprogress/wp-content/uploads/GRAPHOS-Sol-G.pdf

[135] http://www.graphene.it/workinprogress/wp-content/uploads/GRAPHOS-Sol-GO.pdf

[136] Y. Hernandez, M. Lotya, D. Rickard, S. D. Bergin, J. N. Coleman, 2010, Measurement of Multicomponent Solubility Parameters for Graphene Facilitates Solvent Discovery. Langmuir, 26, 3208.

[137] T. C. Merkel, V. I. Bondar, K. Nagai, B. D. Freeman, I. Pinnau, 2000, Gas sorption, diffusion and permeation in Poly(dimethylsiloxane), Journal of Polymer Science Part B: Polymer Physics, 38, 3, 415.

[138] K. Tanaka, H. Kita, K. Okamoto, A. Nakamura, Y. Kusuki, 1989, Gas permeability and permselectivity in polyimides based on 3,3',4,4'-Biphenyltetracarboxylic dianhydride, Journal of Membrane Scince, 203.

[139] N. M. B. Flichy, C. J. Lawrence, S. G. Kazarian, 2003, Rheology of Poly(propylene glycol) and Suspensions of Fumed Silica in Poly(propylene glycol) under High-Pressure CO_2, Industrial & Engineering Chemistry Research, 42, 6310.

[140] T. Guadagno and S. G. Kazarian, 2004, High-Pressure CO_2 Expanded Solvents:Simultaneous Measurement of CO_2 Sorption and Swelling of Liquid Polymers with in-Situ Near-IR Spectroscopy, Journal of Physical Chemistry B, 108, 13995.

[141] R. H. Perry, D. W. Green, Chemical Engineering Handbook, 7th Ed., Mc Graw Hill, New York, 1999.

[142] C. Wu, 2011, Simulated glass transition temperatures of Poly(ethylene oxide). Bulk and film: a comparative study, Journal of Physical Chemistry, 115, 38, 11044.

[143] D. W. van Krevelen, K. te Nijenhuis, Properties of Polymers. Their correlation with chemical structure; their numerical estimation and prediction from additive group contribution, 4th Ed., Elsevier, 2009.

[144] C. P. Ribeiro Jr., B. D. Freeman, D. R. Paul, 2011, Pure and Mixed-gas Carbon Dioxide/Ethane Permeability and Diffusivity in a Cross-linked Poly(ethylene oxide) Copolymer, Journal of Membrane Science, 377, 110.

[145] J. K. Jung, S. N. Joung, H. Y. Shin, S.Y. Kim, Ki-Pung Yoo, W. Huh, C. S. Lee, 2002, Measurements and Correlation of Hydrogen-Bonding Vapor Sorption Equilibrium Data of Binary Polymer Solutions, Korean Journal of Chemical Engineering, 19, 296.

[146] J. Huang, R. J. Cranford, T. Matsuura, C. Roy, 2003, Water Vapor Sorption and Transport in Dense Polyimide Membranes, Journal of Applied Polymer Science, 2306.

[147] A. Lee, J. Seo, J. Jeon, H. Han, 2000, Water Sorption Behaviors in the Polyimide Thin Films with Various Chain Rigidities, Journal of the Korean Institute of Chemical Engineers, 38, 294.

[148] H. Han, J. Seo, M. Ree, S. M. Pyo, C. C. Gryte, 1998, Water sorption and diffusion behaviours in thin films of photosensitive polyimides, Polymer, 39, 2963.

[149] Consolati, G.; Genco, I.; Pegoraro, M.; Zanderighi, L. Positron annihilation lifetime (PAL) in poly(1-(trimethylsilyl) propyne) (PTMSP): Free volume determination and time dependence of permeability. J. Polym. Sci., Part B: Polym. Phys. 1996, 34, 357.

[150] J. Y. Park, D. R. Paul, 1997, Correlation and prediction of gas permeability in glassy polymer membrane materials via a modified free volume based group contribution method, Journal of Membrane Science, 125, 23.

[151] Brian C. Smith, Fundamentals of Fourier Transform Infrared Spectroscopy, CRC Press, 1995.

[152] G.S. Huvard, V.T. Stannett, W.J. Koros, H.B. Hopfenberg, The pressure dependence of CO_2 sorption and permeation in Poly(Acrylonitrile), Journal of Membrane Science, 6, 1980, 185.

[153] Takeo Yamaguchi, Lars M. Boetje, Carl Koval, Richard D. Noble, Christopher N. Bowman, Transport Properties of Carbon Dioxide through Amine Functionalized Carrier Membranes, Industrial an Engineering Chemistry Research, 34, 4071.

[154] Xiao Yuan Chen, Hoang Vinh-Thang, Denis Rodrigue, Serge Kaliaguine, Amine-Functionalized MIL-53 Metal−Organic Framework in Polyimide Mixed Matrix Membranes for CO_2/CH_4 Separation, Industrial and Engineering Chemistry Research, 2012, 51, 6895.

[155] Sarah Couck, Joeri F. M. Denayer, Gino V. Baron, Tom Remy, Jorge Gascon, Freek Kapteijn, An Amine-Functionalized MIL-53 Metal-Organic Framework with Large Separation Power for CO_2 and CH_4, Journal of the American Chemical Society, 131, 2009, 6326.

[156] Aude Demessence, Deanna M. D'Alessandro, Maw Lin Foo, Jeffrey R. Long, Strong CO_2 Binding in a Water-Stable, Triazolate-Bridged Metal-Organic Framework Functionalized with Ethylenediamine, Journal of the American Chemical Society, 131, 2009, 8784.

[157] Genggeng Qi, Yanbing Wang, Luis Estevez, Xiaonan Duan, Nkechi Anako, Ah-Hyung Alissa Park, Wen Li, Christopher W. Jones, Emmanuel P. Giannelis, High efficiency nanocomposite sorbents for CO_2 capture based on amine-functionalized mesoporous capsules, Energy and Environmental Science, 4, 2011, 444.

[158] G.R. Mauze, S.A. Stern, The solution and transport of water-vapor in Poly(acrylonitrile): a re-examination, Journal of Membrane Science, 12, 1982, 51–64.

[159] E. A. McGonigle, J. J. Liggat, R. A. Pethrick, S. D. Jenkins, J. H. Daly, D. Hayward, 2001, Permeability of N_2, Ar, He, O_2, CO_2 through biaxially oriented polyester films-dependence on free volume, Polymer, 42, 2413.

[160] A. W. Thornton, K. M. Nairn, A. J. Hill, J. M. Hill, 2009, New relation between diffusion and free volume: I. Predicting gas diffusion, Journal of Membrane Science, 338, 29.

[161] M. H. Choen, D. Turnbull, 1959, Molecular Transport in Liquids and Glasses, The Journal of Chemical Physics, 31, 1164.

[162] J. S. Vrentas, J. L. Duda, H. C. Ling, 1985, Free-volume theories for self-diffusion in polymer solvent system. I. Conceptual differences in theories, Journal of Polymer Physics, 23, 275.

[163] J. S. Vrentas, J. L. Duda, H. C. Ling, A. C. Hou, 1985, Free-volume theories for self-diffusion in polymer solvent system. I. Predictive capabilities, Journal of Polymer Physics, 23, 289.

[164] J. S. Vrentas, J. L. Duda, H. C. Ling, 1989, Free-volume equations for polymer-penetrant diffusion, Journal of Membrane Science, 40, 101.

[165] A. K. Dolittle, 1951, Studies in Newtonian flow. II. The dependence of the viscosity of liquids on free-space, Journal of Applied Physics, 22, 1471.

[166] H. Lin, B. D. Freeman , 2006, Gas permeation and diffusion in cross-linked poly(ethylene glycol diacrylate), Macromolecules, 39, 3568.

[167]] I. C. Sanchez, R. H. Lacombe, Statistical thermodynamics of polymer solution, Macromolecules 11 (1978) 1145.

[168] R. M. Barrer, J. A. Barrie, J. Slater, 1958, Journal of Polymer Science, 27, 177.

[169] G. C. Sarti, F. Doghieri, 1996, Nonequilibrium Lattice Fluids: A Predictive Model for the Solubility in Glassy Polymers, Macromolecules, 29, 7885.

[170] G. C. Sarti, F. Doghieri, 1998, Solubility of gases in glassy polymers based on the NELF model, Chemical Engineering Science, 19, 3435.

[171] G. K. Fleming, W. J. Koros, Dilation of Polymers by Sorption of Carbon Dioxide at Elevated Pressures.1. Silicone Rubber and Unconditioned Polycarbonate, Macromolecules 19 (1986) 2285.

[172] S. Jordan, W. J. Koros, 1995, Free volume distribution model of gas sorption and dilation in glassy polymers, Macromolecules, 28, 2228.

[173] M. G. De Angelis, T. C. Merkel, V. I. Bondar, B. D. Freeman, F. Doghieri, G. C. Sarti, 2002, Gas Sorption and Dilation in Poly(2,2-bistrifluoromethyl-4,5-difluoro-1,3-dioxole- co-tetrafluoroethylene): Comparison of Experimental Data with Predictions of the Nonequilibrium Lattice Fluid Model, Macromolecules, 35, 1276.

[174] Vito Carlà, Ke Wang, Yazan Hussain, Kirill Efimenko, Jan Genzer, Christine Grant, G. C. Sarti, Ruben G. Carbonell, Ferruccio Doghieri, 2005, Nonequilibrium model for sorption and swelling of bulk glassy polymer films with supercritical carbon dioxide, Macromolecules, 38, 10299.

[175] M. G. De Angelis, G. C. Sarti, 2011, Solubility of gases and liquids in Glassy Polymers, Annual Reviews of Chemical and Biomolecular Engineering, 2, 97.

[176] M. Minelli, M. G. De Angelis, M. G. Baschetti, F. Doghieri, G. C. Sarti, C. P. Ribeiro, B. D. Freeman, 2015, Equation of State Modeling of the Solubility of CO_2/C_2H_6 Mixtures in Cross-Linked Poly(ethylene oxide), Industrial and Engineering Chemistry Research, 54, 1142.

[177] M. Galizia, M. G. De Angelis, M. Messori, G. C. Sarti, Mass transport in hybrid PTMSP/Silica membranes, 2014, Industrial and Engineering Chemistry Research, 53, 9243.

[178] M. G. De Angelis, G. C. Sarti, 2012, Gas sorption and permeation in mixed matrix membranes based on glassy polymers and silica nanoparticles, Current Opinion In Chemical Engineering, 1, 148.

[179] K. Tanaka, H. Kita, K. Okamoto, A. Nakamura, Y. Kusuki, 1989, Gas permeability and permselectivity in polyimides based on 3,3',4,4'-Biphenyltetracarboxylic dianhydride, Journal of Membrane Science, 47, 203.

[180] K. Tanaka, H. Kita, M. Okano, K. Okamoto, 1992, Permeability and permselectivity in fluorinated and non-fluorinated polyimides, Polymer, 33, 585.

[181] N. M. B. Flichy, C. J. Lawrence, S. G. Kazarian, 2003, Rheology of Poly(propylene glycol) and Suspensions of Fumed Silica in Poly(propylene glycol) under High-Pressure CO_2, Industrial & Engineering Chemistry Research, 42, 6310.

[182] Minqiang Hou, Shuguang Liang, Zhaofu Zhang, Jiyuan Song, Tao Jiang, Buxing Han, 2000, Determination and modeling of solubility of CO_2 in PEG200 + 1-pentanol and PEG200 + 1-octanol mixtures, Fluid Phase Equilibria, 258, 108–114.

[183] M. G. De Angelis, T. C. Merkel, V. I. Bondar, B. D. Freeman, F. Doghieri, G. C. Sarti, 1999, Hydrocarbon and Fluorocarbon Solubility and Dilation in Poly(dimethylsiloxane): Comparison of Experimental Data with Predictions of the Sanchez-Lacombe Equation of State, Journal of Polymer Science, Part B, Polymer Physics, 37, 3011.

List of publications

Journal papers:

- L. Olivieri, S. Ligi, M. G. De Angelis, G. Cucca, A. Pettinau, 2015, The effect of graphene and graphene oxide nanoplatelets on the gas permselectivity and ageing behavior of poly(trimethyl sylil propyne) (PTMSP), Industrial and Engineering Chemistry Research, 54, 11199–11211.
- L. Olivieri, A. Tena, M. G. De Angelis, A. Lozano, G. C. Sarti, 2016, Sorption and transport of CO_2 in copolymers containing soft (PEO, PPO) and hard (BKDA-ODA and BPDA-ODA) segments at different temperatures: experimental data and modeling, Paper in revised form for Journal of Membrane Science.

Conference proceedings:

- L. Olivieri, S. Ligi, M. G. De Angelis, E. Treossi, G. C. Sarti, Gas Permeability in PTMSP/Graphene, PTMSP/Graphene Oxide Mixed Matrix Membranes, AICHE 2014 meeting, 16-21/11/2014, Poster.
- L. Olivieri, S. Ligi, M. G. De Angelis, Membrane based on polymeric matrices and graphene nanoplatelets for CO_2 capture processes, X Convegno Nazionale INSTM sulla Scienza e Tecnologia dei Materiali, 28/06/2015-01/07/2015, Oral communication.
- L. Olivieri, S. Ligi, M. G. De Angelis, The effect of small amount of graphene and graphene oxide nanoplatelets on the gas transport properties and ageing behavior of PTMSP, EUROMEMBRANE 2015, 06-10/09/2015, Poster.
- L. Olivieri, A. Lorenzetti, M. G. De Angelis, Amine-functionalized, electrospun polyacrylonitrile (PAN) materials for advanced CO_2 capture processes, EUROMEMBRANE 2015, 06-10/09/2015, Poster.
- L. Olivieri, A.Tena Matias, M. G. De Angelis, A. E. Lozano, J. De La Campa, G. C. Sarti, Sorption, diffusion and permeation of CO_2 in copolymers containing soft (PEO, PPO) and hard (BKDA-ODA and BPDA-ODA) segments at different temperatures: experimental data and modeling, EUROMEMBRANE 2015, 06-10/09/2015, Poster.
- L. Olivieri, S. Ligi, M. G. De Angelis, Membranes based on poly(trimethyl sylil propyne) (PTMSP) and graphene nanoplatelets for gas separation and CO_2 capture, GraphITA 2015, 14-18/09/2015, Poster.